Eur. Phys. J. A (2020) 56:181
https://doi.org/10.1140/epja/s10050-020-00141-9

THE EUROPEAN PHYSICAL JOURNAL A

Review

The joint evaluated fission and fusion nuclear data library, JEFF-3.3

A. J. M. Plompen[1,a], O. Cabellos[2], C. De Saint Jean[3], M. Fleming[4,5], A. Algora[6], M. Angelone[7], P. Archier[8], E. Bauge[3], O. Bersillon[3], A. Blokhin[9], F. Cantargi[10], A. Chebboubi[8,11], C. Diez[12], H. Duarte[3], E. Dupont[13], J. Dyrda[4], B. Erasmus[14], L. Fiorito[4,15], U. Fischer[16], D. Flammini[7], D. Foligno[8], M. R. Gilbert[5], J. R. Granada[10], W. Haeck[17], F.-J. Hambsch[1], P. Helgesson[18], S. Hilaire[3], I. Hill[4], M. Hursin[19], R. Ichou[17], R. Jacqmin[8], B. Jansky[20], C. Jouanne[21], M. A. Kellett[22], D. H. Kim[23], H. I. Kim[23], I. Kodeli[24], A. J. Koning[25], A. Yu. Konobeyev[16], S. Kopecky[1], B. Kos[24], A. Krása[15], L. C. Leal[17], N. Leclaire[17], P. Leconte[8], Y. O. Lee[23], H. Leeb[26], O. Litaize[8], M. Majerle[27], J. I Márquez Damián[10], F. Michel-Sendis[4], R. W. Mills[28], B. Morillon[3], G. Noguère[8], M. Pecchia[19], S. Pelloni[19], P. Pereslavtsev[16], R. J. Perry[29], D. Rochman[19], A. Röhrmoser[30], P. Romain[3], P. Romojaro[31], D. Roubtsov[32], P. Sauvan[33], P. Schillebeeckx[1], K. H. Schmidt[34], O. Serot[8], S. Simakov[16], I. Sirakov[35], H. Sjöstrand[18], A. Stankovskiy[15], J. C. Sublet[25], P. Tamagno[3], A. Trkov[25], S. van der Marck[14], F. Álvarez-Velarde[31], R. Villari[7], T. C. Ware[29], K. Yokoyama[36], G. Žerovnik[1]

[1] European Commission, Joint Research Centre, 2440 Geel, Belgium
[2] Department of Energy Engineering, Universidad Politécnica de Madrid, 28006 Madrid, Spain
[3] CEA, DAM, DIF, 91297 Arpajon, France
[4] OECD Nuclear Energy Agency, 92100 Boulogne-Billancourt, France
[5] UK Atomic Energy Authority, Culham Science Centre, Abingdon OX14 3DB, UK
[6] Instituto de Física Corpuscular, CSIC-Universidad de Valencia, 46071 Valencia, Spain
[7] ENEA, Fusion and Technology for Nuclear Safety and Security Department, 00044 Frascati, Italy
[8] CEA, DEN, DER, SPRC, LEPh, 13108 Saint-Paul-lez-Durance, France
[9] Nuclear Safety Institute of the Russian Academy of Science, Moscow, Russia
[10] Neutron Physics Department, Centro Atomico Bariloche, San Carlos de Bariloche, Argentina
[11] LPSC, Université Grenoble-Alpes, CNRS/IN2P3, 38026 Grenoble Cedex, France
[12] Consejo de Seguridad Nuclear, Madrid, Spain
[13] CEA, IRFU, 91191 Gif-sur-Yvette, France
[14] Nuclear Research and Consultancy Group (NRG), Petten, The Netherlands
[15] Studiecentrum voor Kernenergie-Centre d'Etude Nucléaire, 2400 Mol, Belgium
[16] Institute for Neutron Physics and Reactor Technology, Karlsruhe Institute of Technology, 76021 Karlsruhe, Germany
[17] Institut de Radioprotection et de Sûreté Nucléaire, 92262 Fontenay-aux-Roses, France
[18] Department of Physics and Astronomy, Uppsala University, 751 20 Uppsala, Sweden
[19] Reactor Physics and Systems Behaviour Laboratory, Paul Scherrer Institute, 5232 Villigen, Switzerland
[20] Research Centre Řež, Prague, Czech Republic
[21] CEA, DEN/DM2S/SERMA/LLPR, 91191 Gif-sur-Yvette, France
[22] CEA, LIST, Laboratoire National Henri Becquerel (LNE-LNHB), 91191 Gif-sur-Yvette, France
[23] Nuclear Data Center, Korea Atomic Energy Research Institute, Daejeon 305-35, Republic of Korea
[24] Jožef Stefan Institute (JSI), 1000 Ljubljana, Slovenia
[25] NAPC-Nuclear Data Section, International Atomic Energy Agency, 1400 Vienna, Austria
[26] Atominstitut, Technische Universität Wien, 1040 Vienna, Austria
[27] Nuclear Physics Institute, 250 68 Řež, Czech Republic
[28] National Nuclear Laboratory, Central Laboratory, Sellafield, Seascale, Cumbria CA27 0EF, UK
[29] Wood, Kings Point House, Queen Mother Square, Poundbury, Dorchester DT1 3BW, UK
[30] Technische Universität München, FRM II, 85747 Garching, Germany
[31] Centro de Investigaciones Energéticas, Medioambientales y Tecnológicas (CIEMAT), 28040 Madrid, Spain
[32] Canadian Nuclear Laboratories, Chalk River, ON, Canada
[33] Energy Engineering, UNED, 28040 Madrid, Spain
[34] Rheinstraße 4, 64390 Erzhausen, Germany
[35] Institute for Nuclear Research and Nuclear Energy, 1784 Sofia, Bulgaria
[36] Nuclear Science and Engineering Center, Japan Atomic Energy Agency, Tokai, Ibaraki 319-1195, Japan

Received: 9 September 2019 / Accepted: 17 March 2020 / Published online: 14 July 2020

Communicated by N. Alamanos

Abstract The joint evaluated fission and fusion nuclear data library 3.3 is described. New evaluations for neutron-induced interactions with the major actinides ^{235}U, ^{238}U and ^{239}Pu, on ^{241}Am and ^{23}Na, ^{59}Ni, Cr, Cu, Zr, Cd, Hf, W, Au, Pb and Bi are presented. It includes new fission yields, prompt fission neutron spectra and average number of neutrons per fission. In addition, new data for radioactive decay, thermal neutron scattering, gamma-ray emission, neutron activation, delayed neutrons and displacement damage are presented. JEFF-3.3 was complemented by files from the TENDL project. The libraries for photon, proton, deuteron, triton, helion and alpha-particle induced reactions are from TENDL-2017. The demands for uncertainty quantification in modeling led to many new covariance data for the evaluations. A comparison between results from model calculations using the JEFF-3.3 library and those from benchmark experiments for criticality, delayed neutron yields, shielding and decay heat, reveals that JEFF-3.3 performes very well for a wide range of nuclear technology applications, in particular nuclear energy.

Contents

[a] e-mail: arjan.plompen@ec.europa.eu (corresponding author)

1 Introduction

Since the discovery of radioactivity, nuclear reactions, the neutron and nuclear fission, a considerable knowledge-base was developed in nuclear physics about these processes and their characteristics. This evolved from many sophisticated experiments and the development of advanced models based on phenomenology and theoretical insight. Early on, applications of nuclear science developed that have had and will have an important impact on society – nuclear energy, medicine, security, material characterization, geological exploration, radiation safety and protection, the promise of fusion energy.

Developments are increasingly facilitated and stimulated by better quantitative modeling of physics processes through improved engineering tools and computing power. This allows a reduction in the requirement to use assumptions and approximations in the interpretation, testing and validation of data.

To profit from these advances, physics models have to be coded better and the required input data, in particular the nuclear data, have to be more accurate and complete. In addition, they are required in forms that are compatible with the software that is used for modeling. The input should include full covariance information such that uncertainties can be propagated to derive uncertainty margins of design and operational parameters at a desired confidence level.

In nuclear physics and engineering there is a long tradition to provide nuclear data libraries in response to evolving needs in the field. In this paper the Joint Evaluated Fission and Fusion nuclear data library version 3.3 (JEFF-3.3) is described. It is the last of a series of libraries developed over the past 35 years through a collaborative effort of nuclear laboratories coordinated by the Databank of the OECD Nuclear Energy Agency (NEA). JEFF-3.3 was released on 20 November 2017. The library consists of reaction data files for incident neutrons, protons, deuterons, tritons, helions, alphas and photons, a decay data file, a fission yields file, a thermal neutron scattering file, an activation file, and a displacements per atom (dpa) file. Although the JEFF-3.3 library builds on earlier releases (3.0 [1], 3.1 [2], 3.1.1 [3,4], 3.1.2 and 3.2), it includes substantial changes. For completeness, in particular for neutron activation applications and decay heat estimations, many files were adopted from TENDL [5]. This includes files for charged-particle and photon induced reactions which are of interest for accelerator applications.

Purpose

JEFF-3.3 is a general purpose library serving a wide field of nuclear technology applications, both nuclear energy and non-energy applications. The main effort is directed at improving the data for neutron transport calculations. This part of the library, i.e. the neutron transport sublibrary, is used for the design, performance and safety assessment of industrial and experimental nuclear reactors, criticality safety analyses of spent nuclear fuel, nuclear safeguards and security and basic science.

JEFF-3.3 developments targeted the needs for the following reactor development programmes: ASTRID, a French fast reactor concept with enhanced sustainability and safety and reduced production of high level nuclear waste [6], MYRRHA, a research reactor developed in Belgium, advancing and promoting the development of accelerator driven systems and lead or lead-bismuth cooled fast reactors [7,8], and the ITER and DEMO [9,10] reactors and the IFMIF-DONES material irradiation facility [11] in support to nuclear fusion technology. JEFF-3.3 also aims at maintaining or improving performance for present and prospective pressurised water reactors (PWR) and boiling water reactors (BWR) for which JEFF-3.1.1 and JEFF-3.2 demonstrated excellent performance. Of particular interest are the concerns for safe, economic and ecologic transport, intermediate storage and final disposal of spent fuel. This requires accurate neutron transport and depletion calculations for criticality safety analyses and the prediction of decay heat and radiation source terms.

MYRRHA

MYRRHA, a Multi-purpose Research Reactor for High-tech Applications is being designed at SCK•CEN, Belgium [7,8]. It is envisaged to operate both in critical and sub-critical mode. The reactor has a pool design with Lead-Bismuth Eutectic (LBE) coolant ensuring a fast neutron spectrum. This positions MYRRHA in the class of heavy liquid metal

cooled fast reactors. In case the sub-critical operation mode is chosen, the central sub-assembly hosts a spallation neutron source. High energetic protons, with an energy of 600 MeV, are produced by a high-power linear accelerator with a max. beam current of 4 mA. The protons produce neutrons by interacting with the LBE coolant.

The two operation modes have their specific energy and neutron fluence distributions that permit a wide range of applications, from transmutation research to radionuclide production for medical and industrial applications. A flexible core design envisages many positions for experimental rigs to test new types of fuel and materials for e.g. fusion reactors. A sensitivity and uncertainty analysis revealed the noticeable contribution of lead and bismuth cross sections to the k_{eff} uncertainty [12]. In addition, neutron capture on ^{209}Bi leads through the decay of ^{210g}Bi to the formation of ^{210}Po, a highly radiotoxic nuclide determining the radioactive source term of LBE coolant.

ASTRID

ASTRID, the Advanced Sodium Technological Reactor for Industrial Demonstration, is a Generation-IV sodium-cooled fast reactor project, proposed by the Commissariat à l'Énergie Atomique (CEA) [6]. The main goals of ASTRID are multiple recycling of plutonium for the sustainability of natural uranium resources, minor actinide transmutation to reduce nuclear waste, and an enhanced safety compared to Generation-III reactors, such as the European Pressurized-water Reactor – EPR. Based on the experience with past Sodium-cooled Fast Reactors (SFR), ASTRID has the objective to demonstrate at an industrial scale the relevance and performance of innovations, in particular in the fields of safety and operability. ASTRID, with the related R&D facilities (hot labs, irradiation, technological platform, severe accidents, etc.) is designed to allow the:

- testing and qualification of innovative safety design options towards a commercial reactor,
- qualification of different fuels (transmutation, plutonium burner, etc.),
- collection of the necessary data to justify a useful lifetime of 60 years for future SFR,
- confirmation of the performance of innovative components and systems in order to optimise the design of future commercial reactors from a technical and economical point of view,
- establishment of a reference for SFR cost assessment for construction and operation.

PWR and BWR and Spent Nuclear Fuel

Previous JEFF-3.1.1, JEFF-3.1.2 and JEFF-3.2 releases were tested broadly for pressurized and boiling water reactors. JEFF-3.1.1 was proven to perform well for these reactors in normal conditions [2]. JEFF-3.2 aimed at keeping this good behavior and fixed some issues for applications based on fast neutrons. For JEFF-3.3, the community chose to keep as much as possible this good behaviour and including results from recent studies carried out by WPEC[1] subgroup 34 on the *Coordinated evaluation of Plutonium-239 in the resonance region* [13], subgroup 40, the *Collaborative International Evaluated Library Organisation (CIELO) Pilot Project* for major isotopes ^{235,238}U, ^{239}Pu, Iron, Oxygen and Hydrogen [14,15]. In addition, recommendations resulting from the CHANDA (*solving CHAllenges in Nuclear Data*) project [16], a project supported by the European Commission within the 7th framework, were taken into account. For fission yields and thermal scattering data, additional collaboration through WPEC was co-ordinated under the WPEC subgroup 37 on *Improved fission product yield evaluation methodologies*[2] and subgroup 42 on *Thermal Scattering Kernel* $S(\alpha,\beta)$: *Measurement, Evaluation and Application*2.

With the prospect of phasing out of PWR and BWR there is an increasing emphasis on spent nuclear fuel intermediate storage and final disposal, long term disposal of high level waste and the related encapsulation and transport problems. Therefore, considerable emphasis is placed on criticality safety, decay heat and radiation source term estimates for the proposed solutions and operations.

Fusion applications

The European strategy for the realisation of fusion energy, as expressed in the recent fusion roadmap [9], is built on three main pillars: the international ITER tokamak to demonstrate the scientific and technological feasibility of fusion as an energy source, an accelerator based neutron source, called IFMIF-DONES [11], for the development and qualification of fusion materials and a DEMOnstration power plant (DEMO) [10], which shall deliver a substantial amount of electricity to the grid and operate with a closed tritium fuel cycle. Neutronics simulations play a fundamental role for the design and optimisation of these facilities, including the evaluation and verification of their nuclear performance. Accurate nuclear data are required to predict the tritium breeding capability, assess the shielding efficiency, estimate the nuclear power generated in the system and produce activation

[1] Working Party on Evaluation Cooperation on nuclear data, an expert group of the Nuclear Science Committee of the Nuclear Energy Agency – Organisation for Economic Cooperation and Development.

[2] www.oecd-nea.org/science/wpec.

and radiation damage data for the irradiated materials and components. This applies to the radiation dose fields after shut-down or during maintenance periods [17]. The availability of high quality nuclear data is thus a pre-requisite for reliable design calculations affecting the nuclear design and performance of the facilities, as well as safety, licensing, waste management and decommissioning issues.

A dedicated programme is conducted by the EUROfusion consortium on the development and qualification of nuclear data for fusion. This includes the evaluation of general purpose neutron cross-section data as required for design calculations using particle transport codes, the generation of new activation and displacement damage cross-section data libraries, and the evaluation of deuteron cross-sections as required for the IFMIF-DONES d-Li accelerator. This work is complemented by extensive benchmark, sensitivity and uncertainty analyses to check the performance of the evaluated cross-section data and libraries against integral experiments. Nuclear data evaluations of specific importance to fusion applications, such as those for Cr, Cu, W, and Zr stable isotopes, were contributed to the JEFF-3.3 general purpose neutron cross data library and benchmarked against fusion relevant integral experiments. Specific nuclear data libraries were provided as sub-libraries to JEFF-3.3 including a dedicated neutron activation data file (see Sect. 2.9) and a displacement damage data library (see Sect. 2.6).

2 Components

In this section the components of JEFF-3.3 are presented. We start with the neutron transport sublibrary consisting of data for actinides (Sect. 2.1), structural materials, coolants and fission products (Sects. 2.2 and 2.3) and thermal neutron scattering (Sect. 2.10). The neutron transport sublibrary includes modifications for improved delayed neutron and gamma-ray emission data. We then present covariances related with the neutron transport sublibrary, fission yields, decay data, neutron activation, and displacement damage data.

2.1 Actinide evaluations

2.1.1 ^{235}U in the resonance range

In the late 1980s and early 1990s a ^{235}U Reich–Moore resonance evaluation was performed from thermal energy to 2.25 keV [18] using the SAMMY [19] code. This was the first attempt to use a more rigorous resonance formalism to account for interference effects in the fission channels. The evaluation represented a substantial improvement compared to previous ^{235}U evaluations based on the Single-Level Breit-Wigner (SLBW) formalism combined with background cross-sections. Very little integral benchmark testing was carried out to assess the quality prior to its adoption in an evaluated library. Subsequent benchmark testing demonstrated shortcomings of this evaluation. In particular, these tests suggested that the capture cross-section in the energy region from 22.6 to 454 eV was underestimated [20]. No issues with the fission cross-section were found. It should be pointed out that at the time of the evaluation of Ref. [18] no reliable capture cross section data in the energy range above 100 eV were available. In addition, reported capture cross-section data for neutron energies above 100 eV suffered from bias effects due to normalisation and background corrections. Therefore, in the evaluation process no capture data were included.

The ^{235}U evaluation of Ref. [18] was revised using results of integral benchmark and extensive sensitivity analysis studies [21]. The results were included in the ENDF, JEFF and JENDL libraries. The JENDL project adopted the evaluation up to 500 eV and used an unresolved resonance representation above 500 eV to improve consistency with results of a fast critical assembly benchmark (FCA) [22]. The revised evaluation produced a higher capture cross-section that is not supported by results of both the FCA and the ZEUS benchmark (hmi6 [23]).

The WPEC subgroup 29 [24] investigated this issue and recommended new measurements of the capture cross-section to be considered in future evaluations.

Therefore, capture cross-section measurements with the time-of-flight technique were performed independently at the Rensselaer Polytechnic Institute (RPI) [25] and at the Los Alamos National Laboratory (LANL) [26]. The results of these measurements were included in a resonance analysis to update the ^{235}U resonance parameters in the energy range from thermal energy to 2.25 keV. Using the new resonance parameters the results of integral benchmarks could be better reproduced. Unfortunately, fission cross section data derived from these parameters showed marked differences with those recommended by the standards evaluation [27]. Recently, fission cross-section data resulting from measurements at the n_TOF facility provided strong support to the recommendations in the standards evaluation. Indeed, normalising the n_TOF fission data to the energy integral from 7.8 to 11.0 eV of Ref. [27] (Table 4) results in good agreement between the n_TOF data and the cross-sections from the standards evaluation in the low energy region, supporting the averaged fission cross-sections of Ref. [27] in the resonance region. Therefore, the ^{235}U resonance parameter evaluation for JEFF-3.3 was revised based on results of a new analysis that included the n_TOF experimental fission data.

^{235}U resolved resonance range Resonance parameters for neutron energies between 10^{-5} eV and 2.25 keV were derived from a resonance analysis using the experimental data given in Table 1. These data include the high-resolution transmission, fission cross-section, and eta measurements

Table 1 Experimental data included in the SAMMY resonance analysis of ^{235}U for JEFF-3.3; The references (Refs.) column mentions the lead author to identify the data set of the figures of this section. ER is the energy range (eV). L is the nominal flight-path length (m) of the time-of-flight measurement. n is the atom density times the sample thickness (atoms per barn), T is sample temperature (K)

Refs.	ER	L	n	K
Transmission				
Spencer [28]	0.01–8	18	0.001468	293
Harvey [29]	0.4–68	18	0.03269	77
Harvey [29]	4–2250	80	0.00233	77
Harvey [29]	4–2250	80	0.03269	77
Fission				
Gwin [30]	0.1–20	26		293
Weston [31]	100–2250	86		293
Weston [32]	14–2250	19		293
Paradela [33]	0.7–2250	185		293
Danon [25]	0.01–2250	26		293
Wagemans [34]	0.001–0.4	18		293
Eta (η)				
Wartena [35]	0.0018–1	8		293
Weigmann [36]	0.0015–0.15			293
Capture				
Danon [25]	0.01–2250	26		293
Jandel [26]	100–2250	25		293
Perez [37]	0.01–200	40		293
Saussure [38]	0.01–2250	25		293

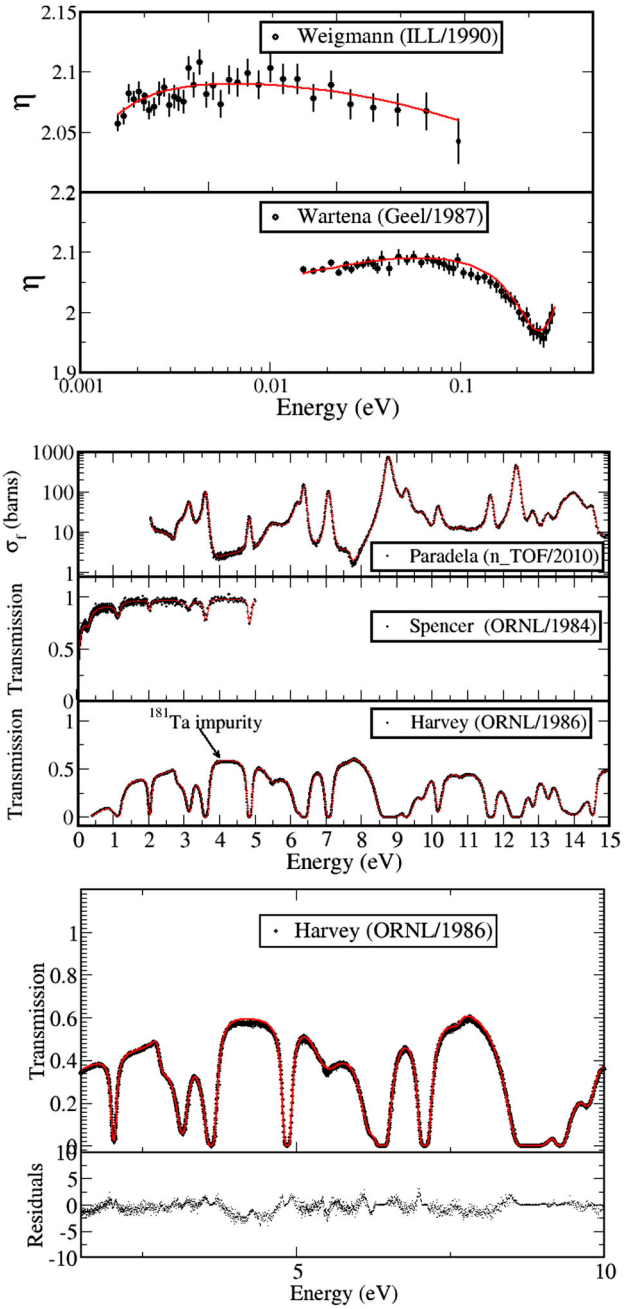

Fig. 1 Top: comparison of the experimental and calculated η(E) for ^{235}U in the thermal energy range. Middle: comparison of the SAMMY fit of the experimental data for ^{235}U. The bottom figure gives a flavor of typical residuals and highlights an unaccounted Ta impurity in the Harvey data. Chi-square varies between 0.94 and 1.8 over the range of the fits (see also the next figure)

that were included in previous evaluations and the data of LANL, n_TOF and RPI, which were not available before. The results of the capture cross section measurements carried out at LANL and RPI were important to unveil issues with the capture cross section above 100 eV. The fission cross-section measurements carried out at n_TOF supported the standard cross section values, which were used as a reference in the analysis.

The Reich–Moore approach implemented in SAMMY was used for fitting the data. Before fitting the data shown in Table 1, the experimental conditions were examined carefully. Experimental resolution, normalisation, background, multiple-scattering and data alignment were inspected to assure consistency between experimental input parameters and the experimental conditions. The experimental data were fitted with typical values for Chi-square between 0.94 and 1.8. An example of the associated residuals is given in Fig. 1 for the transmission data of Harvey et al. in a limited energy range.

Previous evaluations of the ^{235}U resonance parameters made use of several external resonance energies: 14 bound levels and 14 levels above 2.25 keV. This proved not necessary to represent the interference effects in the resonance range from 10^{-5} eV to 2.25 keV. Actually, it was found that the issue of fitting the standard fission cross-section was directly related to the contribution of the external energy levels. The long-range interference effects inherent in the R-matrix methodology precluded finding a good fit of the experimental fission data. It also had an impact on the elastic

Table 2 External levels for the ^{235}U resonance analysis for JEFF-3.3

E_r (eV)	Γ_γ (MeV)	Γ_n (MeV)	Γ_{f1} (MeV)	Γ_{f2} (MeV)	J^π
Bound levels					
−75.405	47.781	507.274	−487.090	−443.345	3^-
−5.253	36.797	12.170	195.681	−160.038	4^-
−0.481	39.228	0.088	129.661	−80.535	3^-
−0.432	38.024	0.033	167.072	−8.283	4^-
-3.7×10^{-5}	39.988	6.5×10^{-8}	−0.509	0.935	4^-
Levels above 2.25 keV					
2281.325	44.083	12.459	155.711	458.850	4^-
2284.014	41.147	3802.461	1956.501	22.864	3^-
3312.563	47.228	11457.53	474.421	571.292	3^-
3819.129	38.494	1242.316	−511.662	67.709	4^-
4500.997	33.681	33.8548	286.623	364.141	3^-

scattering cross section. The present evaluation contains five bound energy levels and five energy levels above 2.25 keV. The 10 external energy levels are listed in Table 2. For each resonance the resonance energy E_r, gamma width Γ_γ, neutron width Γ_n, two fission widths Γ_{f1} and Γ_{f2} and the spin and parity J^π are reported. A negative sign for a partial width reflects the sign of the reduced width. The bound level with an energy close to zero (-3.657×10^{-5} eV) and a very small neutron width is responsible for the curved energy dependence of the η(E) at low energy [39]. Two experimental η(E) measurements (Table 1) were included in the fit (Fig. 1).

An accurate representation of the external resonance contribution provides the basis for the effective scattering radius. The analysis of high-resolution transmission data led to an effective scattering radius of 9.602 fm.

Having fixed the external levels, a sequential analysis of the data was carried out to achieve a reasonable fit of the data with an acceptable χ^2. In the energy range a total of 3170 resonance levels were identified. Not only were the resonance parameters allowed to vary in the fit but also normalisation, resolution parameters, and others. The normalization correction ranges from −1.8% to + 3.1%. These corrections are essential for the consistency of the fit and are achieved by a sequential fitting of the experimental data. The normalization of the fission data of Weston were 1.8% lower than that of Paradela fission data. Likewise, Gwin fission data normalization were about 1.4% lower compared to Paradela's data. This feature has precluded in the past to obtain the 7.8–11.0 eV standard fission integral value. The capture data of Danon and Jandel were in agreement with a normalization correction of about 1.1%. Perez capture data below 200 eV were also consistent with the Danon and Jandel experimental data. However, the De Saussure capture data have a normalization correction of about 3.1%.

The results of a fit to the Harvey [29] (transmission), Spencer [28] (transmission), and the Paradela [33] (fission cross-section) data are shown in Fig. 1. An examination of

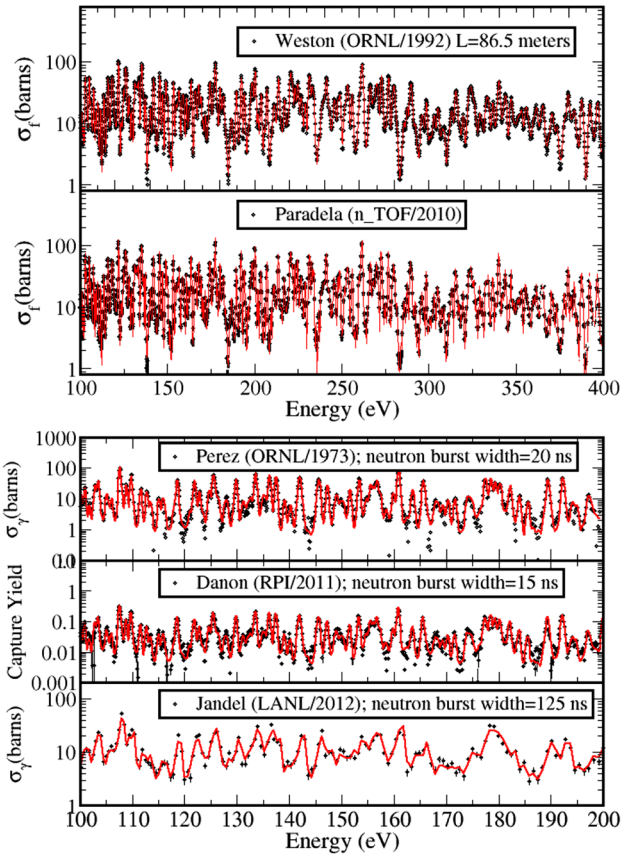

Fig. 2 Top: SAMMY fitting of the ^{235}U fission cross section in the 100–400 eV energy range for JEFF-3.3. Bottom: SAMMY fitting of the ^{235}U capture cross section in the 100–200 eV energy range for JEFF-3.3

the transmission data of Harvey revealed an inconsistency around the energy 4.25 eV. It was found that this is due to an impurity of ^{181}Ta present in the transmission sample. Although the data reduction was suitably done it appears that the effect of the ^{181}Ta impurity was not completely removed.

Table 3 JEFF-3.3 energy-averaged fission cross sections for ^{235}U from the SAMMY resonance analysis compared with the standards [27,40]. For the interval 7.8–11 eV the energy integrated cross section is given

E_n	Standards evaluation		JEFF-3.3
	2009 [27]	2018 [40]	
(eV)	(b eV)	(b eV)	(b eV)
7.8–11	246.4(12)	247.5(30)	246.9
(eV)	(b)	(b)	(b)
100–200	21.17(11)	21.3(3)	21.02
200–300	20.69(11)	20.8(3)	20.77
300–400	13.13(7)	13.2(2)	13.22
400–500	13.78(8)	13.9(2)	13.49
500–600	15.17(9)	15.2(2)	15.20
600–700	11.51(7)	11.57(15)	11.53
700–800	11.10(6)	11.15(14)	11.10
800–900	8.21(5)	8.25(11)	8.15
900–1000	7.50(4)	7.54(10)	7.37
1000–2000	7.30(4)	7.34(10)	7.29

In the analysis an adjustable normalisation factor was included for each fission cross section data set. This normalisation factor was adjusted using the fission integral in the energy range between 7.8 and 11 eV recommended in Ref. [27]. Due to this procedure the Weston [31,32] and Gwin [30] fission data were adjusted by about 2%. The results of a fit to the Weston [32] and Paradela [33] data is shown in Fig. 2 in the energy range 100–400 eV. The resolution of the n_TOF data is excellent, displaying the details of the Porter–Thomas like fluctuations not seen in the Weston data in this energy range. The results in Table 3 confirm that the averaged fission cross sections derived from the final resonance parameters are in very good agreement with those of the standards evaluation [27].

The capture data of Perez et al. [37] were used below 200 eV together with the data of Danon et al. [25] obtained at RPI, which were used up to 2250 eV. The data of Jandel et al. obtained at LANL were used in the region above 100 eV. The three data sets in the energy range 100–200 eV are displayed in Fig. 2 together with the results of a fit. As can be seen, the resolution of the RPI data is excellent for resonance analysis. Since the flight path lengths for the three measurements are about the same, the main difference in resolution is due to the neutron burst width. In the energy range from 100 to 200 eV the results are based on the capture data obtained by Danon (RPI), Jandel (LANL) and Perez (ORNL).

As previously indicated, the main motivation for revising the ^{235}U resonance parameter was to address discrepancies with the ^{235}U(n,f) cross section in the standards file [27]. The revision of the external resonance values, bound energy levels and energies above 2250 eV, allowed a quick convergence to the standard values at thermal energy and the average values for the fission cross section recommended in the 2009 standards evaluation [27]. The values at thermal energy calculated from the new resonance parameters are listed in Table 4 and compared with those of the 2009 [27] and 2018 standards evaluation [40]. The JEFF-3.3 evaluation is seen to be within one standard deviation of both evaluations for all but two energy groups (400–500 and 900–1000 eV).

Table 4 JEFF-3.3 fission σ_f, capture σ_γ and scattering σ_s cross sections of ^{235}U for the 0.0253 eV neutron energy compared with the standards [27,40]. The JEFF-3.3 cross sections are obtained with the SAMMY resonance analysis

	[27] (b)	[40] (b)	JEFF-3.3(b)
σ_f	584.4(10)	587.3(14)	584.4
σ_γ	99.3(7)	99.5(13)	99.2
σ_s	14.09(22)	14.09(22)	14.09

To summarize, for neutron energies below 2.25 keV, a re-evaluation of the ^{235}U resonance parameters was carried out to address discrepancies with cross section standards at thermal energy and average fission cross-section values and to include new capture cross section data above 100 eV. A new fission cross section measurement done at the n_TOF facility of CERN was the primary factor in obtaining good agreement between the results of the new evaluation and the standards evaluation. The new set of resonance parameters includes fewer external levels and provides a better way of calculating the interference effects of the fission channels. The values at thermal energy agree within uncertainties with those recommended in the 2009 standards evaluation. A normalization to the fission integral in the energy range from 7.8 to 11 eV resulted in good agreement with all average fission cross sections of the 2009 standards evaluation below 2 keV. Hence, the new set of resonance parameters presented in this paper are improved compared to those presented in previous JEFF versions.

^{235}U unresolved resonance range In JEFF-3.3 cross section data for neutron interactions with ^{235}U in an URR representation is provided for energies between 2.25 and 46.2 keV. Average resonance parameters were derived with the model implemented in NJOY [41] to ensure full consistency between the evaluation and the files produced with NJOY for application codes (see Sect. 3.6). The Integral Data Assimilation (IDA) procedure of the CONRAD code [42] was used. This procedure allows to include in the analysis both microscopic and integral data. The option within TALYS [43] to run unresolved resonance calculation was used to calculate average parameters. This option, which is consistent with the model implemented in NJOY, allows an adjustment of s-wave parameters to a set of experimental data. For the fission cross section, the values recommended in the 2018

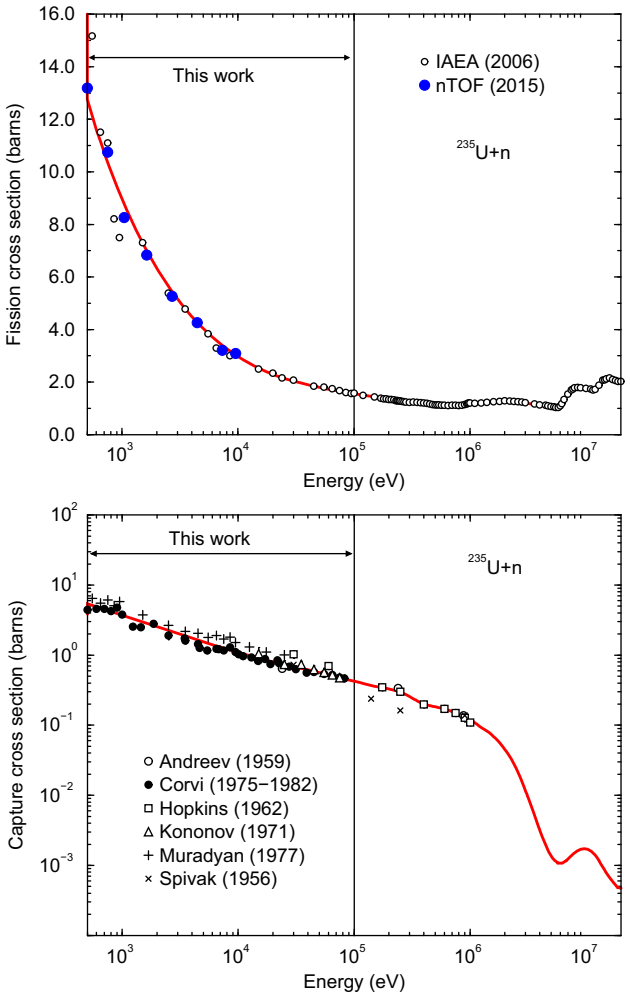

Fig. 3 ^{235}U fission and capture cross sections calculated for JEFF-3.3 with TALYS ($E < 100$ keV), compared with fission cross sections reported in Refs [40] (IAEA 2006) and [33] (nTOF 2015) and with capture data retrieved from the EXFOR data base: [45] (Andreev), [46,47] (Corvi) [48] (Hopkins), [49] (Kononov) [50] (Muradyan), [51] (Spivak)

neutron standards file [40], were used. Capture cross section data in the EXFOR data base are characterised by a large spread. Therefore, it was preferred to use results of the PROFIL integral experiments carried out in the fast reactor PHENIX [44] to optimise the average parameters that are sensitive to the capture reaction. A set of (ℓ,J) dependent average parameters[3] (mean level spacings, reduced neutron widths and partial widths for the capture and fission reactions) was derived in order to calculate self-shielding factors between 2.25 and 46.2 keV. Results were tested on the integral benchmarks ZEUS and MASURCA-1B.

The PROFIL and PROFIL-2 sample irradiation experiments were carried out in the PHENIX reactor of the CEA/DEN Marcoule. These experiments use rods with a large number of samples (130 samples) containing almost pure separated actinides and fission products. The experiments were designed to collect integral information to improve neutron-induced cross sections of interest for fast reactor applications. The PROFIL results were analysed using the ERANOS-2.2 code with the JEFF-3.1.1 nuclear data library. The analyses show that the capture-to-fission ratio α for ^{235}U can be derived from the (^{235}U/^{238}U) and (^{236}U/^{235}U) isotopic ratios. They characterize the fission and capture cross sections for ^{235}U, respectively. In this work, the IDA procedure was used to extract the $\alpha(^{235}\mathrm{U})$ ratio in the neutron energy range 500–150 keV.

Prior values and uncertainties for the s-wave average radiation width $\langle\Gamma_{\gamma 0}\rangle$, mean level spacing D_0 and neutron strength function S_0 were determined from the statistical analysis of the resolved resonance parameters yielding:

$$\begin{aligned}\langle\Gamma_{\gamma 0}\rangle &= 38(4)\ \mathrm{MeV},\\ D_0 &= 0.49(2)\ \mathrm{eV},\\ S_0 &= 0.98(7)\times 10^{-4}.\end{aligned}$$

D_0 and S_0 were determined simultaneously by using the ESTIMA method [52]. ESTIMA provides the most probable neutron strength function and mean level spacing for s-wave levels. We decided to fix the the mean level spacing and to consider the neutron strength function as a free parameter. The posterior value provided by the CONRAD code is close to $S_0 = 1.02\times 10^{-4}$. Final fission and capture cross sections are shown in Fig. 3. The theoretical curves are in good agreement with the microscopic experimental data. The calculated-to-experimental ratios for the (^{235}U/^{238}U) and (^{236}U/^{235}U) isotopic ratios for the PROFIL results [44] deviate by less than 3% from unity.

To understand if for applications the resolved resonance range is best terminated at 0.5, 1 or 2 keV and whether the alpha-ratio extracted with the assistance of the PROFIL data is appropriate, calculations were made with the TRIPOLI-4® [53] Monte Carlo code to simulate the MASURCA-1B and ZEUS hmi6 experiments (See also Sect. 3.1). The ZEUS critical benchmarks consist of four configurations, which are characterised by increasing Energy of the Average Lethargy causing Fission (EALF: 4.44 keV, 9.45 keV, 22.80 keV, and 80.80 keV). For the results in Fig. 4 only JEFF-3.1.1 data were used besides the different options of ^{235}U considered for JEFF-3.3. All three options improve the agreement with experiment, with discrepancies ranging between -300 and $+300$ pcm. The observed trend for increase with EALF of JEFF-3.1.1 between the three first ZEUS benchmarks vanishes. Contrary to the underprediction for the first three ZEUS cases, the fourth ZEUS configuration and MASURCA-1B show an overprediction. Although there is no clear optimum

[3] ℓ is the orbital angular momentum quantum numer, J the total angular momentum quantum number. Both are give in units of $\hbar$.

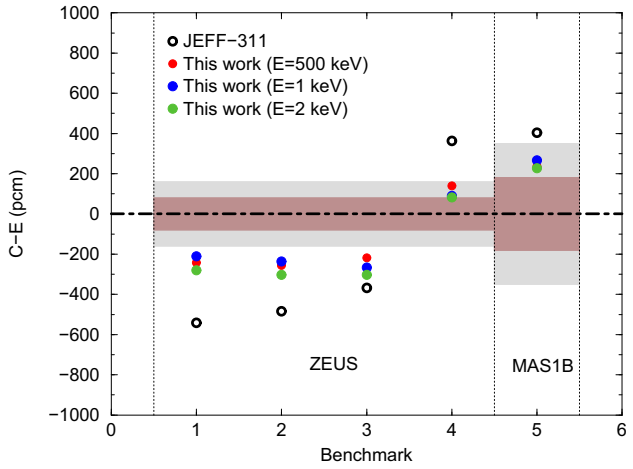

Fig. 4 Integral trends involving JEFF-3.3 ^{235}U obtained with the ZEUS (hmi6) and MASURCA-1B (MAS1B) benchmarks. The brown (grey) band corresponds to 1 (2) experimental standard uncertainty

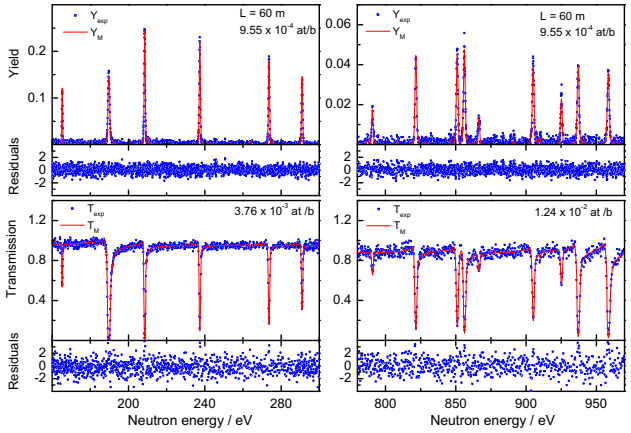

Fig. 5 Comparison of experimental and theoretical observables. The experimental yield Y_{exp} obtained at 60 m with a 9.55×10^{-4} at/b sample is compared with the theoretical yield Y_M. The experimental transmission T_{exp} from measurements with a 3.76×10^{-3} and 1.24×10^{-3} at/b sample at ORELA is compared with the theoretical transmission T_M. The calculated observables were obtained from calculations with REFIT after adjusting the parameters to the experimental data as described in the text. The residuals are calculated considering only the uncorrelated uncertainties due to counting statistics

for the upper limit of the resolved resonance range a choice of 2.25 keV is very reasonable, as is the choice for $\alpha(^{235}\mathrm{U})$.

2.1.2 ^{238}U in the resonance range

^{238}U resolved resonance range The neutron transport sublibrary in the resolved resonance region for ^{238}U, which covers neutron energies from 0 to 20 keV, was constructed by replacing the JEFF-3.2 parameters for resonances below 1200 keV with the parameters reported by Kim et al. [54]. The parameters in JEFF-3.2 were primarily based on the work of Derrien et al. [55]. The parameters reported by Kim et al. [54] were obtained from a least squares fit to the experimental capture yields derived by Kim et al. [54] and the transmission data of Olsen et al. [56,57]. The fission widths were adjusted to reproduce the fission areas of Difilippo et al. [58]. The resonance shape analysis code REFIT [59], which is based on the Reich–Moore [60] approximation of the R-matrix formalism [61], was used. The latest version of the code accounts for various experimental effects such as Doppler broadening, neutron self-shielding, multiple interaction events, the response function of the TOF-spectrometer, properties of the detection system, γ-ray attenuation in the sample and inhomogeneities of the sample [62].

The capture experiments of Kim et al. [54] were carried out at a 12.5 and 60 m measurement station of the time-of-flight facility GELINA [63]. The total energy detection principle in combination with the pulse height weighting technique was applied using C_6D_6 liquid scintillators as prompt γ-ray detectors. The data were normalised to the isolated and saturated ^{238}U resonance at 6.67 eV. The procedures recommended in Ref. [62] were applied to reduce bias effects due to the weighting function, normalisation, dead time and background corrections, and corrections related to the sample properties. Therefore, the options in REFIT [62] to correct for neutron and γ-ray transport in the sample in case of capture data were used. The total uncertainty due to the weighting function, normalisation, neutron fluence and sample characteristics was $\sim$ 1.5%. The transmission data of Olsen et al. [56,57] resulted from time-of-flight experiments at a 42 m and 150 m station of ORELA using 7 samples of different areal density (from 0.0002 at/b to 0.175 at/b). Both the transmission and capture data were analysed without applying any additional background or normalisation correction.

The free gas model with an effective temperature of 295 K was used to account for the Doppler effect. The initial resonance parameters, including parity and spin, and effective scattering radius R′ = 9.48 fm were taken from Derrien et al. [55]. Examples of the result of a simultaneous fit to the capture and transmission data are shown in Fig. 5. To fit the transmission data of Olsen et al. [56,57], without applying a normalisation factor, the contribution of the two bound states at -7 eV and -33 eV were adjusted maintaining the capture cross section at thermal energy $\sigma_\gamma = 2.683\ (12)$ b recommended by Trkov et al. [64]. After this adjustment the elastic scattering cross section at thermal energy was reduced by about 0.5 % compared to the one in JEFF-3.2. The corresponding coherent scattering length $b_c = 8.57\ (2)$ fm is in agreement with the one $b_c = 8.63\ (4)$ fm recommended by Koester et al. [65]. The cross sections at thermal energy and resonance integrals derived from the recommended resonance parameters are listed in Table 5.

Table 5 ^{238}U total, elastic and capture cross sections σ at thermal energy and resonance integrals (RI) between 0.5 eV and 100 keV calculated from the resonance parameter file of JEFF-3.3

	σ (b)	RI (b)
(n, tot)	11.924	593.20
(n, n)	9.240	318.35
(n, γ)	2.684	274.63

^{238}U unresolved resonance range The unresolved resonance range extends from 20 to 150 keV. The so-called infinitely dilute cross sections for the unresolved resonance range was obtained from the statistical model approach presented in Sect. 2.1.4. However, for the sole purpose of calculating self-shielding factors the file retains the evaluation present in the JEFF-3.2 library, which dates from JEFF-2.2. The appropriate flags have been set in the evaluated file to ensure its proper use.

As may be noted from Fig. 9, the JEFF-3.3 evaluation for the neutron capture cross section of ^{238}U is less than those of JENDL-4.0 and ENDF/B-VIII.0 in the energy range around 40 keV and from 150 to 500 keV. In this respect, the JEFF-3.3 evaluation does not follow the result from the evaluation of the standards [27,40].

2.1.3 ^{239}Pu in the resonance range

^{239}Pu resolved resonance range Resonance parameters for n + ^{239}Pu in the RRR, which covers the energy region from 0 to 4 keV, were obtained from a resonance shape analysis with SAMMY using the Reich–Moore approximation [19]. Long-range interference in the R-matrix formalism plays a major role in modeling fissile isotopes. For the present evaluation the first step consisted of finding pseudo resonances, resonances outside of the resolved resonance range of 0–4 keV, that mock-up the contribution and interference due to all resonances not treated explicitly. Five negative levels and three resonances above 4 keV were found that describe well the interference effect. The parameters of these bound states, i.e. resonance energy E_r, gamma width Γ_γ, neutron width Γ_n, two fission widths Γ_{f1} and Γ_{f2} and the spin and parity J^π, are listed in Table 6. Negative signs associated with the fission partial widths Γ_{f1} and Γ_{f2} reflect the sign of the reduced amplitude width γ_{f1} and γ_{f2}. The ground state spin of the ^{239}Pu is $1/2^+$ which leads, for an s-wave ($\ell = 0$) to two J-values 0^+ and 1^+. Higher angular momenta ($\ell > 0$) show negligible contribution to the cross section below 4 keV due to the higher penetrability.

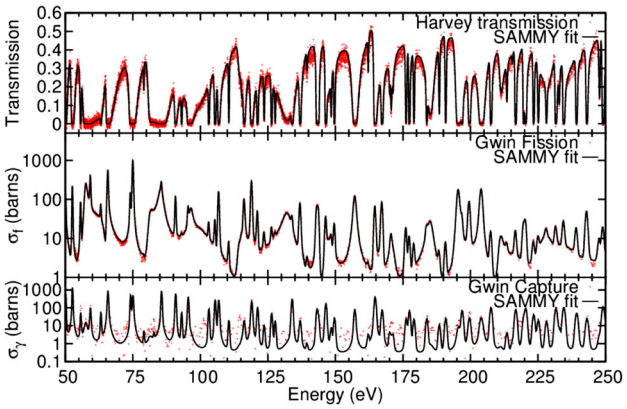

Fig. 6 Comparison of the SAMMY fit for the resolved resonance range of ^{239}Pu JEFF-3.3 to the experimental data

The experimental database used in the new evaluation is essentially the same as the one used in Ref. [66]. The high-resolution transmission data of Harvey et al. [29] allowed extending the resonance range from 2.5 to 4 keV. The results of the SAMMY fitting of the transmission data of Harvey et al. [29] and the fission and capture data of Gwin et al. [30] are shown in Fig. 6. The analysis of the high-resolution transmission data led to an effective scattering radius of 9.41 fm. The number of resonances used in the fit of the experimental data from 0 to 4 keV is 1572.

Table 6 ^{239}Pu resonances external to the resolved resonance range of 0–4 keV used for JEFF-3.3

E_r (eV)	Γ_γ (MeV)	Γ_n (MeV)	Γ_{f1}(MeV)	Γ_{f2}(MeV)	J^π
Bound levels					
− 149.141	47.182	542.357	4226.10	0.0	1^+
− 8.068	49.725	0.141	− 1.499	0.0	1^+
− 7.019	70.066	17.548	− 117.345	223.288	0^+
− 0.514	24.005	0.118	15.237	1189.35	0^+
− 0.020	21.029	6.60×10^{-8}	− 4.880	0.0	1^+
Resonances above 4 keV					
4006.71	39.000	19.901	48.847	0.0	1^+
4022.48	39.000	4.96×10^{-6}	835.807	121.703	0^+
4035.40	39.000	2837.18	− 181.877	0.0	1^+

Table 7 ^{239}Pu thermal cross section values (0.0253 eV) calculated with SAMMY and compared to the Atlas of Neutron Resonances (ANR) and the standards evaluations [27,40]

	ANR	Standard		JEFF		
		2009	2018	3.1.1	3.2	3.3
σ_f	748(2)	750(2)	752(2)	747	747	749
σ_γ	269(3)	272(2)	270(3)	273	270	271
σ_s	7.9(4)	7.8(10)	7.8(10)	8.0	8.1	7.8

The fission, capture and scattering cross sections at thermal energy are displayed in Table 7, together with the values of previous JEFF evaluations, the ones listed in the Atlas of Neutron Resonances [67] and those recommended in the 2009 and 2018 standards [27,40]. The JEFF-3.3 values are within one standard uncertainty in agreement with the 2009 standards evaluation and the Atlas. The fission cross section of JEFF-3.3 differs by 1.5 standard uncertainty from the one in the 2018 standards evaluation.

^{239}Pu unresolved resonance range The URR for n + ^{239}Pu in JEFF-3.3 covers incident neutron energies from 4 to 30 keV. The n + ^{239}Pu average cross sections in the URR were adapted to match the new analysis in the resolved resonance range and in the fast range (Sect. 2.1.4). To generate fluctuations necessary for self-shielding calculations the average resonance parameters for n + ^{239}Pu in JEFF-3.3 are those of JEFF-3.1.1 [3].

The average total cross sections and those for neutron induced fission and capture in JEFF-3.3 and JEFF-3.1.1 are compared in Fig. 7. Also shown are the ENDF/B-VIII.0 and JENDL-4.0u evaluations and for the fission cross section the result from the IAEA standards evaluation. JEFF-3.3 differs from the standards evaluation by a small amount (few %) that is well within the fluctuations in this region, as partly evidenced by the ENDF/B-VIII.0 result. JENDL-4u shows similar differences.

The average fission cross section in JEFF-3.3 and the one recommended in IAEA 2009 and 2018 standard [27,40] are listed in Table 8 for the range below 4 keV (resolved range). The differences vary between less than 1 and up to 8 standard uncertainties. Deviations greater than two standard deviations occur for the energy groups of 300–400, 600–700, 700–800, 800–900 and 1000–4000 eV.

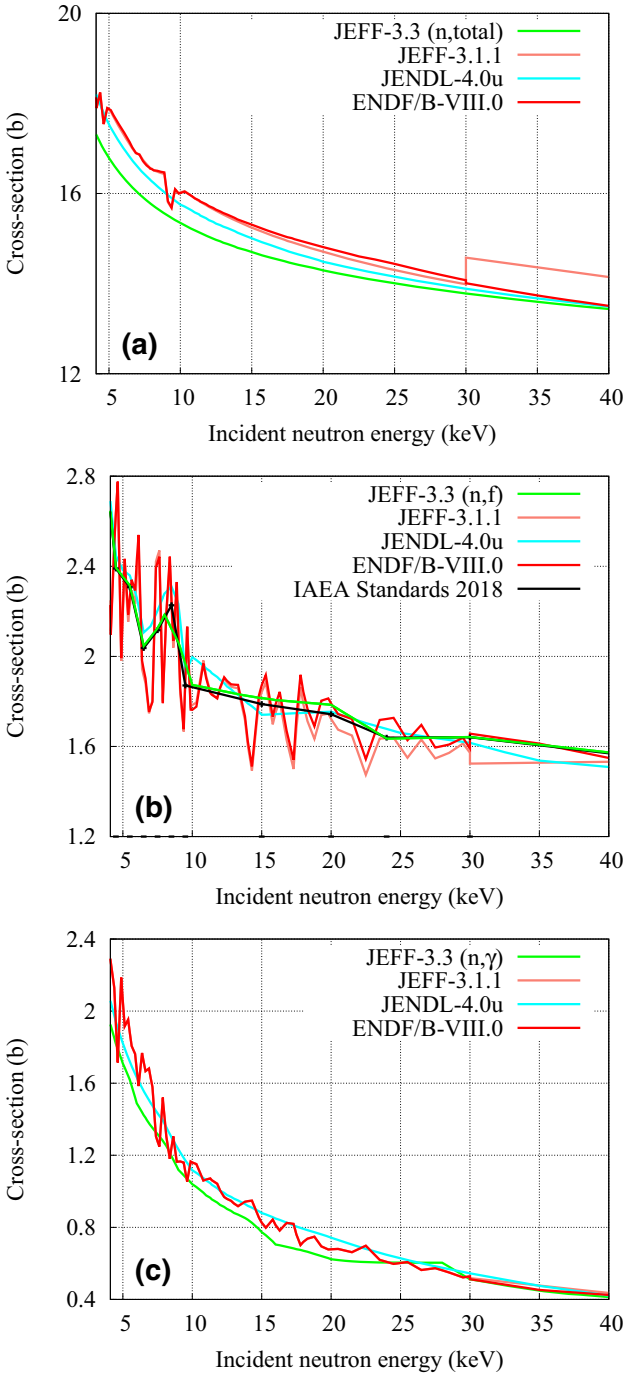

Fig. 7 Unresolved resonance range cross sections for ^{239}Pu total (**a**), fission (**b**) and capture (**c**), with comparisons between JEFF-3.3, JEFF-3.1.1, ENDF/B-VIII.0, JENDL-4.0u and the IAEA 2018 Standards Reference Cross Section

2.1.4 Major actinides beyond a few keV

For incident neutron energies above the URR, that is, beyond a few tens or hundreds of keV, the evaluation for the neutron transport library of the major actinides is performed within the statistical model framework for the continuum region. Results of this evaluation are also used as input for the evaluation process in the URR.

For modeling nuclear reaction cross sections and light particle emission in the continuum region, the "Full Model" approach is used, as described in detail in [68,69]. This approach [69] relies on the use of the TALYS code [43] in

Table 8 ^{239}Pu average fission cross section from the SAMMY resonance fit for JEFF-3.3. The energy-range for the fit is given in column E_n. The standard evaluations are from Refs. [27,40]

E_n (eV)	Standard		JEFF-3.3(b)
	2009 (b)	2018 (b)	
100–200	18.74(11)	18.71(9)	18.55
200–300	18.00(12)	17.86(9)	17.83
300–400	8.56(6)	8.56(5)	8.31
400–500	9.59(6)	9.57(5)	9.56
500–600	15.57(10)	15.49(8)	15.50
600–700	4.53(3)	4.52(3)	4.29
700–800	5.68(4)	5.65(3)	5.51
800–900	5.04(3)	5.04(3)	4.86
900–1000	8.39(6)	8.39(5)	8.50
1000–4000	4.51(3)	4.52(3)	4.37

which the main nuclear reaction models, the optical model for direct interaction mechanisms, the statistical model for compound nucleus decay and pre-equilibrium models are implemented in combination with nuclear structure models and databases. An important source of parameters for TALYS is the IAEA Reference Input Parameter Library (RIPL) [70]. For prompt fission neutron multiplicities and spectra, a modified version of the Madland–Nix model [71] is employed (Sect. 2.1.5).

The optical model is of major importance for the evaluation in the continuum region. It provides the total, elastic and reaction cross sections, as well as transmission coefficients. Together with nuclear level densities, transmission coefficients are the main ingredients of the statistical Hauser–Feshbach model. They distribute the compound nucleus formation cross section into the different open channels at a given neutron incident energy. In the current approach an actinides-specific optical model has been adjusted both for proton and neutron induced reactions using all available experimental data. Since actinides are deformed targets, the coupled channel approach was used, selecting a large enough number of coupled levels to saturate coupling. This saturation is defined by the convergence of the reaction cross section. In practice, levels of the ground state band and of vibrational quadrupole and octupole rotational bands have been coupled. A total of 7, 19 and 9 levels have been coupled for ^{235}U, ^{238}U and ^{239}Pu respectively. As can be observed in Fig. 8, total cross sections have slightly changed from JEFF-3.1.2 to JEFF-3.3, in particular for ^{235}U and ^{239}Pu. The difference between JEFF-3.2 and JEFF-3.3 for ^{238}U is almost negligible.

We note that for the present evaluation the effect of the Engelbrecht–Weidenmüller transformation on the width fluctuation factor in the case of coupled channels calculations was not taken into account. This well-known effect was clarified recently by Kawano et al. [73], but is not widely used, yet. For instance, it leads to an increase of the inelastic scattering cross section by several percent. This may lead to some of the differences between evaluations (see total and inelastic cross sections in Figs. 8 and 9), although these use different optical potentials that already imply differences.

Once optical models are fixed, fission barrier heights and widths, nuclear level densities and gamma ray strength functions were adjusted by simultaneously fitting all available experimental data. The most important data are the total inelastic cross section, the capture cross section and the fission cross section. Evaluated total cross sections and cross sections for some reaction channels that play a key role in neutron transport simulations, i.e. (n,f), (n,γ), (n,n'), are compared with experimental data in Figs. 8 and 9.

An important feature of the "Full model" approach is the coherent analysis of all available data for a given nuclide. This means, for instance, that the set of parameters used to describe photo-fission of ^{238}U is also used for the second chance fission of neutron induced fission of ^{238}U since, in both cases, the same compound nucleus is involved. The price to pay is a more tedious parameter adjustment. The added value of this larger number of constraints is a much better consistency, ensuring a better confidence in model calculations.

The calculated fission cross sections were substituted by those taken from the 2009 IAEA neutron standards project [27]. This choice can be observed in Fig. 8, which illustrates that below a few tens of keV, the evaluation shows sharp oscillations which can hardly be described by a pure model calculation. A comparison between different evaluation libraries reveals that the JEFF-3.3 evaluation is globally closer to the ENDF/B-VIII.0 than the JENDL-4.0 evaluation.

Often microscopic experimental data do not provide enough constraints to obtain satisfactory evaluations from the user point of view. This can be compensated by including results of integral experiments in the evaluation process, as long as the original differential constraints are also respected, as illustrated by the data in Figs. 10 and 11. Figure 10 shows the fission cross section σ_f and average total number of prompt fission neutrons $\bar{\nu}_p$ as a function of incident neutron energy. Experimental data are compared with the values recommended in JEFF-3.3 together with a reduction of 0.15% in the recommended σ_f and an increase of 1% in the recommended $\bar{\nu}_p$. Figure 10 shows that such changes produce recommended data that are within uncertainties in agreement with experimental microscopic data. Combining the variations in σ_f and $\bar{\nu}_p$ simultaneously provides results (blue dots in Fig. 11) that are again very close to those obtained with the JEFF-3.3 evaluation (red dots in Fig. 11). This confirms the study performed in Ref. [74], where strong correlations between the fission cross sections, prompt neutron multiplicities and prompt fission neutron spectra are created when results

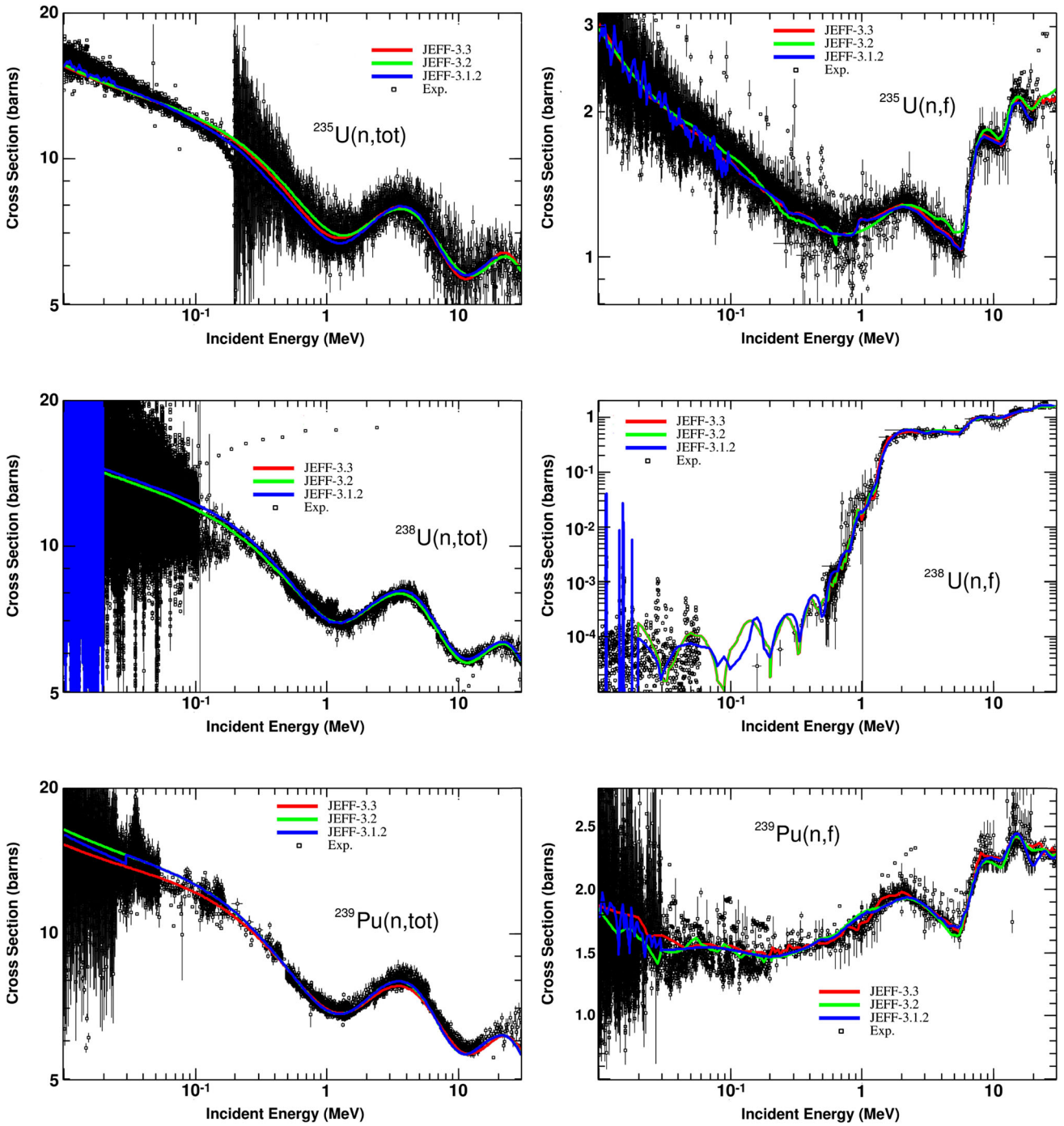

Fig. 8 Comparison between experimental data and the last 3 versions of the JEFF library for ^{235}U (top), ^{238}U (middle) and ^{239}Pu (bottom) total (left) and fission (right) cross sections as function of the incident neutron energy

of integral benchmarks are used in the adjustment process.

In the current evaluation, it is important to mention that the use of standard fission cross sections has removed the possibility of adjusting the fission cross section. Therefore, the average prompt fission neutron multiplicity was adjusted to account for integral benchmark data. The adjustement involved an iterative procedure to achieve an overall good agreement with various benchmarks sensitive both to low and high energy multiplicities. Depending on the results obtained with respect to the selected benchmarks, a small re-normalisation was applied to the prompt neutron multiplicities with typical changes of the order of a few tenths of a percent. The delayed neutron multiplicity was of course not modified. This small adjustment is clearly not the same for each incident neutron energy since each benchmark has its

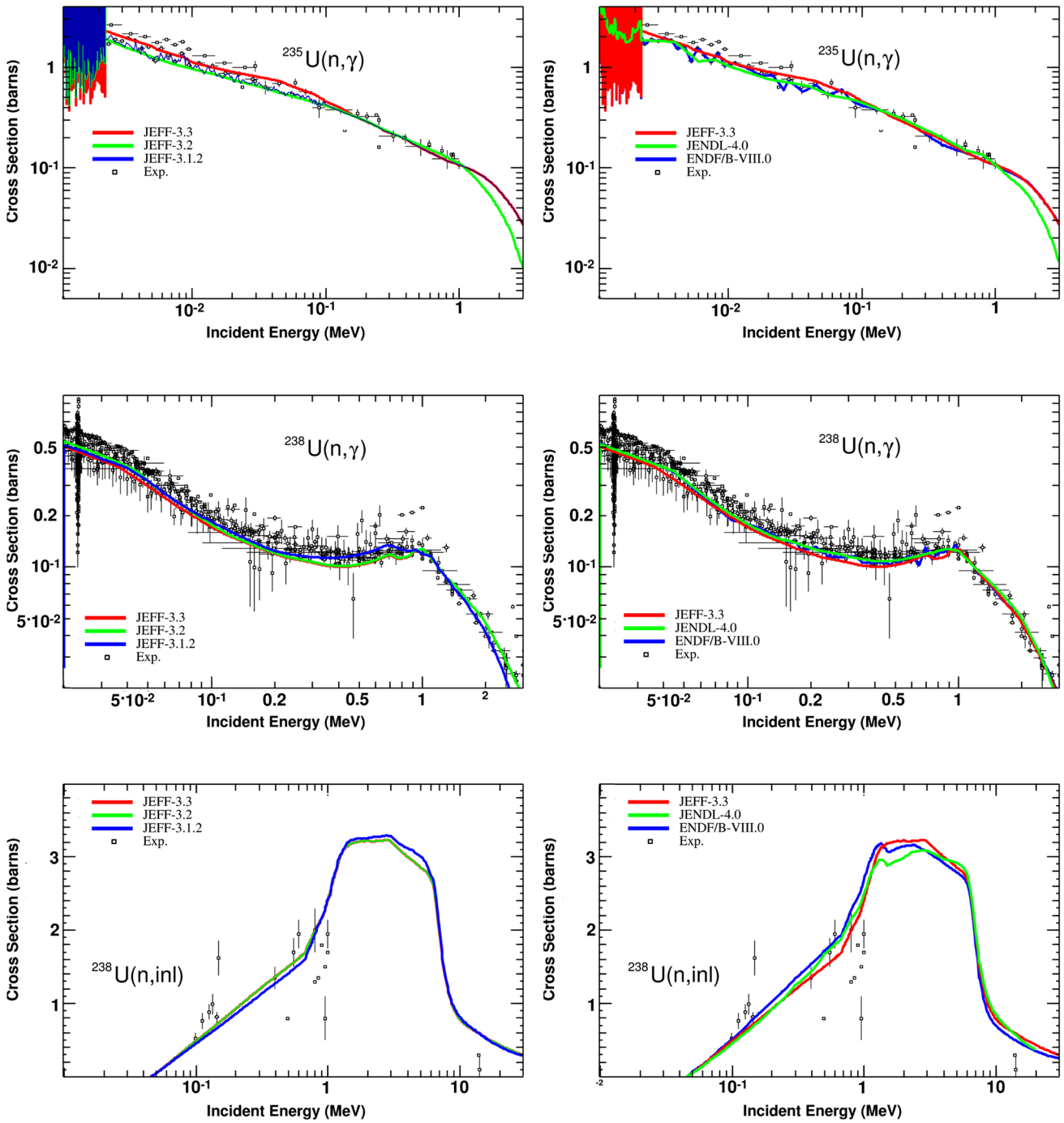

Fig. 9 Comparison between experimental data and the last three versions of the JEFF library (left) and with other evaluations (right) for the ^{235}U capture cross section (top), ^{238}U capture (middle) and ^{238}U inelastic (bottom) cross sections as function of the incident neutron energy

own neutron spectrum sensitivity, but the final multiplicity remains compatible with the experimental uncertainties as shown in Fig. 10.

2.1.5 Prompt fission neutrons

Actinide evaluations require mean prompt fission neutron multiplicities $\bar{\nu_p}$ and prompt fission neutron spectra χ_ν (PFNS). While the most satisfactory approach would consist in computing these spectra from each fission fragment decay, we adopted a more pragmatic and simple approach, the so-called "Los Alamos" or "Madland–Nix" model, which is extensively described in [71,78]. With this model, the PFNS are calculated from the decay of two average fragments, a light and heavy one and $\bar{\nu}$ is then deduced from an energy average involving the mean neutron energy of the

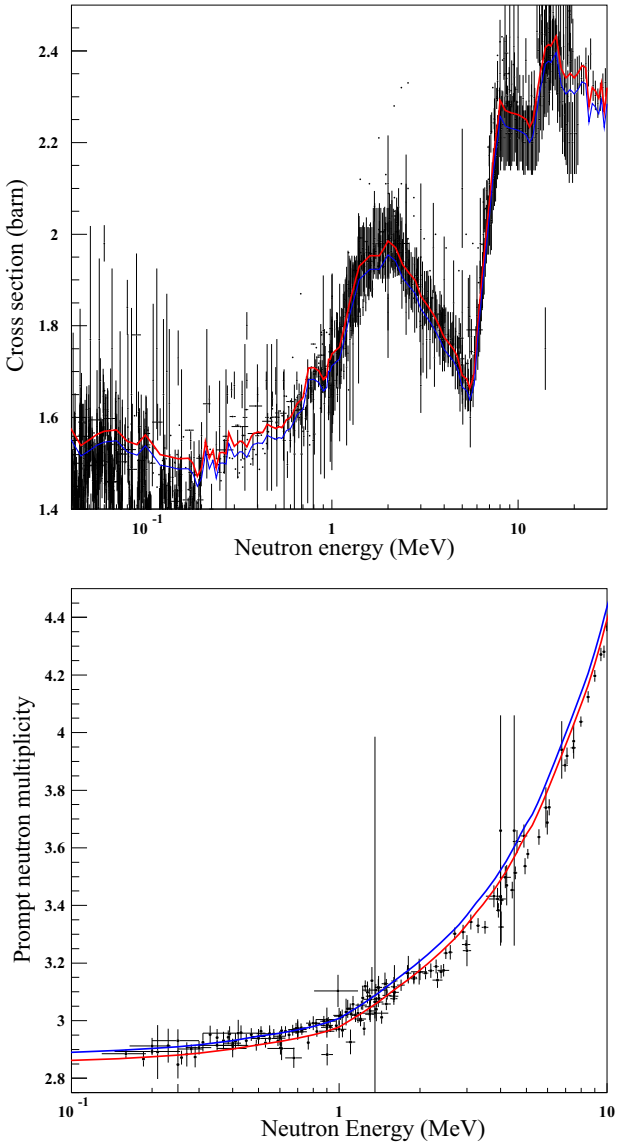

Fig. 10 ^{239}Pu fission cross section (top) and prompt neutron multiplicit $\bar{\nu}$ (bottom) as function of the incident neutron energy. The red curves correspond to the JEFF-3.3 evaluation and the blue curves to a reduction of 0.15% for the fission cross section (top) and an increase of 1% of $\bar{\nu}$ (bottom) of the JEFF-3.3 evaluation

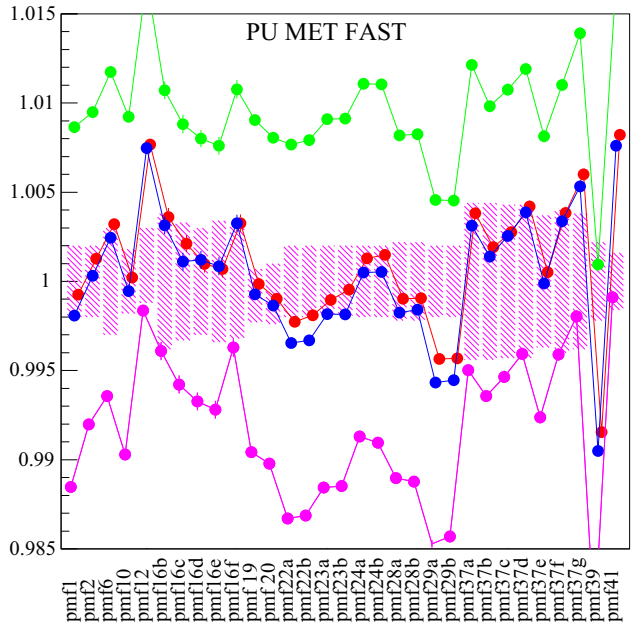

Fig. 11 Neutron multiplication factors (vertical) of ICSBEP Pu fast metallic critical assemblies [23]. Comparisons between experiments and simulations performed using MCNP5 [72] with several choices for the ^{239}Pu evaluations. The red dots correspond to the results obtained with the JEFF-3.3 library. The green dots are obtained increasing by 1% the $\bar{\nu}$ of ^{239}Pu in the JEFF-3.3 library. The pink dots are obtained decreasing by 0.15% the ^{239}Pu fission cross section in the JEFF-3.3 library. The blue dots are obtained by simultaneously increasing $\bar{\nu}$ by 1% and decreasing by 0.15% the fission cross section in the ^{239}Pu evaluation of the JEFF-3.3 library

modelled PFNS. The model parameters are those extracted from the systematics of Tudora [79] with a slight modification for some of them, in order to have a better agreement with experimental data. With increasing incident neutron energy, multiple fission channels open up and partial fission cross sections corresponding to each fission channel must also be accounted for to produce the final PFNS and $\bar{\nu}$. The latter are taken from the modeling of the continuum cross sections mentioned above. Moreover, whereas in the original work of Madland and Nix, the evaporation spectrum due to neutron emission prior to fission was obtained from a Weisskopf spectrum, in the current approach, this contribution was extracted from the aforementioned continuum cross section modeling, as done by Maslov [80].

As one of the difficulties is to account for the strong fission neutron energy dependence of the PFNS, an approach relying only on experimental data is not possible and was therefor not adopted JEFF-3.3. This is illustrated by the ratio of the experimental data to a reference Maxwellian. In Fig. 12, the ratio of the PFNS to a Maxwellian is shown for four different incident neutron energies inducing fission on ^{235}U. By default, in the Los Alamos model, the light and heavy fragment spectra (pink and blue curve) are averaged to produce the total PFNS. As can be observed, the shape of the calculated curve is rather different from the experimental one. The calculated spectrum is too hard and disagrees with the experiments below 500 keV and above 1.5 MeV. A simple way to get softer prompt fission neutron spectra is to assign a different weight to the light and heavy fragments spectra. This has been done for ^{239}Pu(n,f) and ^{235}U(n,f) in order to improve the agreement with experimental data. These predictions are shown in Fig. 12. More precisely, for the first chance fission of n + ^{235}U and n + ^{239}Pu we weighted the light spectrum with a 0.7 factor and the heavy spectrum with a factor of 1.3. For second and higher chance fission, the weights are set to 0.75 and 1.25, respectively. Even if clear differences remain,

the agreement with the data is much better than expected when one sees the two component spectra of the light and heavy fragments.

Using the aforementioned weighting factors, the mean prompt fission neutron energy can be computed as a function of the energy of the neutron inducing fission. The resulting predictions are compared in Fig. 13 with experimental data and with other libraries. It can be noticed that, for ^{235}U and ^{239}Pu neutron induced fission, the mean prompt fission neutron energies are reduced compared to JEFF-3.2 and JEFF-3.3. For ^{239}Pu(n,f), differences between libraries are larger than the differences for ^{235}U(n,f) and ^{238}U(n,f). However, these differences are small compared to the scatter and uncertainty of the experimental data (Fig. 14) so that all recommended values for $\bar{\nu}_p$ are consistent with the experimental microscopic data.

At the time the JEFF-3.3 prompt fission neutron spectra and nu-bar evaluations were completed, the results of a new campaign at the Los Alamos Chi–Nu setup carried out for ^{239}Pu were not yet available. The preliminary results obtained by a collaboration led by CEA show that the n + ^{239}Pu are in similarly good agreement with the JEFF-3.3 evaluation. Tests were also made for the fast criticals of the Mosteller suite replacing the JEFF-3.3 PFNS with that of this experimental campaign above 1 MeV incident neutron energy. The resulting effective multiplication factor was in similar agreement with the benchmarks as the JEFF-3.3 evaluation. As these results are preliminary, details will be published elsewhere. A second campaign at Chi–Nu by the same collaboration is planned for n + ^{235}U.

2.1.6 ^{241}Am in the resonance range

For n+^{241}Am the JEFF-3.2 library with some minor changes was adopted in JEFF-3.3. The RRR covers an energy region between 0 to 150 eV and the URR a region from 150 eV to 40 keV. For energies above 40 keV the evaluation produced for JEFF-3.2 was maintained applying the principles described in Sect. 2.1.4. This resulted in an excellent description of the ^{241}Am(n,2n) cross section [81].

The re-evaluation of the resolved and unresolved resonance ranges was triggered by an overestimation of the k_{eff} values for MOX fuels identified with Monte-Carlo (TRIPOLI-4® [53]) and deterministic (APOLLO2 [82]) calculations based on JEFF-3.1.1. The overestimation becomes sizeable with plutonium ageing, reaching a reactivity change of $\Delta\rho \simeq +700$ pcm for integral measurements carried out with MOX fuel containing a large amount of americium (see also below).

The evaluation in the resolved and unresolved resonance ranges for n + ^{241}Am is the result of a collaboration between JRC-Geel and CEA Cadarache. A detailed explanation of the evaluation work and the benchmark results can be found in Refs. [83,84]. Resonance parameters for n + ^{241}Am were derived by adjusting them in a least squares fit to experimental data that are reported in the EXFOR library together with the transmission and capture data obtained by Lampoudis et al. [85] at the GELINA facility. From a simultaneous analysis of the data sets, listed in Table 9, energies and partial widths of 211 resonances ($l = 0$) up to 150 eV were determined. The REFIT code [59] was used for the analysis.

In the analysis, the transmission data of Lampoudis et al. [85] were considered as a reference. They were obtained from measurements at a 26.45 m station of GELINA with a homogeneous sample prepared by the sol-gel method. The sample, with an areal density of $n = 2.068(10) \times 10^{-4}$ at/b, was especially designed to derive accurate parameters for the strong s-wave resonances at 0.306, 0.574 and 1.270 eV.

The transmission data of Derrien and Lucas [88] were obtained from measurements at 17.9 m and 53.4 m stations using three AmO_2 powder samples with different areal density, i.e. 0.18, 0.63 and 1.87 g/cm^2. The results of the three data sets were merged into one single experimental total cross section from 0.8 eV to 1 keV so that the individual transmission factors are not reported in EXFOR. As noted in Ref. [62], parameters of strong resonances derived from measurements with powder samples will be biased, unless their particle size distributions are taken into account in the analysis. Unfortunately, not enough detail is provided to account for the particle size distribution by the procedure that has been implemented in REFIT [90,91]. To reduce bias effects due to the sample properties an average areal density was determined from a fit to the data. In addition, transmission data involving the strong resonances with energies below 8 eV were not included in the fit.

Since the neutron widths for most of the low energy resonances are much smaller than their radiation widths, the neutron widths derived from the transmission data of Lampoudis et al. were used to normalize the capture yields of Refs. [85–87]. The capture data of Lampoudis et al. [85] were obtained from experiments with a detection system consisting of two C_6D_6 detectors using the same sample as the one used for the transmission measurements. The energy dependence of the neutron fluence was derived in parallel from measurements with a detector placed one meter before the sample. The detector consisted of two ionisation chambers with a common cathode loaded with two layers of ^{10}B. Fixed background filters were used to reduce bias effects due to the background corrections. Given the low amount of ^{241}Am in the sample the impact of the neutron flux attenuation in the sample was negligible and no correction due to the attenuation of the neutron beam was required.

Van Praet et al. [87] derived a capture yield from measurements with C_6D_6 detectors at a 8.6 m station of GELINA. The energy distribution of the neutron fluence was measured with a B_4C disc at the place of the capture sample.

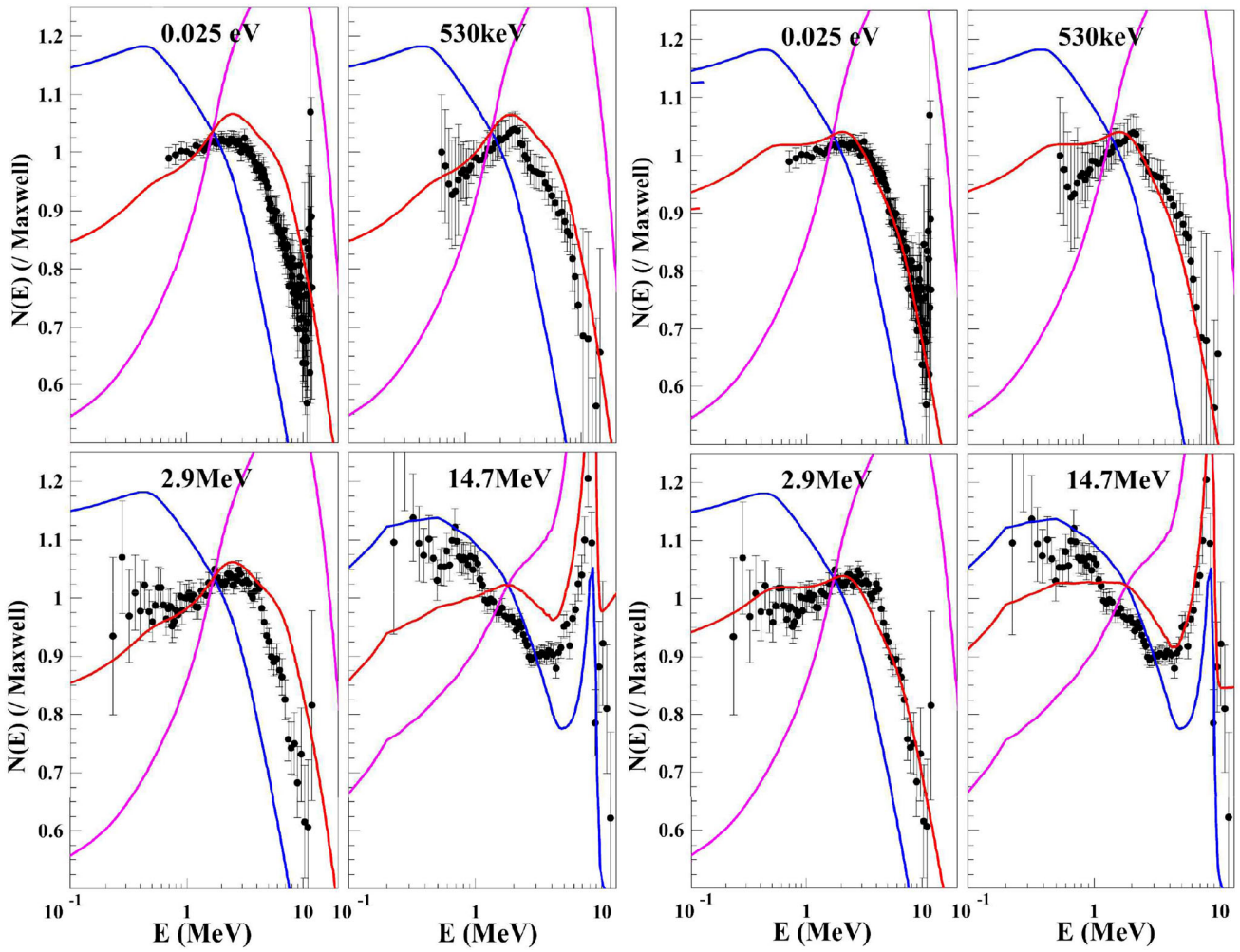

Fig. 12 PFNS for n + ^{235}U as function of the energy of the outgoing neutron for 4 incident neutron energies (from 0.025eV up to 14.7 MeV). The pink (blue) curve shows the neutron spectrum of the light (heavy) fragment and the red curve shows the total PFNS. The data for 0.025 eV are from Ref. [75], those for 530 keV from Ref. [76] and those for 2.9 and 14.7 MeV from Ref. [77]. The two leftmost columns show the total PFNS according to the Madland–Nix weighting of the light and heavy fragment spectra, while the rightmost columns display the PFNS with the weights of the JEFF-3.3 evaluation

Although a relatively thick metallic ^{241}Am sample (areal density of 1.063×10^{-3} at/b) was used, no special procedure was applied to correct for the neutron attenuation and related gamma-ray transport in the sample.

The capture yield of Jandel et al. [86] resulted from measurements at LANSCE with a 4π total absorption detector placed at 20.2 m from the neutron producing target. A thin ^{241}Am sample, prepared by electroplating was used.

Figure 15 shows the result of an adjustment with REFIT. The theoretical and experimental capture yield and transmission obtained at the JRC-Geel facility are compared. Compared to JEFF-3.1.1 the new evaluation results in an increase of the capture cross section at thermal energy and the capture resonance integral by 15% and 20%, respectively, while the fission resonance integral is decreased by 14% (Table 10).

The average resonance parameters of interest for a partial wave breakdown of the neutron cross sections in the resonance region are the mean level spacing, the neutron strength function and the average radiation and fission widths. Parameters for s-wave levels were determined from a statistical analysis of the resolved resonance parameters. For higher values of angular momentum $\ell > 0$, average resonance parameters are obtained from systematics and by means of optical and statistical model calculations.

For 14 resonances, both the neutron and radiation width were determined. From these data an average radiation width was derived (Table 10).

This average value is in good agreement with the average value reported by Derrien and Lucas [88] and Lampoudis et al. [85]. The ESTIMA method [52] was used to determine simultaneously the most probable neutron strength function

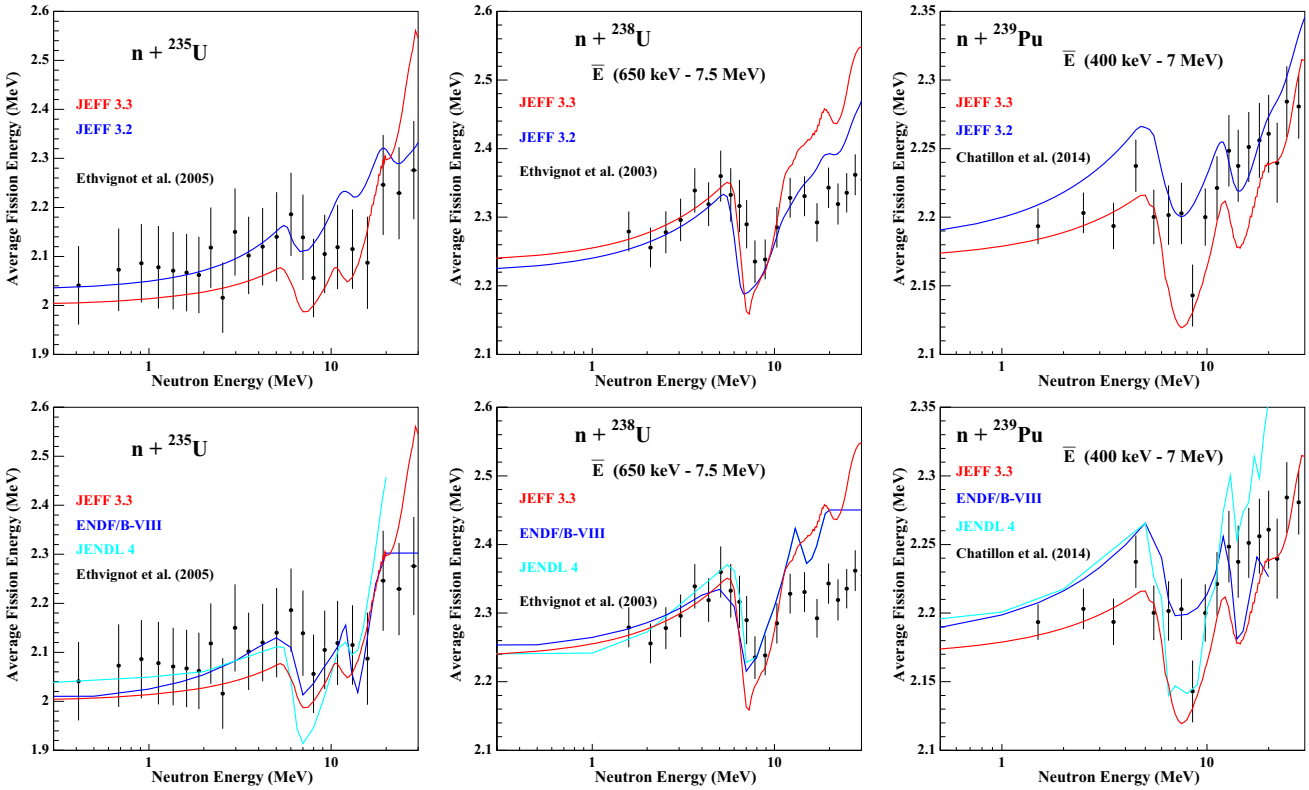

Fig. 13 Mean prompt fission neutron energy as a function of the energy of the neutron inducing fission for $n+^{235}U$ (left), $n+^{238}U$ (middle) and $n+^{239}Pu$ (right). Comparisons are made with experimental data, with JEFF-3.2 (top) and other libraries (bottom). For $n+^{238}U$ and $n+^{239}Pu$ the mean energy is calculated over the range of prompt fission neutron energies measured by the mentioned experiment (The values in brackets following the label $\bar{E}$)

S_0 and mean level spacing D_0 for s-wave levels from the properties of the cumulative Porter–Thomas distribution of reduced neutron widths [92]. Such a procedure also accounts for the number of missing levels. In the present analysis, we obtain for the neutron width

$$\langle \Gamma^0_{nJ} \rangle = 6.03(70) \times 10^{-5}\ \text{eV}.$$

The neutron strength function S_0 is derived from the ratio of the reduced neutron width $\langle \Gamma^0_{nJ} \rangle$ to the mean level spacing D_0. The uncertainty of S_0 is obtained from the quadratic sum of the variances of D_0 and $\langle \Gamma^0_{nJ} \rangle$ (Table 10).

ECIS calculations were performed on the basis of the rigid rotor model using the optical model established by Soukhovitskii [95] and ^{241}Am file of the JENDL neutron library. As proposed in Ref. [96], five ground-state rotational band levels ($5/2^-$, $7/2^-$, $9/2^-$, $11/2^-$ and $13/2^-$) were included in the coupled-channel calculations. The deformation parameter β_2 was slightly optimised to improve the agreement with the S_0 value established with the ESTIMA method. Uncertainties and correlation matrix for the optical model parameters of interest for this work (geometrical parameters, depth of the potentials and deformation parameters) were determined by propagating the uncertainties of the experimental total cross section of Philips and Howe [93] and the s-wave neutron strength function provided by ESTIMA, using the conventional uncertainty propagation applied in least squares adjustments. In Fig. 16, the total cross section calculated with ECIS is compared with the EXFOR data.

In the unresolved resonance range, the ^{241}Am(n, γ) reaction was calculated with the TALYS code [43], in which the partial cross sections are calculated by means of the Hauser–Feshbach formula with width fluctuation correction factor using Moldauer's prescription. The ^{241}Am capture cross section calculated with the TALYS code by using the mean level spacing $D_0 = 0.6$ eV and the average radiation width $\langle \Gamma_{\gamma_0} \rangle = 43.3$ meV is compared in Fig. 16 with data available in the EXFOR data base. The option within TALYS to run unresolved resonance calculation was then used to automatically generate the average resonance parameters in ENDF-6 format.

To account for the uncertainties of systematic effects the Monte Carlo procedure proposed by De Saint Jean [97] was applied. This procedure was used to propagate the uncertainties of the equivalent distance ($\Delta L = 1$ cm), time offset ($\Delta t_0 = 1$ ns), sample temperature ($\Delta T = 5$ K), the normalizaton factors and areal densities. The resulting relative

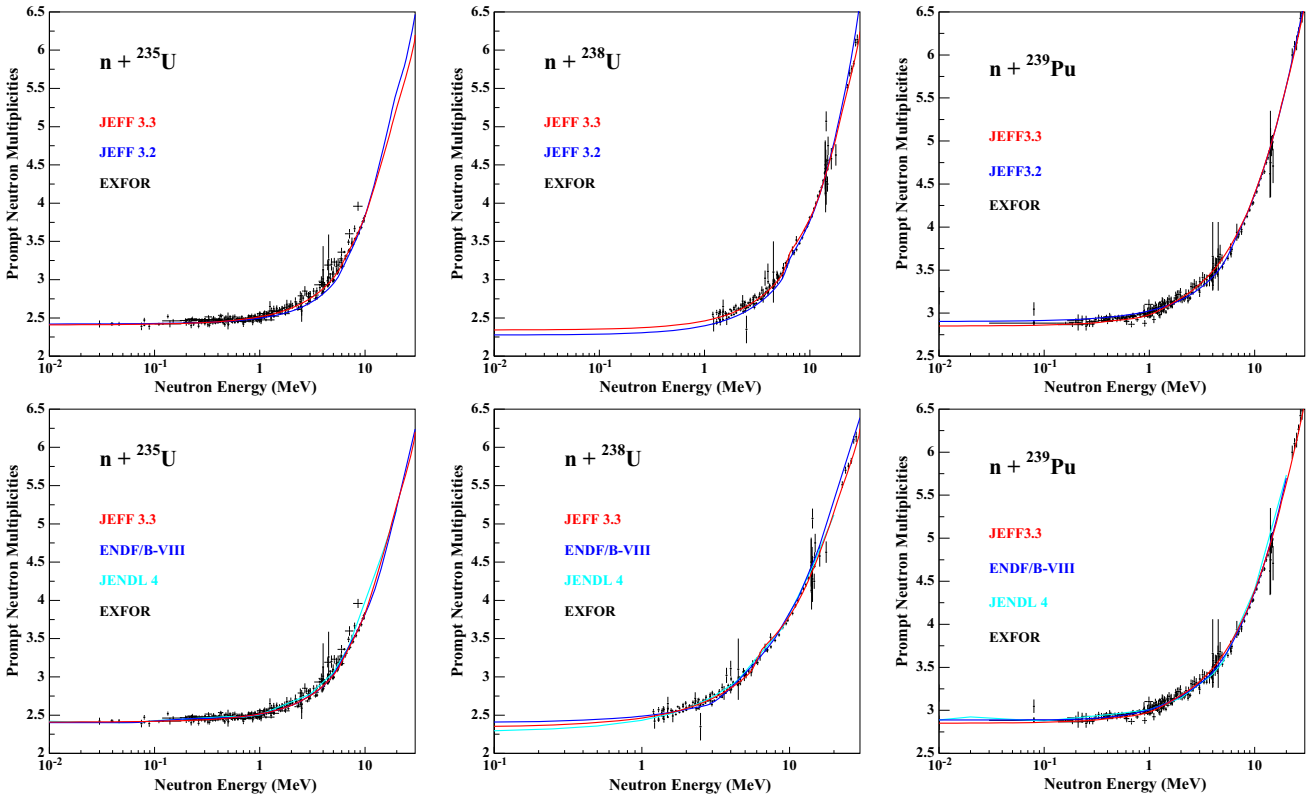

Fig. 14 Prompt neutron multiplicity $\bar{\nu}_p$ as a function of the energy of the neutron inducing fission for n + ^{235}U (left), n + ^{238}U (middle) and n + ^{239}Pu (right). Comparisons are made with experimental data and with JEFF-3.2 (top) and other libraries (bottom)

Table 9 List of capture, fission and transmission data used in the evaluation for n + ^{241}Am in the resolved resonance range

Author	Year	References	Facility	Data type
Jandel	2008	[86]	DANCE	Capture yield
Van Praet	1986	[87]	GELINA	Capture yield
Lampoudis	2013	[85]	GELINA	Capture yield
				Transmission
Derrien	1975	[88]	Saclay	Transmission
			LINAC	Fission
Dabbs	1983	[89]	ORELA	Fission

uncertainties and correlations on the capture cross section calculated over a broad energy mesh (15 groups) are shown in Fig. 17.

To understand the impact of the new evaluation, the above mentioned integral experiments performed at the zero power reactor EOLE in Cadarache were revisited. Material buckling B_m^2 was analysed with APOLLO2 and k_{eff} measurements with TRIPOLI-4® (Fig. 17). As the JEFF-3.2 and JEFF-3.3 evaluations for n + ^{241}Am are the same the conclusions are valid for both (see also Sect. 3.1.6). The results are shown as a function of plutonium ageing from MH1.2 (no ageing) to MISTRAL-2, -3 and -4 (20 years old Pu for MISTRAL-4). The observed trend confirms the increasing discrepancies with Pu ageing between calculation and experiment. The worst result reaches a maximum close to $\Delta\rho \approx +800$ pcm for the reference configuration of the MISTRAL-4 program carried out in 1999. The Japanese code MVP confirms the k_{eff} estimates. The increase of the ^{241}Am(n, γ) cross section in the new evaluation (+20% compared to JEFF-3.1.1 and the Atlas and 9% compared to ENDF/B-VIII and JENDL-4, see Table 10) improves significantly the reactivity calculations of the MOX configurations over a wide range of moderation ratios. The mean value $\langle\Delta\rho\rangle$ calculated over the five reference configurations of the FUBILA, MH1.2 and MISTRAL-2-3-4 programs is now:

$$\langle\Delta\rho\rangle = 50(180) \text{ pcm}.$$

Resonance parameter uncertainties of ^{241}Am were propagated to k_{eff} [98] and contribute 131 pcm for MISTRAL-2 and 143 pcm for MISTRAL-3, a considerable fraction of the total uncertainty.

2.1.7 Curium

Neutron cross sections for curium isotopes, i.e. $^{240-250}$Cm, were evaluated at KAERI. A more detailed description of this

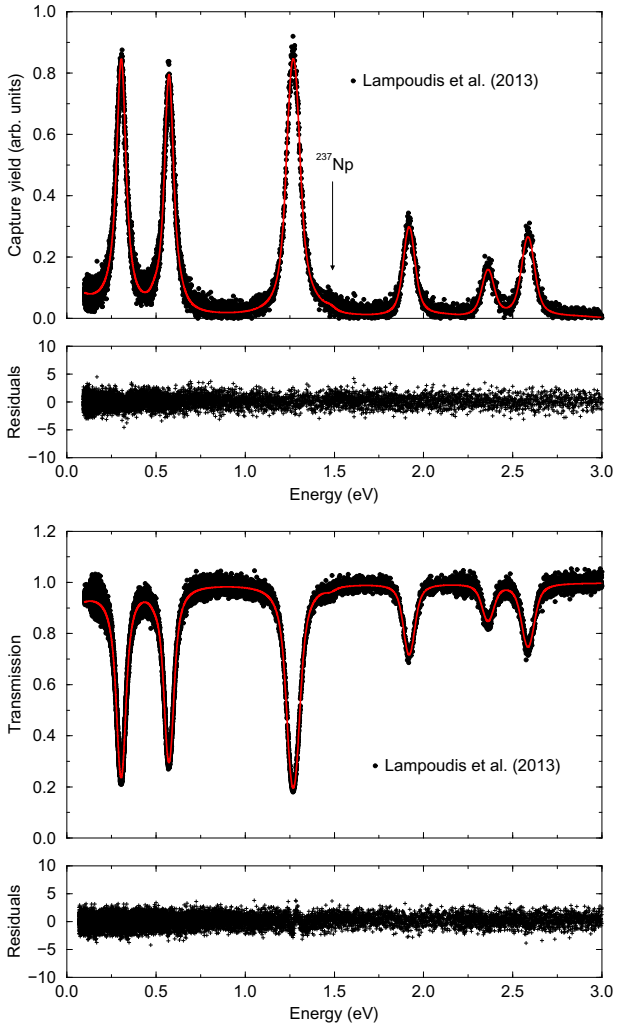

Fig. 15 Comparison of the REFIT curves with experimental capture yield and transmission measured at the JRC-Geel facility for ^{241}Am up to 3 eV

Table 10 ^{241}Am thermal capture cross section, capture (fission) resonance integral and average parameters of JEFF-3.3 compared to ENDF/B-VIII, JENDL-4 and Atlas values

	JEFF-3.3	ENDF/B-VIII.0	JENDL-4	Atlas
σ_γ (b)	748(35)	684	684	587
I_γ (b)	1826(55)	1590	1588	1425
I_f (b)	15.2(5)	15.9	15.0	14.4
$\langle \Gamma_{\gamma_0} \rangle$ (meV)	43.3(11)			45.0
$10^4 S_0$	1.01(12)		1.0	0.9
D_0 (eV)	0.60(10)			0.55

evaluation is given in Refs. [99,100]. The upper boundaries of the RRR and URR, together with the half-lifes and the experimental data that are available in the EXFOR data library, are listed in Table 11. The data in the resonance region were adopted from JENDL-4 [101]. For neutron interactions above

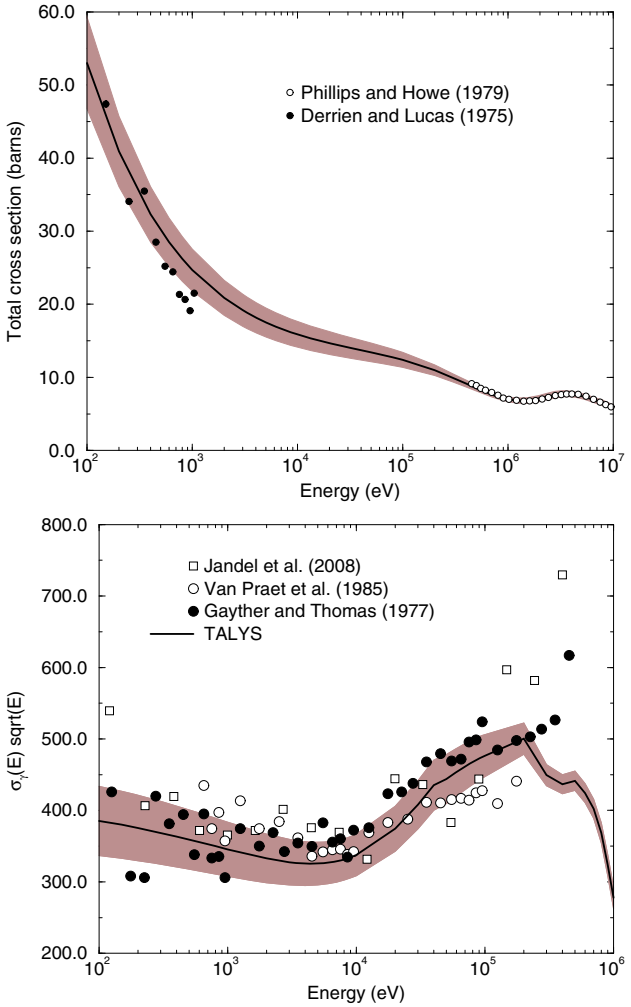

Fig. 16 Top: ^{241}Am total cross section calculated with the ECIS code and compared with EXFOR data [88,93]. Bottom: Comparison of the theoretical ^{241}Am capture cross section (TALYS) with data retrieved from the EXFOR data base [86,87,94] multiplied by the square root of the incident neutron energy

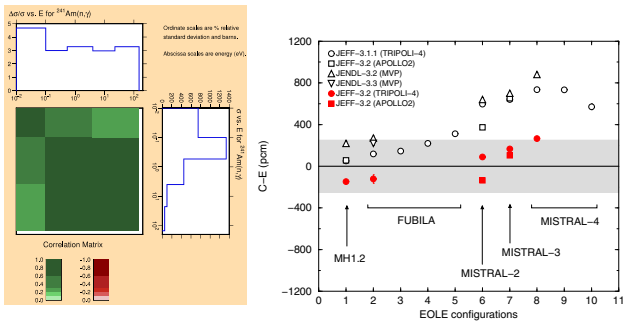

Fig. 17 Top: relative uncertainties and correlation matrix for the ^{241}Am(n, γ) reaction up to 150 eV. Bottom: integral trends obtained with the JEFF-3.1.1, JENDL-3.2 and JEFF-3.2 libraries for material buckling B_m^2 (APOLLO2 calculations) and critical k_{eff} measurements (TRIPOLI-4® and MVP calculations)

Table 11 Experimental data for $^{240-250}$Cm reported in the EXFOR library, together with the half-lives ($T_{1/2}$) and upper energy boundary of the resolved (RRR) and unresolved resonance region (URR). Only fission data (f) are available for $^{242-248}$Cm. The half-lives are from the JEFF-3.3 radioactive decay data file (Sect. 2.8). 1 a(nnus) is 365.242198 d [4]

Isotopes	Data	$T_{1/2}$	RRR (eV)	URR (keV)
^{240}Cm	–	27 (1) d	–	–
^{241}Cm	–	32.8 (2) d	–	–
^{242}Cm	f	162.93 (7) d	275	100
^{243}Cm	f	28.9 (4) a	100	40
^{244}Cm	f	18.0 (1) a	1000	100
^{245}Cm	f	8250 (70) a	100	40
^{246}Cm	f	4730 (150) a	400	140
^{247}Cm	f	$1.60(5) \times 10^7$ a	60	40
^{248}Cm	f	$3.40(4) \times 10^5$ a	1500	200
^{249}Cm	–	64.15 (3) m	–	–
^{250}Cm	–	$8(4) \times 10^3$ a	150	200

the resonance region, evaluated cross section and covariance data were derived from model calculations using the EMPIRE code [102]. Table 11 reveals that experimental data that can be used to adjust the model parameters and to validate the results are rather scarce. In addtion, for ^{240,241,249}Cm, which have a very short half-life, no resolved or average resonance parameters are available. For these isotopes only averaged cross sections derived by the EMPIRE code are given. The lower energy boundaries for these cross sections are at 3.0 eV, 1.1 eV and 3.1 eV for ^{240}Cm, ^{241}Cm and ^{249}Cm, respectively. Given the limited number of experimental data a procedure similar to the one applied for Nd-isotopes was followed [103]. This procedure relies on model parameters, such as the parameters of the optical model potential and the asymptotic value of the level density parameter, that vary smoothly as a function of mass number.

The EMPIRE code calculates cross sections for all relevant reaction channels, angular distributions, exclusive and inclusive particle- and γ-ray emission spectra, double-differential cross sections, and spectra of recoils. Nuclear reaction models in the Empire code can be classified into three major classes: (i) optical model and direct reactions (Coupled-channels (CC) and Distorted-wave Born approximation (DWBA)), (ii) preequilibrium emission, and (iii) Hauser–Feshbach statistical decay. An isospin-dependent coupled-channel optical model potential containing a dispersive term (DCCOMP) as suggested by Capote et al. [104] was used. The model parameters were taken from the RIPL-2 data base [70]. The Empire-specific level density formulas were employed and their parameters adjusted by a fit to known nuclear discrete levels and available experimental data. The gamma strength function proposed by Plujko et al. [105] was

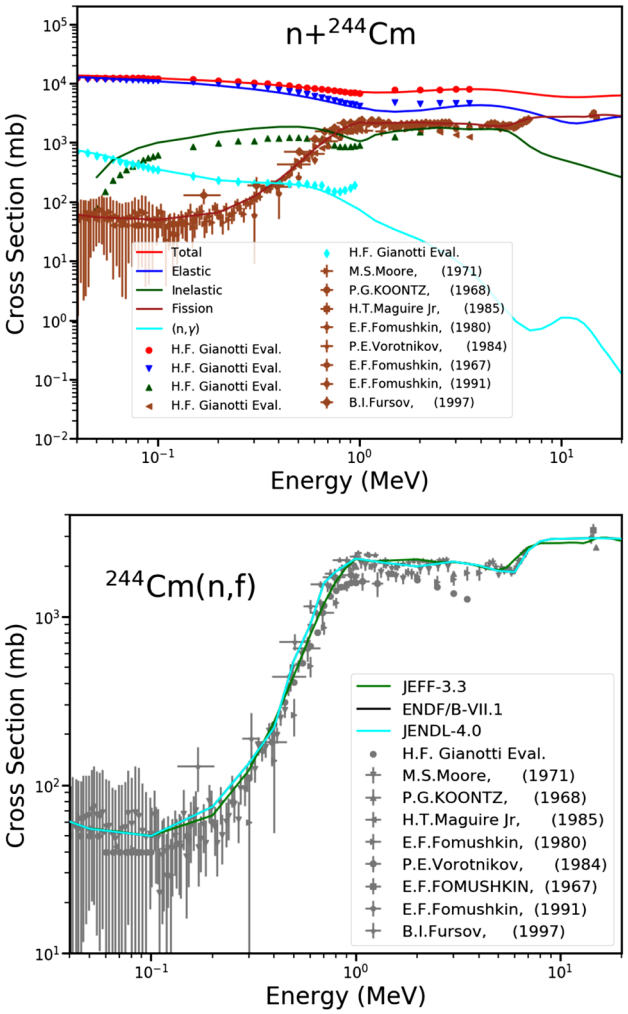

Fig. 18 Top: total, elastic, inelastic, fission and capture cross sections for ^{244}Cm compared to the Gianotti model calculations [106] and the measurements [107–112]. Bottom: fission and capture cross sections for ^{244}Cm compared to the JENDL-4.0 and ENDF/B-VII.1 evaluations, the Gianotti model calculations [106] and the measurements [107–112]

used. Fission cross sections were derived in the WKB approximation supposing a double-humped fission barrier with free parameters that were adjusted to experimental cross section data [99]. Results of the evaluation are illustrated in Figs. 18 and 19. Figure 18 compares the evaluated and experimental total cross section for ^{244}Cm together with those for the capture reaction and elasitic and inelasting scattering. A comparison of the evaluated fission cross section for ^{244}Cm with experimental data reported in the EXFOR library is shown in Fig. 18. The results for the other isotopes are shown in Fig. 19. The total cross section and the cross section for elastic scattering are compared with an evaluation reported by Fernandez Gianotti [106]. Figure 19 also compares the fission cross sections reported in this work with the results of experiments of Refs. [107–112].

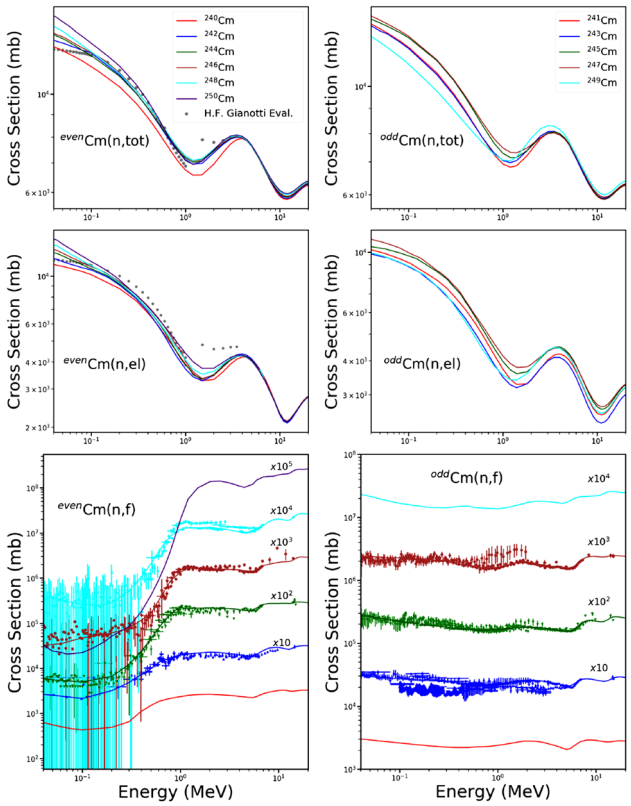

Fig. 19 Total, elastic, and fission cross sections for all Cm isotopes [106–112]

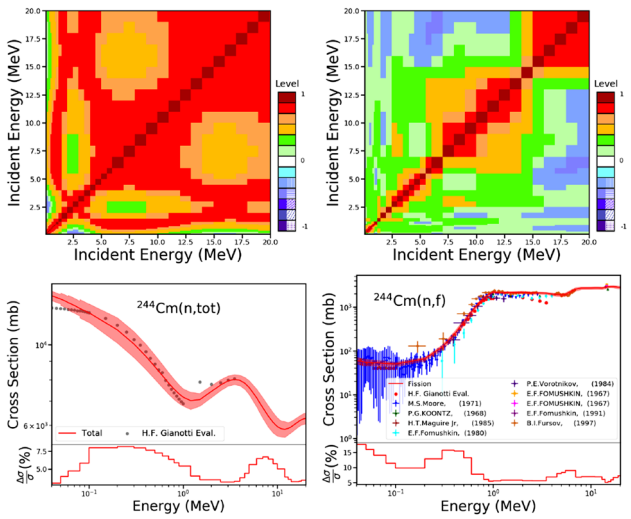

Fig. 20 The correlation of total and fission cross sections for ^{244}Cm and the uncertainties compared to the measurements [106–119]

Covariance data were generated by the Kalman code implemented in the EMPIRE system supposing a 10% uncertainty on the model parameters. These uncertainties were complemented in a Bayesian updating procedure with the experimental fission cross section data listed in Table 11.

Table 12 Some actinide evaluations in JEFF-3.3 adopted from other evaluations

Nuclide	Origin
^{232}Th	IAEA Th/U CRP [120]
^{231,233}Pa	IAEA Th/U CRP [120]
^{232}U	JENDL-4 [101]
^{233,234}U	ENDF/B-VII.1 [121]
^{237}Np	ENDF/B-VII.1 [121]
^{238}Pu	JENDL-4 [101]
^{240}Pu	JEFF-3.1 [2]
^{241,242,244}Pu	JEFF-3.0 [1]
^{242m}Am	JENDL-3.3 [122]
^{243}Am	JENDL-4 [101]

Figure 20 shows the resulting uncertainties for total and fission cross sections together with their correlation matrix.

2.1.8 *Other actinides*

In the previous sections the three major actinides ^{235,238}U and ^{239}Pu and the minor actinides ^{241}Am and $^{240-250}$Cm were presented. Evidently, this does not cover all actinide nuclear data of importance. For instance, the thorium-uranium fuel cycle takes interest in ^{232}Th, ^{233}U and minor actinides such as ^{231,233}Pa and ^{232,234}U. For use of MOX, high level waste management, spent nuclear fuel transport, storage and fuel disposal and in particular transmutation, data are needed for ^{237}Np, $^{238,240-242,244}$Pu, ^{242m,243}Am. For JEFF-3.3 these are either taken from earlier JEFF releases or from other evaluations. Table 12 shows the primary source of the evaluations and the references providing further details.

2.1.9 *Delayed neutrons*

Delayed neutrons (DN) are of great importance for a safe reactor operation. The uncertainty of DN production due to the quality of nuclear data resulted in a strong conservatism in the design and operation of reactor control systems. An international effort has been made by the NEA/WPEC Subgroup 6 to improve the nuclear data that is required to predict the DN production. This resulted in the recommendations for the major actinides that are specified in the Subgroup 6 report [123]. These recommendations, which are based on an 8-group structure with a fixed set of half-lifes, were already adopted in JEFF-3.1.1 and are restored in the official release of JEFF-3.3.

It is a common procedure to sort the approximately 300 delayed-neutron precursors into groups (typically 6 or 8) and to represent their aggregate behavior through group parameters [124]. The most important application of the group con-

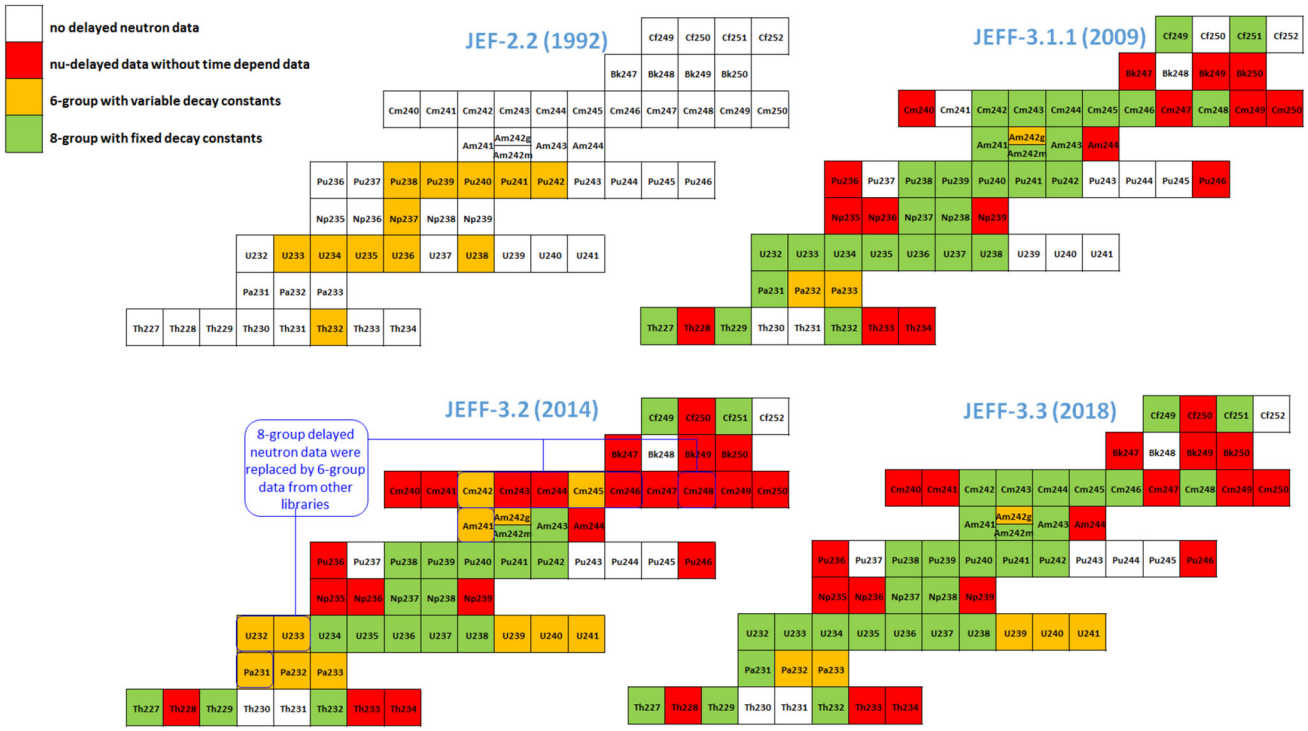

Fig. 21 Evolution of the JEFF library with respect to DN data

stants is the estimation of the reactivity (ρ) from the measurement of the reactor period (T), through the Inhour equation in which the average delayed neutron precursor half-life ($\overline{T_{1/2}}$) plays an important role [125].

The average precursor half-life can be computed by adding up the individual contributions (second expression in Eq. 1) or by using the group approximation (third expression in Eq. 1):

$$\overline{T_{1/2}} = \sum_{i}^{n} \frac{CY_i \; P_{n,i} \; T_{1/2,i}}{\overline{\nu_d}} = \frac{\sum_j^G a_j \; T_{1/2,j}}{\sum_j^G a_j}, \tag{1}$$

where a_j is the abundance of group j and $T_{1/2,j}$ its half-life [124].

Delayed-neutron parameters can be found by either a macroscopic approach, based on experiments carried out on irradiated samples, or by a microscopic approach by investigating the properties (i.e. cumulative fission product yield, half-life, neutron emission probability) of individual neutron precursors. The data from the NEA/WPEC-6 report published in 2002 [123] is based on an 8-group structure. The abundances a_i come from the expansion of a 6-groups data set that Keepin obtained in 1957 through results of an integral measurement [126]. The uncertainties of the 8-group abundances have been estimated to preserve the reactivity uncertainty based on a 6-group estimation [125]. The main feature of the new set is that the group decay-constants are valid for any fissioning system at any incident neutron energy, thus simplifying the modeling of multiple fissioning nuclides. The data recommended by Subgroup 6 were extensively validated for thermal and fast reactors (see Refs. [2,3])

The JEF-2.2 library, released in 1992, only contained delayed-neutron data for the major nuclides, as shown in Fig. 21. Reliable estimates of the β_{eff} for fast reactor systems or for end-of-cycle-conditions could not be made since DN data for Am and Cm isotopes were missing. The time dependence of the DN production was reproduced by the 6-group parameters with a fitted set of decay constants (one set per fissioning nuclide). The effect of the incident neutron energy could not be represented.

The Subgroup 6 recommendations were adopted in JEFF-3.1.1 for most of the U, Np, Pu, Am and Cm isotopes. The data for minor isotopes were taken from other libraries. The incredible effort of delayed neutron data compilation done by the international community led to the marked improvement reflected in JEFF-3.1.1, as seen in Fig. 21.

In JEFF-3.2, which was released in 2014, the neutron transport sublibraries for $^{242-246,248}$Cm, ^{241}Am, ^{232,233}U and ^{231}Pa, including the DN data, were replaced by results of other evaluations. Since no new experimental data was produced or became available after the work of Subgroup 6 there was in principle no justification to replace the DN data. In the process of developing JEFF-3.3, it was demonstrated that for ^{235}U the DN data taken from ENDF/B-VII.0 lead to a wrong evaluation of the average DN precursor's half-life

[127]. In addition, IPEN and SPERT benchmarks both concluded that JEFF-3.1.1 data provides the best C/E agreement on the dynamic reactivity from the Inhour equation, due to the better evaluation of the a_i and λ_i data.

The United States library ENDF/B-VII.1, on the other hand, is still relying on the 6-group a_i and λ_i from the Brady and England fit of the decay-curve computed by a summation method [128].

All the considerations mentioned above motivated the restoration of the 8-group data for ^{227,229,232}Th, ^{231}Pa, $^{232-235}$U, ^{237}Np, ^{238,241}Pu, ^{241,243}Am, $^{242-246,248}$Cm and ^{249}Cf. For nuclides without DN data in JEFF-3.1.1, i.e. ^{250}Cf, ^{241}Cm and $^{239-241}$U, data coming from other libraries were adopted in JEFF-3.3. As the ENDF-6 format cannot handle uncertainties on DN group constants, the information in the Subgroup 6 report for ^{235,238}U and ^{239,241}Pu was summarised in the header of their files.

2.2 Structural materials and coolants

An overview of the origin of evaluations for coolants, moderators, structural and shielding materials is given in Table 13. As indicated in the table, below we describe the evaluations for JEFF-3.2 and JEFF-3.3.

2.2.1 Deuterium

In JEFF-3.2 a new evaluation for n+D reactions was introduced [132]. The elastic and breakup cross sections are computed by solving the three-body Faddeev equations with the semi-realistic MTI-III [133] and the realistic INOY [134] nucleon-nucleon potentials. The n-d reaction is considered as a three particle problem for nucleons interacting via pairwise potentials. The solution has been obtained numerically by means of standard methods used in few-body problems. They are based on a spline expansion of the Faddeev amplitudes which transform the set of partial differential equations into a homogeneous linear system [135].

For JEFF-3.3 the evaluation modifies the JEFF-3.2 evaluation by correcting for masses and Q-values and adding covariances for the total, elastic (n,2n) and (n,γ) reactions. The covariances were based on an analysis of the experimental data. Finally, decay data were added for tritium.

The cross sections calculated with the INOY potential (JEFF-3.3) are compared to the existing experimental data in Figs. 22, 23 and 24. Figure 22 shows the excellent agreement with the very accurate low energy scattering cross section. Similar agreement is obtained by ENDF/B-VIII.0 and JENDL-4u which is hidden by the other two evaluations in the figure. The total cross section data are well described by the three evaluations, as well. Slight differences are observed that are well within the experimental uncerainties. Even if the three evaluations show some dis-

Table 13 Origin of evaluations for structural materials, coolants and moderators in JEFF-3.3

Nuclide	Evaluation
^{1,3}H	ENDF/B-VII.1 [121]
^{2}H	JEFF-3.2, this paper
^{6,7}Li	ENDF/B-VII.1 [121]
^{9}Be	JEFF-3.1, EFF-3.6 [2]
^{nat}C	ENDF/B-VII.1, JEFF-3.2 [121]
^{13}C	TENDL-2015 [5]
^{16}O	ENDF/B-VII.1 [121]
^{17,18}O	TENDL-2015 [5]
^{19}F	ENDF/B-VII, JEFF-3.1.2 [129]
^{23}Na	this paper
^{24,25,26}Mg	JENDL-3.3 [122]
^{27}Al	ENDF/B-VI, this paper
^{28}Si	EFF-3.0
^{29,30}Si	ENDF/B-VII.1 [121]
^{31,32}Si	TENDL-2015 [5]
$^{44,46-50}$Sc	TENDL-2015 [5]
^{50,51}V	TENDL-2015 [5]
$^{50,52-54}$Cr	this paper
^{55}Mn	IAEA [121,130]
^{54,57,58}Fe	JEFF-3.1 [2], JEFF-3.2
^{56}Fe	JEFF-3.2/1, EFF-3.1
^{59}Co	ENDF/B-VI.3 [131]
^{58,60}Ni	EFF-3.1 [1], this work
^{61,64}Ni	ENDF/B-VII.1 [121]
^{62,63}Ni	TENDL-2015 [5]
^{63,65}Cu	this paper
$^{64-70}$Zn	TENDL-2015 [5]
$^{90-92,94,96}$Zr	JEFF-3.2, this paper
^{93}Zr	ENDF/B-VII.1 [121]
^{88,89,95}Zr	TENDL-2015 [5]
^{93}Nb	TENDL-2015 [5]
^{92,94,96,97,98,100}Mo	JENDL-4 [101]
^{95}Mo	ENDF/B-VII.1 [121]
^{180m}Ta	TENDL-2015 [5]
^{181}Ta	JEFF-3.2, this paper
^{180}W	TENDL-2015 [5]
$^{182-184,186}$W	JEFF-3.2, this paper
^{197}Au	this paper
^{196,204}Hg	ENDF/B-VII.1 [121]
$^{198-202}$Hg	TENDL-2015 [5]
^{204}Pb	JEFF-3.1, JEFF-3.2
$^{206-208}$Pb	JENDL-4, this paper
^{209}Bi	JENDL-4, this paper

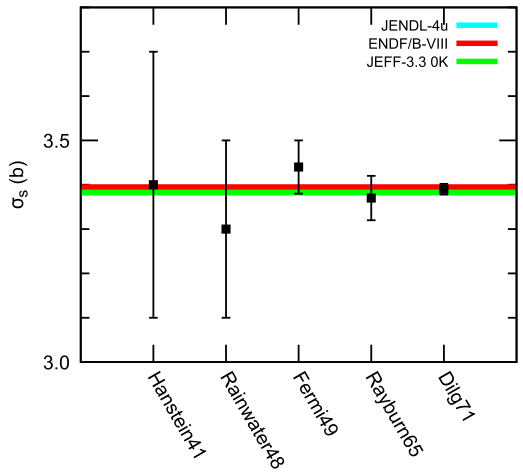

Fig. 22 Low energy cross section for n+D scattering. The weighted average of the experimental data is 3.390(11) b in agreement with the most accurate value obtained by Dilg et al. [136]. The remaining data are from Rayburn et al. [137], Fermi and Marschall [138], Rainwater et al. [139] and Hanstein [140]

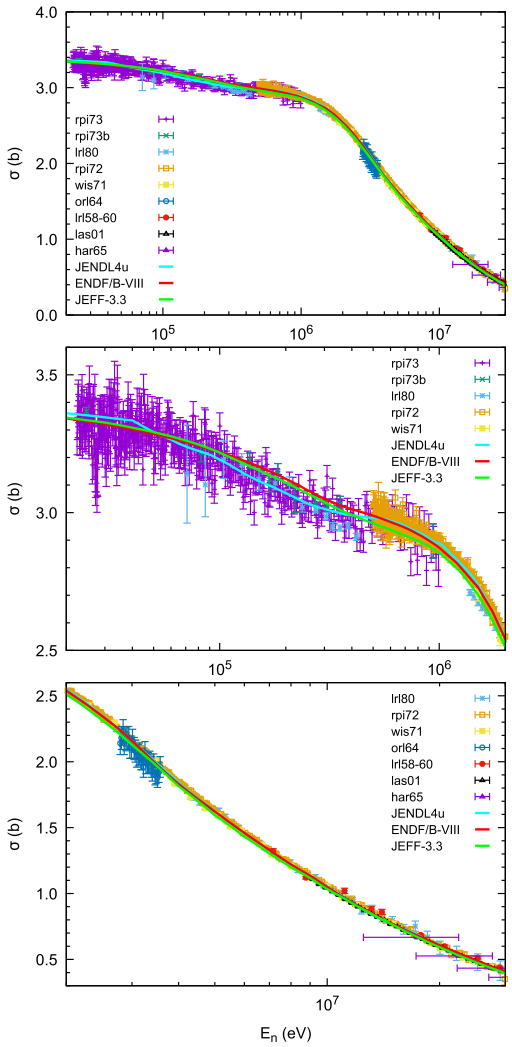

Fig. 23 Total cross section data for n+D scattering compared to JEFF-3.3, ENDF/B-VIII.0 and JENDL-4u for 20 keV to 30 MeV (top), 20 keV to 2 MeV (middle) and 2 MeV to 30 MeV (bottom). The data labels refer to the following references: rpi73(b for filtered beam) [141,142], lrl80 [143], rpi72 [144], wis71 [145], orl64 [146], lrl58-60 [147,148], las01 [149], har65 [150]

tinct weak and different trends there is no conclusive answer as to which is best. At low energy the behaviour of JEFF-3.3 and ENDF/B-VIII.0 are smooth whereas JENDL-4u shows a stronger energy dependence. For the angular distributions a comparison is only made with the data of Schwarz et al. [151]. The comparison is similar to that of Ref. [132] but here we include the calculation that led to JEFF-3.3 which is based on the INOY potential. This calculation follows very closely that of the AV-18 potential and shows overall good agreement with the data that correspond to 20 neutron energies between 2.5 and 30 MeV. A recent measurement for n+d scattering by Pirovano et al. shows good agreement with JEFF-3.2 (and therefore JEFF-3.3) for the backward–forward scattering ratio for neutron energies between 0.2 and 2 MeV [152].

The multiplication factors k_{eff} of heavy water benchmarks obtained by Monte Carlo simulations including this evaluation can be found in [132]. Further comparisons may be found below.

2.2.2 *Sodium*

The JEFF-3.1.1 [3] sodium evaluation shows large discrepancies in the MeV range with the microscopic experimental data that is available in EXFOR , even though it behaves well in integral experiment benchmarking. Furthermore, cross section covariance matrices, which are of interest for fast reactor applications in sensitivity and uncertainty analysis, are not available. In the framework of the ASTRID project (French sodium fast reactor), a new evaluation for sodium from 0 to 20 MeV [153] was carried out using the CONRAD code [154]. The results are included in the JEFF-3.3 library. The file contains both re-evaluated nuclear data and covariances and is divided in two energy regions: the resolved resonance range and the continuum part.

The resonance range, which had an upper limit of 350 keV in previous versions, has been extended to 2 MeV. For the continuum region, a simultaneous analysis of total, inelastic, capture and charged particle cross section data was performed with the ECIS [155] and TALYS [43] codes, interfaced with CONRAD. An overall good agreement between experimental and theoretical cross sections was achieved. The covariance data were produced with a Monte Carlo marginalisation procedure which consists in propagating the uncertainties of the most important systematic

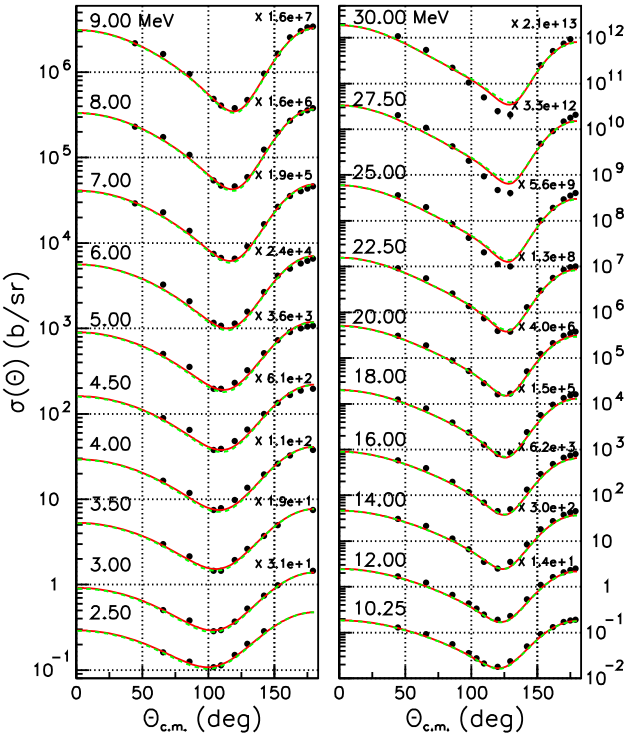

Fig. 24 Differential scattering data by Schwarz et al. [151] compared with model calculations using the AV-18 nucleon–nucleon potential (red line) and the INOY potential (dashed green line – JEFF-3.3, [132])

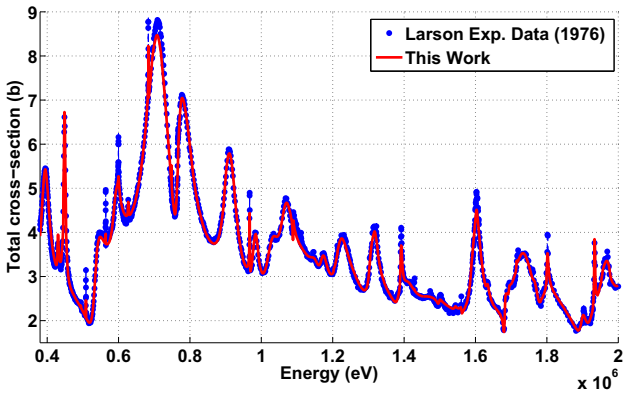

Fig. 25 Evaluated ^{23}Na total cross-section (red) compared to Larson experimental data (blue dots [157])

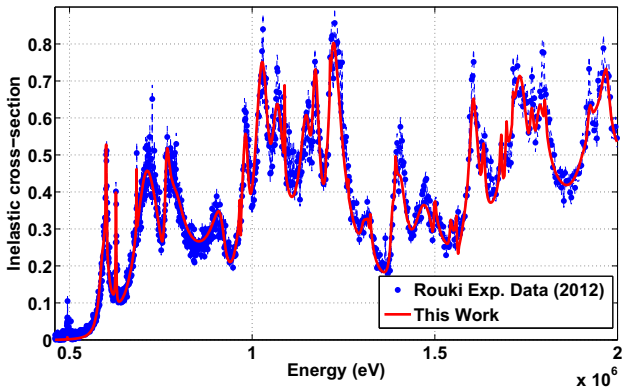

Fig. 26 Evaluated ^{23}Na inelastic cross-section (red) compared to Rouki experimental data (blue dots [158])

effects to the uncertainties of the nuclear reaction model parameters.

The resolved resonance range for sodium in JEFF-3.1.1 was described up to 350 keV using the Multilevel Breit-Wigner approximation. With this R-Matrix approximation in the ENDF-6 format, the upper energy value cannot exceed the first inelastic threshold which is at 459.3 keV for ^{23}Na.

To produce improved resolved resonance parameters for JEFF-3.3, the high resolution experimental total cross section data of Rahn [156] and Larson [157] and the inelastic cross-section data of Rouki et al. [158] were used. These data show large and detailed resonant structures up to 5 MeV. This is the primary motivation to extend the resonance range up to 2 MeV, just before the opening of the second inelastic scattering channel. For a better representation of the elastic-inelastic scattering interferences the Reich–Moore approximation of the R-matrix formalism was used. An energy-dependent effective scattering radius (R_{eff}) was required in order to obtain a good agreement with the experimental data above 1 MeV. The energy dependence was derived from results of optical model calculations.

For the resonance analysis the starting parameters were mainly taken from the Atlas of Neutron Resonances [67]. The neutron widths for resonances below 450 keV were adjusted to the total cross section data of Rahn [156] and Larson [157]. Above this energy, the inelastic data of Rouki et al. [158], obtained at the GELINA facility of the JRC Geel, were used to derive the neutron elastic and inelastic scattering widths and total angular momentum. The good agreement between the results of the adjustment and experimental data is shown in Figs. 25 and 26.

In the continuum region, i.e. for neutron energies larger than 2 MeV, optical model and statistical model parameters (level density, giant dipole resonance, pre-equilibrium…) were derived with the ECIS [155] and TALYS [43] codes. We used a spherical dispersive parameterisation derived from the global optical model of Morillon and Romain [159] found in the RIPL-3 database [70].

In this energy range, we use the data from Rouki et al. [158] for the first six inelastic channels up to 3.5 MeV. Above this energy, we derived our parameters set from the Larson measurements and various experimental data available in EXFOR for the (n, γ), (n, p), (n, α), $(n, 2n)$ reactions. The agreement with respect to Larson data is excellent. Concerning the partial and total inelastic cross-sections, an overall good agreement has been achieved with the data obtained by Rouki et al.

Experimental uncertainties, in particular a normalisation uncertainty of 3% for the data of Larson and 6% for those of Rouki et al. were propagated to the model parameters using a Monte-Carlo marginalisation technique [97] for both energy domains at the same time. This procedure creates correlations between resonance and statistical parameters and also between the resonance range and the continuum region.

2.2.3 Aluminum

The aluminum evaluation of ENDF/B-VI.8 was adopted in JEFF-3.0. For JEFF-3.3, it was modified to include inelastic scattering, in particular the emitted gamma rays (Sect. 2.4). In addition, covariances were generated for the resonance parameters and the cross sections using the TENDL method [5].

2.2.4 Chromium

New evaluated data files were prepared for n + ^{50,52,53,54}Cr interactions for the JEFF-3.2 release [160]. With one modification to the evaluation of n + ^{52}Cr data these were adopted for JEFF-3.3. The resonance range evaluations were performed at Oak Ridge National Laboratory, USA. The data were analysed using the SAMMY [19] resonance analysis code. The experimental data that were included and the quality of the fit are comprehensively summarized in Ref. [161]. In the fast energy range the data for n + ^{52}Cr were evaluated up to 150 MeV using the GNASH code while the data for n+^{50,53,54}Cr were evaluated with TALYS-1.0 up to 200 MeV using the geometry dependent hybrid pre-equilibrium model [162]. Particular attention was paid to reproducing the available experimental data for the total cross section and the (n,xn), (n,xp) and (n,xα) channels especially when these lead to radioactive residual nuclei [160]. Figure 27 shows the evaluation compared with data for the ^{52}C(n,2n) [163–172] and ^{52}Cr(n,p) [164,169,170,172–176] reactions and for the production of protons and alphas on natural chromium. The latter are important for the effect of gas production on material damage.

For JEFF-3.3 this evaluation was modified to account for a change of normalization of the data for neutron inelastic scattering of Mihailescu et al. by 12.5% ([177,178], see also Sects. 2.2.14, 2.2.15). The change implied replacing the data for inelastic scattering to the first level up to 4.5 MeV, to levels 2, 3, 4, 5 and 9 up to 4 MeV and to levels 6, 7 and 8 up to 3.9 MeV with the renormalized experimental data as available in EXFOR [179]. The cross sections above these energies were smoothly matched to the existing evaluated cross sections at 20 MeV by a multiplicative factor depending linearly on the energy (Fig. 27).

2.2.5 Iron

Recently, the CIELO project developed new evaluations for the stable iron isotopes, that were adopted in the ENDF/B-VIII.0 library [14,180]. The evaluations in JEFF-3.3 for ^{54,56,57,58}Fe are unchanged from those in JEFF-3.2. The files in JEFF-3.2 were modifications of those in JEFF-3.1. Besides a few corrections, new capture gamma data were included (Sect. 2.4). For ^{56}Fe covariance data for the elastic, inelastic and capture cross sections were obtained by an adjustment to the PERLE experiment at the Eole zero power reactor and the gas-benchmark at the Masurca zero power reactor. These experiments were carried out in Cadarache, France, and featured iron reflectors for a typical Generation-III PWR configuration and a typical Generation-IV fast reactor (see also Sect. 3.1.6). An iterative non-linear regression was performed using the RDN code to arrive at the posterior covariance matrix [181].

For ^{56}Fe in JEFF-3.1 the original JEFF-3.0 (EFF-3.1) file with an evaluation up to 20 MeV was extended up to 200 MeV using the TALYS code by Koning and Duijvestijn [1,2,43]. The evaluations for ^{54,57,58}Fe were newly introduced by these authors in JEFF-3.1 and were left untouched, aside from the inclusion of capture gamma-ray emission for JEFF-3.2 (Sect. 2.4).

The decision to leave the iron files for JEFF-3.3 untouched was due to the fact that these files are competitive in terms of the description of available microscopic data, are performing well in criticality benchmarking and are better than the CIELO files in shielding benchmarks (Sects. 3.1 and 3.3). The choice has the unfortunate consequence that new insights in inelastic scattering are not included in the evaluation [182–186].

2.2.6 Nickel

From Table 13 it is clear that the stable isotopes for nickel were taken from either TENDL-2015 (^{62,63}Ni), from ENDF/B-VII.1 (^{61,64}Ni) or from EFF-3.1 (^{58,60}Ni). For JEFF-3.3 only the radioactive product data of the ^{58}Ni(n,p) channel were added. For the unstable nuclides, evaluations were added for ^{56,57,59}Ni. For ^{56,57}Ni these were taken wholesale from TENDL2015. For ^{59}Ni a Talys based statistical method was pioneered that is of interest to evaluations for future libraries such as JEFF-4.

^{59}Ni is interesting because of its non-threshold (n,α) and (n,p) reactions. The isotope is unstable, but has a half-life of 76,000 years and is produced in thermal neutron spectra from neutron capture in ^{58}Ni. For austenitic materials, including a wide range of common stainless steels, nickel may be sufficiently transmuted to reach as much as 3% of the nickel content and ^{59}Ni reactions have been shown to contribute the vast majority of displacement damage in some

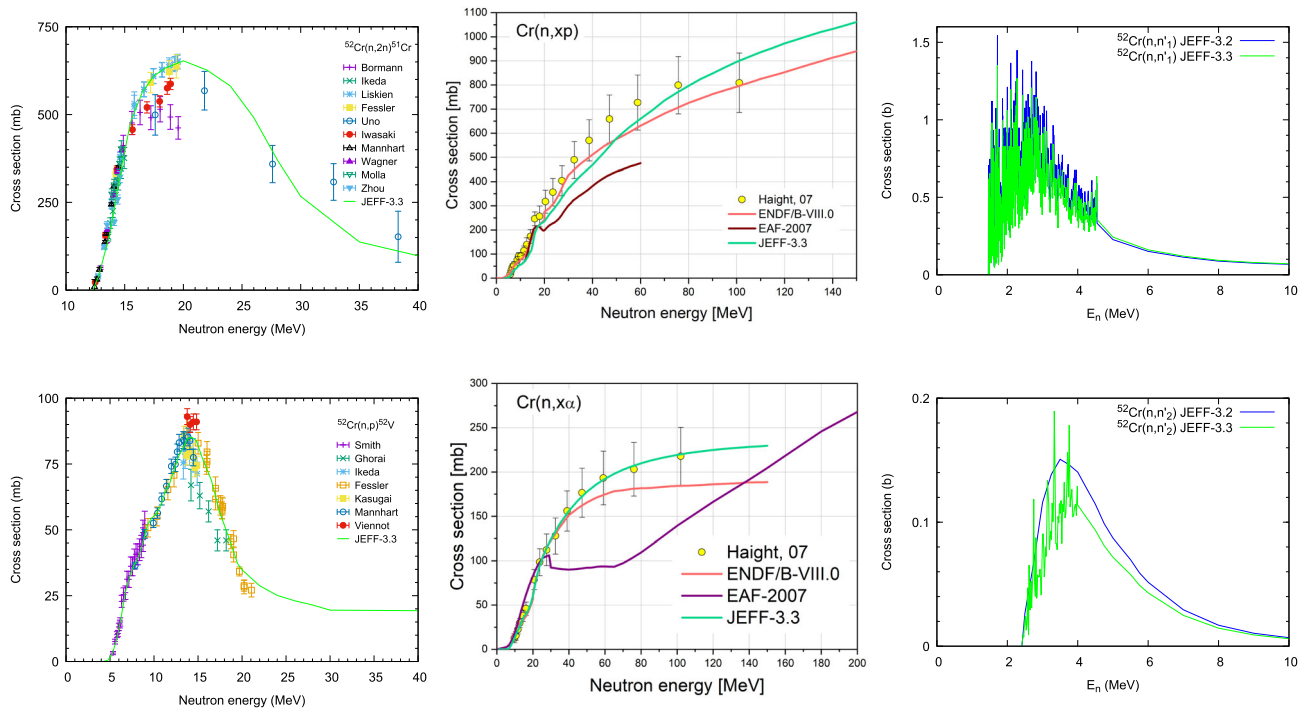

Fig. 27 Left: The ^{52}Cr(n,2n)^{51}Cr and ^{52}Cr(n,p)^{52}V evaluations compared with the experimental data. Middle: The production of protons (left) and alphas (right) on natural chromium. Right: Examples of the modifications to the neutron inelastic scattering channels of ^{52}Cr from JEFF-3.2 to JEFF-3.3. Left, inelastic scattering to the first excited level, right, inelastic scattering to the second excited level. The data are labeled by the first author of the reference

heavily thermalised environments [187]. Since nickel is one of the constituents of many stainless steels, the (n,α) and (n,p) reactions may also contribute a large fraction of the gas production reactor components [187].

The previous JEFF evaluation [188] did not contain any covariance data and only ranged up to 20 MeV. The new evaluation work is focused towards covariances, and contains, e.g., cross-channel correlations over the whole energy range, up to 200 MeV. The evaluation contains several novel features, e.g. a sampling of experimental errors merged with the sampling of resonance and model parameters; sampling from the latter two is similar to Total Monte Carlo [189]. A summary of the evaluation is presented below and further details are given in Ref. [190].

Since the thermal cross sections of ^{59}Ni are judged to be most important for applications, the evaluation is focused on these. Also, most available experiments are for thermal cross sections.

The publications (or, if not available, the EXFOR entries [179]) of thermal cross section experiments are studied in some detail, and the evaluators try to identify experimental uncertainty components which are not included in the experimenters' analyses. Seemingly missing uncertainties are added using assumed default values, which are intended to be somewhat conservative. Uncertainty components which are in common for different experimental points are identified (even for different experiments, for example originating from the use of the same target or monitor cross section).

Table 14 Estimated expected values $\langle\sigma\rangle$ and standard uncertainty u in barns for the thermal cross sections of the current ^{59}Ni evaluation, compared to the values from Mughabghab [67] and the previous JEFF evaluation. The uncertainties of the standard deviations are determined using the method described in Ref. [191]

	(n, α)		(n, p)		(n, γ)		(n, tot)	
	$\langle\sigma\rangle$	u	$\langle\sigma\rangle$	u	$\langle\sigma\rangle$	u	$\langle\sigma\rangle$	u
This work	12.7	0.7	1.5	.2	74	4	95	5
[67]	12.3	0.6	2.0	0.5	78	4	–	–
JEFF-3.2	13.5	–	1.7	–	81	–	98	–

After this analysis, the error components are sampled. In this way, random realisations of the different experiments are obtained. For each set of realisations, estimates for each of the (n,α), (n,p), (n,γ), and (n,tot) thermal cross sections are obtained using generalized least squares. In this way, a sample from the full joint distribution of the thermal cross sections is obtained. Physical constraints (a non-negative (n,el) cross section and the matching to other data) are included by redrawing and thus discarding "unphysical" results. This procedure impacts the distribution of the thermal cross sec-

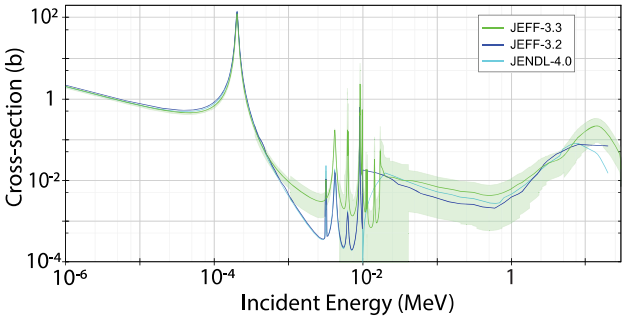

Fig. 28 The cross sections of (n,α)for the ^{59}Ni JEFF-3.3 evaluation (green with error bands) as functions of energy compared to JEFF-3.2 (blue, no error bands) and JENDL-4.0 (cyan no- error bands)

tions. The resulting mean values and uncertainties are presented and compared to the previous JEFF evaluation and the Mughabghab *Atlas of Neutron Resonances* [67] in Table 14. The values are generally different from, but compatible with, both Mughabghab and JEF(F) 2.2–3.2.

The thermal cross sections are combined with resonance parameters from experiment [192–194] and other data from TALYS-1.8 [43] using the parameter distribution of TENDL 2015 [5]. Both these sets of data are also sampled. For each realisation of data, the resonance parameters are matched with the thermal cross sections by sampling bound resonances ($E < 0$) based on average level spacings and widths from the corresponding TALYS run, and the resonance widths of these bound resonances are adjusted such that the thermal cross sections are reproduced. If the adjustment fails, the *combination* of sampled thermal cross sections and sampled resonance parameters is considered unphysical, and both sets of data are redrawn, as can be motivated by Bayes' theorem. For further details see Ref. [190].

The procedure results in 300 sets of complete nuclear data, which implicitly includes uncertainties of almost all the data. Also, all subsets of the data are correlated, since the sampling of bound resonances is based on TALYS results, and because of the matching between resonance parameters and thermal cross sections. For illustration, Figure 28 shows the (n,α) cross sections for the ^{59}Ni JEFF-3.3 evaluation compared to JEFF-3.2 and JENDL-4.0. JEFF-3.2 is copied from previous JEF(F) versions since JEF-2.2. ENDF/B-VIII.0 is also based on this evaluation. More illustrations of the new JEFF-3.3 evaluation are found in Ref. [190].

The 300 sets of nuclear data are condensed into one single ENDF file with covariances. Because of format limitations, correlations between some subsets of data are lost, e.g., between URR parameters and the cross sections. Higher moments than covariances are also lost. The impact of cross correlations can however be studied by the direct use of the 300 ENDF formatted files (the so-called random-files) which also were produced.

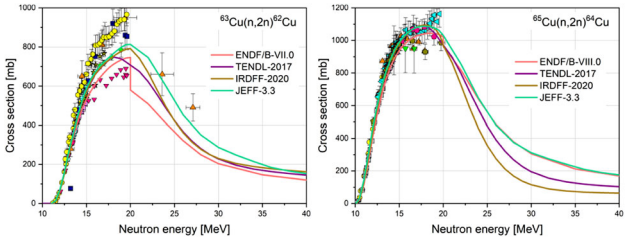

Fig. 29 Left: evaluated ^{63}Cu(n,2n)^{62}Cu cross section. Right: evaluated ^{65}Cu(n,2n)^{64}Cu cross section

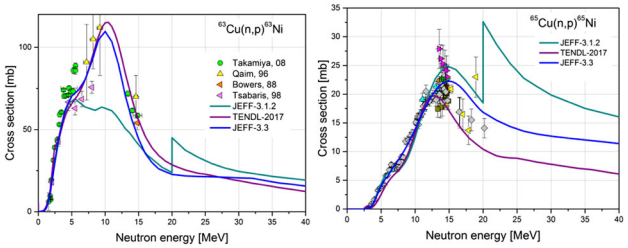

Fig. 30 Left: evaluated ^{63}Cu(n,p)^{63}Ni cross section. Right: evaluated ^{65}Cu(n,p)^{65}Ni cross section

2.2.7 *Copper*

For the ^{63}Cu and ^{65}Cu isotopes the resonance region was set from 10^{-5} eV to 300 keV. Resolved resonance parameters for neutron interactions with ^{63}Cu and ^{65}Cu in the energy region below 6 keV were taken from the work of Tsuchiya et al. [195]. They result from a combination of the radiation widths reported by Weigmann and Winter [196] and a resonance shape analysis of transmission data obtained at GELINA using REFIT [59]. To account for external contributions the bound state parameters of JEFF-3.2 were adopted. This contribution is not consistent with the one used in Ref. [195]. This explains the inconsistencies observed in Ref. [197] between experimental transmission data and the calculated ones using the parameters in JEFF-3.3. The results in Ref. [197] reveal also problems with the parameters recommended by Mughabghab [67], Sobes et al. [198] and ENDF/B-VIII.0 [180].

The nuclear model simulations of the n + ^{63,65}Cu reactions were performed using the TALYS-1.8 code [43] for neutron energies between 1 keV and 200 MeV [199]. In spite of the general predictive power of TALYS, certain improvements can be gained by inclusion of an extra model for preequilibrium reactions, known as the Geometry Dependent Hybrid model (GDH) [162]. With the GDH model added to TALYS-1.8, the system provides more accurate results for n+Cu reactions compared to the existing models within the code. The nuclear level density was described with a back-shifted Fermi-gas model [200].

All optical model calculations for neutrons and protons were performed using TALYS built-in Optical Model Poten-

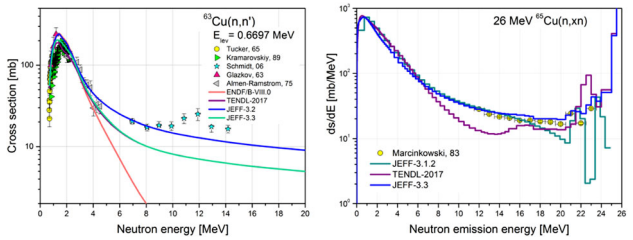

Fig. 31 Left: evaluated ^{63}Cu(n,n') cross section for the first excited level. Right: evaluated neutron emission spectra for n + ^{nat}Cu at 26 MeV

tials (OMPs). In the case of other charged particles, external global OMPs were used for deuterons [201] and alphas [202]. For tritons and helions, new OMPs were elaborated using a large experimental database and available OMPs for some target nuclides. The parameters of the global OMPs for charged particles (except incident protons) were separately prepared and used in TALYS calculations invoking the cycling through the available options. For all OMPs, the same incident energy range from keVs up to 200 MeV was used to keep continuity and consistency of the evaluated data. All changes arising in the evaluations due to the adjustment procedure of the reaction cross sections are accounted for in the elastic scattering cross section, keeping the total cross section unchanged.

The procedure applied to these nuclear data evaluations is based on an optimised fit to the experimental data [203]. The nuclear model parameters were adjusted stepwise, resulting in an optimal set that results in evaluated data that best fits the experimental results. Shown in Fig. 29 are the newly evaluated (n,2n) cross sections for ^{63,65}Cu. The results for ^{63,65}Cu(n,p) cross sections compared to the measured and other evaluated data are presented in Fig. 30. Great attention was paid to the evaluation of the inelastic scattering cross sections for all excitated states of the ^{63,65}Cu. The latest measured data of Takamiya et al. [204] cannot be reproduced by any nuclear model simulations considered and they were not used for the adjustment of the nuclear model parameters. The results of the evaluation for ^{63}Cu(n,n') inelastic scattering cross sections are given in the Fig. 31. The inclusion of the new GDH option enabled significant improvements in the calculated pre-equilibrium particle emission spectra compared to the original TALYS-1.80 results (Fig. 31). The JEFF-3.3 and JEFF-3.2 results are compared with ENDF/B-VIII.0 [180], TENDL-2017 [5] and IRDFF-2 [205].

2.2.8 Zirconium

The evaluation n+Zr data was performed in the same way as in the n+Cu case [199]. However, for zirconium the n + ^{90,91,92,94,96}Zr resonance data for the resolved and unresolved ranges were taken from the ENDF/B-VII.1 [121]. For

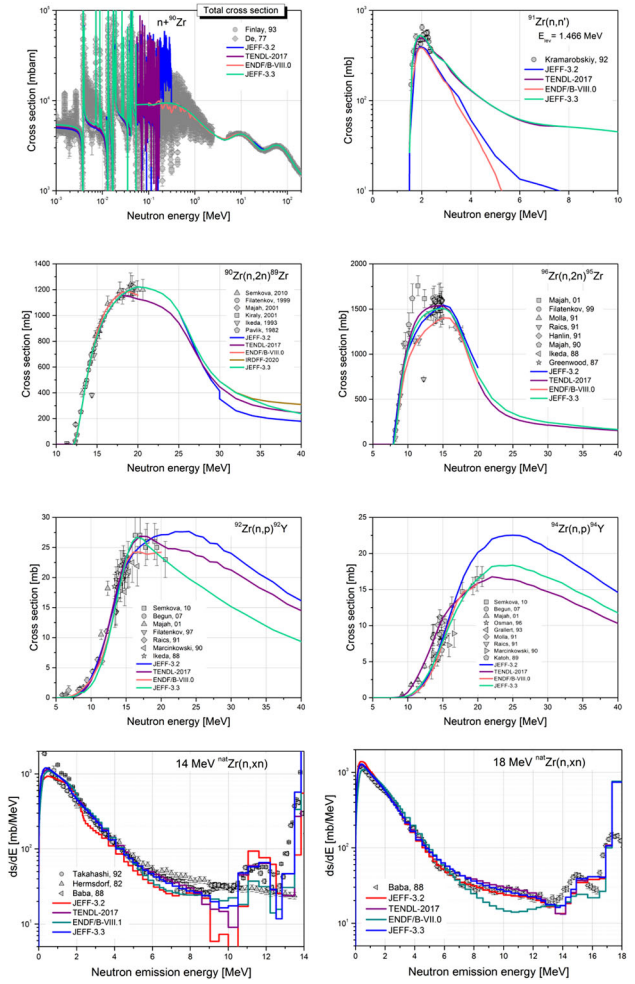

Fig. 32 Top left: evaluated total cross section for the n+^{90}Zr. Top right: the evaluated (n,n') cross section for the 2^{nd} excited level of the ^{91}Zr. Row 2 left: evaluated ^{90}Zr(n,2n) cross section. Row 2 right: evaluated ^{96}Zr(n,2n) cross section. Row 3 left: evaluated ^{92}Zr(n,p) cross section. Row 3 right: evaluated ^{94}Zr(n,p) cross section. Row 4 left: neutron emission spectrum for $^{nat.}$Zr at 14 MeV. Row 4 right: neutron emission spectrum for $^{nat.}$Zr at 18 MeV. Comparisons are with experimental data, JEFF-3.2, ENDF/B-VIII.0 and TENDL-2017 [5,180]

the fast range, the available experimental database was used to apply a consistent procedure for the evaluation of the exclusive reaction cross sections. Examples of evaluated cross sections compared with experimental data and other evaluations are given in Fig. 32 for the evaluated total cross section of n + ^{90}Zr, where the resonance data are quite different in various libraries, for the evaluated neutron inelastic scattering cross section (n,n') for the 2nd excited state of ^{91}Zr and for evaluated exclusive (n,2n) and (n,p) cross sections are given. The new evaluations account for the latest measured data and show a good agreement with the available experimental data below 20 MeV, as well as a significant improvement compared with other evaluations. The neutron emission spectra presented in Fig. 32 also demonstrate an improvement in the

pre-equilibrium components due to the inclusion of the GDH model. In the figure, the JEFF-3.3 and JEFF-3.2 results are compared with ENDF/B-VIII.0 [180], TENDL-2017 [5] and IRDFF-2 [205]. The JEFF-3.3 evaluation generally compares well to its predecessor and these other evaluations.

For the ENDF-6 representation of the data, the following structure of the data files was adopted: below 20 MeV the full detailed information for all open reaction channels is given and above 20 MeV total and elastic scattering cross sections are provided alongside total particle emission spectra and total cross sections for the production of the residual nuclides with their recoil spectra.

2.2.9 Cadmium

An ENDF-6 compatible evaluation for neutron induced reactions in the resonance region has been completed for ^{106,108,110,111,112,113,114,116}Cd. The resonance parameters were derived from an analysis of experimental data available in the literature together with a parameter adjustment to transmission and capture data obtained at the time-of-flight facility GELINA. The REFIT code [59] was used for the resonance shape analysis. A detailed description of the experimental data and the analysis in the resolved resonance region was reported by Volev et al. [206]. For neutron induced reactions in the unresolved resonance region the JENDL-4.0 evaluation for ^{111}Cd and ^{113}Cd was adopted. The evaluated files have been processed with the latest updates of NJOY.99 to test their format and application consistency as well as to produce a continuous-energy data library in ACE format for use in Monte Carlo codes. The ACE files have been utilised to study the effect of the evaluated resonance parameters on results of integral experiments. The production of the file together with its validation is described by Sirakov et al. [207].

2.2.10 Hafnium

Hafnium is a ductile metal which does not exist as a free element in nature. The stable hafnium isotopes for A = 174,176,177,178,179 and 180 are found combined in zirconium compounds with a respective natural abundance of 0.16%, 5.26%, 18.60%, 27.28%, 13.62% and 35.08%. Hafnium is very corrosion resistant, has impressive mechanical properties and shows good absorption for thermal and epi-thermal neutrons. Due to these properties, it is commonly selected in reactor engineering as a neutron absorbing material in steel clad control rods to regulate the fission process.

In JEFF-3.3, hafnium evaluations are based on the TENDL files produced in 2015 [5]. They were used as templates for the six stable hafnium isotopes. The resolved resonance parameters were replaced by those of Ref. [208]. The unresolved resonance parameters and the neutron cross sections

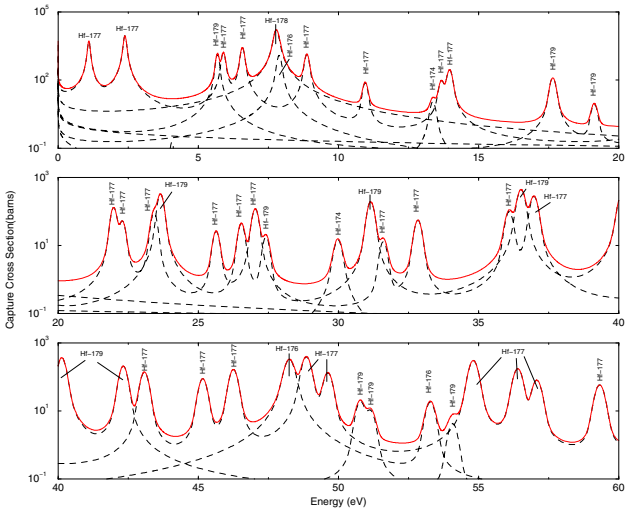

Fig. 33 The solid line represents the natural hafnium capture cross section calulated with the Reich–Moore formalism using the resonance parameters compiled in the JEFF library. The dashed lines show the contributions of the six hafnium isotopes

above the upper energy limit of the resolved resonance range are from Ref. [209]. The covariance files for the neutron cross sections are derived from the work reported in Ref. [210].

In contrast, the ENDF/B-VII.1 resonance region data is taken from JEFF-3.1 for ^{174,176,178,180}Hf and JENDL-3.3 for ^{177,179}Hf, with some adjustments to bound levels, RRR upper limits and URR average parameters. ENDF/B-VIII.0 [180] uses the ENDF/B-VII.1 resonance region data with cross sections and energy spectra above the resonance region produced by Kawano (LANL) using the CoH3 code in 2016.

The resolved resonance parameters established by Trbovich from RPI data [211] were introduced in the JEFF-3.1 evaluations. They were replaced by the new parameters determined with time-of-flight data measured at the GELINA facility of JRC-Geel [208]. The natural hafnium capture cross section reconstructed with the parameters compiled in the JEFF-3.3 (and JEFF-3.2) library is shown in Fig. 33. The complex resonance structure is dominated by the ^{177}Hf isotope. The peak cross section values of the resonances at 1.1 eV and 2.4 eV reach respectively 5200 barns and 8800 barns ($T = 300$ K). For reactor applications, these two first ^{177}Hf resonances represent the most important contribution to the Hf reactivity worth. Near 7.8 eV, one can distinguish the non-negligible contribution of the ^{178}Hf isotope. Between 15 and 45 eV, the behavior of the natural Hf capture cross section is characterized by several multiplets of ^{177}Hf resonances overlapping resonant structures of the ^{179}Hf(n, γ) reaction.

In order to determine accurate resonance parameters, a wide experimental program was carried out at the JRC-Geel facility. Detailed explanations can be found in the PhD thesis of Tim Ware [212]. Sixteen sets of capture data were collected

Table 15 Upper energy limit of the resolved resonance range and number of resonances

Hf isotope	Upper energy		Nr. of resonances	
	JEFF-3.1.1	JEFF-3.3	JEFF-3.1.1	JEFF-3.3
^{174}Hf	220	250	12	14
^{176}Hf	700	3000	19	74
^{177}Hf	250	1000	94	331
^{178}Hf	1500	3000	23	55
^{179}Hf	250	1000	50	219
^{180}Hf	2500	3000	16	21

at different repetition rates (50 Hz, 800 Hz) and different flight paths (12.89 m, 28.82 m, 58.586 m) with 4 natural Hf samples (0.024 mm, 0.079 mm, 0.26 mm, 1 mm) and additional samples enriched in ^{176}Hf (65%), ^{177}Hf (85.4%), ^{178}Hf (92.4%) and ^{179}Hf (72.1%). The transmission of a thick natural Hf sample (16 mm) was also measured at the 49.34 m station. Resonance parameter were determined with the REFIT code [59]. Previous capture and transmission data were also included in the analysis such as those reported in Refs. [211,213,214]. As shown in the Table 15, the upper energy limits of the resolved resonance range and the number of resonances were significantly increased.

The variances and covariances of the Hf resonance parameters were obtained with the CONRAD code [153]. A retroactive analysis [215] was used in order to determine the resonance parameter covariance matrix without changing the resonance parameters reported in Refs. [208,212]. Systematic uncertainties related to experimental parameters (normalisation, background, temperature ...) were propagated by using a marginalisation procedure [97]. Uncertainties on the thermal capture cross section and on the capture resonance integral were used as constraints. For the thermal capture cross sections and resonance integrals, we obtain:

$$\begin{aligned}
\sigma_{th}(174) &= 651 \pm 110 \ (17\%),\\
\sigma_{th}(174) &= 651 \pm 110 \ (17\%),\\
\sigma_{th}(176) &= 16.8 \pm 2.0 \ (12\%),\\
\sigma_{th}(177) &= 371 \pm 13 \ (3.5\%),\\
\sigma_{th}(178) &= 85 \pm 5 \ (6\%),\\
\sigma_{th}(179) &= 40 \pm 3 \ (7.5\%),\\
\sigma_{th}(180) &= 13.1 \pm 1.1 \ (8.4\%),
\end{aligned}$$

$$\begin{aligned}
I_{\gamma}(174) &= 453 \pm 21 \ (4.7\%),\\
I_{\gamma}(176) &= 634 \pm 21 \ (3.2\%),\\
I_{\gamma}(177) &= 7165 \pm 218 \ (3.0\%),\\
I_{\gamma}(178) &= 1798 \pm 64 \ (3.5\%),\\
I_{\gamma}(179) &= 530 \pm 16 \ (3.0\%),\\
I_{\gamma}(180) &= 37.4 \pm 1.8 \ (4.8\%).
\end{aligned}$$

Above the upper energy limit of the resolved resonance range up to 20 MeV was carried out as follows (for further details see Ref. [209]). The strength and originality of this work lie in the Reich–Moore interpretation of the resolved resonance range in association with optical model calculations based on parameters established by Morillon et al. [216,217] with deformation parameters initially proposed by Avrigeanu et al. [218]. Links between the collision matrix elements calculated by the optical model code ECIS [155] and the average R-Matrix parameters (neutron strength function S_l and distant level parameters R_l^{∞}) were established by using the ESTIMA [52] and SPRT methods [219]. Inherent difficulties in assessing unambiguous average resonance parameters from neutron spectroscopy measurements are not only the correct determination of the s-wave parameters but also the generalisation of the obtained results to higher order partial waves ($l = 1, 2, 3 \cdots$). These difficulties can be partially solved with a sequential (and iterative) analysis of the low and high neutron energy ranges. The accuracy of the final results depends mainly of the quality of the experimental data available in the unresolved resonance range, and of the choice of the optical model parameters established for the nuclei involved in the nuclear reactions of interest. The consistency of the resulting neutron strength functions, mean level spacing and average radiation width was tested by comparing experimental total and capture cross sections with theoretical curves calculated with the nuclear data code CONRAD [153]. Results are reported in Fig. 34 up to 1 MeV.

For JEFF-3.3, the neutron cross section files up to 20 MeV were produced with the TALYS code [5]. The option for unresolved resonance calculation implemented in TALYS allows users to simultaneously create a consistent set of unresolved resonance parameters. Covariances between the neutron cross sections were generated with a two-step CONRAD calculation, involving a standard least-square fit followed by the marginalisation of the nuisance parameter uncertainties. Results for the ^{177}Hf(n, γ) reaction is shown in Fig. 35.

Trends for the natural hafnium capture cross section have been deduced from critical experiments performed in zero-power reactors located at Cadarache [220–222]. Interpretations of these experiments with the APOLLO2 deterministic lattice code [82] and with the Monte-Carlo code TRIPOLI-4® [53] have demonstrated the good description of the low energy natural hafnium capture cross section compiled in the JEFF-3.1.1 and JEFF-3.2 libraries. Integral trends obtained for the CAMELEON and AMMON programs are summarized in Table 16. Discrepancies between the calculated and experimental reactivity worth remain less than 3% on average. The slight increase of the reactivity worth (+0.5%) indicates that the capture resonance integral in JEFF-3.1.1 [211] and JEFF-3.2 [208] are consistent. Similar trends are expected with the hafnium evaluations of the JEFF-3.3

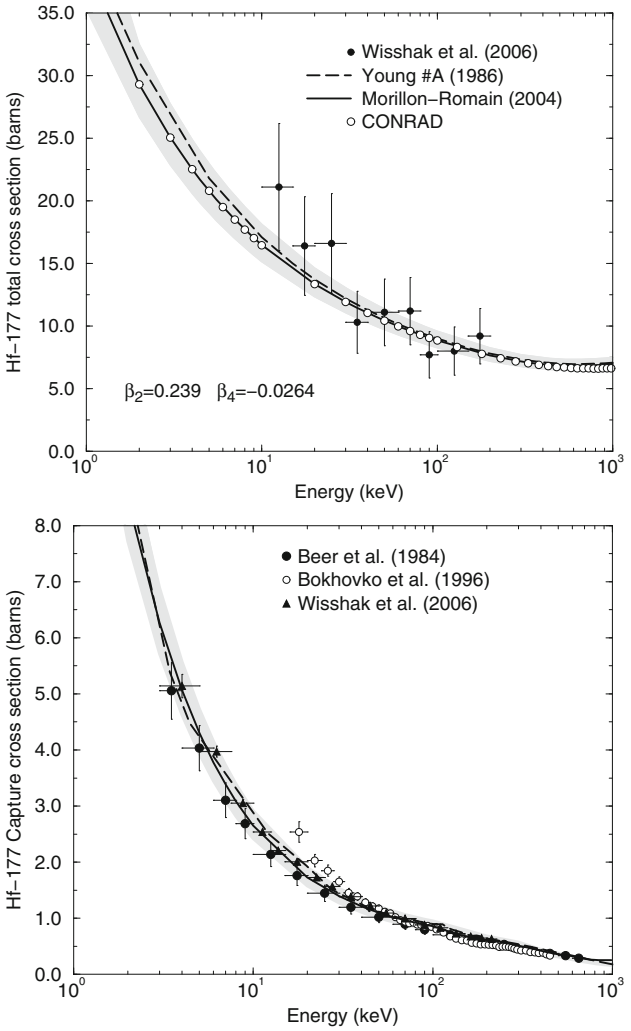

Fig. 34 Top: CONRAD results (open circle) and uncertainties (gray zones) compared with ECIS calculations based on the optical model parameters of Morillon et al. [216,217] and Young (see Ref. [218]) using deformation parameters from Ref. [209]. Experimental data were measured at the VdG facility of Karlsruhe with the time-of-flight technique. Bottom: CONRAD results (solid line) and uncertainties (gray zones) obtained by using the average parameters and the uncertainties reported in Ref. [209]. They are compared with calculations (dashed line) based on the local approach and parameters given in Ref. [218] with the average radiation widths of Ref. [209]. The experimental data were retrieved from the EXFOR data base [179]

library, as JEFF-3.3 and JEFF-3.2 evaluations share the same resolved resonance parameters.

Impact of the Hf nuclear data accuracy on integral calculations were investigated with the experimental data measured in the frame of the CAMELEON program [210]. Final uncertainties are reported in Table 17 for two CAMELEON configurations (17 Hf pins, 25 Hf pins). Results obtained for each configuration differ from a factor 1.5 which is consistent with the ratio between the Hf reactivity worth of $\sim$ 10, 000 pcm (25 Hf pins) and $\sim$ 7000 pcm (17 Hf pins). The global uncertainty of $\sim$300 pcm (3%) is consistent with the integral trends reported in Table 16.

2.2.11 Tantalum

Nuclear data for n + ^{181}Ta were evaluated for JEFF-3.2 and this evaluation was adopted for JEFF-3.3. The GNASH Hauser–Feshbach code described in Ref. [236] was used, which includes statistical, pre-equilibrium and direct-reaction models. The global optical model potentials of Koning and Delaroche [237] were used in coupled-channels calculations for incident neutrons and protons in the energy region from 0 to 150 MeV. The Bojowald potential [238] was used for deuterons. For tritons and ^{3}He the simplified folding approach of Watanabe [239] was used with the neutron and proton potentials of Ref. [237]. This approach leads to underestimation of cross sections for all energies. Below 20 MeV (n,t) and (n,^{3}He) cross sections were calculated by folding with the Becchetti-Greenlees potential [240]. For alphas the Avrigeanu global potential was used [202]. The ECIS code [155] was used for the couple-channels and Distorted Wave Born Approximation (DWBA) calculations. The gamma transmission coefficients were calculated using the Kopecky-Uhl model [241]. The parameters of Gurevich [242] were used for the description of the giant dipole resonances. The model of collective excitations [243] included for continuum inelastic scattering and the GNASH multiple particle emission option improved the neutron emission spectra.

The resonance range evaluation was taken from JENDL-3.3 [122]. Elastic scattering cross sections and angular distribution in the range from 0.5-3 MeV are from JENDL-3.3, as well. For the (n,2n) reaction JEFF-3.0 activation data are taken below 12 MeV neutron energy. This gives an excellent description of the data by Fréhaut et al. when renormalized by a factor 1.1 [225]. Above 12 MeV the GNASH results are taken. Below 4 MeV the neutron capture cross section is from JENDL-3.3 and above the GNASH results normalized to the JENDL data are used. The capture gamma-rays are from JENDL-3.3. For the (n,p) channel the GNASH calculation is normalized to the data of Refs. [234,235]. GNASH (n,t) channel estimates are normalized to the systematics of Ref. [244].

Results for the ^{181}Ta(n, 2n)^{180}Ta, ^{181}Ta(n, p)^{181}Hf, ^{181}Ta (n, 3n)^{178}Ta and ^{181}Ta(n, α)^{178}Lu cross sections and the ^{181}Ta(n, xn) spectra for 6.7 MeV and 14 MeV incident neutrons are shown in Fig. 36. The evaluation agrees well with the experimental data and clearly compares well with the recent TENDL-2017 and ENDF/B-VIII.0 evaluations. Differences between evaluations are noteworthy for the (n,p) and (n,3n) cross sections and for the neutron emission spectra in the energy region just below the incident neutron energy.

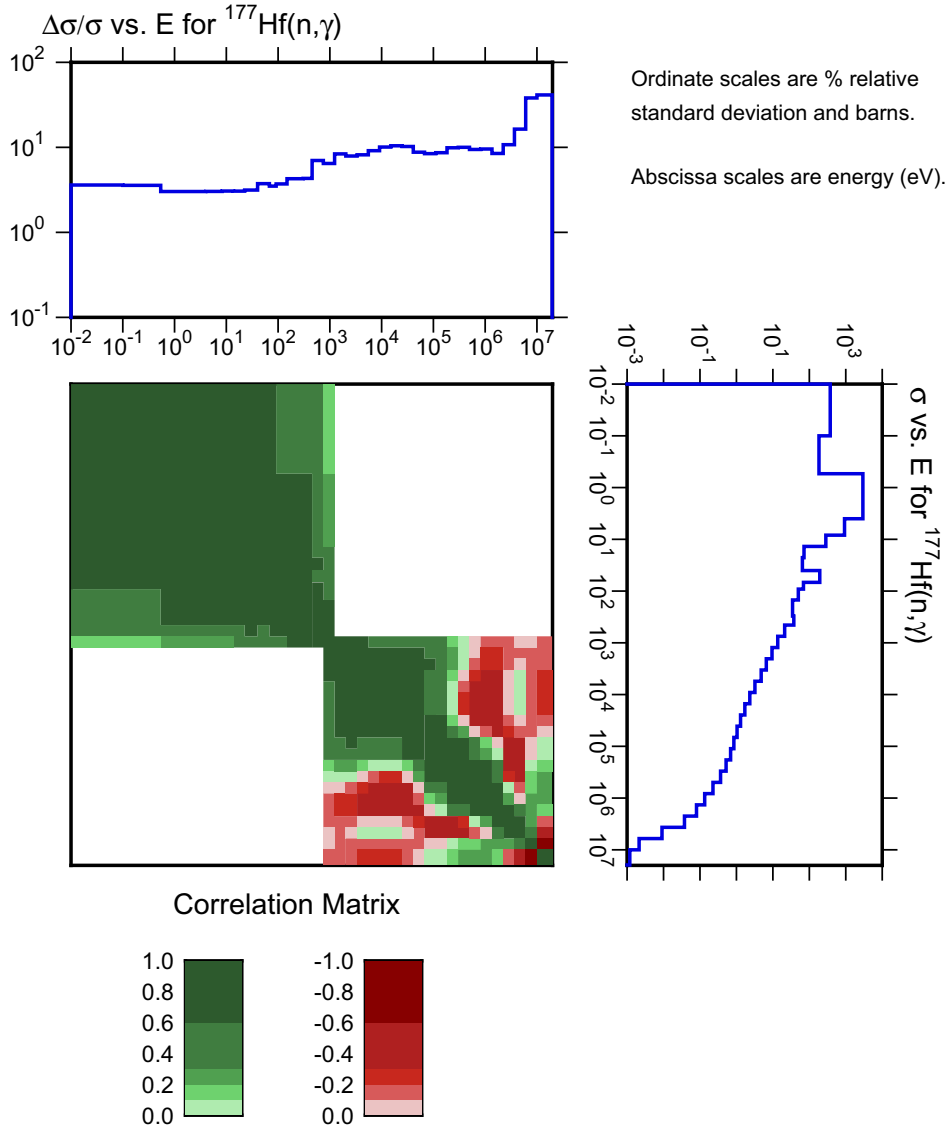

Fig. 35 Relative uncertainties in % (top) and correlation matrix for the ^{177}Hf(n, γ) reaction up to 20 MeV. The ordinate scales are neutron energy in eV

Table 16 Integral trends on the Hf reactivity worth calculated with the Monte-Carlo code TRIPOLI-4®[53] for the CAMELEON (17 and 25 Hf pins) and AMMON program carried out in the EOLE facility of CEA Cadarache

JEFF	CAMELEON		AMMON
	17 Hf	25 Hf	
3.1.1	$2.7 \pm 0.3\%$	$2.8 \pm 0.2\%$	$1.8 \pm 1.8\%$
3.2	$2.9 \pm 0.3\%$	$3.2 \pm 0.2\%$	$2.4 \pm 1.8\%$
Diff.	0.2%	0.4%	0.6%

Table 17 Reactivity worth uncertainty (in pcm) due to the accuracy on the Hf capture cross sections. The Hf reactivity worths calculated with APOLLO2 are close to 7000 pcm and 10,000 pcm for the 17 Hf and 25 Hf pins configurations, respectively

Pins	^{176}Hf	^{177}Hf	^{178}Hf	^{179}Hf	^{180}Hf	Total
17	10	208	41	74	32	227
25	15	306	60	111	48	334
Uncer.	$> 0.2\%$	3.0%	0.6%	1.1%	0.5%	3.3%

2.2.12 Tungsten

New evaluations of neutron induced cross-sections up to 150 MeV were performed for the stable ^{182,183,184,186}W isotopes [245]. A good description of the available total cross section and neutron elastic and inelastic (differential) cross section data was obtained by adapting the optical potentials of Koning and Delaroche [237] and Young. The reaction data were calculated with ECIS95 and GNASH using both global and local potentials for neutrons, protons, deuterons, tritons and alphas and taking into account collective excitations.

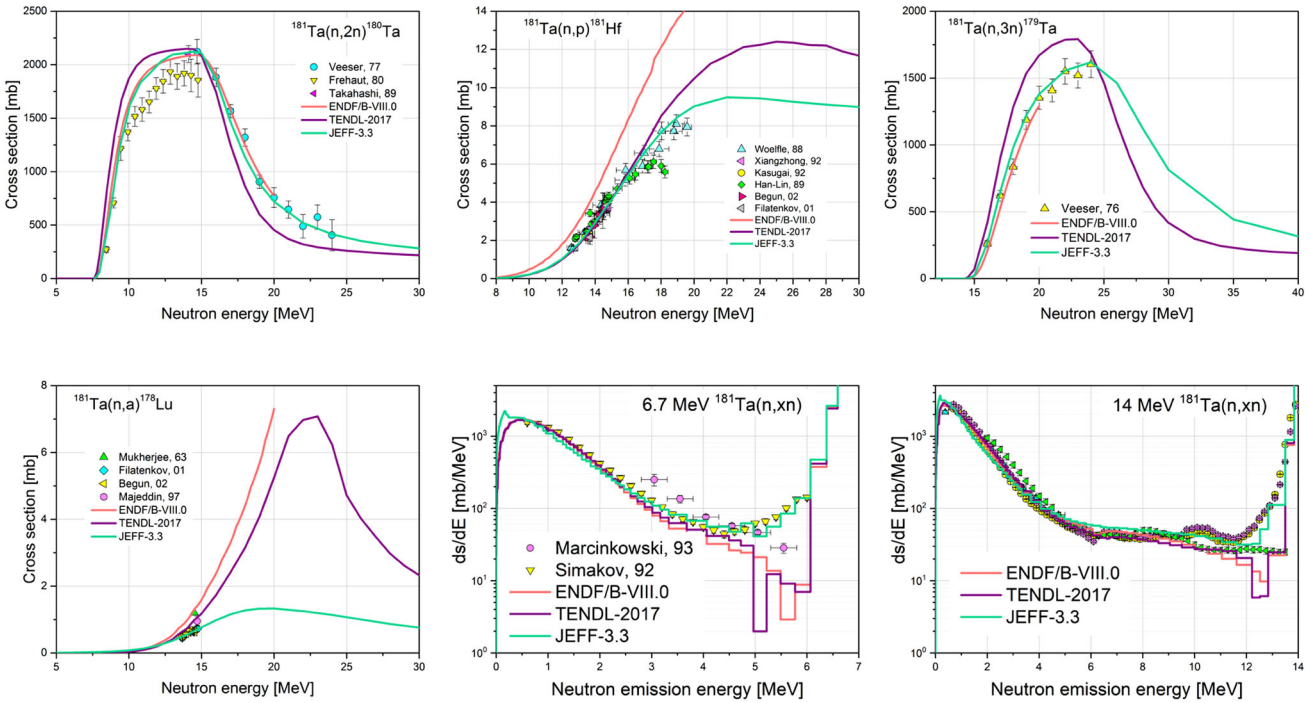

Fig. 36 Experimental data for n + ^{181}Ta cross sections and spectra compared with the JEFF-3.3 evaluation, TENDL-2017 and ENDF/B-VIII.0. The JEFF-3.2 evaluation was adopted in JEFF-3.3. The data are from Refs. [223–235]

In Fig. 37 the JEFF-3.3 evaluation is compared with experimental data, the TENDL-2017, JENDL-4 and ENDF/B-VIII evaluations. The evaluated JEFF-3.3 total cross sections for n + ^{182,184,186}W follow the data well above 10 MeV and are in reasonable agreement with the data below that energy, although the evaluation is clearly on the low-side of the data for n + ^{182,184}W. The other evaluations are higher for these nuclides but none is uniformly best. The ^{184,186}W(n,2n) cross section data are well described by the JEFF-3.3 evaluation and the latter compares well with ENDF/BVIII.0 and TENDL-2017. The data for inelastic scattering to the second level (4^+) of ^{182}W and the first level ($2+$) in ^{186}W compare best with ENDF/B-VIII.0, while JEFF-3.3 is somewhat low near the maximum and TENDL-2017 is respectively in the middle and high. Angular distribution data for one particular energy above the maximum are shown for each of these cases. The distributions are similarly described by the three libraries and the normalization differences reflect the difference in cross section.

Good agreement is observed for JEFF-3.3 with the (n,xn) neutron spectra at 14 and 26 MeV. Also the elastic scattering angular distribution of JEFF-3.3 at 14 MeV for natural tungsten describes the available data reasonably well up to a scattering angle of 100 degrees after which only JENDL-4 remains in reasonable agreement with the data.

The evaluations were further optimized to obtain good agreement for the available data for the (n,p), (n,α) reaction cross sections on ^{182,183,184,186}W and the remaining experimental data not shown in the figure.

Neutron resonance parameters for the ^{182,183,184,186}W isotopes were obtained in the energy region below 2 keV from a resonance shape analysis with REFIT of transmission and capture data that were measured at GELINA [63]. Details about the measurements and the analysis are given in Reference [246]. Starting parameters for the least squares adjustment were obtained by combining the results of transmission and capture measurements reported by Camarda et al. [247] and Macklin et al. [248], respectively. The parameters of negative resonances have been adjusted to match the coherent scattering lenghs of Ref. [249] and the capture cross sections at thermal energy of Ref. [250]. General purpose data files for transport calculations were prepared in ENDF-6 data format, processed with NJOY [41] and tested with MCNP calculations of the output ACE files.

2.2.13 Gold

An evaluation for neutron induced interactions with ^{197}Au in the resolved and unresolved resonance region was produced starting from the ENDF/B-VII.1 library file [121]. Despite the importance of neutron capture reactions on gold in the energy region between 5 keV and 150 keV for astrophysical applications, no unresolved resonance region (URR) has previously been considered in the major general purpose nuclear data libraries, in particular in ENDF/B-VII.1 [121]. This was

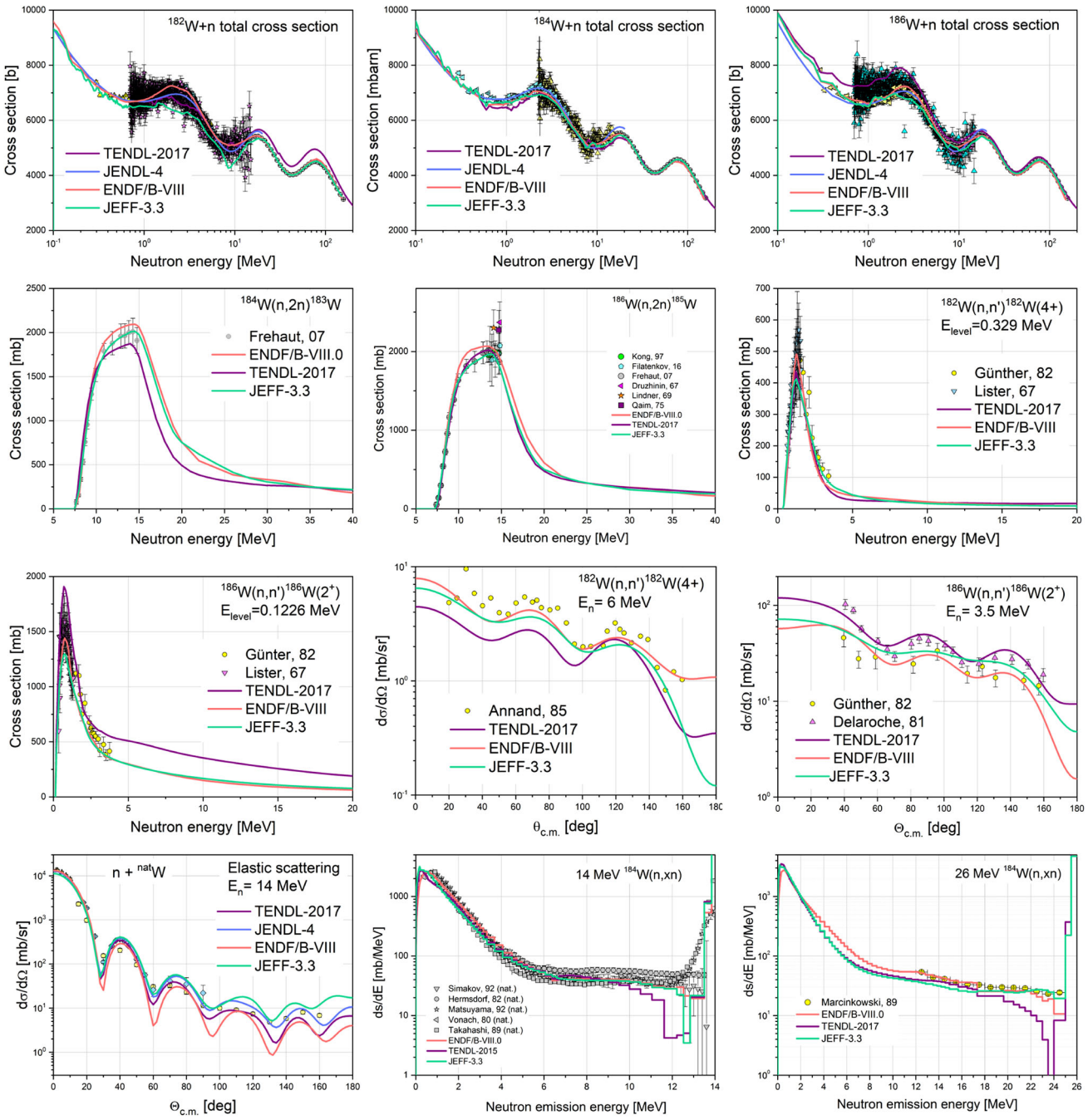

Fig. 37 Comparisons of the JEFF-3.3 evaluation for n + ^{182,184,186,nat}W to experimental data and the TENDL-2017, JENDL-4 and ENDF/B-VIII.0 evaluations. Some cross sections, angular distributions and spectral are shown

a reason for the former unjustified extension of the resolved resonance region (RRR) up to 5 keV. The only other evaluation for ^{197}Au in terms of average resonance parameters can be found in the TENDL nuclear data library [5]. Unfortunately, this evaluation was performed with incorrect values of the elastic degrees of freedom for five of the spin sequences. In addition, the upper limit of the URR is restricted up to the inelastic scattering threshold of 77.75 keV.

To evaluate the cross section data for ^{197}Au in the RRR the resolved resonance parameters in ENDF/B-VII.1 [121] were inspected and partly revised based on a resonance shape analysis of transmission, capture and self-indication data using the REFIT code [59]. The experimental data were obtained at the time-of-flight facility GELINA [63] by Massimi et al. [251]. The upper limit of 5 keV of the RRR, as adopted in ENDF/B-VII.1, was reduced to 2 keV due to the lack

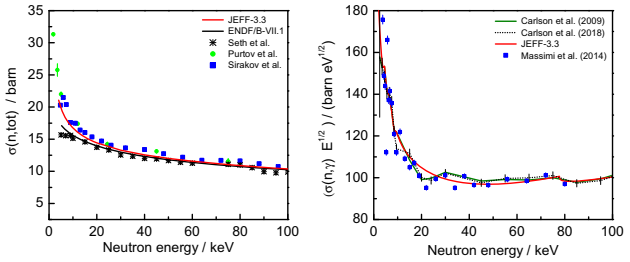

Fig. 38 Left: Average total cross section for neutron induced reactions in ^{197}Au as a function of neutron energy in the URR. The cross section in JEFF-3.3 is compared with the experimental data of Seth et al. [255], Purtov et al. [256] and Sirakov et al. [253] and with the one recommended in ENDF/B-VII.1 [121]. Right: Average neutron induced capture cross section for ^{197}Au as a function of neutron energy in the URR. The cross section in JEFF-3.3 is compared with the one recommended by Carlson et al. [27] and the experimental data of Massimi et al. [257]

of reliable capture data above 2 keV which are needed for the analysis of weak resonances. This solution seems to be a more justified alternative than generating unobserved 'resolved' resonances as in the IRDFF file of Ref. [252]. In addition, it resulted in a better agreement between calculated and experimental results of lead slowing-down experiments (Ref. [253]). The sum of the p- and d-wave contribution to the capture cross section at the 2-keV boundary of the RRR was estimated to be 86 mb or about 2%. This estimation was based on the average parameters resulting from the URR evaluation. To match the capture cross section at the boundary between the RRR and URR, a smoothly increasing background cross section was introduced from thermal energy to 2 keV as compensation for the missing p- and d-waves. This procedure is similar to the one used in the IRDFF file [252]. Parameters of the negative resonance with $J = 2$ were adjusted to reproduce both the thermal capture cross ection $\sigma_\gamma = 98.67(10)$ b by Holden and Holden [254] and the bound coherent scattering length $b_c = 7.9\ (7)$ fm by Koester et al. [65]. The value of Holden and Holden [254] is also adopted in the 2009 standards file of Carlson et al. [27]. The corresponding calculated cross sections at thermal energy together with some resonance integrals are summarised in the file description.

The evaluation of the URR between 2 keV and 100 keV is based on a generalised single-level representation compatible with the energy-dependent option of the ENDF-6 format as described in Ref. [258]. The average partial cross sections are expressed in terms of transmission coefficients by applying the Hauser–Feshbach statistical reaction theory including width fluctuations. The transmission coefficients and the scattering radius were deduced from a combined analysis of the capture cross section resulting from the standards evaluation project [27] and theoretical non-fluctuating cross sections derived from a dispersive coupled channel optical model [70]. The parameters at zero energy used to describe the average total and partial cross sections were: a hard-sphere scattering radius independent from the orbital angular momentum ℓ; neutron strength functions for s-, p- and d-wave ($\ell = 0$, 1 and 2) and capture transmission coefficients for positive and negative parity. The neutron strength functions and scattering radius were adjusted to reproduce both the compound formation cross sections and the shape elastic cross section of the dispersive coupled channel optical model (DCCOM) potential RIPL1483 derived by Capote et al. [70]. The DCCOM smooth and weak energy dependence at energies below 100 keV were approximated by second order polynomials. The coupled-channel OPTMAN code [95,259] incorporated into the EMPIRE system [102] was used for the optical model calculations. The capture transmission coefficients at zero energy were adjusted by fitting to the capture cross section recommended by Carlson et al. [27]. This cross section, which resulted from international cooperative efforts of the IAEA, NEA, and CSEWG to improve cross section standards for neutron induced reactions, was based on a simultaneous analysis of data from 62 experiments that are specified in Refs. [27,260]. The evaluated average parameters together with their relative uncertainty and correlation matrix are reported in the description of the library file. The covariance matrix was calculated for the present ENDF-6 convention supposing a zero uncertainty for the scattering radius. A small background capture cross section was introduced between 3.75 keV and 11.75 keV to make the capture cross section in this energy region identical to the one of Carslon et al. [27].

The total cross section from 5 to 20 keV in ENDF/B-VII.1 is substantially (up to 15%) lower than the results of the DCCOM and the present evaluation. This is mainly due to the fact that the cross section in ENDF/B-VII.1 is largely based on the data by Seth et al. [255] and disregard the data by Purtov et al. [256]. Measures were taken in the URR to reduce the non-Hauser–Feshbach processing for the J^π-sequences $(1^+, 2^+)$ of double-orbital contribution. The flexibility of the ENDF-6 format was used to achieve this goal. As known, the above short-coming is due to the ENDF-6 simplifying (but anti-Hauser–Feshbach) assumption for orbital momentum conservation. The latter removes the competition e.g. of the s-wave elastic channel for the above d-wave reactions. The effect for gold at 100 keV reaches an increase of 10% in the capture cross section. To solve the problem, a reduction and adjustment of the corresponding d-wave contribution was used. The total cross section remains intact in such a procedure, so that the elastic cross sections is also corrected. The results were compared making use of a URR code that can process with and without the assumption for ℓ-conservation.

The results of the present evaluation were validated by a comparison with results of transmission [253] and capture [257] experiments carried out at the time-of-flight facility

GELINA. The results of these experiments were not included in the present evaluation. The good agreement between the experimental and evaluated data in the URR is shown in Fig. 38, for the total and capture cross section. The capture cross section resulting from the latest neutron standards evaluation reported by Carlson et al. [40], which included the data of Massimi et alo. [257], is also shown in Fig. 38. In addition, ACE files were produced to compare results of Monte Carlo simulations using the MCNP-5 code [72] and results of measurements with a lead slowing-down spectrometer carried out by Perrot et al. [261]. Also this comparison shows a good agreement between the cross section data in JEFF-3.3 and the experimental results. A more detailed discussion on this validation exercise can be found in Reference [253].

2.2.14 Lead

The neutron transport sublibraries for ^{204,206,207,208}Pb of JENDL-4 were adopted in JEFF-3.3. Above the resonance region modifications were made to the inelastic cross sections due to experimental data reported in Refs. [178,262]. The choice of JENDL-4 is based on a study of nuclear data relevant for MYRRHA as part of the CHANDA project. The quality of the data recommended in independent versions of the main data libraries, i.e. CENDL, ENDF, JENDL, JEFF and TENDL, was verified using energy dependent microscopic cross section data and results of integral measurements including lead slowing down and integral benchmark experiments.

The inelastic scattering cross sections in JENDL-4 were modified for ^{206,207,208}Pb on the basis of time-of-flight data taken at the GELINA facility of the JRC Geel, i.e. data for ^{207,208}Pb reported by Mihailescu et al. [262] and those for ^{206}Pb reported by Negret et al. [178]. The data of Mihailescu et al. [262] were renormalized according to the procedure described in Ref. [178] and as detailed in the respective EXFOR entries [179]. For ^{206}Pb the cross sections of Reference [178] were adopted up to 3.1 MeV for levels 1,3-10. For ^{207}Pb the cross sections from Mihailescu et al. [263] were taken for levels 1-2,4-6 and 8 up to 3.2 MeV and for ^{208}Pb the levels 1-3 up to 4.1 MeV. From these maximum energies to 20 MeV a linear factor was used to multiply the JENDL-4.0 evaluation for each affected level to ensure continuity at the transition energy and no correction above 20 MeV. The total cross section of JENDL-4.0 was left unchanged by modifying the elastic cross section to respect the sum rule.

2.2.15 Bismuth

A study of cross section data for neutron interactions with Bi was part of the CHANDA project. Similar to the evaluations for the Pb isotopes, the JEFF-3.3 file for ^{209}Bi was created using JENDL-4.0 as a basis and by including modifications based on results of inelastic scattering cross section measurements by Mihailescu et al. [264] at GELINA. The time-of-flight data for level inelastic cross sections of [264] were used to replace the cross sections for the levels 1-11 up to 4 MeV. The data were renormalised following the same procedure as the one applied for the Pb isotopes.

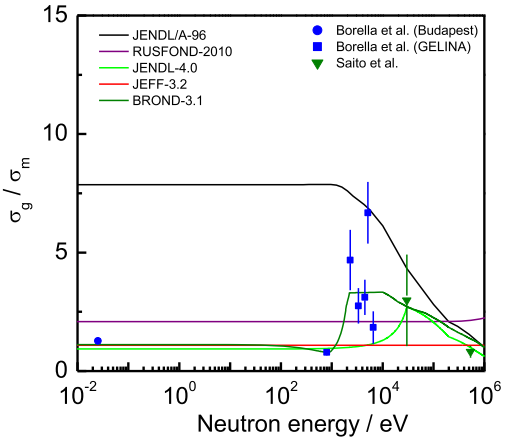

Fig. 39 Comparison of the branching ratio BR=σ_γ/σ_m of the capture cross section to the ground state ^{209}Bi(n, γ)^{210g}Bi and to the isomeric state ^{209}Bi(n, γ)^{210m}Bi as a function of incident neutron energy. The ratios resulting from measurements of Refs. [265,266] are compared with the ratios derived from the evaluated cross sections in the JENDL-4.0, JEFF-3.2, BROND-3.1, JENDL/A-96 and ROSFOND-2010 libraries

Neutron capture on ^{209}Bi leads to the formation of ^{210}Po through the decay of ^{209}Bi in its ground state. Since ^{210}Po is a highly radiotoxic nuclide, it is an important contribution of the radioactive source term of a LBE coolant. To predict the production of ^{210}Po the branching ratio BR $= \sigma_\gamma/\sigma_m$), i.e. the ratio of the cross section σ_γ for production of the ground state ^{210g}Bi to the cross section σ_m for production of the isomeric state ^{210m}Bi, is required. Unfortunately, the energy dependence of this BR is difficult to measure. Experimental data that can be used to evaluate this ratio above thermal energy are limited to the results of activation measurements at 30 keV and 534 keV by Saito et al. [265], and measurements by Borella et al. [267] at GELINA. The BR derived from these experimental data together with the one derived from measurements at the cold neutron beam of the research reactor in Budapest [266] are plotted as a function of energy in fig. 39. The BR obtained from ^{209}Bi(n, γ) cross sections in the JENDL-4.0, JEFF-3.2, BROND-3.1, JENDL/A-96 and ROSFOND-2010 files are also shown.

At low energies, the BR in JENDL-4.0, JEFF-3.2 and BROND-3.1 are consistent with the experimental value determined in Ref. [266]. The BR from the JENDL/A-96 and ROSFOND-2010 files are larger by a factor 6.7 and 1.8, respectively. In general the best agreement between experimental and evaluated BR is obtained with the BROND-3.1

data. Therefore, this BR that has not been included in JEFF-3.3 file for ^{209}Bi is recommended for future JEFF-4.0 evaluation. Nevertheless, to reduce the uncertainty on the estimated production of ^{210}Po additional experimental data of the energy dependent BR are required. In addition, results obtained within the CHANDA project reveal that both the total and capture cross sections of ^{209}Bi can be improved by new TOF cross section measurements.

2.3 Use of TALYS and TENDL

In its latest release, the JEFF library uses 312 TENDL-2015 evaluations for the neutron sub-library. This is not a unique step in the recent JEFF history, as the JEFF-3.2 library already used about 150 evaluations from TENDL-2012. Additionally, the complete charged-particle and photon sub-libraries from TENDL-2017 are also adopted in JEFF-3.3 and the JEFF-3.3 neutron activation sub-library corresponds to TENDL-2017 neutron sub-library produced in the European Activation File (EAF) format. Details about these evaluations are given below.

2.3.1 The TENDL environment

A short description of the TENDL methodology will be presented here. For further details, see the different references proposed in this section.

TENDL stands for the "Talys Evaluated Nuclear Data Library" and it has been produced since 2008. In its early versions, it was largely based on the TALYS nuclear reaction code [43] and the TEFAL data parsing program. Over the years, the TENDL production relied on additional codes, such as TASMAN (for the production of random model parameters), TARES (for the resonance range), TAFIS (for the number of fission neutrons $\overline{\nu}$ and fission yields) and TANES (for the prompt fission spectra). These six programs (all starting with a "T") are simply named T6 and are driven by the wrapping script "*autotalys*", allowing to produce the full TENDL library.

Additional databases are used within T6 by the different programs. One such database contains all the necessary model parameters to produce the adequate nuclear data quantities. The adjustment of such model parameters, as for any other evaluation work, represents the traditional evaluation effort. All the other aspects, including the formatting, checking and processing, are taken care of by the T6 system. In some regards, TENDL can be seen as an output database of the T6 system.

A special feature of the T6 system of particular help in the evaluation process is referred to as "*autonorming*". In the TENDL evaluation process, the evaluator first adjusts the different model parameters (as for TALYS), in order to reproduce the desired experimental data. In some cases, the different models do not have the required flexibility, possibly due to theoretical shortcomings. A solution is then to calculate the ratio between the desired cross section and the calculated cross sections, and to multiply all related quantities by this ratio. In this way, the desired cross sections are obtained, together will the other quantities such as angular or energy distributions.

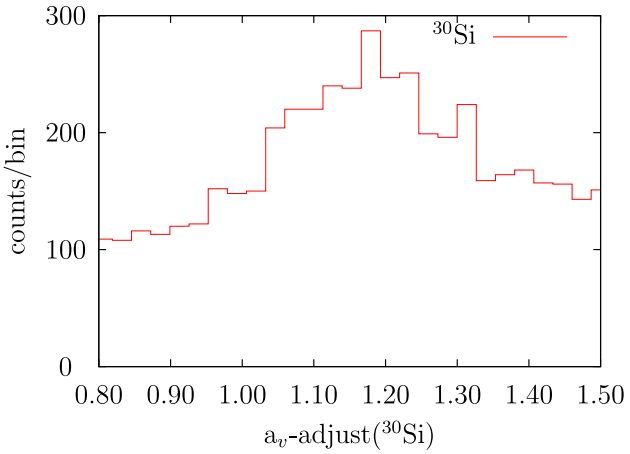

Fig. 40 Example of the posterior parameter distribution obtained with the TENDL Bayesian Monte Carlo method (BMC) for the optical model parameter a_v of ^{30}Si. The prior distribution, not shown here, is uniform

The TASMAN code can generate sampled model parameters to provide varied inputs that simulate the space of possible evaluations based on our understanding of the input parameters and their uncertainties. This code is used for the generation of the covariance matrices using a Monte Carlo approach. Before 2015, all model parameters were sampled using un-correlated multi-variate Gaussian distributions. The widths of such distributions were chosen so that selected experimental data from the EXFOR database were covered by the random cross sections obtained from the use of random parameters (see Ref. [268] for details). From 2015 a different method is used, known as the Bayesian Monte Carlo (BMC) approach (see Refs. [269–271] for details). This is a two-step approach where the model parameters are first sampled in an independent and uniform manner, with a relatively large standard deviation – typically 5 times larger than the normally adopted value. A comparison with selected experimental differential cross sections is performed and each random realisation is weighted according to its agreement with the experimental values. A weighted distribution is then obtained for each model parameter, reflecting the experimental data information. An example is presented in Fig. 40 for the optical model parameter a_v of ^{30}Si.

In a second step, a sampling based on the posterior parameter distributions is done to generate the TENDL random cross sections. In this way covariance matrices can be obtained from calculating the moments associated with these sam-

ples. They are formatted with TEFAL in the MF33 format and added to the nominal TENDL file.[4]

In the resonance range, a different approach is followed. The cross sections are not represented in a pointwise format, but rather with resonance parameters, following the MF2 format. The following steps are followed:

- resonance parameters are obtained from compilations or experimental databases;
- uncertainties for the bound levels and the low energy resonance are estimated to reproduce the thermal cross section uncertainties;
- such parameters and their uncertainties are used by SAMMY and the retroactive method to generate a complete parameter covariance matrix, as well as a cross section covariance matrix; and
- these matrices, in the MF32 or MF33 format are included in the TENDL nominal file.

Up to (and including) the TENDL-2015 version, the MF32 data is calculated and stored in the resonance range. Starting from the 2017 TENDL version, the MF33 format is used in the resonance range, merged with the MF33 file coming from the fast energy range, allowing to use cross section covariances over the entire energy range. In general, TENDL evaluations contain MF31-35 and MF40 for various types of covariance data.

In the following, specific details for each sub-library adopted in JEFF-3.3 are presented.

2.3.2 *Neutron files*

As mentioned, a total of 312 TENDL-2015 evaluations were adopted in JEFF-3.3. The complete list is too long to be given here, but some representative examples are presented in the following.

Stable isotopes

The majority of the adopted TENDL files are not for stable isotopes, although for 111 stables isotopes listed in Table 18 TENDL-2015 was adopted. These isotopes were either not present in the previous JEFF releases, or were present in the form of very incomplete evaluations (e.g. only cross sections were given, without the so-called MF6, or gamma production data). These TENDL evaluations allow JEFF-3.3 to globally bring a uniform and complete format. An example of improvements from JEFF-3.2 to JEFF-3.3 are presented in Fig. 41 for a specific stable isotope.

Table 18 The 111 stable nuclide evaluations from TENDL adopted in the JEFF-3.3 neutron sub-library

Nuclides
^{17,18}O, ^{20,21,22}Ne, ^{31}P, ^{32,33,34,36}S, ^{36,38}Ar, ^{39,41}K,
^{40,42,43,44,46}Ca, ^{45}Sc, $^{46-50}$Ti, ^{51}V, $^{64,66-68,70}$Zn
^{69,71}Ga, ^{75}As, $^{74,76-78,80}$Se, ^{79,81}Br,
$^{80,82-84,86}$Kr, ^{85}Rb, $^{84,86-88}$Sr, ^{93}Nb, ^{100,101}Ru,
^{102,110}Pd, ^{107}Ag, ^{122,124}Sn, ^{120,122,124,126}Te,
^{124,126,131}Xe, ^{136,138,140}Ce, ^{142,143,145}Nd, ^{150,152}Sm,
^{156,158,160,164}Dy, $^{166-168,170}$Er, ^{169}Tm,
$^{168,170-174,176}$Yb, ^{175}Lu, ^{180m}Ta, ^{185}Re,
$^{184,187-190,192}$Os, $^{192,194-196,198}$Pt,
$^{198-202}$Hg and ^{203,205}Tl

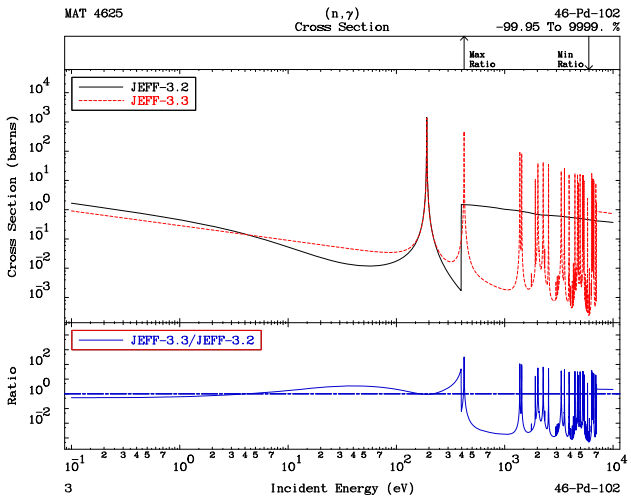

Fig. 41 Example of the new evaluated capture cross section for the ^{102}Pd stable isotope from TENDL

Filling the gaps

Many TENDL-2015 isotopes adopted in JEFF-3.3 are long-lived isotopes, allowing to provide a full isotopic chain for specific elements, complemented with original JEFF evaluations or evaluations adopted from other libraries. This is of importance for activation calculations, as demonstrated in Ref. [273]. Due to the TENDL data, more complete chains can be found for C, O, Si, P, S, Cl, Ar, Ca or Sc, amongst others. Isotopes from TENDL have been adopted so that at least all isotopes with a half life longer than 1 year are now in JEFF. For many of these isotopes, experimental data are relatively scarce, and the evaluations heavily rely on default TALYS calculations in the fast neutron range and on systematics in the resonance range. In the resonance range, the

[4] Nuclear data libraries are stored in files in the ENDF format. This format is fully described in Ref. [272]. MF2 is the section where resonance range information is stored, the MF3 section stores tabulated cross sections. MF32 and MF33 are the accompanying sections storing the covariance information for resonance parameters and tabulated cross sections. MF4 and MF5 store angular distributions and double diferential cross sections and yields and MF34 and MF35 are the corresponding covariance sections. MF40 stores covariances for radionuclide production data.

so-called High Fidelity Resonance (HFR) method is applied, producing statistically-generated resonances where no measurement exists [274]. The HFR approach utilises average resonance parameters from TALYS calculations extended to the low energy region. Such parameters can either be formatted using the unresolved formalism, or used to generate one set of resonances calculated from statistical sampling of these parameters. Such resonances are then adjusted to reproduce thermal cross sections from a systematics developed for the EAF library [275]. It also allows TENDL to reach consistency between the low and high energy range, as the TALYS parameters are used from 0 to 200 MeV. The prediction of thermal cross sections is almost impossible, due to the fact that only a very limited number of resonances determines these values and thus no statistical assumption can be applied. However, in spite of the expected very large uncertainty in these predictions, they account at least for the global trends. Starting from the expression for the average capture cross section in the statistical region, after several simplifications, the parameterised formula

$$\sigma_{\mathrm{th}}(n,\gamma) = C \times (a \times U)^{x} \tag{2}$$

can be used to fit the constants C and x to the measured data. U is the effective excitation energy defined as the neutron separation energy minus the pairing energy, and a is the level density parameter. The application of this approach at 30 keV is generally justified, however, at thermal energy the influence of the resonance region on the cross section value is dominant and any dependence on $a \times U$ is masked by large Porter-Thomas fluctuations. Nevertheless, a least square fit was applied to the thermal cross section data. In the case of the fission cross section, we use $\sigma_{\mathrm{th}}(n,f) = \sigma_{\mathrm{th}}(n,\gamma)/(A^2/15930)$ for non-fissile nuclei, and $\sigma_{\mathrm{th}}(n,f) = \sigma_{\mathrm{th}}(n,\gamma) \times (A^2/1593)$ for the other ones. An example for the capture cross section of ^{58}Co is presented in Fig. 42, showing the improvement in the resonance range compared to the JEFF-3.2 library.

Meta-stable states

The final category for the isotopes coming from the TENDL-2015 library concerns the evaluations for reactions on the relatively long-lived isomeric states as targets. These were relatively few in number in the JEFF-3.2 library (12, from which 4 came from TENDL-2012), and are still limited in JEFF-3.3 with 16 evaluations. Among these 16, 12 evaluations come from TENDL-2015: ^{58m}Co, ^{62m}Co, ^{84m}Nb, ^{106m}Ag, ^{127m,129m,131m}Te, ^{135m}Xe, ^{148m}Pm, ^{152m}Eu, ^{166m}Ho and ^{180m}Ta. For these isotopes, a limited amount of measurements are usually available, and the same approach as for the previous category is applied. If the thermal capture cross section is not known, a similar systematics as in Eq. (2) is used,

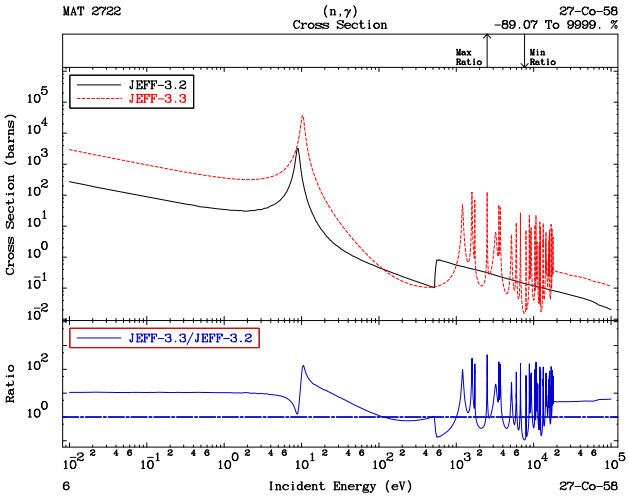

Fig. 42 Example of the new evaluated capture cross section for the short-lived ^{58}Co isotope ($t_{1/2}$ = 70 days) from TENDL

multiplied by the ratio of the average radiation width of the isomer over the one for the ground state.

2.3.3 Photon and charged particle sub-libraries

Following the same approach as for the neutron sub-library, charged particle induced evaluations are produced with TALYS. JEFF-3.3 takes advantage of the TENDL-2017 data (not 2015) by adopting the entire sub-libraries for incident protons, deuterons, helions, tritons, alphas and gammas. In total, there are 2804 proton evaluations, 2811 deuteron evaluations, 2805 triton evaluations, 2806 He3 evaluations, 2809 alpha evaluations and 2809 gamma evaluations. To compensate for the weakness of the TALYS models for the light elements, a number of isotopic evaluations are imported from the ENDF/B-VIII library and are replacing the original TALYS files. These include all the isotopes below ^{19}F which are included in ENDF/B-VIII [180].

Covariance matrices based on a simple Monte Carlo approach are included for proton and gamma induced reactions. The applied procedure is not the BMC method, but a simple variation of all input parameters using default input parameter distributions.

2.4 Gamma emission

2.4.1 Fission products

In 2011, a study was undertaken to provide gamma production data for 89 major fission products. The optimal solution would be to automatically adopt all available data from EGAF [276], but this feature has not yet been added to the TENDL library. Instead, for all 89 nuclides capture gamma

data from the TENDL-2011 evaluated library replaced the existing capture gamma data, with cross-section data taken from either JEFF-3.1.1 or ENDF/B-VII.0. This implies that the capture gamma-rays are obtained from a TALYS calculation combining continuum and discrete level decay as described in Ref. [43]. These fission product files were released in JEFF-3.1.2 and retained for JEFF-3.2.

For JEFF-3.3, new or updated evaluations have been adopted for many of the 89 fission products and a significant number of these did not include gamma production data. It was necessary to reinstate the gamma production data for these nuclides. This was done by following the methodology of the earlier study by adopting gamma production data from the TENDL library. For JEFF-3.3, the required data were taken TENDL-2015.

There were two classes of nuclides for which the gamma production data needed to be reinstated. The first included those nuclides for which there were no capture gamma data in the evaluations adopted for JEFF-3.3. The nuclides in this class were Ru-102, Ru-103, Ru-104, Pd-107, I-131, I-135, Xe-130, Xe-132, Xe-134, Xe-136, Ba-134, La-139, Ce-141, Pr-143, Pm-148m, Eu-154 and Eu-155.

The second set were nuclides for which the evaluated files contained capture gamma data but as continuum spectra only, with no discrete gamma lines. For the majority of these, the files were taken from ENDF/B-VII.1 and the gamma data were unchanged from the ENDF/B-VII.0 data that were considered in the original study. Thus, the original decision, to replace the gamma data for these files, was still valid. For these nuclides, the existing MF6/MT102 data were replaced by discrete data taken from TENDL-2015. The nuclides in this class were; Y-89, Zr-93, Mo-95, Pd-104, Pd-105, Pd-106, Pd-108, Cs-133, Cs-135, Pr-141, Nd-144, Nd-146, Nd-147, Pm-149, Pm-151, Sm-144, Sm-148, Sm-149, Sm-153, Sm-154, Eu-157, Dy-161, Dy-162 and Dy-163.

For the remainder of the 89 fission product nuclides, gamma production data were already present in the evaluated files adopted for JEFF-3.3 and no update was necessary. These again fell into two sets. The first, covered nuclides that were either unchanged from JEFF-3.2, adopted from TENDL-2015 or were new evaluations that included discrete capture gamma data. The nuclides in this set were; Zr-91, Zr-95, Zr-96, Tc-99, Ru-105, Rh-103, Ag-109, I-127, I-129, Xe-135, Pm-147, Pm-148, Gd-155, Gd-156, Gd-157, Gd-158, Cd-110, Cd-111, Cd-113, Kr-83, Ru-100, Ru-101, Rh-105, Xe-131, Cs-134, Cs-137, Nd-143, Nd-145, Nd-148, Nd-150, Sm-147, Sm-150, Sm-151, Sm-152, Eu-153, Eu-156 and Tb-159.

The final set were files that were adopted from JENDL-4.0 evaluations that contained gamma data only for the total non-elastic reaction and not for individual reactions. As the capture component could not be isolated in these data, the choice was either to retain the existing JENDL-4.0 gamma data or replace all the gamma data with MF6 MT102 data taken from TENDL-2015. The decision was taken to retain the JENDL-4.0 gamma data as the alternative involved the loss of some data. The nuclides in this set were; Nb-95, Mo-96, Mo-97, Mo-98, Mo-100, In-113, In-115, Xe-128, Xe-129, Xe-133, Ce-142 and Ce-144.

2.4.2 TALYS and EGAF

Gamma emission evaluations for neutron radiative capture by ^{54,56,56,58}Fe, ^{107,109}Ag, ^{113,115}In, ^{113}Cd, ^{155,157}Gd, ^{174,177,178,179,180}Hf were made combining TALYS calculations with the discrete gamma-rays from the EGAF database. These were included in JEFF-3.2. They were taken over in JEFF-3.3 except for ^{107}Ag and ^{113,115}In for which other evaluations were adopted (TENDL-2015 and JENDL-4). The evaluations correct major deficiencies in total gamma-energy release for predecessors of JEFF-3.2. Above 1 keV incident neutron energy the evaluated file sections were entirely made with the TALYS code. The default composite Gilbert-Cameron model was used for the level density model and the default Kopecky-Uhl model for the gamma-ray strength function [5,43]. Below a neutron energy of 1 keV use was made of the Evaluated Gamma-ray Activation File (EGAF [276]) to include an evaluated set of experimentally determined discrete gamma-rays. These were judiciously combined with estimates for the continuum contribution made with TALYS. For the iron nuclides the discrete data were so complete that a continuum contribution was not needed (it would be redundant). Even when the continuum contribution was dominant, such as for silver and hafnium, important corrections result from including the discrete gamma-rays from EGAF. The gamma emission data were stored in the MF6/MT102 section.

2.4.3 Prompt fission gammas

Motivation for new evaluations

For several years and following the request from the High Priority Request List (HPRL) [277], significant efforts have been made by the community of experimenters to improve our knowledge of the prompt fission gamma characteristics (spectra, multiplicities and energies). These characteristics are very important for the modeling of current and innovative reactors. According to Rimpault et al. and Luthi et al. [278,279], the γ-heating in the center of a typical fast reactor core comes from several components:

- 20% from the γ produced in radiative capture;
- 10% from the inelastic scattering reactions;
- 30% from the delayed γ produced by fission products; and
- 40% from the prompt γ emitted by fission fragments.

Table 19 Survey of the experimental data for the four n-induced fission reactions investigated for JEFF-3.3: the average γ-ray multiplicity ($\langle M_\gamma \rangle$), the mean photon energy ($\langle \epsilon_\gamma \rangle$) and the average total γ-energy released ($\langle E_\gamma \rangle$). N is the target nucleus and E_n the incident neutron energy (T for thermal and F for 2.4 MeV). T_w corresponds to the coincidence time used during the experiment

N	E_n	T_w (ns)	$\langle M_\gamma \rangle$	$\langle \epsilon_\gamma \rangle$ (MeV)	$\langle E_\gamma \rangle$ (MeV)
^{235}U [280]	T	5	8.19(11)	0.85(2)	6.92(09)
^{238}U [281,282]	F	2	6.38(19)	0.81(4)	5.15(21)
^{239}Pu [283]	T	3	7.35(12)	0.85(2)	6.27(11)
^{241}Pu [284]	T	3	8.21(09)	0.78(1)	6.41(06)

The first three components are rather well known, while the fourth is poorly known. In the previous JEFF evaluated nuclear data files (JEF-2.2, JEFF-3.1.1, JEFF-3.1 and JEFF-3.2), evaluations of both Prompt Fission Gamma Spectra (PFGS) and Prompt Fission Gamma Multiplicities (PFGM) were based on measurements from the 1970s. In addition, PFGS was not given for the ^{241}Pu(n,f) reaction. These may explain the strong observed discrepancies (from 10 to 28%) for C/E ratios in various benchmarks [278,279].

Recent measurements

After about 40 years since the first prompt fission gamma observable measurements related to the reactions ^{235}U(n_{th}, f) [285–287], ^{252}Cf(sf) [285], ^{233}U(n_{th}, f) [288] and ^{239}Pu(n_{th}, f) [285,288], new experimental results are now available thanks to the development of experimental techniques for the gamma detection (as explained in Ref. [289]). In particular, reliable data (see Table 19) obtained for 4 neutron induced fission reactions ^{235}U(n_{th}, f) [280], ^{239}Pu(n_{th}, f) [283], ^{238}U($n_{2.4MeV}$, f) [281,282] and ^{241}Pu(n_{th}, f) [284]) were used for a re-evaluation of the PFGS and PFGM in JEFF-3.3.

Each measurement is characterised among others by a low and high gamma detection thresholds ([E_l-E_h]) and by a time window (T_w) corresponding to the coincidence time between the fission fragment detection and the prompt gamma detection. In Table 19, E_l = 0.1 MeV and E_h = 6 MeV (7 MeV for ^{239}Pu). As discussed later on, these experimental conditions are important for the simulation with the de-excitation Monte Carlo codes.

Advanced modeling of prompt fission γ-ray emission

Parallel to improvement of experimental technique, new computer codes were developed aiming at predicting characteristics of both prompt neutrons and prompt gamma [290–293]. In the context of a new evaluation of the PFGS and PFGM for the JEFF-3.3 library, we have decided to use the code FIFRELIN. In this code, the de-excitations of the fission fragments are simulated from statistical Hauser–Feshbach model [294], following Becvar's procedure [295]. It accounts for the competition between neutron and gamma emission as well as for the conservation of energy, spin and parity of the initial and final states. Note that conversion electrons emission is also taken into account. All the details related to the code can be found in Refs. [293,296,297]. The reference case of ^{252}Cf(sf) has been chosen to validate our calculation scheme. The PFGS calculated with FIFRELIN is then compared to the experimental data obtained by Bilnert et al. [298] in Fig. 43.

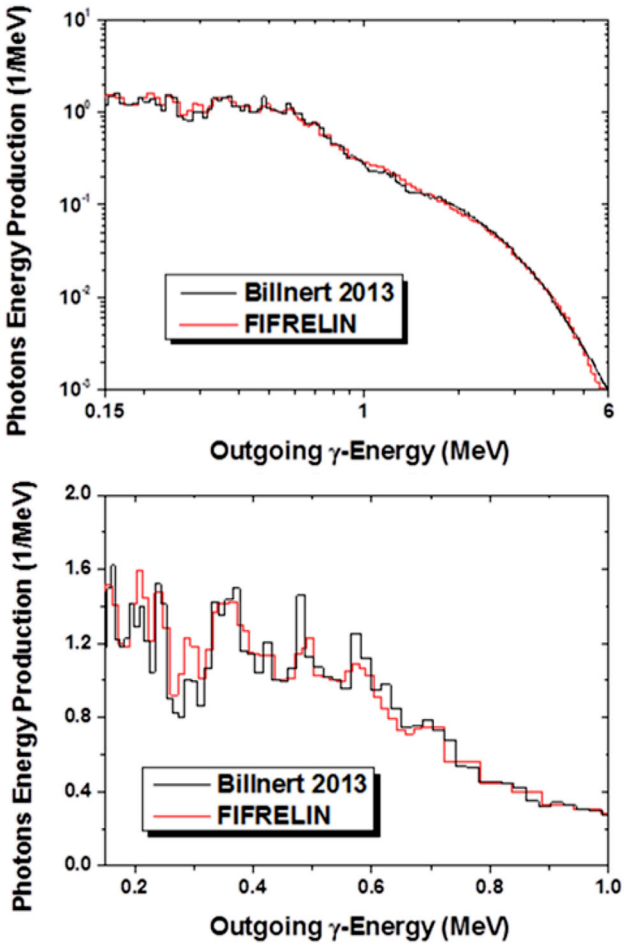

Fig. 43 PFGS measured by Bilnert [298] for ^{252}Cf(sf) (black line) compared to FIFRELIN calculation (red line). The calculation is normalised to the experimental γ-multiplicity in [140 keV–10 MeV] γ-energy range. In order to see the whole spectra, a log-log scale is used (top), while to enlighten structures below 1 MeV, a lin-lin scale is chosen (bottom)

The calculation is normalised to the average measured γ-multiplicity ($\langle M\gamma \rangle$ = 8.14) in the [140 keV–10 MeV]

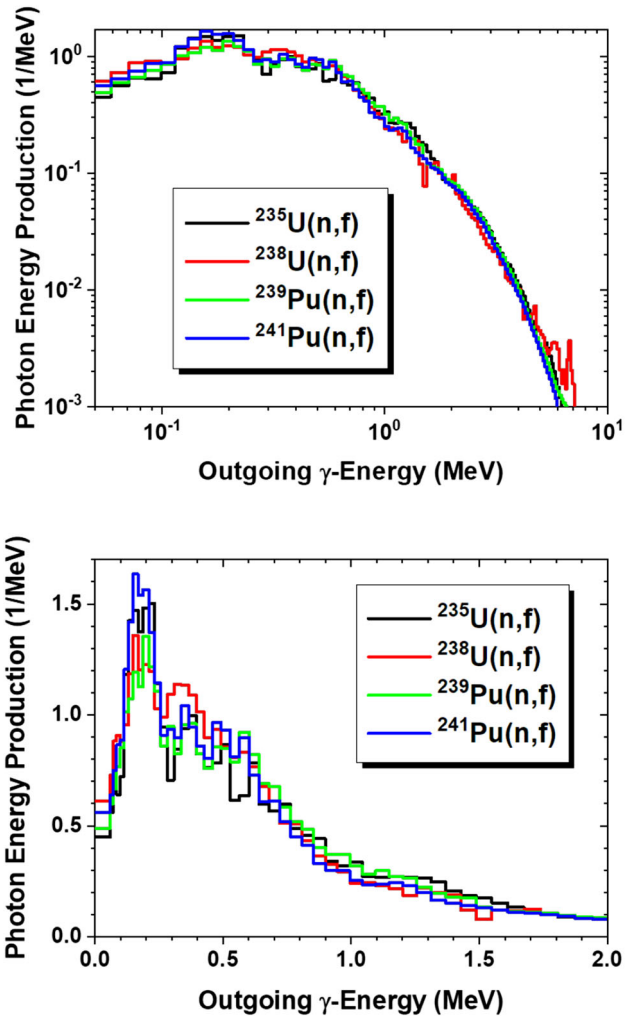

Fig. 44 Evaluations of the PFGS adopted in JEFF-3.3. In order to see the whole spectra, a log-log scale is used (top), while to enlighten structures below 1MeV, a lin-lin scale is chosen (bottom)

γ-energy range. It can be observed that the shape of the PFGS is nicely reproduced as well as the structures of the spectrum which are visible below 1 MeV. This nice result is partly obtained thanks to the coupling between FIFRELIN and RIPL3 reference input parameter library [70] which provides the nuclear level scheme at low energy (the scheme being completed at higher energy by FIFRELIN).

Prompt fission gamma spectra/multiplicities

The strategy for the PFGS evaluations in JEFF-3.3 is to adopt the experimental results and to complete them (below E_l and above E_h) by a FIFRELIN calculation normalised to the experimental average γ-multiplicity (Table 19). Results obtained in this way for the 4 neutron-induced fission reactions are shown in Fig. 44.

All spectra are defined on the same energy grid and are re-normalised to 1 as requested in evaluated nuclear data libraries. Lastly, due to the lack of data, PFGS in JEFF-3.3 are assumed to be independent of the incident neutron energy. The average γ-multiplicity over the whole γ-energy range can be deduced and are given in Table 20. A comparison between the PFGS evaluations in JEFF-3.1.1 and JEFF-3.3 libraries for ^{235}U and ^{238}U can be seen in Fig. 45.

The dependence of the average PFGM ($\langle M_\gamma \rangle$) with the incident neutron energy E_n is calculated from an empirical law proposed by Oberstedt [299]:

Table 20 Survey of the average prompt fission gamma multiplicities (PFGM) at thermal incident neutron energy ($\langle M_\gamma(E_{th}) \rangle$) adopted in JEFF-3.3 for the four investigated (n,f) reactions. Values from previous JEFF evaluated nuclear data files are also given

	JEF-2.2	JEFF-3.1.1	JEFF-3.2	JEFF-3.3
^{235}U	7.04	7.17	7.04	8.74(12)
^{238}U	8.18	8.18	8.18	7.49(22)
^{239}Pu	7.78	Not given	7.78	7.89(13)
^{241}Pu	Not given	Not given	Not given	8.90(10)

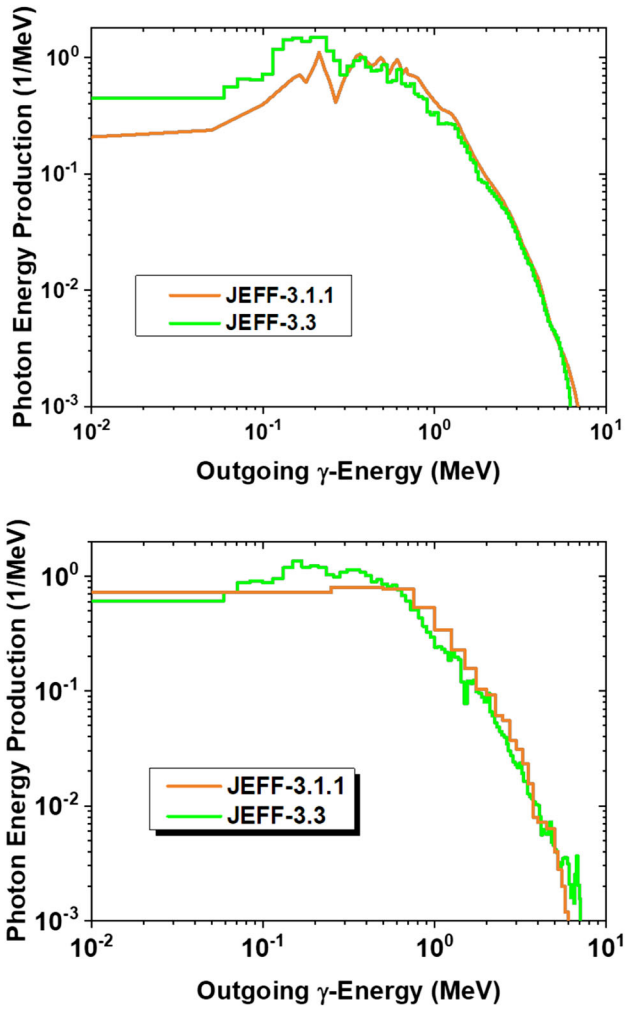

Fig. 45 Comparison between JEFF-3.1.1 (black line) and JEFF-3.3 (red line) PFGS evaluations for ^{235}U(n,f) (top) and ^{238}U(n,f) (bottom) reactions

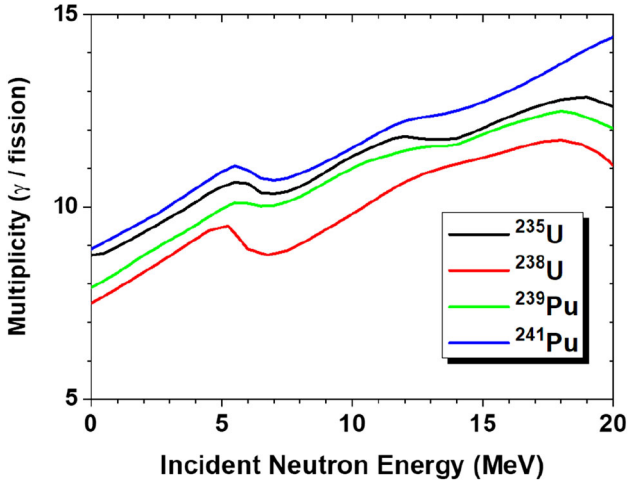

Fig. 46 Evaluations of the PFGM as a function of the incident neutron energy (adopted in JEFF-3.3)

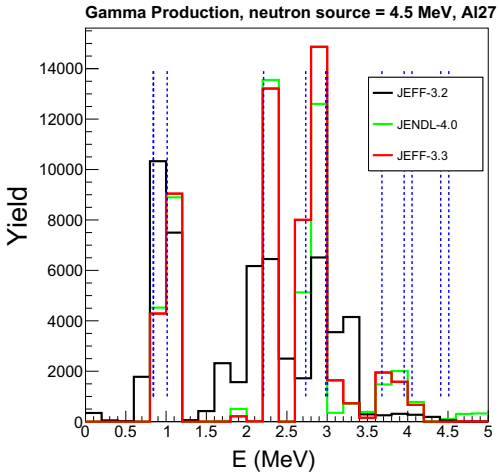

Fig. 47 Monte-Carlo simulations of gamma spectra from Al-27 inelastic scattering with 4.5 MeV neutrons, with excited level energies of Al-27 shown in blue

$$\langle M_\gamma(E_n)\rangle = \langle M_\gamma(E_{th})\rangle + (C_0 + C_1 Z^{5/3} A^{-1/2})(\langle \nu_P^{corr}(E_n)\rangle - \langle \nu_P^{corr}(E_{th})\rangle) \quad (3)$$

where $\langle \nu_P^{corr}(E_n)\rangle$ is the average prompt fission neutron multiplicity, Z and A are the nuclear charge and mass of the compound nucleus. The C_0 and C_1 constants were obtained from a fit of experimental data: $C_0 = 16.6 \pm 0.5$; $C_1 = -(11.0 \pm 0.4) \times 10^{-2}$. The average PFGM at thermal energy ($\langle M_\gamma(E_{th})\rangle$) is taken from Table 20. The corrected average prompt fission neutron multiplicity $\langle \nu_P^{corr}(E_n)\rangle$ is calculated by removing from the total prompt neutron multiplicity $\langle \nu_P(E_n)\rangle$ the contribution of neutrons emitted prior to fission:

$$\langle \nu_P^{corr}\rangle = \frac{\langle \nu_P\rangle \sigma_{n,f} + (\langle \nu_P\rangle - 1)\sigma_{n,n'f} + (\langle \nu_P\rangle - 2)\sigma_{n,2n'f}}{\sigma_{n,f} + \sigma_{n,n'f} + \sigma_{n,2n'f}} \quad (4)$$

where $\sigma_{n,f}$, $\sigma_{n,n'f}$ and $\sigma_{n,2n'f}$ correspond to the first, second and third fission chance cross-sections respectively. All the quantities needed for the $\langle \nu_P^{corr}(E_n)\rangle$ calculation are taken from JEFF-3.1.1. Evaluations of the PFGM for the four neutron-induced fission reactions are shown in Fig. 46.

Up to now, γ-heating calculations have not yet been performed with the new PFGS and PFGM adopted in JEFF-3.3. In view of their average γ-energies and multiplicities, it seems that JEFF-3.3 will not be able to correct for the significant underestimation of the total γ-heating observed in various benchmarks. Nevertheless, since γ-spectrum shapes are also very important, these calculations have to be done.

2.4.4 Inelastic scattering photon correlations

Discrete inelastic scattering produces a nucleus in an excited state that typically returns to its ground state by emitting one or more photons. The ENDF-6 format offers two main options for storing these data. The first option is to use the MF12 format for photon production multiplicities, allowing us to define all the intermediate states of the decay. In this case, it is easy to reconstruct the decay cascade. The second is the use of the double differential format of MF6 for which data on photon production are given in the form of total photon multiplicity and probabilities for each photon in the decay. In this case, the average statistical behavior is respected but it is no longer possible to define the photon decay chain of the excited state.

This offers the ability to generate more accurate gamma spectra from inelastic scattering. This is demonstrated in Fig. 47, where the total energy of the photons emitted event by event for the interaction of 4.5 MeV neutrons in an Al-27 sphere is shown. The results presented are obtained with the libraries JENDL-4.0 (green), JEFF-3.2 (black) and JEFF-3.3 (red). The JEFF-3.3 Al-27 evaluation corresponds to the JEFF-3.2 evaluation corrected for the gamma production of inelastic scatterings. The blue dashed lines indicate the energies of the excited levels of Al-27. We observe the good agreement between JENDL-4.0 and JEFF-3.3. The peaks observed correspond to the energies of the excited states of Al-27. These results are obtained with the Monte-Carlo code TRIPOLI-4®.

We have modified 31 evaluation files to restore these correlations between decay photons, which are very important in the case of analog Monte Carlo simulation.

The general methodology for this work was to:

1. use the SIXPAK module [300] to generate neutron angular distributions (MF4 files) from MF6 Files;
2. use the ENSDF database [301] to define gamma cascade for each excited state in agreement with data used in the evaluated file, including all the excited states describe in MF12; and
3. add new MF4, MF12 and MF14 (photon angular distributions) for discrete inelastic scatterings in a modified evaluation file.

The list of modified evaluation files includes: Al-27, Eu-153, Eu-156, I-127, I-129, In-113, In-115, Mo-92, Mo-94, Mo-96, Mo-97, Mo-98, Nd-148, Pb-206, Pb-207, Pb-208, Pd-104, Pd-106, Pd-108, Rh-103, Sn-112, Sn-114, Sn-115, Sn-116, Sn-117, Sn-118, Sn-119, Sn-120, Xe-128, Xe-129 and Xe-133.

2.5 Covariances

Nuclear data evaluated files are of major interest for fission and fusion applications. Until recently, the performance of existing nuclear data libraries is demonstrated by calculating an exhaustive list of public integral experiment benchmarks (ICSBEP/IRPHE) with complementary validation coming from internal sets of experiments from different participating institutions. This benchmarking allows an estimation of residual biases of nuclear data files. An extensive international work is underway not only to properly quantify these biases but also to evaluate the uncertainties associated with these nuclear data files. These uncertainties express a certain degree of confidence in the use of the nuclear data files for various energy domains and various nuclear data types. A modern general purpose nuclear data library is meant to provide these data for end-users with well estimated and realistic uncertainties.

A covariance working group was proposed in 2013 in the JEFF community with the objectives of defining a work plan for next JEFF Mandates. The strategy is to increase the number of covariance estimations for next JEFF releases, identifying missing data and performing evaluations.

2.5.1 Major isotope list

About 25-30 high priority nuclides were identified as being the major tasks for JEFF releases. Of those, the nuclides in Table 21 were addressed by dedicated efforts for either the JEFF-3.2 or JEFF-3.3 release.

To allow the evaluation of proposed covariances, various tools were provided: testing tools for simple verification (such as for example positive definiteness of matrices), treatment (from parameters or cross sections uncertainty to multigroup cross sections), more elaborate tools quantifying final uncertainty contributions to a limited set of applications (fission, fusion, integral experiments) and, finally, visualisation tools (figure/plots) to allow a simple representation of this type of data.

Table 21 List of isotopes with new covariance data in JEFF-3.3, which were not taken from TENDL files

Coolant	^{23}Na
Structural materials	^{24,25,26}Mg
	^{27}Al, ^{50,52,53,54}Cr, ^{55}Mn,
	^{56}Fe, ^{59}Ni, ^{63,65}Cu
	^{90,91,92,94}Zr, ^{182,183,184,186}W
Fission product	^{103}Rh
Absorbers	^{174,176,177,178,179,180}Hf
Actinides	^{235,238}U, ^{239,240}Pu

2.5.2 JEFF-3.3 covariance data description

In principle, for each evaluated file we should have covariances for all quantities possible. It is not always the case for various reasons, including formatting issues, file size, evaluator choices and technical capability. In JEFF-3.3, 50 files contain MF31 values, 442 files contain at least MF32 or MF33 and 34 files contains MF35 information. For cross section covariances (MF33), various energy group structures were proposed and all processed matrices are block diagonal (blocks for the resonance range and the high energy range) except for ^{23}Na and ^{59}Ni. No cross correlations between different types of data are given, except for cross sections where cross correlation of reactions for one isotope are available. Some formatting issues exist with the ENDF format that do not permit cross correlations between, for example prompt fission neutron spectra, neutron multiplicities and fission cross sections. A general international work is underway to propose a new generic format that may solved this kind of issue within WPEC Subgroup 44 [302].

For neutron induced cross sections covariances are available for the full energy range for ^{23}Na, ^{235,238}U, ^{239,240}Pu, Hf, Co and ^{58,59}Ni. In addition, covariance data for the prompt fission neutron spectrum PFNS and the mean prompt neutron multiplicity from fission $\bar{\nu}$ are now available for ^{235,238}U and ^{239}Pu. The main missing covariance information concerns ^{241}Am neutron induced cross sections and missing official releases of covariances for fission yields, thermal scattering data, delayed neutrons and prompt gamma fission spectra and multiplicities.

To obtain the evaluated covariances, various methods were used by different evaluators, including Bayesian inference based on Monte-Carlo or Generalised Least Square (GLS) algorithms (for example for ^{239}Pu and ^{23}Na). These consist of a comparison of nuclear reaction models to experiments with *a posteriori* parameters and vectors of uncertainties. Other

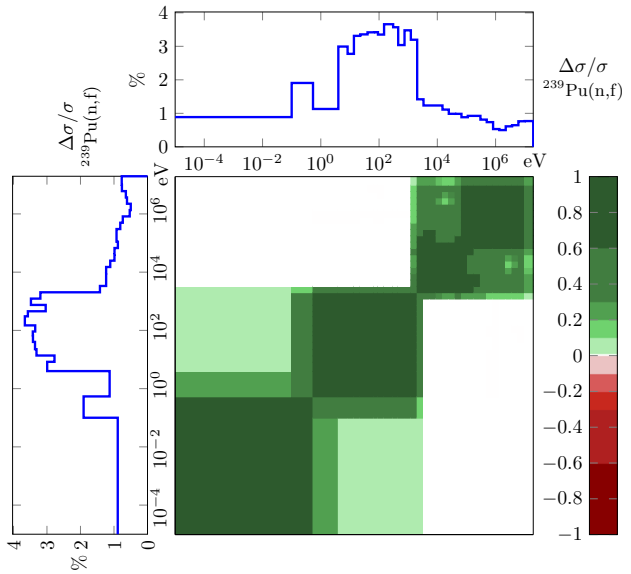

Fig. 48 ^{239}Pu fission multigroup cross section correlations. Energies are in eV, uncertainties in % and cross-sections in barns

Monte-Carlo propagation methods use sampling of initial model parameter distributions with parameter distribution moments adjusted to reproduce experimental uncertainties (example of TENDL covariances and ^{235}U high energy range for cross sections, PFNS and $\bar{\nu}$). The experimental information could have been treated differently, taking into account only microscopic data, or data from integral experiments, or both.

Even if this first set of covariances may seem a patchwork that might have benefitted from a stronger coherence, a large effort was made that is a major step forward and that makes JEFF-3.3 a competitive library with respect to the availability of covariance data. Section 4.2 contains several examples where JEFF-3.3 covariances have been used to propagate uncertainties into integral benchmark or reactor concepts.

2.5.3 JEFF-3.3 covariance highlights

^{235,238}U and ^{239,240}Pu

In JEFF-3.3 a complete set of covariances for ^{235,238}U and ^{239,240}Pu in the resonance range and the high energy range were provided. Not only are cross section covariances given but also PFNS and nu-bar.

Figure 48 clearly shows that the ^{239}Pu fission cross section in the unresolved resonance range is much less known than the thermal and high energy ranges. This is mainly due to the lack of precise experimental data from both microscopic and integral experiments. Table 22 presents classical integral values for resonance analysis and the related uncertainties.

Covariances for the ^{235}U resolved resonance parameters were determined with the CONRAD code [153]. A retroactive analysis [215] was used with the marginalisation procedure of CONRAD [97] to determine the resonance parameter covariance matrix without changing the resonance parameters that was established before. Constraints were applied to the thermal cross sections and to the fission integral between 7.8 eV and 11 eV by using the latest values and uncertainties recommended by the "neutron cross section standards" group of IAEA [40]. According to an independent analysis with the CONRAD code of the thermal constants reported by Axton [303] and of the experimental review reported in Ref. [179], relative uncertainties on the thermal fission and capture cross sections were set to ±0.6% and ±2.2%, respectively. Analysis of several time-of-flight data have provided a 7.8–11 eV integral uncertainty close to 2%. Results obtained for JRC-Geel fission data are shown in Fig. 49. Final uncertainties of the ^{235}U resonance parameters were propagated on the calculated multiplication factor k_{eff} of the critical Benchmark UH1.2 carried out in the EOLE reactor of CEA Cadarache. A realistic uncertainty of 316 pcm was obtained. This result provides an order of magnitude which is valid for UOX configurations in a PWR-type neutron spectrum. Figure 50 shows the correlations and uncertainties evaluated for the ^{238}U neutron induced capture cross sections.

Table 22 Integral values for ^{239}Pu

Integrated observable	Value (barn)
Thermal fission cross section	747 ± 7 (0.9%)
Thermal capture cross section	270 ± 12 (4.4%)
Fission resonance integral	309 ± 7 (2.3%)
Capture resonance integral	180 ± 10 (5.7%)

^{23}Na

A new evaluation of sodium is proposed in JEFF-3.3 ([153], Sect. 2.2.2). This work has been motivated mainly because the earlier JEFF-3.1.1 sodium evaluation showed large differences with microscopic measurements and did not provide covariance data. A new experiment performed at the JRC Geel [158] was analyzed in conjunction with high-resolution measurements from Larson [157] with the data assimilation code CONRAD [153]. In addition, a proper covariance estimation was done for the whole energy range. A previous paper [304] pointed out effects of consistent uncertainties treatment over a "large" energy range requiring two nuclear reaction models for the analysis. It showed that, if only experimental statistical uncertainties are considered, no cross correlation appears for the cross section between the energy ranges analyzed by the two models. On the contrary, when systematic uncertainties (such as normalisation, background, detector efficiency, ...) are considered, it is possible to propagate cross correlations all the way, from experiment to evaluated cross section. The result for the sodium neutron-induced inelastic cross section is given in Fig. 51. Experimental systematic uncertainties have been propagated to nuclear reac-

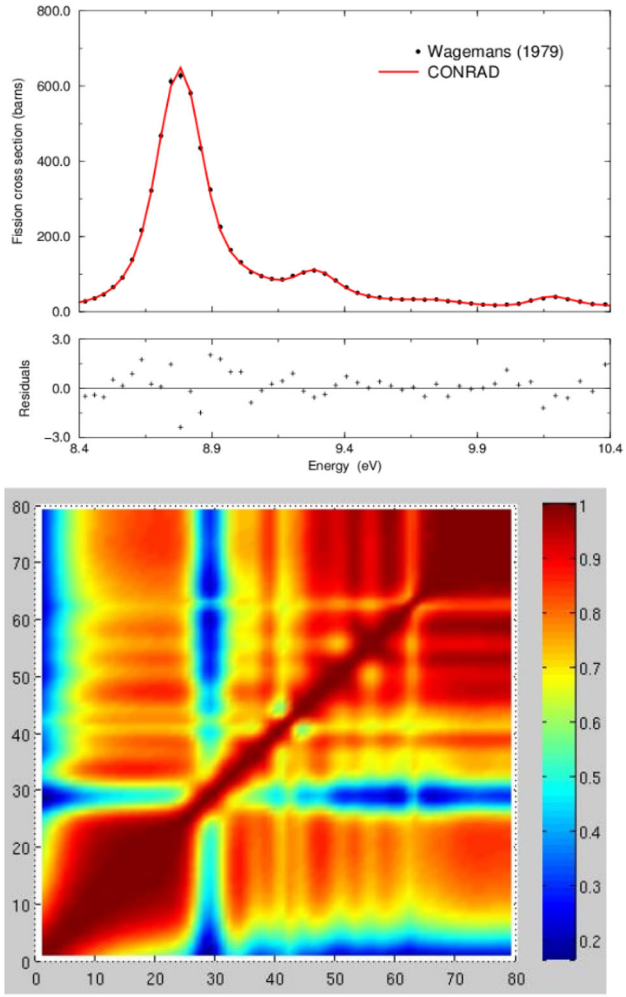

Fig. 49 Fission cross sections and correlation matrix obtained with the CONRAD code between 7.8 and 11 eV. The theoretical curve is compared with data retrieved from the EXFOR data base [179]. The ordinates of the correlation matrix are neutron energy in eV

tion model parameters in order to produce a consistent set of covariance data over a large energy range of 0 eV–20 MeV.

^{16}O

During a sensitivity and uncertainty analysis an error was detected in the JEFF-3.3 covariance matrix for ^{16}O inelastic scattering (standard deviations up to and above 10,000 %, probably an error of a factor of 100). This can lead to severe overestimation of uncertainty. Prior to use the covariance matrix should be corrected, e.g. by reducing the standard deviations to a maximum of 100% as was done in the latest version of the XSUN-2017/SUSD3D package [305] (Fig. 51).

2.5.4 JEFF-4 covariance data

Covariance add-ons to JEFF-3.3

A significant effort was devoted to propose uncertainties for thermal scattering data ($S_{\alpha\beta}$). Figure 52 gives the impact of this work on the effective hydrogen elastic cross section covariance matrix. A difficulty arises with the ENDF format that cannot represent $S_{\alpha\beta}$ uncertainties and covariance matrix in a suitable format.

Furthermore, proposals for fission yields covariance data were made for the JEFF-3.1.1 set of fission yields. These data are availiable for the JEFF community and explanations of these can be found in the literature [271,306,307]. These contributions are not part of the official JEFF-3.3 release but they will form the basis of ongoing and future activities in the field.

Covariances data for JEFF-4

For the future JEFF-4 library the aim is to provide full covariance data from evaluations considering the full energy range and accounting for all microscopic data constraints in a consistent way. Integral experiments should be included in a second step through a systematic approach leading to a separate file. JEFF-4 must keep the momentum gained with developing covariance data for JEFF-3.2 and JEFF-3.3 taking advantage of international collaborations under the auspices of OECD-NEA and IAEA. In particular, the JEFF working group will try to assess the main difficulties related to the evaluation of uncertainties

2.6 Displacement damage data

Atomic displacement cross sections were calculated using the standard NRT [308] model and the recently proposed athermal recombination-corrected dpa (arc-dpa) model [309,310]. The arc-dpa model makes possible a more accurate estimate of the damage production in irradiated materials.

According to the arc-dpa concept the number of stable defects produced under irradiation is parameterized in the following form

$$N_d = \begin{cases} 0 & \text{when } T_{dam} < E_d \\ 1 & \text{when } E_d < T_{dam} < \gamma \\ (1/\gamma)\ \xi_{arc}\ \ T_{dam} & \text{when } \gamma < T_{dam} \end{cases} \quad (5)$$

where $\gamma = 2E_d/0.8$, E_d is the average displacement threshold energy [311], and T_{dam} is the 'damage energy' or energy available for atom displacements in elastic collisions calculated using the Robinson formula [312].

The defect generation efficiency ξ_{arc} in Eq. (5), equal to the ratio of the calculated number of defects to one predicted by the NRT model, is calculated as follows [309,310]

$$\xi_{arc} = \frac{1 - c_{arc}}{\gamma^{b_{arc}}}\ T_{dam}^{b_{arc}} + c_{arc} \quad (6)$$

where b_{arc} and c_{arc} are parameters obtained based on results of molecular dynamics simulations or experimental data [311,313].

For Fe, Ni, Cu, Pd, Ag, W, Pt, and Au the parameters included in the arc-dpa formalism were taken from Refs.

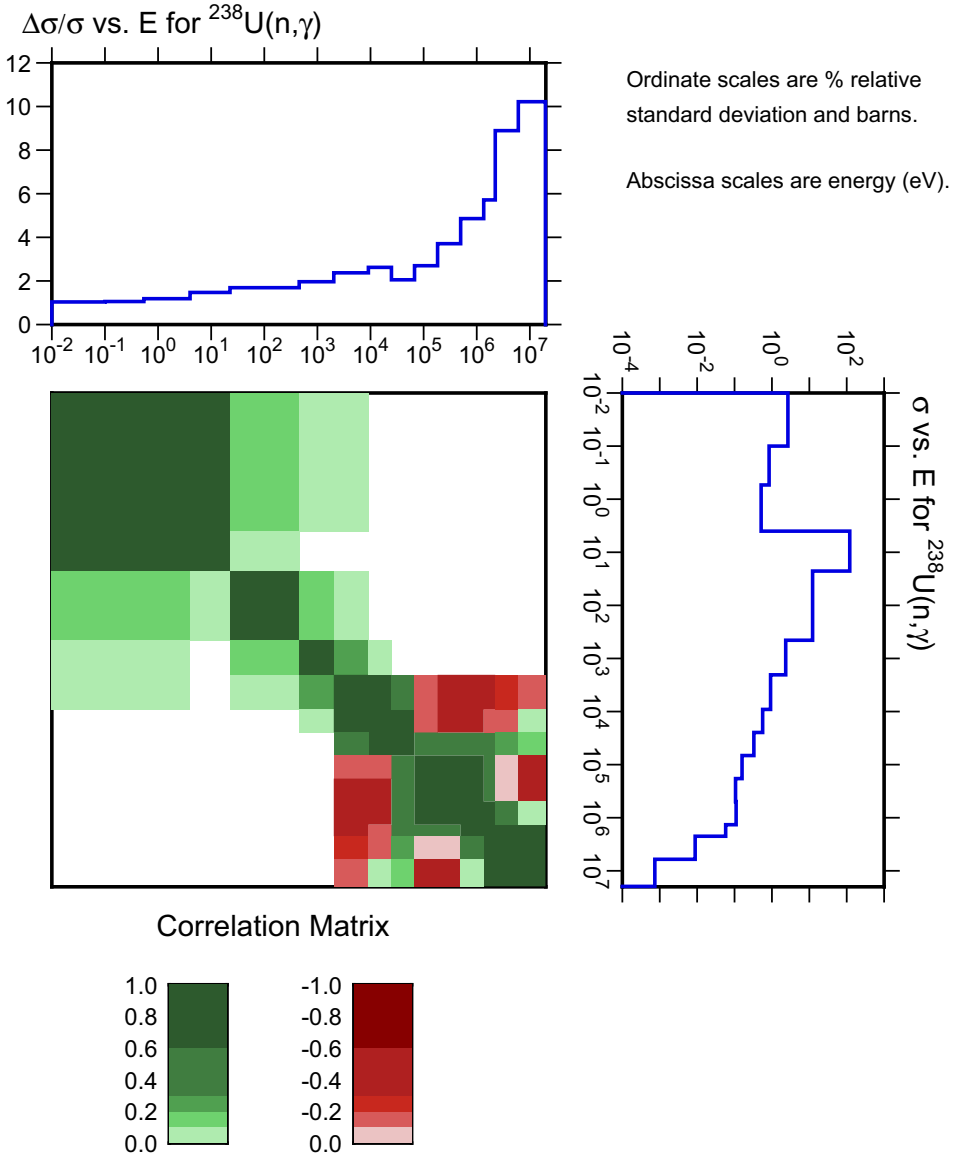

Fig. 50 ^{238}U capture multigroup cross section correlations. Energies are in eV, uncertainties in % and cross-sections in barns

[309,310,314] and for other materials were estimated using a semi-empirical systematic approach [315]. The approach uses the correlations between minimum, averaged, and effective threshold displacement energies and a number of quantities such as melting temperature, material density, cohesive energy, and others.

As an illustration Fig. 53 shows the c_{arc} parameters evaluated using experimental data and systematics [315]. Obtained E_d, b_{arc}, and c_{arc} values [315] and data from References [309,310,314] were employed for the calculation of atomic displacement cross sections for elements from lithium to uranium. The NJOY code with Eqs. (5) and (6) implemented was used for calculations.

Figure 54 shows a typical example of atomic displacement cross sections calculated using Eqs. (5), (6) and the NRT model for Al. The plotted data represent the energy group averaged values.

The data obtained on the basis of JEFF-3.3 were extended, if necessary, up to 200 MeV incident neutron energy using TENDL-2015. Figure 54 shows an example of such an extension for Ni. The displacement cross sections were recorded in ENDF-6 and ACE formats.

Because results of arc-dpa calculations are absolute numbers of stable displacements, the final values were recorded as cross sections in barns. This data representation is different from the common recording of "damage energy production cross sections" with MT = 444 by the NJOY processing. In the latter case, the displacement cross section varies according to the E_d value, which is not reasonable for the current results. The resulting arc-dpa cross sections were recorded in the file MF = 3 and the section MT = 900. Absolute val-

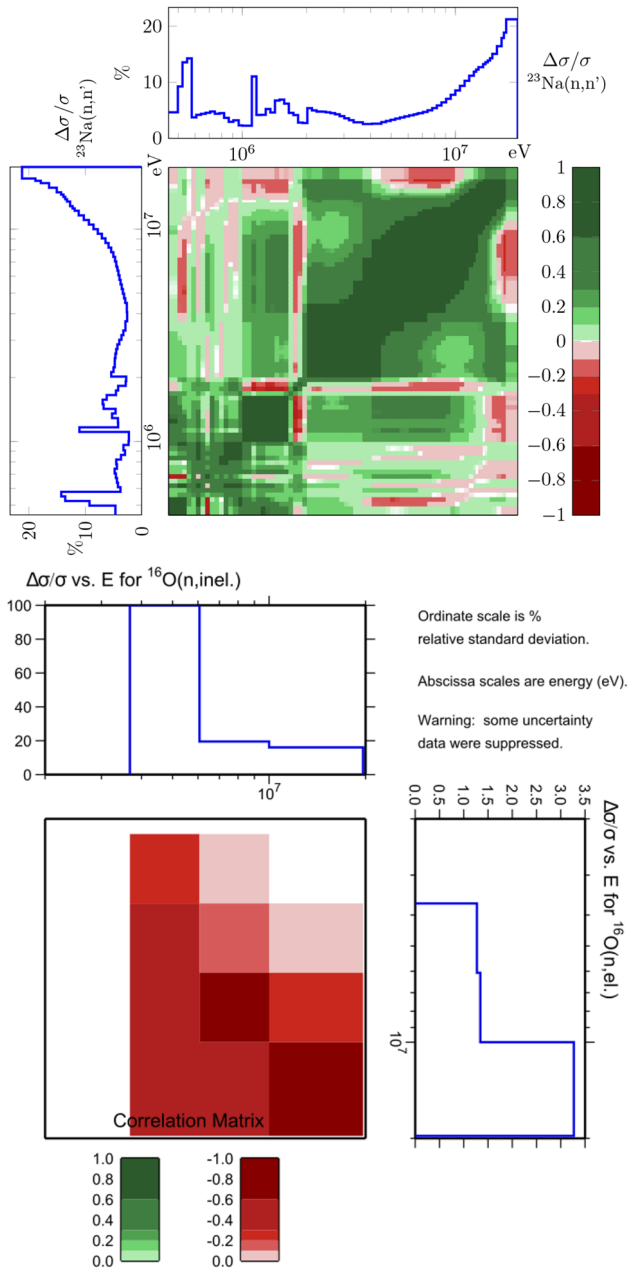

Fig. 51 Covariances of neutron-induced inelastic cross section of sodium (left). The results take full account of systematic uncertainty over the wide energy range. The corrected JEFF-3.3 covariance matrix for ^{16}O inelastic scattering (right)

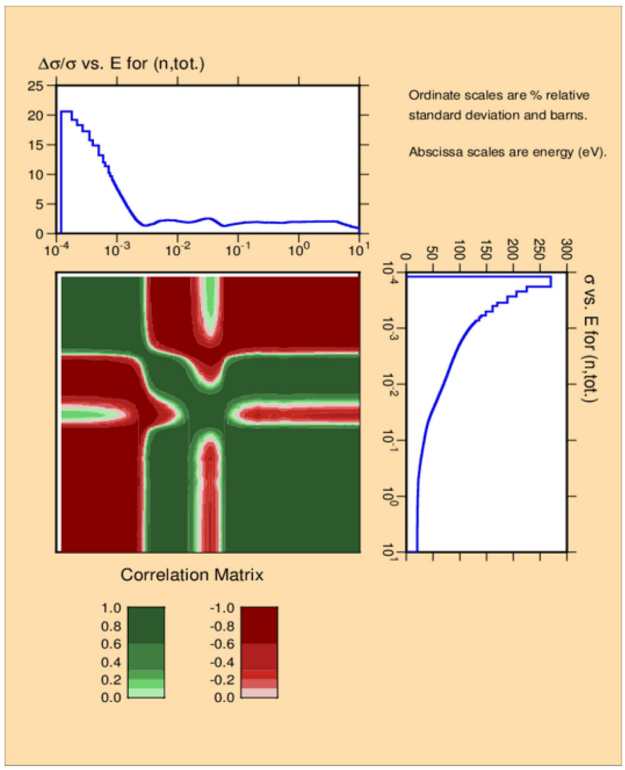

Fig. 52 Propagation of thermal scattering uncertainties to the total cross section of hydrogen in water

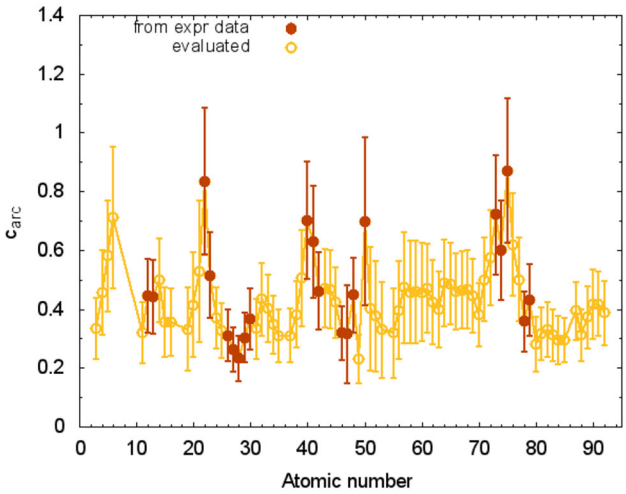

Fig. 53 The c_{arc} values evaluated for different materials with red points for experimental data and yellow for systematics

ues of displacement cross sections obtained using the NRT model [308] were written in MF = 3, MT = 901 for better comparison with arc-dpa cross sections.

2.7 Fission yields

A new fission yield library, UKFY-3.7 [316], has been created as part of the JEFF collaboration and is included in the JEFF-3.3 release. This includes 19 neutron-induced fission yield files, with thermal, fast and/or high-energy evaluations, as well as three spontaneous fission yield evaluations, for ^{252}Cf, ^{242}Cm and ^{244}Cm. The neutron-induced isotopes have been selected, as indicated in Table 23, based on their contribution to the overall number of fissions in thorium, uranium and MOX-fuelled thermal and fast reactors. This is complemented by a small set of 'high'-energy, 14 MeV fission yield data sets and ^{236}U.

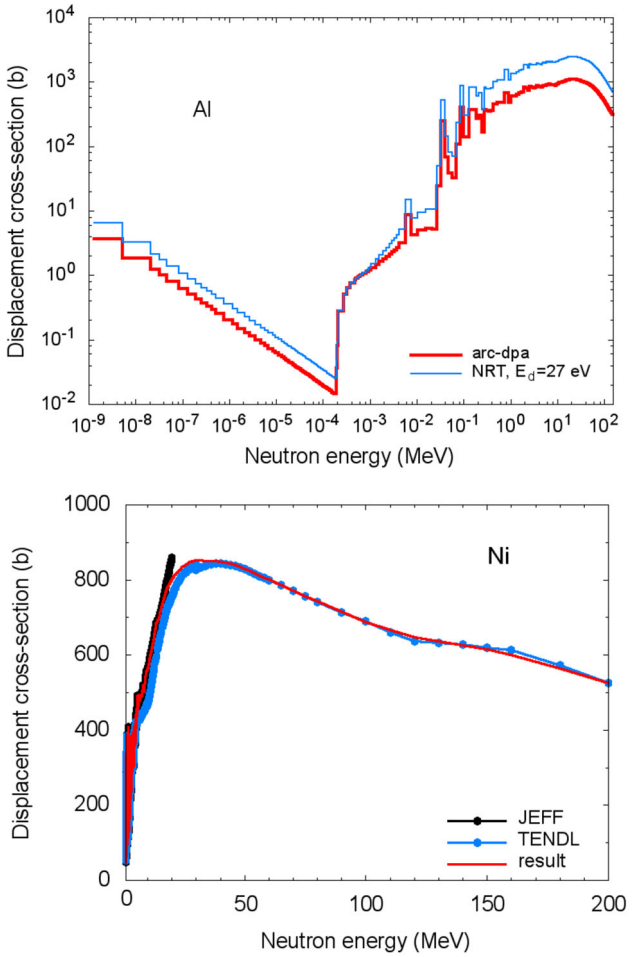

Fig. 54 Displacement cross section for aluminum calculated using the arc-dpa and NRT models (top). Displacement cross sections for nickel obtained using JEFF-3.3 and TENDL-2015 data using the arc-dpa model (bottom)

2.7.1 Evaluation methodology

The JEFF-3.3 fission yield library was built using the same general evaluation methodology that was employed for all UKFY evaluations made in the past 20 years [317]. This employs the following eleven sequential steps:

1. perform statistical analysis of a database of experimental measurements to estimate a set of recommended chain, independent and cumulative fission yields and their corresponding uncertainties;
2. for all required fissioning systems, use a suitable model to predict the independent yields and their uncertainties for all fission product nuclides- the uncertainities being based upon the model parameters uncertainities;
3. calculate the chain yield distributions from a model and adjust these to fit the recommended chain yields;

Table 23 Fission yield evaluations in the JEFF-3.3 sub-library, classified by the maximum fraction of fission rates in UOX- and MOX-fuelled thermal or fast reactors. *T, F,* and *H* refer to thermal, fast and high energy incident neutron spectra, respectively

Maximum fraction of fission rate		
> 10%	1–10%	0.1–1%
U-233 T,F,H	Pu-240 F	Th-232 F,H
U-235 T,F,H	Cm-245 T,F	U-234 F
U-238 T,F,H		U-236 F
Pu-239 T,F		Np-237 T,F
Pu-241 T,F		Np-238 T,F
		Pu-238 T,F
		Pu-242 F
		Am-241 T,F
		Am-242m T,F
		Am-243 T,F
		Cm-243 T,F
		Cm-244 T,F

4. use the modelled independent yields to derive fractional independent yields and then combine these with the chain yield distributions to produce a modified set of independent yields;
5. adjust the modified independent yields to fit the physical constraints, such as mass or charge conservation, as well as detailed complementary element balances;
6. calculate isomeric branching ratios based on the Madland-England model;
7. split the independent yields using the isomeric branching ratios;
8. calculate cumulative fission yields using the isomeric split adjusted independent yields and the most recent decay data evaluation decay branching ratios;
9. increase the uncertainities on the recommended cumulative yields by the difference between the recommended and calculated cumulative yields;
10. from the cumulative yields with uncertainities (i.e. those with measurements) use the independent yield uncertainities to estimate the cumulative yield uncertainities on their parent nuclides higher in the decay chain; and
11. parse all data into an ENDF-6 formatted data file.

2.7.2 New data considered in the evaluation

The previous JEFF-3.1.1 fission yield files [4] were based on experimental data found in literature reviews performed up to the year 2000. A new review was carried out between 2013-2016, identifying 1234 new data measurements that have been used in the JEFF-3.3 evaluation. These are summarised in Table 24 for all systems that had an updated experimental database. Notably, this updated data set includes new

Table 24 Number of experimental measurements used in the evaluation of all fissioning systems with new data in the JEFF-3.3 fission yield sub-library

Neutron spectrum	Fissioning nuclide	JEFF-3.1.1	JEFF-3.3	New data
Thermal	Th-229	337	409	72
Thermal	U-233	757	945	188
Thermal	U-235	2390	2541	151
Thermal	Np-238	115	178	63
Thermal	Pu-239	861	1086	225
Thermal	Pu-241	334	397	63
Thermal	Cm-245	161	380	219
Thermal	Cf-249	305	544	239
Fast	U-235	725	729	5
Fast	Pu-239	390	395	5
Fast	Pu-241	111	116	5
Total		6486	7720	1234

Table 25 Fast neutron spectrum ^{148}Nd cumulative yields determined from statistical analysis of experimental measurements

Fissioning nuclide	JEFF-3.1.1	JEFF-3.3
U-235	1.696 ± 0.019	1.677 ± 0.020
Pu-239	1.699 ± 0.025	1.700 ± 0.029
Pu-241	1.946 ± 0.045	1.943 ± 0.041

fast neutron spectrum measurements for ^{148}Nd, which are summarised in Table 25.

The integration of these new data into the database provides two kinds of improvements. In some cases, the addition of more precise data improves the accuracy of the fission yield evaluation or reduces their uncertainties. In other cases, the measurements are first-of-a-kind and allow the evaluation to rely directly upon experimental data, rather than model calculations and/or the application of constraint equations in the evaluation process. Examples of the latter include the thermal fission of ^{238}Np, where measurements are available for masses between 74 and 85; thermal fission of ^{239}Pu, where masses 80, 82 and 130 have now been measured; and thermal fission of ^{249}Cf, where masses 69–82 have now been measured.

2.7.3 New modelling methods

In the previous JEFF-3.1.1 evaluation, the 5-Gaussian and Wahl Zp models were used to supplement experimentally-measured yields with semi-empirical data [4]. The parameterisation of these models were fitted separately for each fissioning system, where possible, or the parameters were extrapolated where there was insufficient data to perform a reliable fit.

The development of the '**GE**neral description of **F**ission observables' (GEF) code [290] since the previous JEFF fission yield evaluation has offered another model for the calculation of fission yields. This uses a single set of physically-inspired semi-empirical parameters for all fissioning systems and offers impressive predictive capability for fissioning systems ranging from thorium to californium, and beyond. It has been used for incident neutron energies ranging from thermal to tens of MeV, and includes multi-chance fission.

Following several preliminary comparison studies, it was decided to use the GEF code as the model to estimate independent and chain yields required as an input to the evaluation. Although GEF also possesses an isomeric branching simulation feature, the Madland-England model was retained in JEFF-3.3. The isomeric splitting has a significant effect on short-term decay heat from fission products, and thus it was decided to keep the existing Madland and England model until any improvements from using the GEF code could be quantified.

2.8 Decay data

The JEF-2.2 library included the reference decay data in Europe since being released in the early 1990s. However, various shortcomings, both in content and evaluation methodology, led to the establishment of a new decay data evaluation system developed through the JEFF project. The initial construction of the JEFF-3.0 decay data sub-library [4] used the most recent versions of the NUBASE [318] and Evaluated Nuclear Structure Data File (ENSDF) [301] databases, complemented with specialised decay data evaluations from the United Kingdom Activation Product Decay Data (UKPADD) and Heavy Element and Actinide Decay Data (UKHEDD) libraries [319], the Decay Data Evaluation Project (DDEP) [320], the IAEA Actinide Decay Data Library [321] and the International Reactor Dosimetry and Fusion File (IRDFF) [252]. The different data sources are sequentially processed with various quality checks, e.g. intensity and energy balance verification, performed in each step. The result is a library

Table 26 Source libraries and the number of evaluations adopted in the JEFF-3.3 decay data sub-library

Source library	Number
NUBASE	2295
ENSDF	849
DDEP	140
UKPADD-6.12	441
UKHEDD-2.6	59
IAEA	66
IRDFF	2
Total	3852

that recognises and incorporates the most rigorous available evaluation for each of the 3852 radionuclides, whether that represents a bespoke evaluation or a translation of an ENSDF file into the ENDF-6 format. For the JEFF-3.3 release the source libraries are listed in Table 26, including updates to the UKPADD and UKHEDD versions and several newly evaluated files from the DDEP, including ^{18}F, ^{59}Fe, ^{82}Rb, ^{82}Sr, ^{88}Y, ^{89}Zr, ^{94m}Tc, ^{109}Cd, ^{133}Ba, ^{140}Ba, ^{140}La, ^{151}Sm and ^{169}Er.

2.8.1 Inclusion of TAGS measurements

The well-known Pandemonium effect [322] results in misallocation of beta and gamma decay intensities, and has resulted in several experimental campaigns to provide new non-spectroscopic data to improve the decay data evaluations. The initial benchmarking of the JEFF-3.1 decay sublibrary [4], alongside work of the OECD-NEA Working Party on International Evaluation Co-operation subgroup 25 [323] highlighted inconsistent simulation results for decay heat calculations. These were a direct result of the mean gamma and beta decay energies calculated from the discrete decay scheme data suffering from the Pandemonium effect, and it was assumed these mean energies could be better determined using Total Absorption Gamma-ray Spectroscopy (TAGS) experiments. A set of 29 nuclei, shown in Table 27 had their mean energies updated from the work of Greenwood et al. [324] for JEFF-3.1.1 [4]. For the release of JEFF-3.3, nine new nuclei were updated using data from the groups at Valencia, Spain and SUBATECH, the University of Nantes, France, working at the University of Jyväskylä, Finland, as shown in Table 28. The differences are often substantial.

The JEFF-3.3 radioactive decay data library does not contain beta or neutrino spectra. Estimates of these spectra are of interest to various problems and require additional models besides the data provided in the present and previous JEFF radioactive decay data library. Examples of such estimates may be found in Refs. [328,329] for the estimation of reactor anti-neutrino spectra and in Ref. [330] for beta (β^- and β^+) and (anti-)neutrino spectra.

Table 27 Nuclei updated in JEFF-3.1.1 using Greenwood et al.'s [324] TAGS mean energy values (in MeV, [4]). (An uncertainty of 10% was applied to the adopted mean energies.)

Nuclide	JEFF-3.1 $\langle E_\beta \rangle$	TAGS (MeV)	JEFF-3.1 $\langle E_\gamma \rangle$	TAGS (MeV)
^{90}Rb	2.049	1.916	1.982	2.270
^{90m}Rb	1.403	1.118	3.240	3.869
^{91}Rb	1.612	1.368	2.269	2.706
^{95}Sr	2.208	1.901	1.118	1.790
^{139}Cs	1.640	1.671	0.345	0.305
^{141}Cs	1.935	1.506	0.770	1.701
^{143}Ba	1.417	1.195	1.417	1.341
^{144}Ba	1.040	0.930	1.040	0.785
^{145}Ba	1.860	1.285	1.860	1.833
^{142}La	0.868	0.962	2.325	2.121
^{143}La	1.237	1.235	0.252	0.439
^{144}La	1.382	0.986	2.330	3.085
^{145}La	1.499	0.762	0.624	2.144
^{148}Ce	0.713	0.586	0.713	0.486
^{147}Pr	0.899	0.669	0.899	0.929
^{148}Pr	1.679	1.348	0.938	1.776
^{148m}Pr	1.701	1.239	0.937	2.050
^{149}Pr	1.286	0.811	0.305	1.332
^{151}Pr	1.394	1.114	1.394	1.363
^{153}Nd	1.112	1.153	1.112	0.509
^{154}Nd	0.937	0.856	0.937	0.551
^{155}Nd	1.500	1.085	1.500	1.543
^{152}Pm	1.326	1.304	0.285	0.345
^{153}Pm	0.686	0.663	0.073	0.123
^{154}Pm	1.321	0.849	1.321	1.876
^{156}Pm	1.717	1.206	1.717	2.206
^{157}Pm	1.453	1.540	1.453	0.849
^{157}Sm	0.912	0.839	0.912	0.585
^{158}Sm	0.667	0.512	0.667	0.590

2.9 Neutron activation

The JEFF-3.3 files are complemented by an activation library that includes 2797 neutron-induced reaction files in the so-called European Activation File (EAF) format. All previous JEFF-3 libraries utilised the most recent version of the European Activation File, with the EAF-2010 library [331,332] being the last release of that project. Since 2010, the development of the TALYS-based TENDL [5] files has replaced this activity within Europe and several verification and validation exercises that had been performed for the EAF libraries (c.f. [333]), have been redone using the TENDL files with superior results [273]. In order to maintain compatibility with the activation simulation codes that have traditionally relied upon EAF formatted data files, a special processed version

Table 28 Nuclei updated in JEFF-3.3 using recently measured TAGS mean energy values (in MeV) at the University of Jyväskylä by the Valencia [325,326] and Nantes [327] groups (Uncertainties not shown)

Nuclide	JEFF-3.1 $\langle E_\beta \rangle$	TAGS (MeV)	JEFF-3.1 $\langle E_\gamma \rangle$	TAGS (MeV)
Valencia				
^{87}Rb	1.577	1.170	3.089	3.938
^{88}Rb	2.394	1.706	3.112	4.609
^{94}Rb	3.102	2.450	2.747	4.063
^{105}Mo	1.922	1.049	0.552	2.407
^{104}Tc	1.595	0.931	1.890	3.229
^{105}Tc	1.310	0.764	0.671	1.825
^{106}Tc	1.906	1.457	2.191	3.132
^{107}Tc	1.920	1.263	0.515	1.822
Nantes				
^{92}Rb	3.639	3.496	0.170	0.464

of TENDL-2017 was prepared and has been the subject of validation activities under the EUROfusion nuclear data programme [334]. As a result, the JEFF-3.3 library has adopted this EAF formatted TENDL-2017 neutron library. Work is in progress on the generation of a EAF-type 211 group cross-section data library (up to 60 MeV) which can be used by any activation code.

2.10 Thermal scattering

The thermal neutron scattering sublibrary contains 20 evaluations for 16 materials. The evaluation for heavy water was updated and now has components for deuterium and oxygen bound in heavy water. Nine new materials (sapphire-Al_2O_3, silicon, mesitylene, toluene, ortho- and para- hydrogen, ortho- and para-deuterium, and light water ice) were included, and the remaining evaluations were carried forward from JEFF-3.2. The current status of the evaluations is summarized in Table 29. Details of the evaluation and validation methodologies are given below for each of the new and updated materials.

Table 29 Thermal scattering libraries included in JEFF 3.3. Notation: Al_2O_3 for sapphire, L for liquid, *o-* for *ortho-*, *p-* for *para-*, Mes. for phase II Mesitylene, $(CH_2)_n$ for polyethylene

Mat.	Eval.	T (K)	Origin
L(o-H_2)	H	14, 15, 16, 17 18, 19, 20	New
L(p-H_2)	H	14, 15, 16, 17 18, 19, 20	New
$(CH_2)_n$	H	293.6, 350	JEFF-3.2
H_2O	H	293.6, 323.6, 373.6 423.6, 473.6, 523.6 573.6, 623.6, 647.2 800, 1000	JEFF-3.2
H_2O ice	H	77, 115, 233, 243 253, 263, 273	New
Mes.	H	20,120	New
Toluene	H	20,120	New
CaH_2	Ca, H	293, 400, 500, 600, 700, 800, 1000, 1200	JEFF-3.2
ZrH	H	293.6, 400, 500, 600.0, 700, 800, 1000, 1200	JEFF-3.2
D_2O	D, O	283.6, 293.6, 300, 323.6, 350, 400, 423.6, 450, 473.6, 500, 523.6, 550, 573.6, 600, 623.6, 650	ENDF/B-VIII
L(o-D_2)	D	19, 20, 21, 22, 23	New
L(p-D_2)	D	19, 20, 21, 22, 23	New
Be	Be	293, 400, 500, 600, 700, 800 1000, 1200	JEFF-3.2 JEFF-3.2
Al_2O_3	Al, O	293	New
Mg	Mg	20, 100, 296, 773	JEFF-3.2
Si	Si	296	New

2.10.1 Silicon and sapphire

Silicon and sapphire (Al_2O_3) are two materials used in single crystal form as neutron filters at neutron beam facilities. For this application, single crystals are aligned to the neutron beam in a way that the incident neutrons do not satisfy any Bragg condition. A precise representation of this system requires the calculation of the interaction of neutron waves with the single crystal and consider the extinction of reflections caused by destructive interference [335]. This cannot be computed using neutron transport codes which assume non-oriented, isotropic materials. Therefore, in order to introduce filters into these codes a simplification was applied: we only consider inelastic interactions. This approximation works for simulating neutron filters [336], but also was found to be satisfactory for the calculation of the neutron irradiation of silicon single crystals for transmutation doping [337].

The models use a simple Debye spectrum with Debye temperature $T_D = 485$ K for silicon and $T_D = 1032$ K for sapphire. The models show a good agreement with measurements of the total neutron cross section, as shown in Fig. 55. Details of the evaluation can be found in Reference [338]. The libraries are evaluated at T = 293 K for sapphire and T = 296 K for silicon. When the libraries are reconstructed

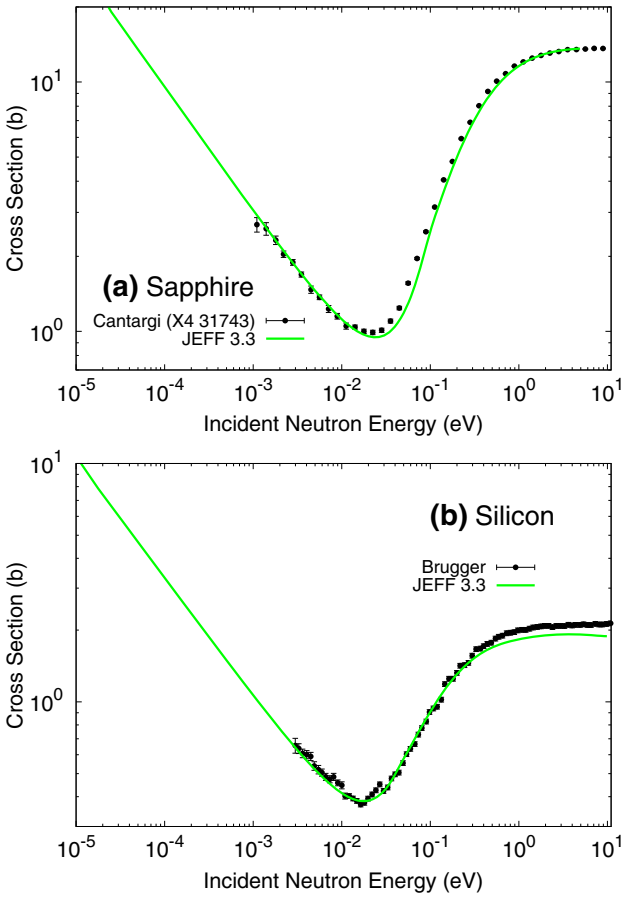

Fig. 55 Inelastic scattering cross section of sapphire (top) and silicon (bottom) at room temperature. The calculations are compared with experimental data by Cantargi [338], and Brugger [339]. The evaluation for silicon is normalized to the free gas scattering cross section of Si-28, whereas the measurements by Brugger correspond to natural silicon

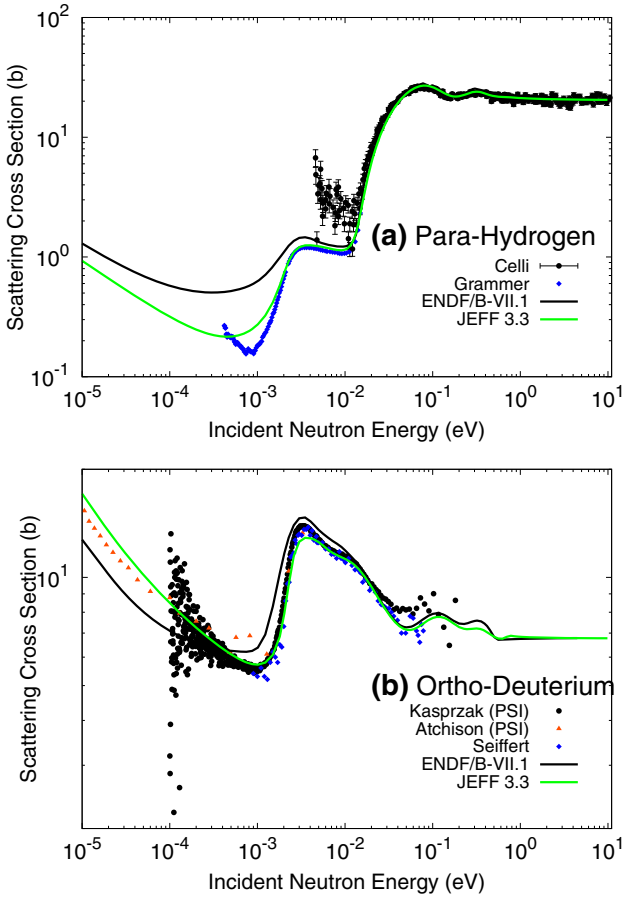

Fig. 56 Total scattering cross section of liquid para-hydrogen (top) and liquid ortho-deuterium (bottom) at 19 K. The calculations are compared with experimental data by Celli [344], Grammer [345], Kasprzak [346], Atchison [347], and Seiffert [348]

using NJOY to produce ACE libraries, the parameter `mte` should be set to 0 to create a library without the elastic component.

2.10.2 Liquid hydrogen and deuterium

Liquid hydrogen and liquid deuterium are among the most used materials for the production of cold neutrons in pulsed neutron sources and nuclear research reactors. Hydrogen and deuterium form diatomic molecules with two spin states: symmetric (ortho) and antisymmetric (para). At low temperatures, for which few rotational levels are excited, the selection rules caused by the correlation between the total nuclear spin **I** and total angular momentum **J** affect the neutron interaction probability changing the cross section [340].

Compared with previous models by Keinert and Sax [341] included in ENDF/B-VII.1, this evaluation improves the calculation of interference effects by including a Sköld correction computed using molecular structure factors derived from measurements performed by Zoppi [342]. The structural correction, as in a previous evaluation by Granada and Gillette [343], is separated into an analytical component that is applied to the internal dynamics of the molecule, and a numerical component that is applied to the rigid-body dynamics of the molecule.

Calculations for para-hydrogen show a better agreement with experimental measurements of the total cross section by Celli [344] and Grammer [345] (Fig. 56a), and calculations for ortho-deuterium show an improvement over previous models when compared with measurements performed at Paul Scherrer Institut by Kasprzak [346] and Atchison [347] (Fig. 56b).

The libraries are evaluated at $T = 14$, 15, 16, 17, 18, 19 and 20 K for ortho- and para-hydrogen, and $T = 19$, 20, 21, 22 and 23 K for ortho- and para-deuterium.

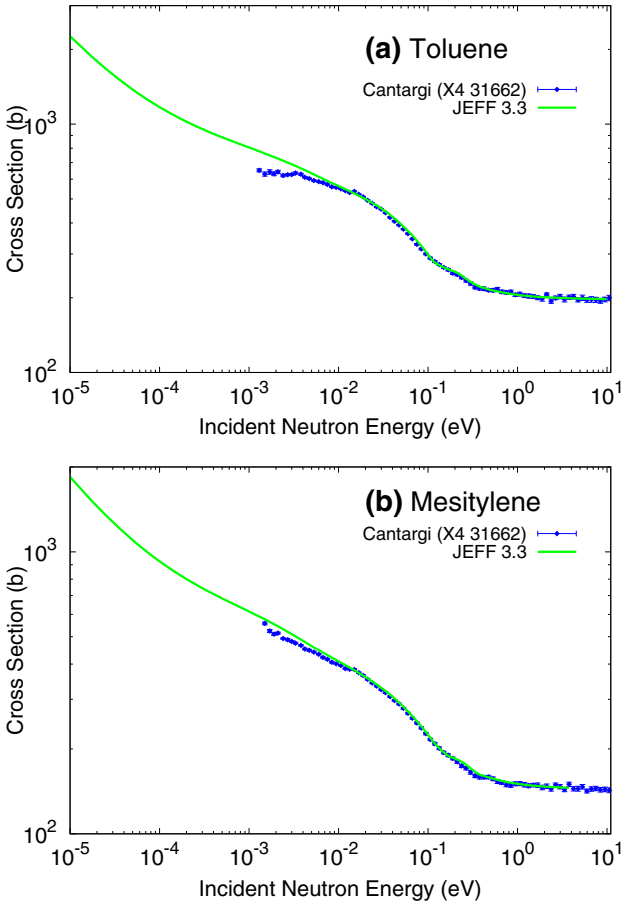

Fig. 57 Total cross section of toluene (top) and mesitylene (bottom) computed at 120 K compared with experimental data measured at the CAB LINAC [352]

2.10.3 Solid mesitylene and toluene

Toluene and mesitylene are aromatic hydrocarbons with metyl groups replacing hydrogen positions in a benzene ring, one in the case of toluene and three in the case of mesitylene. The presence of these metyl groups add low energy rotational modes to the dynamics of benzene, reducing the effective temperature of the material and improving the production of cold neutrons. As other aromatic hydrocarbons, toluene and mesitylene have a higher radiation resistance compared to solid methane, with a significant neutron production [349,350].

The models are based on inelastic neutron scattering measurements at the IBR-II reactor [351] combined with synthetic data [352]. The models show good agreement with measured total neutron cross section data, as shown in Fig. 57. The libraries are evaluated at $T = 20\,\mathrm{K}$ and $T = 120\,\mathrm{K}$ for both H bound in solid mesitylene in phase II, and solid toluene.

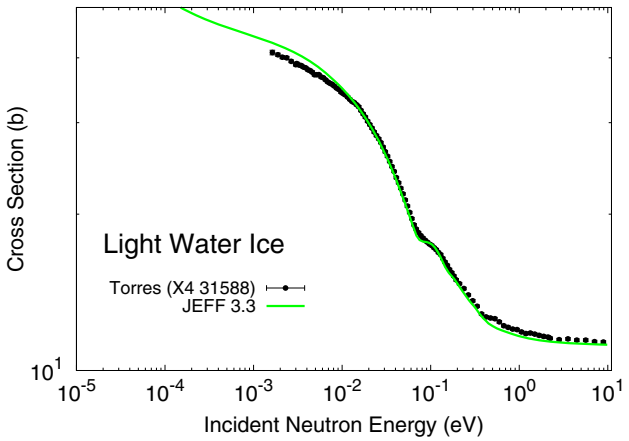

Fig. 58 Total scattering cross section of light water ice at 115 K. The calculations are compared with experimental data measured at the CAB LINAC [357]

2.10.4 Light water ice

Although light water ice is not a very efficient cold moderator due to its relatively high effective temperature, it has been studied in the past in the context of advanced neutron sources to take into account the effect of ice layers, and as a component of methane clathrates [353,354]. Aside of this, nuclear fuel material transportation conditions might include the presence of ice [355] and would require thermal scattering data for the assessment of criticality safety.

The model is based on experimental data measured by Kolesnikov [356] and shows a good agreement with measurements performed at the Bariloche LINAC, as shown in Fig. 58. The library for hydrogen bound in light water ice is evaluated at $T = 77$, 115, 233, 243, 253, 263 and 273 K.

2.10.5 Heavy water (D_2O)

The evaluations for deuterium and oxygen in D_2O are based on the *CAB Model for Heavy Water* [358] and were prepared using NJOY99.396 with updates to extend the calculation grids. Details of the model and its validation with experimental data can be found in Ref. [358]. Compared with the JEFF-3.2 D-D_2O evaluation by Mattes and Keinert [359], the following changes are introduced:

- Low energy interaction has been changed from a free gas model to molecular diffusion using the Egelstaff-Schofield diffusion model.
- The coherent inelastic component has been computed in the Sköld approximation, using correction functions computed from molecular dynamics and validated with experimental data from Soper [360], instead of the analytical model used by Mattes.

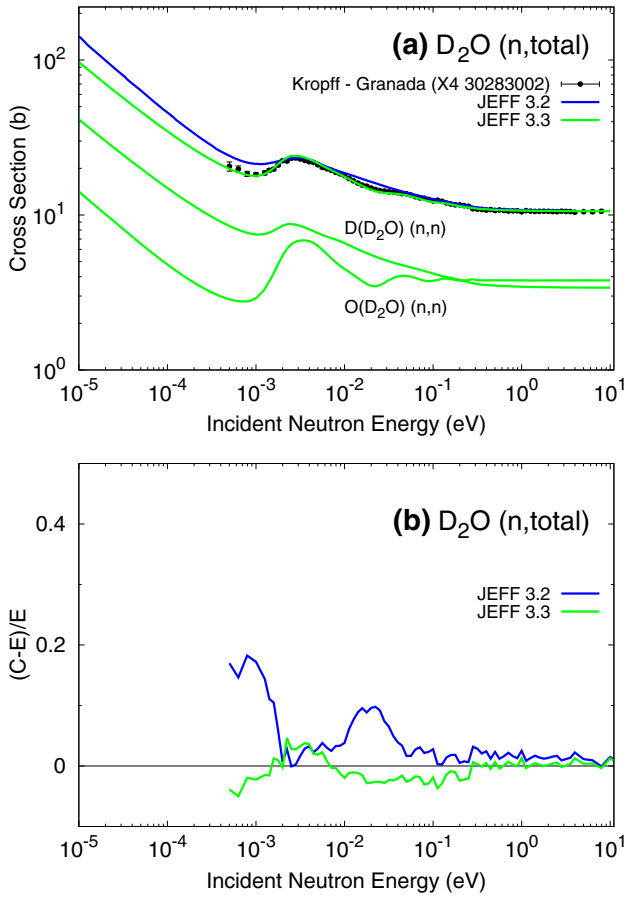

Fig. 59 Evaluated D_2O(n,tot) cross section at 293.6 K, compared with data retrieved from EXFOR

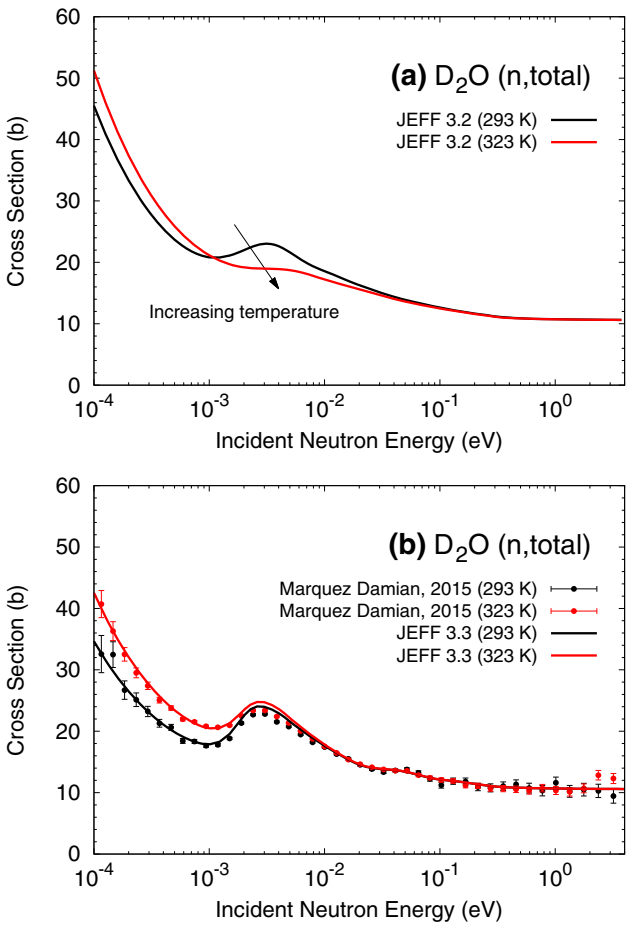

Fig. 60 Temperature dependence of the evaluated D_2O(n,tot) total cross section in the JEFF 3.2 library (**a**), and JEFF 3.3 library (**b**) compared with transmission measurements by Márquez Damián [362]

- A continuous spectrum derived from molecular dynamics simulations [361] replaces the continuous spectra from Haywood and Page.
- Alpha and beta grids have been refined to allow a better representation of the low energy interaction.
- Scattering by oxygen bound in heavy water is now treated explicitly in the O(D_2O) evaluation. In heavy water oxygen-16 contributes to approximately 1/3 of the total cross section and a explicit model is needed to correctly reproduce the features found in the experimental cross section, whereas in light water oxygen-16 contributes less than 8% to the total cross section and it can be modeled as a free gas.

The changes introduced in the evaluation allowed for a much better comparison with experimental neutron cross section data. In Fig. 59 we compare the evaluated data with measurements by Kropff and Granada retrieved from EXFOR. The new evaluation represents better the reduction in the total cross section at sub-thermal energies (0.3–3.0 MeV), which was already found in the JEFF-3.2 evaluation, but also reproduces a reduction of the experimental total cross section in the thermal range (10–50 meV) which was not possible with previous evaluations. This reduction in the total scattering cross section can be traced to the effects of coherent scattering in oxygen, which was not included in earlier JEFF releases.

The new evaluation also solves an anomalous behavior of the evaluation by Mattes, which predicts a reduction of the total scattering cross section when the temperature is increased from 293 to 350 K (Fig. 60a). The new evaluation shows an increase of the total cross section with increasing temperature (Fig. 60b), and compares well with new total cross section data from transmission experiments at Indiana University [362]. The evaluation was generated at the following temperatures: 283.6, 293.6, 300.0, 323.6, 350.0, 373.6, 400.0, 423.6, 450.0, 473.6, 500.0, 523.6, 550.0, 573.6, 600.0, 623.6, and 650 K.

The effect of the new evaluation in critical systems is significant, with changes of up to 1200 pcm in sensitive critical experiments [363]. Benchmarking with experiments in the ZED-2 reactor resulted in a reduction of 100–300 pcm in the multiplication factor when the new thermal scattering

libraries where introduced [364]. The uncertainty associated to this library was studied for the OPAL reactor [365] using the Total Monte Carlo method [366]. The results show a 41 pcm uncertainty caused by the thermal scattering library used for the calculation of the heavy water reflector.

3 Benchmarking and testing

The performance of the JEFF-3.3 nuclear data library for applications in nuclear fission and fusion was evaluated by comparing experimental and derived data from integral experiments with model estimates based on JEFF-3.3 data. For brevity we refer to this performance evaluation as benchmarking of the library. Benchmarking concerned estimates of criticality, delayed neutron yields, neutron shielding, decay heat and Maxwellian-averaged cross sections.

Data and models for integral experiments were obtained from the International Criticality Safety Benchmark Evaluation Project (ICSBEP) Handbook [23] and the Shielding Integral Benchmark Archive and Database (SINBAD [367]). In addition, results from well-known experimental campaigns were contributed by the co-authors. For delayed neutron yields, decay heat and Maxwellian averaged cross-sections dedicated compilations were used that are described in the respective sections, below.

Moving from JEFF-3.2 to JEFF-3.3 four test releases (JEFF-3.3T1 through JEFF-3.3T4) were issued that were evaluated based on benchmarking results presented by the co-authors following each test-release. The results for these test releases were used to guide choices of evaluations and of dedicated improvements. This implies that important feedback from integral experiments is already included in the JEFF-3.3 library. For completeness we note that JEFF-3.3T4, the final test library, was adopted as JEFF-3.3 without further change. A summary of benchmarking and validation activities for the first test releases of JEFF-3.3 can be found in Reference [368].

Below we present the benchmarking of the publicly released JEFF-3.3 library and compare its performance with earlier releases and recent releases from the United States (ENDF) and the Japanese (JENDL) nuclear data libraries.

3.1 Criticality

Criticality benchmarking was carried out independently by several co-authors providing complementary views on library performance. Results were obtained for several selections (suites) from the ICSBEP Handbook and for additional well-known experiments and applications. The transport codes MCNP, MORET 5 [369] and Tripoli were used with the associated processing codes, including NJOY and GAIA [370]. This variety adds confidence that the library will perform for a wide range of processing routes and application codes.

Results of benchmarking are commonly reported as C/E ratios where C stands for the computed result with the nuclear data library of choice and E stands for the result of the integral experiment. For good performance C/E should be close to one, ideally within one standard uncertainty of the experimental result. Results are often presented for larger subsets of critical integral experiments to ensure that (1) the library is tested broadly for all relevant features and that (2) a statistical indication can be provided of its performance outside the range of benchmarking. Besides straightforward outlier analysis, such testing based on suites of benchmarks is often summarized by a single number, the metric. Since reliable uncertainty estimation is an important goal for modern nuclear data libraries, here we favor a metric (Chi-square) that includes the uncertainty of the integral experiment.

C/E may deviate from one for several reasons. For physics and hence nuclear data implications we need a reliable integral experiment result and a model that represents it, accurately. Besides the experimental or derived effective multiplication factor k_{eff} this requires a reliable uncertainty of k_{eff} based on a detailed, credible uncertainty budget. The inclusion of correlations between integral experiments is ongoing work that is not included in this paper.

Below we demonstrate that significant changes in Chi-square occur for several suites when only the library is changed. Those suites then indicate the way forward with the library and provide a measure of confidence for applicability. It is important to remember that remaining issues do not necessarily reflect the nuclear data.

The primary set used for optimization of JEFF-3.3 during its development is the NEA extended Mosteller-suite of 123 integral experiments from the ICSBEP Handbook [371,372]. This suite containing high-quality integral physics experiments effectively tests the main nuclides of interest – major actinides, structural materials, moderators – in a range of neutron spectra from fast to thermal using fissile materials ranging from pure metals to oxides and solutions and a range of enrichments. Besides the common major actinides the suite includes ^{233}U. Additions to the 119 cases of Ref. [371] are 4 cases discussed in Ref. [372].[5]

[5] The ICSBEP Handbook uses three qualifiers, a rank number and a subrank number to uniquely identify a benchmark and categorize the main features [23]. Here, the abbreviated notation abcn-m is used where 'a' specifies the main fissile component, 'b' the fuel composition, 'c' the spectrum, 'm' the rank number and 'n' the subrank number. 'a' is either 'h' for highly (HEU - $^{235}U \geq 60\%$), 'i' for intermediate (IEU - $10\% < ^{235}U < 60\%$), 'l' for low (LEU - $^{235}U < 10\%$) enriched uranium, 'p' for plutonium, 'm' for mixed, 'u' for U-233 or 's' for special. 'b' is 'm' for metal, 'c' for compound, 's' for solution. 'c' is 'f' for fast, 't' for thermal and 'i' for intermediate. Besides this systematic name, a common name is often used in addition (Godiva, Jezebel, Big-Ten, ...). A spectrum is fast if $>$ 50% of fissions is above 100 keV,

To test ^{237}Np data smf8 was added, for Cu data in the fast range hmf73, for deuterium data hsi1-1 and for enhanced thermal testing of Pu pst9-1. The suite consists of a deck of MCNP inputs and established benchmark results and is referred to as the NEA benchmark suite.

A much larger subset of 2530 cases from ICSBEP was compiled by Steven van der Marck (NRG suite). A second large subset of the ICSBEP Handbook (about 1700 cases) is the IAEA suite compiled by Andrej Trkov starting from the suite of MCNP inputs developed and maintained by Skip Kahler of Los Alamos National Laboratory. These two large subsets of NRG and IAEA were not used for optimizing the library and mainly serve for a statistical analysis. These two sets were analyzed differently, providing complementary indications about library performance and improvement over earlier releases.

Several co-authors employ dedicated subsets of ICSBEP benchmarks for qualifying their calculational schemes for performance and safety assesments of advanced reactors under development, operational reactors, spent fuel storage, transport and fuel cycle processes. Below we mention the IRSN and PSI suites that are used for criticality safety analyses in support of studies performed for their respective national safety authorities. Including these suites here therefore provides an important link with safety applications that are context specific. These suites partly overlap with each other and with the Mosteller suite.

The indications provided by these suites are complemented by dedicated experimental campaigns supporting Pressurized Water Reactors (PWR) and advanced reactor (ASTRID, MYRRHA, ALFRED) development.

3.1.1 The NEA extended Mosteller suite

The results for the NEA extended Mosteller suite are shown in Fig. 61 using the reduced Chi-square (χ^2/N) as defined in Eq. (7)

$$\chi^2/N = \frac{1}{N}\sum_{i=1}^{N}\frac{(k_{C,i}-k_{E,i})^2}{\Delta k_{E,i}^2}\,, \tag{7}$$

where N is the number of benchmarks, $k_{C,i}$ is the computed neutron multiplication factor for benchmark i using a particular library and $k_{E,i}$ is the experimental neutron multiplication factor with $\Delta k_{E,i}$ its standard uncertainty.

The cumulative plot for the OECD-NEA-suite (Fig. 61) clearly shows the improvement from JEFF-3.0 (24, not shown) over JEFF-3.1.1 (6.9) to JEFF-3.2 (6.3) and finally the latest release JEFF-3.3 with a rather good $\chi^2/N = 2.2$. Clearly, for this metric and benchmark suite the JEFF-3.3 library performs similarly to the ENDF/B-VIII.0 library [180]. JENDL-4.0, not shown, has 11 [101].

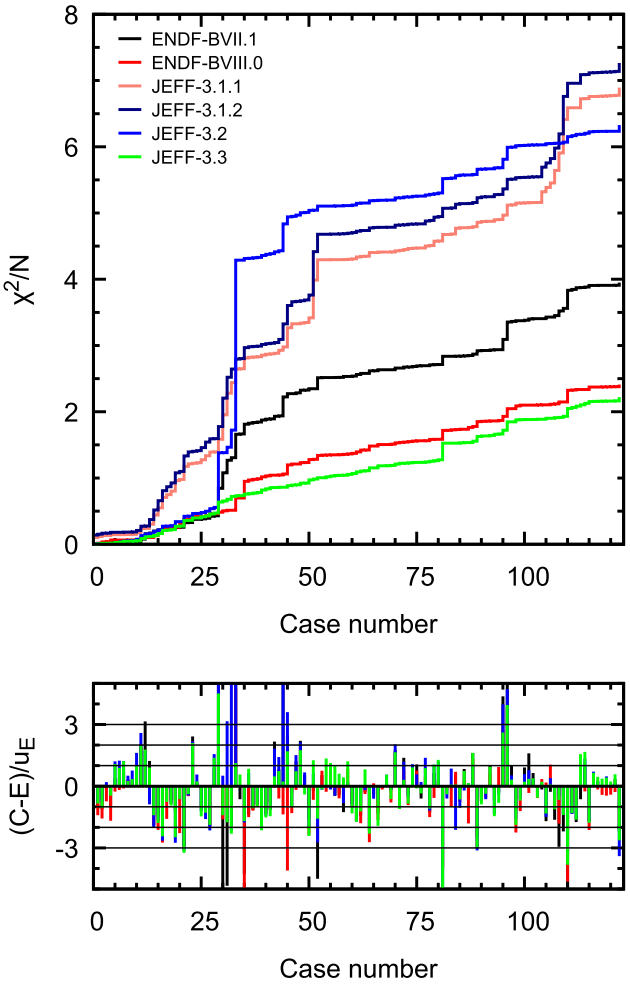

Fig. 61 Cumulative χ^2/N (top) and residuals (bottom) for the Extended Mosteller suite of 123 benchmark cases from the ICSBEP Handbook [23]. The horizontal axis shows the benchmark number sorted first by fuel as in Table 30, then by material (metal, compound, solution), then by spectrum (fast, intermediate, thermal). For brevity, $C = k_{C,i}$, $E = k_{E,i}$, $u_E = |\Delta k_{E,i}|$

From the figure it is clear that these improvements are obtained through the elimination of significant outliers. Larger steps are associated with an absolute residual greater than 3 standard deviations. JEFF-3.2 has 13 such cases with values as high as 18, while JEFF-3.3 has only 6 with highest value 5.5. The number of cases with absolute residual less than 1 is 61 for both libraries. This is less than the 84 cases expected from a Gaussian distribution where the uncertainty is determined by the benchmarks alone. The residual dispersion is due to imperfect agreement between calculation and benchmark values. The large number of outliers (deviation more than 3σ) suggests the same: we should have between none and one ($0.2\% \times 123 = 0.25$).

thermal if > 50% of fissions is below 0.625 eV, intermediate if > 50% of fissions is between these energies and it is mixed otherwise.

Table 30 Comparison of χ^2/N values for the NEA suite by fuel category and spectrum (Th. for thermal, Int. for intermediate)

Fuel	N	ENDF/B-VII.1	ENDF/B-VIII.0	JEFF-3.1.1	JEFF-3.2	JEFF-3.3
HEU	42	5.5	3.1	8.4	12.8	2.5
IEU	12	6.4	3.1	14.6	7.4	1.5
LEU	13	1.1	1.5	1.1	0.8	1.7
MIX	8	0.8	0.8	0.9	0.9	0.8
PU	29	3.1	2.3	2.9	3.3	2.8
U233	18	3.4	1.9	11.1	1.4	1.9
SPEC	1	4.9	3.8	14.3	11.6	6.9
Spect.						
Fast	73	3.8	2.3	8.7	4.7	2.5
Th.	42	2.1	1.6	1.5	1.7	1.7
Int.	8	15.4	7.8	19.4	45.5	2.3
Total	123	3.9	2.4	6.9	6.3	2.2

The most important improvements in JEFF-3.3 over JEFF-3.2 are for:

- hmf73 The unmoderated Zeus benchmark with a high sensitivity to copper data. A small step remains in JEFF-3.3 that is not in the ENDF/B-VIII.0 library, leaving room for improvement for future JEFF releases,
- hmi6-4 and hmi6-3 The initial Zeus experiments with graphite-HEU core and Cu reflector,
- imf1-3 JEMIMA unreflected cylindrical stacks of natural and highly-enriched uranium,
- pst9-1 and pst9-3 plutonium solution benchmarks for which smaller steps remain.

Had JEFF-3.2 had a better copper evaluation, avoiding the hmf73 and hmi6 discrepancies, it would have been uniformly better than JEFF-3.1.x and similar in performance to ENDF/B-VII.1. The JEFF-3.3 copper data play an important role in the improvement, but it must be noted that all steps occurring in JEFF-3.3 are smaller than in JEFF-3.2. This must be attributed to significant improvements for the major actinides.

Even if the χ^2/N of JEFF-3.3 is rather good, it is still substantially greater than 1, indicating the importance of the remaining outliers. The following benchmarks differ more than 3 standard deviations: hmf15-1 (unreflected HEU cylinder), hmf73 (see above), pmf8-1 (a thorium shell around a plutonium sphere), pmf21-2 (a stack of cylindrical Pu disks with BeO cylindrical reflectors), pst9-3 (see above), and umf4-2 (a high purity ^{233}U sphere reflected by W). Clearly, significant progress can be made if these cases could be resolved by a future evaluation. If the contribution of these six cases were negligible Chi-square would drop to 1.4.

The remaining discrepancies due to systematic errors are more difficult to trace. Other ways of examining the data are warranted. One method would be to look at further outliers. After all we should have only 5–6 cases outside 2σ, where we have 15 with JEFF-3.3. The additional cases from worst to best are smf8-1 (Np sphere in HEU shell), pst9-1 (see above pst9-3), hmf13 (steel reflected HEU sphere), hmf9-2 (BeO relected HEU sphere), imf6-1 (duralumin relected HEU sphere), hmi6-3 (copper and graphite reflected HEU sphere), lst7-3 (unreflected cylinder), hst13-3 (unreflected sphere), hmf19-1 (graphite reflected HEU sphere). If these were also negligible Chi-square would be one (but statistics would be violated).

Table 30 shows average performance per category of fuel and spectrum. JEFF-3.3 shows good improvement over JEFF-3.2 and JEFF-3.1.1 for highly and intermediate enriched uranium and a clear improvement for plutonium over JEFF-3.2 making it slightly better than JEFF-3.1.1. For low enriched uranium and ^{233}U performance is somewhat worse, although it is better than the overall average of JEFF-3.3. Given that JEFF-3.1.1 and JEFF-3.2 were excellent for low-enriched fuel, this change is unfortunate. On the other hand the number of LEU cases is small and they are atypical for power applications. Further validation is needed for an unambiguous assessment of JEFF-3.3 for power reactors.

Looking at the spectrum there is a clear improvement for fast systems and a very similar behaviour for thermal systems compared to earlier versions of the library. This indicates that the library has improved overall performance for advanced reactor modeling. Pending further validation this indicates that it would maintain good performance for present and near term power (thermal) reactors. For intermediate spectra the improvement is dramatic owing to the elimination of the outlying hmi6 case (Zeus, see above). The SPEC case smf8 (Np sphere with HEU shell) improved but not as much as in ENDF/B-VIII.0. Since the HEU cases improved considerably this points at a need to further improve the ^{237}Np evaluation.

Table 31 Number of benchmarks in the NRG-suite per ICSBEP category

	COMP				MET				SOL				MISC			
	t	i	f	m	t	i	f	m	t	i	f	m	t	i	f	m
LEU	462	–	–	–	31	–	–	–	67	–	–	–	–	–	–	–
IEU	33	4	2	–	–	–	28		60	–	–	–	–	–	–	–
HEU	156	6	6	8	51	5	294	6	402	–	–	–	–	–	–	–
MIX	100	–	9	–	–	–	33	–	53	–	–	–	60	–	11	–
PU	–	1	–	34	–	5	100	6	385	–	–	–	–	–	–	–
^{233}U	8	–	–	–	1	–	10	–	60	33	–	–	–	–	–	–
Total	759	11	17	42	83	10	465	12	1027	33	–	–	60	–	11	–

Table 32 Average $C/E - 1$ value in pcm (100 pcm = 0.1%) for the NRG-suite compound and metal cases for JEFF-3.3 (roman) and *JEFF-3.1.1* (italics)

	COMP				MET			
	Therm	Inter	Fast	Mixed	Therm	Inter	Fast	Mixed
LEU	-21 ± 522				49 ± 255			
	−55 ± 534				*323 ± 495*			
IEU	-1 ± 437	-437 ± 1254	216 ± 140				136 ± 326	
	−240 ± 431	*−468 ± 2548*	*189 ± 69*				*−176 ± 389*	
HEU	784 ± 1267	2283 ± 5008	-298 ± 138	-943 ± 522	-12 ± 857	181 ± 617	-34 ± 438	467 ± 553
	472 ± 1395	*−1912 ± 4569*	*−362 ± 172*	*−1221 ± 432*	*−43 ± 854*	*235 ± 971*	*−220 ± 511*	*422 ± 708*
MIX	-356 ± 1122		458 ± 184				317 ± 288	
	−264 ± 1108		*306 ± 164*				*164 ± 370*	
PU		−191		2245 ± 960		469 ± 585	197 ± 487	1170 ± 299
		692		*1798 ± 890*		*619 ± 1353*	*92 ± 497*	*478 ± 220*
^{233}U	415 ± 130				−3373		-13 ± 192	
	−312 ± 102				*−3898*		*363 ± 199*	

The table further shows that ENDF/B-VIII.0 performs better for Pu benchmarks and worse for HEU and IEU. Otherwise the libraries show rather similar performance.

3.1.2 The NRG suite

The NRG suite contains 2530 benchmarks for a variety of fuel types, physical forms of the fissile component and neutron spectra (Table 31). It therefore allows a better statistical analysis of performance of a library than the NEA-suite discussed above.

The results for the NRG suite[6] using JEFF-3.3 and JEFF-3.1.1 are summarized in Tables 32 and 33. The $(C - E)$ values in pcm (parts per 100,000) are averaged by ICSBEP category as indicated and the standard deviation of the population is given. A second analysis is reported in Fig. 62 where results are lumped by spectrum. For each group the distribution of $(C/E - 1)/u_E$ is displayed together with a normal-distribution fit. If the nuclear data and the benchmark evaluations were not subject to biases, the $(C/E-1)/u_E$ distribution would converge to a normal distribution centered on zero and with standard deviation equal to one.

The improvement of JEFF-3.3 with respect to JEFF-3.1.1 for the thermal cases is small and mainly signalled by the slightly more peaked distribution. For the intermediate and mixed spectrum cases the sample size is too small to draw any statistically significant conclusion. However, for the intermediate spectrum the bias in the calculated k_{eff} seems to be roughly identical for the two libraries, with the mean lying more than one standard deviation below the benchmark values. For the mixed spectrum the mean lies more than one standard deviation above the benchmark value and this bias seems to have increased from JEFF-3.1.1 to JEFF-3.3. For fast spectrum cases the width of the distribution hardly changed, but a slight bias in JEFF-3.1.1 seems gone with JEFF-3.3.

Despite the overall agreement between the two libraries some differences stand out that may be correlated with the changes itemized below:

[6] The results for JEFF-3.1.1 differ from those in Ref. [373] because many benchmark cases have been added since.

Table 33 Average $C/E-1$ value in pcm (100 pcm = 0.1%) for the NRG-suite for JEFF-3.3 (roman) and *JEFF-3.1.1* (italic) for solution and miscellaneous systems

	SOL		MISC	
	Therm	Inter	Therm	Fast
LEU	118 ± 305			
	179 ± 289			
IEU	140 ± 534			
	87 ± 539			
HEU	157 ± 947			
	40 ± 1102			
MIX	-482 ± 396		150 ± 536	-53 ± 285
	−374 ± 381		*57 ± 491*	*−863 ± 419*
PU	114 ± 547			
	196 ± 557			
^{233}U	485 ± 680	-1591 ± 814		
	229 ± 684	*−1638 ± 804*		

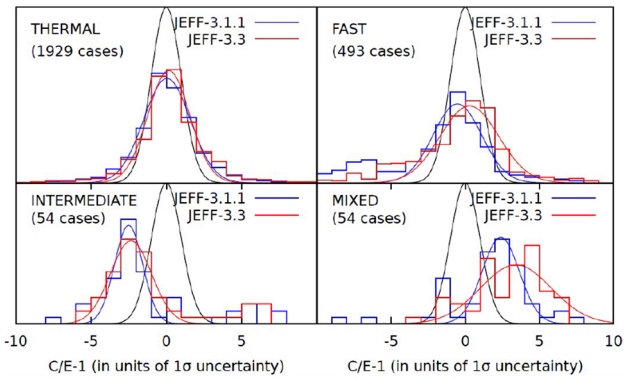

Fig. 62 The distribution of $C/E-1$, in units of the combined benchmark and statistical uncertainty. The normal distribution (in black) would be the perfect situation

- predictions for some well-known benchmarks such as hmf-1 (Godiva) and imf7 (Big Ten) improved;
- the new thermal scattering data for heavy water yield better results for lmt15 (lattices of 2% enriched uranium in heavy water);
- results for hst49 (uranyl nitrate solution containing cadmium) improved, presumably thanks to the amelioration of the ^{113}Cd data.
- results for hmf67 (ZPR-9 assemblies with tungsten, graphite and aluminum) are much better;
- results for lct60 improved because of the new carbon evaluation.

From the tables and the figure, it stands out that the rather obvious improvement in χ^2/N for the NEA-suite is not reflected by distributions significantly more normal for JEFF-3.3 than for JEFF-3.1.1. This confirms the conclusion of the previous section based on a small subset of ICSBEP that systematic effects leading to biases and plain discrepancies dominate the distributions. It is therefore of interest to further investigate and categorize these discrepancies in order to clearly identify where future development should be directed.

3.1.3 The IRSN suite for criticality safety

A total of 238 ICSBEP benchmark cases [374] were selected by IRSN for the thermal, intermediate and fast energy range. The diversity of media and configurations makes these benchmarks representative of criticality safety considerations for fuel cycle operations. The selection is wider than the NEA-suite discussed above and provides further indications about the performance of JEFF-3.3. Here a subset is presented that highlights remaining deficiencies with the aim of identifying the way forward. Experiments with unrealistic uncertainties were systematically discarded (uncertainties less than Godiva – hmf1).

The multiplication factor k_{eff} of the selected benchmarks was calculated using the Monte Carlo code MORET 5.D.1. The nuclear data libraries were processed with GAIA-1.1.1, based on NJOY2016.35. The results for JEFF-3.3 are compared with JEFF-3.2 and JEFF-3.1.1 (Fig. 63) and ENDF/B-VIII.0 (Figs. 63, 64).

Figure 63 shows the residuals for 138 cases by ICSBEP category. For many cases JEFF-3.3 performs better than JEFF-3.1.1 and JEFF-3.2 and has comparable residuals with ENDF/B-VIII.0. These conclusions are, however, not uniform as a detailed inspection of the figure shows. If we focus on outliers of JEFF-3.3 Table 34 shows the 45 cases that deviate more than 2 and more than 3 (19 cases) benchmark standard uncertainties in the combination of the NEA and IRSN suites. Special materials for these benchmarks, i.e. materials other than the major actinides, oxygen or water are listed in Table 35. The table mentions only 35 benchmarks. Therefore the number of outliers in which a particular material features

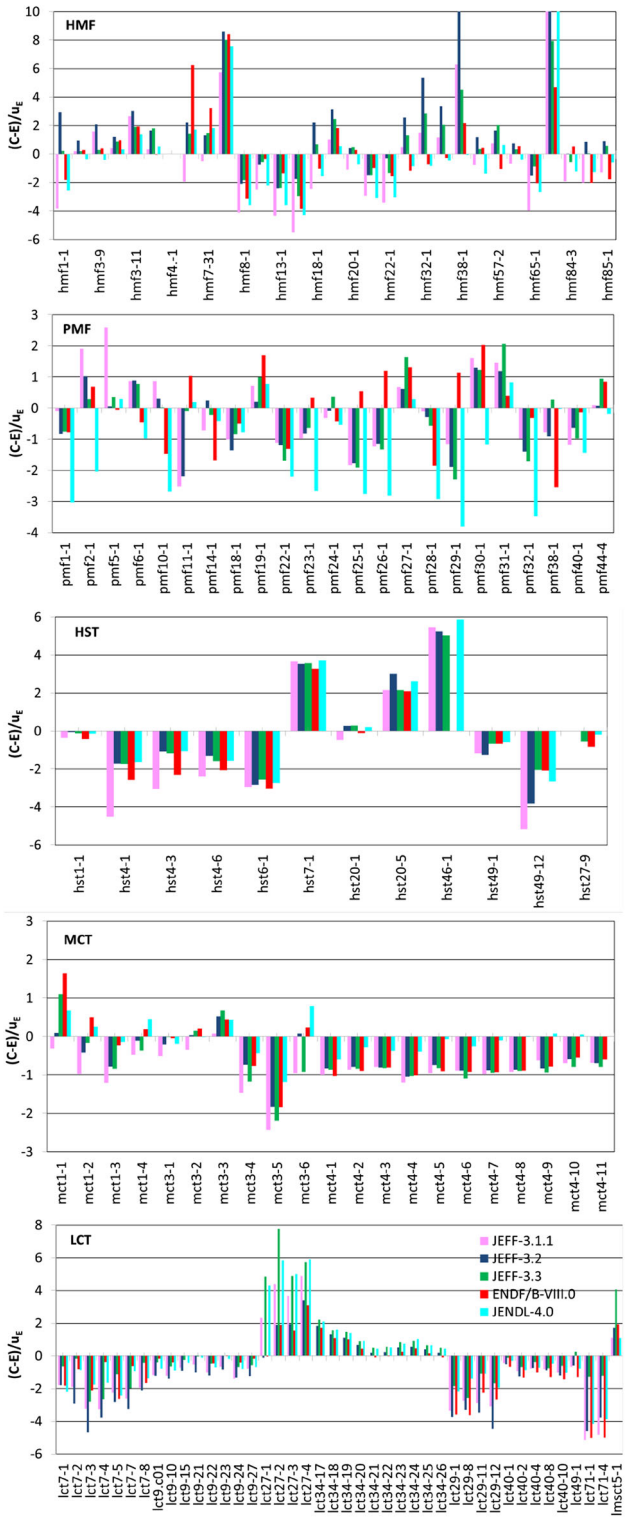

Fig. 63 Comparison of JEFF-3.3, JEFF-3.2, JEFF-3.1.1 and ENDF/B-VIII.0 for the IRSN selection of ICSBEP benchmarks for criticality safety of the fuel cycle. Highly-enriched metallic uranium with fast spectra (HMF), the same for plutonium (PMF), highly-enriched U-235 solutions (HST), mixed oxide fuel (MCT), and low-enriched U-235 in lattices (LCT)

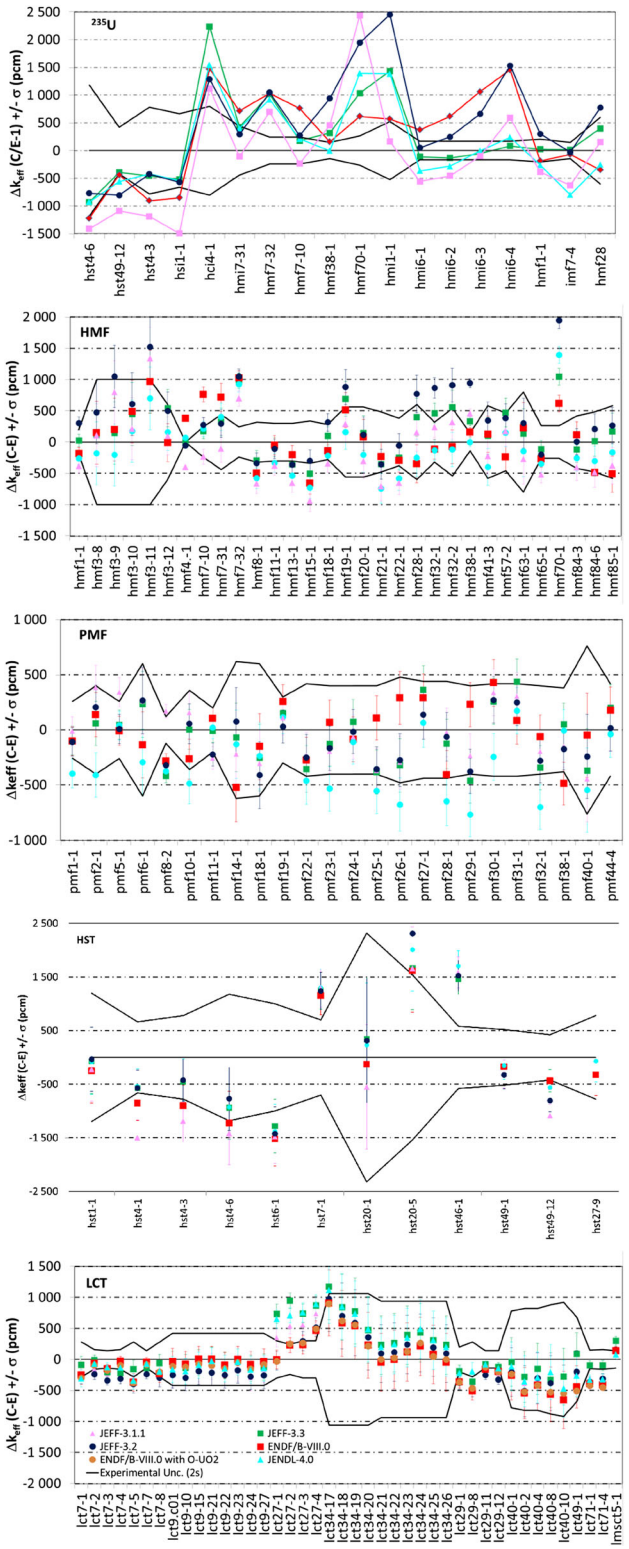

Fig. 64 Comparison of JEFF-3.3 and ENDF/B-VIII.0 for the IRSN selection of ICSBEP benchmarks for criticality safety of the fuel cycle. U-235 (U235), highly-enriched metallic uranium with fast spectra (HMF), the same for plutonium (PMF), highly-enriched U-235 solutions (HST) and low-enriched U-235 in lattices (LCT)

Table 34 Summary of outliers for JEFF-3.3 in the NEA and IRSN suites sorted by ICSBEP category. Cases shown are more than 3 experimental standard uncertainties off (> 3s) or between 2 and 3 standard uncertainties (2-3s). The geometry (geo) is either rectangular (Rec), spherical (Sph), cylindrical (Cyl) or hexagonal (Hex). The main reflector material is given in Column (ref)

Case	> 3s	2–3s	Geo	Ref	Comment
hmf7-32	x		Rec	Bare	Teflon mod.
hmf9-2		x	Sph	BeO	
hmf13		x	Sph	Steel	
hmf15-1	x		Cyl	Bare	
hmf19-1		x	Sph	C	
hmf32-1		x	Sph	U-nat	10 cm U-nat
hmf32-2		x	Sph	U-nat	9 cm U-nat
hmf38-1	x		Cyl	U-dep	Be+BeO moderator
hmf57-2		x	Sph	Pb	16.5 cm lead
hmf70-1	x		Cyl	Al_2O_3	In-core W, Al
hmf73	x		Cyl	Cu	Unmoderated
hmi1-1	x		Cyl	Steel	
hmi6-3		x	Sph	Cu	C moderated
hci4-1	x		Cyl	Be	
hst6-1		x	Cyl	Bare	
hst7-1	x		Rec	Concrete	
hst13-3		x	Sph	Bare	
hst20-5		x	Cyl	Bare	D_2O, fluoride
hst46-1	x		Cyl	BeO, C	Sulfate
hst49-12		x	Cyl	Water	Cd in fuel
imf6-1		x	Sph	Al	Duralumin
lct7-3		x	Rec	Water	2.1 cm pitch
lct7-4		x	Rec	Water	2.52 cm pitch
lct7-7		x	Hex	Water	2.26 cm pitch
lct27-1	x		Rec	Pb	0 cm gap
lct27-2	x		Rec	Pb	0.5 cm gap
lct27-3	x		Rec	Pb	1.0 cm gap
lct27-4	x		Rec	Pb	1.5 cm gap
lct29-8		x	Rec	Water	Hf plates
lct34-17		x	Rec	Water	Cd in steel
lmt5-1	x		Rec	PE	ErO, HEU-Al
lst7-3		x	Cyl	Bare	
mct3-5		x	Rec	Water	
pmf8-1	x		Sph	Th	
pmf21-2	x		Cyl	BeO	
pmf29-1		x	Sph	Bare	
pmf31-1		x	Sph	PE	
pst9-1		x	Sph	Bare	
pst9-3	x		Sph	Bare	
pst18-1		x	Cyl	Water	
pst28-1		x	Cyl	Water	
pst30-1		x	Cyl	Water	
pst32-1	x		Cyl	Water	
smf8-1		x	Sph	Bare	Np in HEU
umf4-2	x		Sph	W	

Table 35 Non-actinide materials (mat.) featuring in outliers of the NEA and IRSN suites. N is the number of cases. Bold are cases off by more than 3 experimental standard uncertainties

mat.	N	Cases
PE	2	**lmt5-1**, pmf31-1
D_2O	1	hst20-5
Be&BeO	5	hmf9-2, **hst46-1, pmf21-2, hmf38-1, hci4-1**
C	3	hmf19-1, hmi6-3, hst46-1
F	2	**hmf7-32**, hst20-5
Al	3	**hmf70-1**, imf6-1, **lmt5-1**
concrete	1	**hst7-1**
S	1	**hst46-1**
Steel	4	hmf13, hmf7-1, lct34-17, **hmi1-1**
Cu	2	**hmf73**, hmi6-1
Er	1	**lmt5-1**
Hf	1	lct29-8
W	2	**umf4-2, hmf70-1**
Pb	5	hmf57-2, **lct27-1 to -4**,
Th	1	**pmf8-1**
Np	1	smf8-1

is small, i.e.it is at most 5 (for Pb and Be/BeO). The table shows iron and aluminum with few cases (2 and 3, resp.) as it ignores that iron and aluminum are almost always present as container or support material. For lead 5 cases are mentioned, four of which are correlated (lct27-1 to lct27-4) as only the water gap between the lead reflector and the fuel assembly was varied. However, the indication is clear (see also Sects. 3.1.7, 3.3.2). A case like lmt5-1 is ambiguous as it involves the three: Er, polyethylene and aluminum. Similarly, hst46-1 involves both BeO and sulfate and hmf70-1 involves W and Al.

With all these considerations it seems that progress can be made by working on improvements for the special materials involved in the main outliers polyethylene, beryllium or beryllium-oxide, fluor, aluminum, concrete, sulphur, steel, copper, erbium, tungsten, lead, and thorium and with a second priority for deuterium or heavy water, graphite, hafnium, and neptunium.

The 16 additional outliers do not concern any of these materials implying they are strictly concerned with the major actinides, oxygen and water. So, important work lies ahead in improving these major constituents of nuclear systems and some of the statements concerning the special materials above are conditioned by the state of play for these materials.

In more detail, Fig. 64 (top panel) presents the results for benchmarks highly sensitive to the ^{235}U cross sections, in particular capture. The selection is ordered by Energy of Average Lethargy causing Fission (EALF) from 0.2 eV to 850 keV.

- hci4-1, hmf7-32, hmf70-1 and hmi1-1 show the largest discrepancies for JEFF-3.3;
- for hci4-1, hmf70-1 and hmi1-1 ENDF/B-VIII.0 performs better. The reflectors vary from Be, to Al2O3 and steel. These are among the materials mentioned as requiring further scrutiny in future evaluations;
- as noted before significant improvement was brought by the new evaluation of copper in JEFF-3.3;
- for the selected suite, JEFF-3.3 and ENDF/B-VIII.0 produce equal or better results than JEFF-3.2, with the exception of hci4.

For the study of performance of JEFF-3.3 in fast systems 24 plutonium and 64 highly-enriched metallic uranium cases were inspected (Figs. 63, 64). These had reflectors, ranging from none to water, depleted uranium, CH_2, alumina, tungsten and steel. Uranium-235 enrichments range between 89.5 wt% and 97.7 wt%. Pu concentrations vary from 1.8 wt% to 20.16 wt%. Specific tendencies due to the reflectors can be observed:

- JEFF-3.3 and ENDF/B-VIII.0 ^{238}U cross sections reduce the overestimation observed with JEFF-3.2 for hmf28 and hmf32 while JEFF-3.1.1 agrees better than JEFF-3.3;
- hmf57-2 having a lead reflector is 2 standard uncertainties off for JEFF-3.3 and is better described by ENDF/B-VIII.0;
- pmf25, pmf26 and pmf32 having iron reflectors are within 2 standard uncertainties for JEFF-3.3 but are better described by ENDF/B-VIII.0;
- benchmarks with nickel and copper show a systematic bias of several hundreds of pcm between JEFF-3.3 and ENDF/B-VIII.0, which results in JEFF-3.3 performing slightly better for the selected cases.

JEFF-3.3 was also tested on several thermal systems, including experiments with high-enriched uranium (HEU) in solution and low-enriched uranium (LEU) in fuel rod lattices. Again, various reflectors were considered, including light water, heavy water, beryllium oxide and unreflected systems. Eleven HEU solution experiments with ^{235}U enrichment higher than 89.3 wt% and with concentrations ranging from 13.24 g/l to 516.6 g/l were investigated to test the modification of the ^{235}U cross sections in the resonance range.

- JEFF-3.3 shows a general agreement for benchmarks with solutions in heavy water such as hst4 and hst20;
- the new oxygen evaluation (not included in JEFF-3.3) and the new thermal scattering data for deuterium in D_2O and oxygen in D_2O (both in JEFF-3.3) improve the results when compared with the previous JEFF evaluations.

Finally, for UO_2 lattices (LCT cases), Fig. 64 (bottom panel), we find:

- Many of the observed discrepancies in the LCT cases may originate from the structural materials of the absorbing canisters or the reflectors surrounding the lattices;
- a significant deterioration of the results for benchmarks with thick lead reflector (lct27) for JEFF-3.3 compared with JEFF-3.2 with the k_{eff} being overestimated;
- for the whole series the oxygen evaluations adopted by JEFF-3.3 and ENDF/B-VIII.0 shift the k_{eff} results upward compared to the results of JEFF-3.2.
- the effect of the thermal scattering data of oxygen in UO_2 appear to be negligible.

3.1.4 The PSI suite for criticality safety

The considered area for future criticality safety evaluation (CSE) applications at PSI is currently restricted to light water reactors (LWR) spent fuel storage pools and transport casks with (possibly borated) steel as separator/absorber materials. Therefore, the present validation calculations were performed based on a suite of 15 low-enriched thermal compound uranium (LCT) and 4 mixed plutonium uranium thermal compound (MCT) benchmarks yielding a total of 149 critical experiments. All experiments were extracted from ICSBEP [23] and the selection of benchmark configurations was based on their similarity to designs found in today's LWR compact storage pools and transport casks. The ratios between calculated (C) and experimental (E) values obtained by applying MCNP-6.1.1 with JEFF-3.3 cross section library are reported in the left part of Fig. 65, along with the experimental values and results from previous versions of the JEFF libraries. Error bars represent the benchmark and calculated uncertainties at one standard uncertainty, the latter with respect to the calculations (12–20 pcm statistical uncertainty).

Results show that JEFF-3.3 predicts on average a higher k_{eff} than JEFF-3.2 with an average difference of 78 ± 69 pcm. In particular, this overestimation appears mostly in the subset of LCT benchmarks, where the average deviation increases to 102 ± 43 pcm. Preliminary tests with MCNP correlate such a trend to the changes in ^{16}O and ^{238}U cross sections. A statistical analysis (for details see Ref. [375]) was performed to determine the weighted average k_{eff}, the standard deviation of the sample, and the biases given by bias $= |1 - \langle k_{\text{eff}} \rangle|$ for all

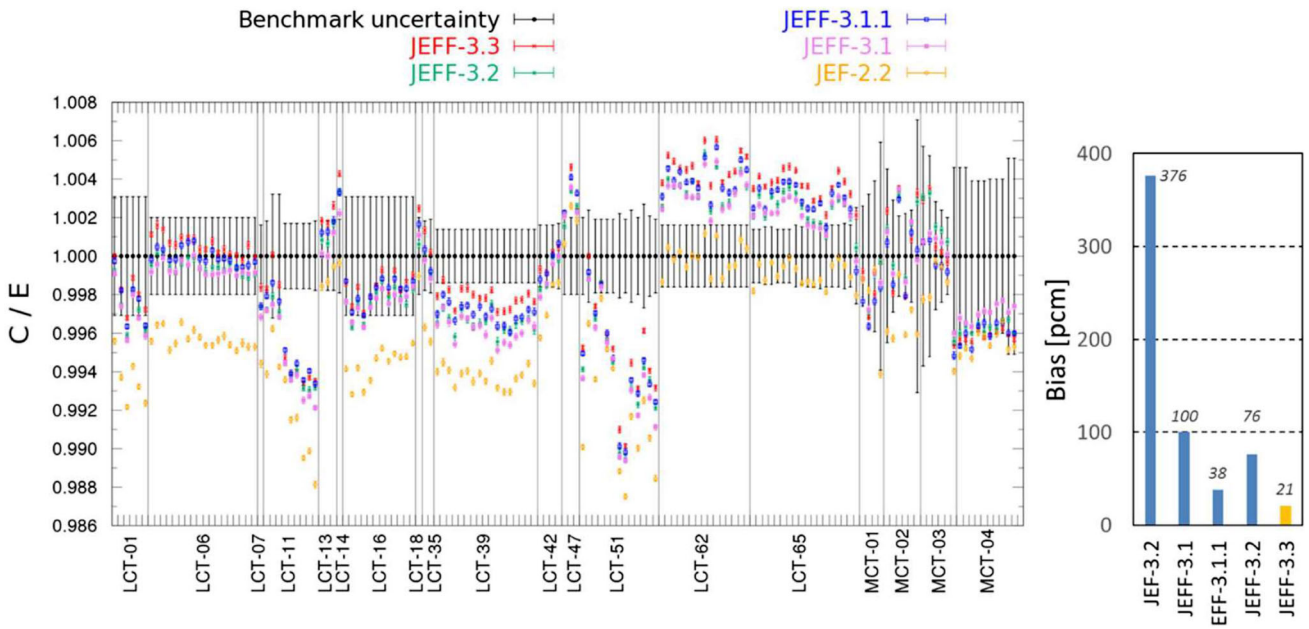

Fig. 65 (Left) Benchmark and calculated C/E values separated by vertical lines and are ordered by increasing benchmark and case number; (Right) Biases as function of cross section data library

cross section libraries. The obtained values for the biases are reported in the right part of Fig. 65, showing that JEFF-3.3 has the lowest value; hence, it performs better than JEFF-3.2 and even JEFF-3.1.1 for the selected set of benchmark cases.

3.1.5 The IAEA suite

The analysis for the NRG suite showed the importance of statistical validation with the main conclusion that systematic effects dominate the distributions of $(C - E)/u_E$. Clear improvements were made, but for further progress the important issues must be identified and tackled. The IAEA suite of about 1700 ICSBEP benchmarks [376] was studied by analysing the cumulative Chi-square plot shown in Fig. 66.

On the whole the recent ENDF/B-VIII.0 and JEFF-3.3 libraries follow each other closely, with the latter coming out somewhat lower at $\chi^2/N = 7$ and the former at $\chi^2/N = 8.5$. Of interest are the major steps and what they could be caused by. The largest contributions (here not included) come from the ORNL bare cylinders of hmf51, some of which have unrealistically low uncertainties of 10 pcm. Large steps, still shown, are due to hmt11, the Valduc water-moderated highly-enriched uranium benchmarks and hmf076 (ORCEF-PE) which both have low uncertainties, as well. This is unfortunate, since no conclusions about nuclear data are possible for those steps. In fact, if we would eliminate all benchmarks with an uncertainty below 100 pcm (256 cases) then χ^2/N with N = 1740 for JEFF-3.3 drops to 2.9 (or 3.4 if N = 1484). So, more than half the score is due to benchmarks with a very low uncertainty. Even when these are eliminated 398 cases remain with absolute residuals between 3 and 100! (537 with absolute residuals over 2). It is clear that so many outliers are difficult to analyze on a case by case basis and that this is even more difficult if the quality of the benchmark may be the issue. For the time being we satisfy ourselves with the more in-depth analysis of Ref. [376] providing additional indications that Fe, Cu and W should be investigated further. For Fe this is suggested by hmf88, hmt13, hmt15 in addition to the already mentioned hmi1 ICSBEP case. Besides the materials already mentioned in Table 35, Ref. [376] indicates improvements are warranted for chromium (hci5-4) and gadolinium (lct5).

3.1.6 Masurca and Eole

The JEFF versions from JEFF-3.1.1 to JEFF-3.3 have been tested on three types of core configurations: fast, UOX and MOX. For the fast spectrum, two configurations, performed at the Masurca facility have been considered. These were ZONA2A and ZONA2B from the CIRANO program [377]. The ZONA2A core has a fertile blanket whereas the ZONA2B core is surrounded by a reflector made of a mix of steel and sodium.

For the UOX cores three configurations are shown, all of them representative of a PWR and performed at the EOLE facility. The UH1.2 configuration from the EPICURE program [378] and the MISTRAL1 [379] configuration both have an enrichment of 3.7% but have different moderation ratios (VH_2O/VUO_2): 1.2 for UH1.2 with a lattice pitch of 1.26 cm and 1.7 for MISTRAL1, so slightly over-moderated

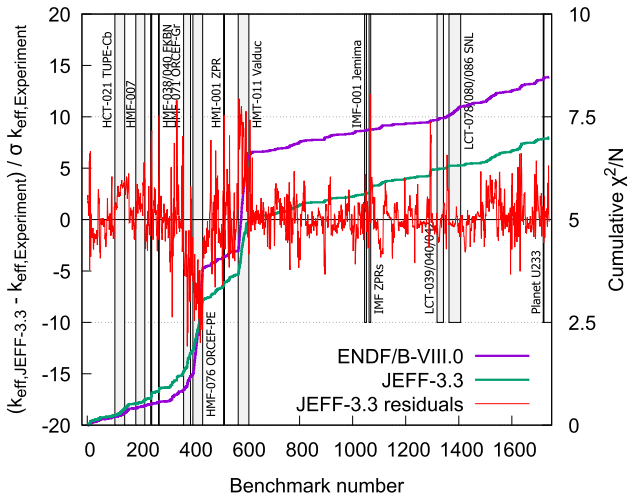

Fig. 66 Cumulative χ^2/N for the full IAEA suite of 1740 benchmark cases from the ICSBEP handbook

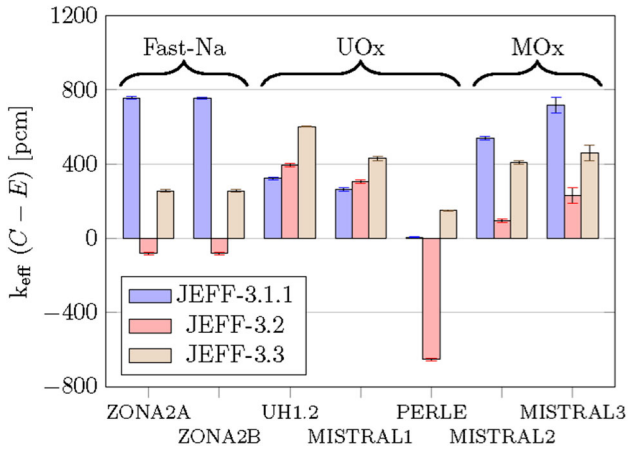

Fig. 67 Comparison of k_{eff} using different versions of JEFF libraries on experimental reactor cores. Experimental uncertainty can be taken to be ±200 pcm including technological uncertainty

with a lattice pitch of 1.32 cm. The PERLE core [380] is different as it is surrounded by a 22 cm thick stainless steel reflector representative of a GEN III core. The fuel composition of the PERLE core is also 3.7% ^{235}U enriched UO_2 with a 1.32 cm lattice pitch. The PERLE core is a 27 x 27 square lattice, whereas UH1.2 and MISTRAL1 have cylindrical cores (radius 26.76 cm and 20.11 cm, resp.).

The two MOX configurations (MISTRAL2 and MISTRAL3) are also from the EOLE facility. The difference is again the moderation ratio (1.7 and 2.1, resp.) [379] MISTRAL2 has the same lattice pitch as MISTRAL1 but for MISTRAL3 the lattice pitch is 1.39 cm. Both configurations use the same fuel enrichment of 7% in Am-PuO_2. Both configurations are 100% MOX loaded. The cores are modeled as cylinders with radii 28.48 cm for MISTRAL2 and 29.40 cm for MISTRAL3. In the MISTRAL3 case criticality is

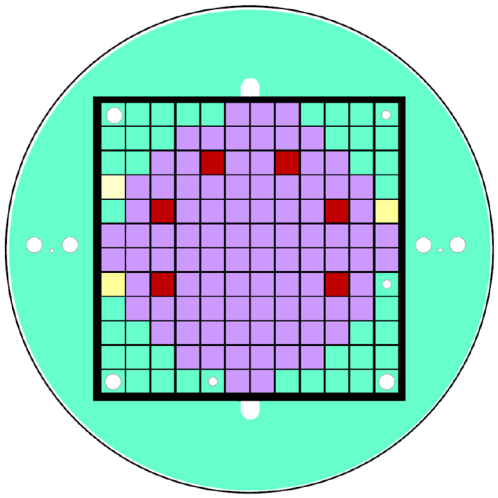

Fig. 68 The CR0 configuration of the VENUS-F reactor. The vessel is 160 cm diameter. Violet: fuel assemblies, green: lead reflector, yellow B_4C control rod, red B_4C safety rod, white air, black: stainless steel

reached by adjusting the boron concentration whereas for MISTRAL2 clear water is used.

The performance of the JEFF evaluation versions on the fast, UOX and MOX cores are shown in Fig. 67. The Monte Carlo code, TRIPOLI-4® [381], was used to obtain these results. Consistent trends can be observed in the sense of a marked increase of k_{eff} moving from JEFF-3.2 to JEFF-3.3. With the exception of the PERLE experiment this change is away from agreement with the experiments. For the fast spectrum and the MOX cases agreement is still better than it was for JEFF-3.1.1, but not for the UOX cases. For the PERLE experiment, which exhibits the strongest change from JEFF-3.2 to JEFF-3.3 reactivity was strongly underestimated in the previous former release, but is now restored to a value closer to experimental data. Given the common trend the changes are most likely due to the changes in the major actinides.

3.1.7 VENUS-F

For VENUS-F, a zero-power critical facility [382], k_{eff} and β_{eff} were calculated using various versions of the JEFF-3 library. MCNP5-1.60 was used to model the critical configuration "CR0", which includes 30 wt%-enriched metallic uranium fuel rods and solid lead as coolant-simulator and reflector (Fig. 68). This configuration exhibits an epithermal to fast neutron spectrum in the fuel region, with a peak between 200 and 700 keV. The flux drops below 1% of the maximum below 10 keV and above 10 MeV.

Table 36 shows a comparison of k_{eff} predictions calculated with different nuclear data libraries [383]. Significant changes from JEFF-3.2 to JEFF-3.3 include the following individual effects:

Table 36 Calculated k_{eff}-values for the VENUS-F CR0 core. The statistical uncertainty of the calculated values is less than 5 pcm

Library	k_{eff}	Library	k_{eff}
JEFF-3.1.2	1.0059	JENDL-4.0	1.0031
JEFF-3.2	1.0083	ENDF/B-VII.1	1.0069
JEFF-3.3	1.0073	ENDF/B-VIII.0	1.0054

- an increase in the ^{235}U capture cross section in the URR (22.5–160 keV) causing a drop in k_{eff} by 900 pcm;
- a decrease in the ^{238}U capture cross section in the URR (20 keV–1 MeV) causing a k_{eff} increase by 350 pcm;
- an increase of k_{eff} by 500 pcm due to ^{208}Pb;
- intermediate impacts of ^{206}Pb, ^{207}Pb and ^{209}Bi, quantified respectively as a k_{eff} increase by 100 pcm, a k_{eff} decrease by 80 pcm and a k_{eff} decrease by 70 pcm.

The net decrease is 100 pcm. The k_{eff} improvement for the VENUS-F CR0 core is therefore small and the remaining 730 pcm discrepancy suggests taking a closer look at the lead data of JEFF-3.3 in close combination with ^{235}U and ^{238}U. This indication for lead adds to the evidence found in Table 35 (ICSBEP hmf57 and lct27, see also Sect. 4.2.4).

3.1.8 FRM II

FRM II is a 20 MWth research reactor of TU Munich that operates on highly enriched uranium fuel (93% enrichment), is heavy water moderated and cooled and has massive metallic hafnium control and safety rods. The fuel element is a compact hollow cylinder with dispersion fuel. The control rod moves inside the cylinder and has a beryllium follower. The fuel element with bent fuel plates is surrounded by five massive safety rods (metallic Hf, diameter 10 cm), which approach the core vertically in case of a shut down. In Fig. 69 they are shown in their closest neighborhood location to the central channel tube (26 cm diameter).

Figure 69 shows k_{eff} calculations using different versions of the ENDF/B and JEFF-3 libraries for a fresh fuel element at first critical. This means the safety rods are moved out of the way and the control rod is at the highest position consistent with $k_{\text{eff}} = 1$ for beginning of cycle. The calculations use a 3d model and MCNP5. The model is detailed and more complicated than shown, as a result of the experimental channels surrounding the fuel element in the full 3d representation. The calculations trace the history of FRM-II beginning-of-cycle situations from its design, when ENDF/B-V was used, to the present with JEFF-3.3 and visualize the impact of a new evaluation introduced for hafnium in ENDF/B-VI. JEFF-3.3 does very well as it is only 50 pcm below critical. ENDF/B-VI gave also a nearly perfect $k_{\text{eff}} = 1$, but this agreement is destroyed when taking the new evaluation for hafnium. As a conclusion, a general trend with ENDF/B-VI to higher k_{eff}

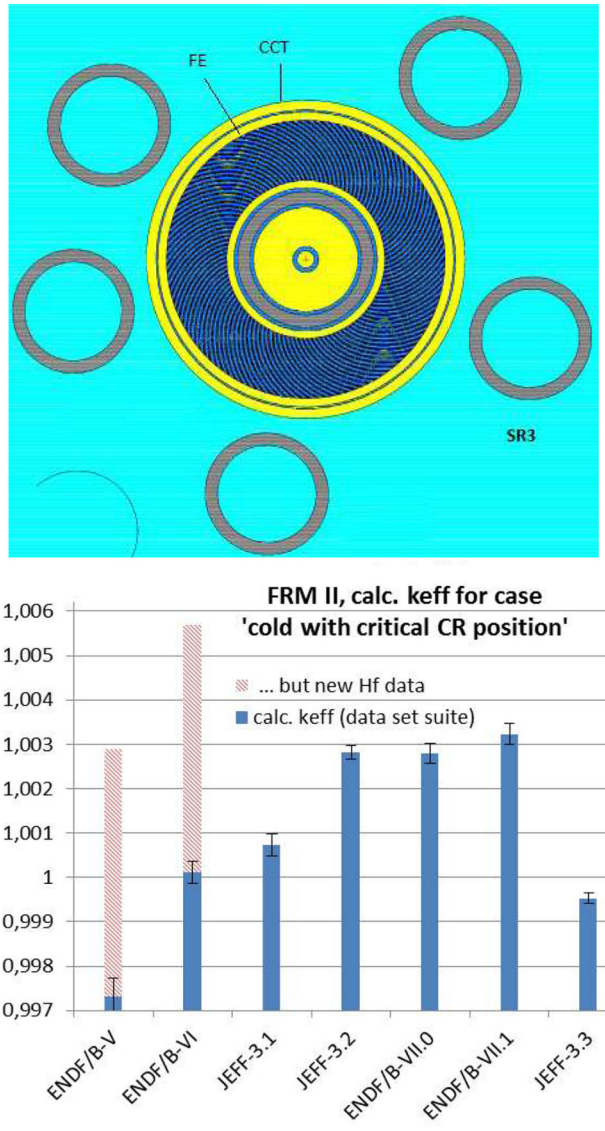

Fig. 69 Top: horizontal cross section view of the compact fuel element (dark blue) in the central channel tube, that separates the primary coolant circuit from the heavy water in the tank (D_2O is light blue) at FRM II. The Hf of the control and safety rods is given in grey. Aluminum is shown in yellow. Bottom: effective multiplication factors calculated for FRM-II using different versions of the ENDF/B and JEFF-3 libraries

with ^{235}U data had been compensated with higher absorption for the inserted Hf control rod at FRM-II. For JEFF a new set of hafnium files was introduced in JEFF-3.2 along with a new file for deuterium. This meant that JEFF moved from + 70 pcm with JEFF-3.1 to + 280 pcm with JEFF-3.2. The change from JEFF-3.2 to JEFF-3.3 is most likely due to the changes introduced for ^{235}U with a possible impact of the new scattering law for heavy water.

At FRM-II the main concern with the new data is the confirmation that the reactivity grasp of the control and safety rods is consistently described as large enough so that one or even two of the safety rods are not needed for safe shutdown.

Table 37 Differences between calculated and measured boron concentration and axial offset versus burnup along an actual cycle operation of a PWR (Westinghouse), three loops, 157 fuel assemblies and 2775 MWth. Calculations were performed with the original SEANAP system and the upgraded version that includes the JEFF-3.3 (J-3.3) nuclear data library

Power (%)	Burnup $\left(\frac{GWd}{tM}\right)$	Boron concentration			Axial Offset		
		Meas. (ppm)	SEANAP		Meas. (%)	SEANAP	
			Orig. (ppm)	J-3.3 (ppm)		Orig. (%)	J-3.3 (%)
50	0.015	1200	1150	1165	7.7	5.6	5.9
75	0.031	1113	1071	1085	3.8	3.7	3.9
100	0.134	985	1000	1011	− 0.7	0.7	0.8
100	1.34	870	897	896	− 1.6	− 1.2	− 1.2
100	2.487	779	806	797	− 2.4	− 2.9	− 2.9
100	2.842	755	778	768	− 2.8	− 3	− 3.1
100	3.591	688	714	701	− 3.8	− 4.9	− 5
100	4.441	604	645	629	− 3.2	− 3.8	− 3.9
100	5.549	504	544	526	− 3.9	− 4.4	− 4.6
100	6.692	412	439	420	− 4.2	− 4.4	− 4.5
100	7.716	319	340	321	− 4.7	− 5.1	− 5.2
100	8.823	227	239	219	− 3.6	− 2.8	− 2.8
100	10.284	101	100	79	− 3.5	− 1.6	− 1.5
100	11.351	4	− 7	− 29	− 3.4	− 2.1	− 2.1

A clearly increased consistency of modeling with the newer data sets is therefore an excellent support to this goal [384].

3.1.9 Pressurized water reactor

JEFF-3.3 has been processed into WIMSD5 format and used to upgrade the SEANAP system, a computational system for the 3D core analysis of the Spanish pressurized water reactors [385]. The original version of the SEANAP system, which uses WIMSD4 and its own adjusted nuclear database from 1981, has demonstrated a very good agreement with the broad sets of parameters and cycles analyzed for the Spanish PWR units. SEANAP showed excellent predicting capabilities for the critical boron concentrations along many completed operating cycles. The calculations showed a general agreement with the measurements within a factor of 20–50 ppm. Also, the calculated axial asymmetry of incore power – incore axial offset – is within 1–4% of the actual measurement, including the cycle start-up and operation maneuvers at different powers along the whole cycle.

Table 37 reports the results for a typical cycle operation of one of the Spanish Units used for the SEANAP validation. The upgraded SEANAP system with JEFF-3.3 shows the following maximum deviations of calculated to measured values:

- 35 ppm of boron concentration;
- 2% of axial offset.

These differences are within the range of validation for the SEANAP system. It can be concluded that JEFF-3.3 integrated in the SEANAP system gives equivalent or even better results for PWR analyses than those produced with ad-hoc nuclear data evaluations.

3.2 Delayed neutrons

In contrast with k_{eff}, there are only a handful of effective delayed neutron β_{eff} measurements reported with sufficiently detailed information. In Ref. [386] more than twenty measurements are listed, including several measurements of Rossi-α. The latter is closely related to β_{eff} through the prompt neutron generation life time. Earlier, these experimental data[7] were used by van der Marck for testing ENDF/B-VII.0 [386] and JEFF-3.1.1 [373].

The fast spectrum cores considered include fuels of ^{235}U (Masurca, FCA, SNEAK, ZPR, Godiva), but also plutonium (FCA, ZPR, Jezebel) and a mix of the two (Masurca, FCA, SNEAK, ZPR) and finally ^{233}U (Skidoo). Using these fast spectrum cases, the ^{233,235,238}U and ^{239}Pu data were tested. One should bear in mind that the tests performed here are assumed to be only sensitive to the total delayed neutron yields. The delayed neutron yields per group are not tested, nor are the values for the decay constant per group.

[7] We avoid the term "benchmark" for these cases because a good benchmark description, comparable to those given in the ICSBEP Handbook [23], is not available.

Table 38 $C/E-1$ in % for β_{eff}. The quoted uncertainty includes only the statistical uncertainty of the calculation. All the cases have a fast spectrum, except for TCA and IPEN/MB01. The experimental β_{eff} is given in pcm with a relative uncertainty r. $C/E-1$ deviating more than $3r$ are underlined

		Experiment β_{eff}	JEFF-3.3	JEFF-3.1.1
	TCA	771 (2.2%)	2.3 ± 0.8	3.9 ± 0.7
	IPEN/MB01	742 (0.9%)	$\underline{4.2} \pm 0.9$	$\underline{4.6} \pm 1.0$
	Masurca/R2	721 (1.5%)	2.1 ± 1.1	2.9 ± 1.1
	Masurca/ZONA2	349 (1.7%)	2.6 ± 1.7	1.1 ± 1.7
	FCA/XIX-1	742 (3.2%)	3.0 ± 1.2	3.6 ± 1.2
	FCA/XIX-2	364 (2.5%)	3.3 ± 1.6	3.8 ± 1.6
	FCA/XIX-3	251 (1.6%)	4.4 ± 1.9	-1.2 ± 2.0
	SNEAK/9C1	758 (3.2%)	-1.8 ± 1.1	-0.8 ± 1.1
	SNEAK/7A	395 (5.1%)	1.0 ± 1.5	-1.0 ± 1.5
	SNEAK/7B	429 (4.9%)	3.5 ± 1.4	3.7 ± 1.3
	SNEAK/9C2	426 (4.5%)	-4.9 ± 1.5	-5.4 ± 1.5
hmi1	ZPR-9/34	667 (2.2%)	0.7 ± 2.2	4.2 ± 2.2
	ZPR-U9	725 (2.3%)	2.6 ± 1.9	0.8 ± 1.9
mmf11-1	ZPPR-21/B	381 (2.4%)	$-\underline{8.9} \pm 2.3$	-4.5 ± 2.2
pmi2	ZPR-6/10	222 (2.3%)	5.9 ± 3.8	3.9 ± 0.7
hmf1	Godiva	659 (1.5%)	0.3 ± 1.1	-1.7 ± 1.1
hmf28	Topsy	665 (2.0%)	4.1 ± 1.0	2.4 ± 1.0
pmf1	Jezebel	194 (5.2%)	-3.1 ± 1.6	-1.0 ± 1.6
pmf6	Popsy	276 (2.5%)	$\underline{7.6} \pm 1.7$	4.3 ± 1.4
umf1	Skidoo	290 (3.4%)	0.7 ± 1.4	1.7 ± 1.4
umf6	Flattop	360 (2.5%)	3.1 ± 1.3	4.2 ± 1.3

Table 39 The values for $C/E-1$ in % for the Rossi-α calculations. The uncertainty quoted for $C/E-1$ includes only the statistical uncertainty of the calculation. $C/E-1$ values deviating more than three times the relative experimental uncertainty are underlined. All the cases have a thermal spectrum, except for Big Ten. The Rossi-α is in s^{-1}

		Experiment Rossi$-\alpha$	JEFF-3.3	JEFF-3.1.1
	SHE/8	6.53 (5.2%)	-1.5 ± 1.0	-3.5 ± 1.0
lst1-1	Sheba-II	200.3 (1.8%)	-4.4 ± 1.4	4.7 ± 1.4
lst4-1	Stacy/29	122.7 (3.3%)	-2.9 ± 1.2	3.5 ± 1.2
lst4-3	Stacy/33	116.7 (3.3%)	-0.6 ± 1.2	0.2 ± 1.2
lst4-5	Stacy/46	106.2 (3.5%)	-0.1 ± 1.1	0.7 ± 1.1
lst7-2	Stacy/30	126.8 (2.3%)	-1.1 ± 1.2	0.9 ± 1.2
lst16-3	Stacy/125	152.8 (1.7%)	-4.1 ± 1.2	3.2 ± 1.2
lst21-215	Stacy/215	109.2 (1.6%)	-4.6 ± 1.1	0.0 ± 1.2
hst38	Winco	1109.3 (0.1%)	$-\underline{4.4} \pm 1.0$	$\underline{0.7} \pm 1.0$
imf7	Big Ten	1.17×10^5 (0.9%)	0.1 ± 1.4	-0.3 ± 1.5

For Rossi-α most of the available experimental data are from cores with a thermal spectrum with ^{235}U fuel. Most cores have low enrichment (Sheba-II, SHE-8, Stacy cores, TCA cores and the IPEN/MB01 core) and only one has highly enriched uranium (Winco slab tank). As a consequence, for thermal spectra only the ^{235}U delayed neutron data are tested.

The β_{eff} and Rossi-α results based on JEFF-3.3 are given in Tables 38 and 39, as well as the results based on other libraries. The results for the Proteus experiment have been omitted, because of concerns about the representativity of the model that was used. The comparison is in favor of JEFF-3.1.1. For the 31 experiments and taking account of the limited simulation statistics, JEFF-3.3 has 6 cases for which the difference with experiment is more than 2 standard deviations while JEFF-3.1.1 has only 2. JEFF-3.3 differs by 3 or more standard deviations for the β_{eff} of IPEN/MB01 (4.7s), ZPPR-21/B (-3.7s) and POPSY (3.0s) and for the Rossi-α of WINCO. JEFF-3.1.1 differs by 3 or more standard deviations for the β_{eff} of IPEN/MB01 (5.1s) and the Rossi-α of WINCO. The WINCO Rossi-α has a very low uncertainty. Note, however (see below), that the data uncertainty is about 3%.

Table 40 Calculated and experimental β_{eff}-values for the VENUS-F CR0 core. The statistical uncertainty of the calculated values is 2 pcm

Library	β_{eff}	Library	β_{eff}
JEFF-3.1.2	730	JENDL-4.0	724
JEFF-3.2	733	ENDF/B-VII.1	727
JEFF-3.3	729	ENDF/B-VIII.0	727
Experiment	730(11)		

For imf7 (Big Ten) the accurate Rossi-α value of Paxton [387] is given in Table 39 which is very well reproduced by JEFF-3.3 and JEFF-3.1.1 certainly considering that only a partial uncertainty is shown for the calculated values. The Big Ten β_{eff} has been discussed before as well, even if no direct experimental result is available. The ICSBEP Handbook quotes an "accepted value" that "appears to be $\beta_{\text{eff}} = 720 \pm 37$ pcm", a number less accurate than the Rossi-α [23]. Calculations of β_{eff} were made using several evaluations with MCNP [388]. The delayed *prompt k-ratio* method and the *KOPTS* method were used. For JEFF-3.2 β_{eff} was overestimated by 3.3% (KOPTS method) and 4.5% (prompt k-ratio). Both are within 1 standard uncertainty. For JEFF-3.3 the overestimations are 1% and 1.1%, resp. JEFF-3.3 therefore agrees even better with the "accepted" β_{eff} than JEFF-3.1.1 and the slight method bias disappeared.

Finally, the effective delayed neutron fraction β_{eff} of the VENUS-F CR0 core, mentioned earlier (Fig. 68, was measured to be 730 ± 11 pcm [389].

Table 40 shows that the calculated β_{eff}-values are all in excellent agreement with experiment. The calculations were performed with MCNP using the KOPTS card.

In conclusion, JEFF-3.3 performs well for estimates of β_{eff} and Rossi-α with admittedly a slight deterioration over JEFF-3.1.1. An uncertainty analysis could not be performed because of the missing covariances for delayed neutron data in JEFF-3.3. Previous studies using the covariances from JENDL-4.0u indicate that the uncertainties due to nuclear data are around 3%, and up to 7% for ^{233}U reactor systems [388].

3.3 Neutron Shielding and Transmission

Clean shielding and transmission experiments have a simple geometry, one predominant material and a well characterized irradiation source, i.e. either

- a well-characterized ^{252}Cf spontaneous fission neutron spectrum with a mean neutron energy of 2.1 MeV;
- a ^{2}H$+^{3}$H neutron source with quasi monoenergetic neutrons peaked at 14 MeV; or
- a fission reactor fast neutron spectrum.

Table 41 List of ToF experiments employing a 14 MeV neutron source used to test JEFF-3.3. The LLNL experiments are from MCNP-6 suite. Mat. is Material, Okt. Oktavian

Mat.	FNS	LLNL	Okt.	Mat.	FNS	LLNL	Okt.
Li		X		Be	X	X	
Graphite	X	X		N_2	X	X	
O_2	X			Al			X
Si			X	Ti			X
Cr			X	Mn			X
Fe	X	X		Co			X
Cu			X	As			X
Se			X	Zr			X
Nb			X	Mo			X
W			X	Pb	X	X	
^{235}U, ^{238}U		X		^{239}Pu		X	
Mat.	FNS	MCNP-6	Okt.				
Li2O	X						
Iron-duct		X					
+SS304		X					
+PE		X					
Concrete		X					
Water		X					
LiF			X				
Teflon			X				

Typical geometries involve spheres, slabs or rods. The measured quantities are the energy-differential neutron or γ-leakage or transmission fluxes normalized per source neutron. The relevant information about the experimental setups is usually available in either the SINBAD [367] or the ICSBEP [23] database. Alternatively, one must resort to the original publications. When important details are not available an experiment cannot be used for testing and validating of nuclear data.

Experimental data are confronted with MCNP6.1 [390] calculations using ACE libraries prepared with NJOY-2012.99 [41].

3.3.1 ToF shielding experiments

An overview of time-of-flight (TOF) shielding and transmission experiments that used a 14-MeV dT neutron source is given in Table 41. They were performed at Oktavian or FNS or are taken from the MCNP-6 shielding suite (MCNP-6_SS) [391,392]. Here the performance of JEFF-3.3, FENDL-3.1b and ENDF/B-VIII.0 is compared.

For OKTAVIAN, fifteen validation studies were carried out for different materials. Figure 70 shows the simulations for Cr, Mo and W. To highlight the differences C/E values averaged over broad energy groups are calculated and shown in Table 42.

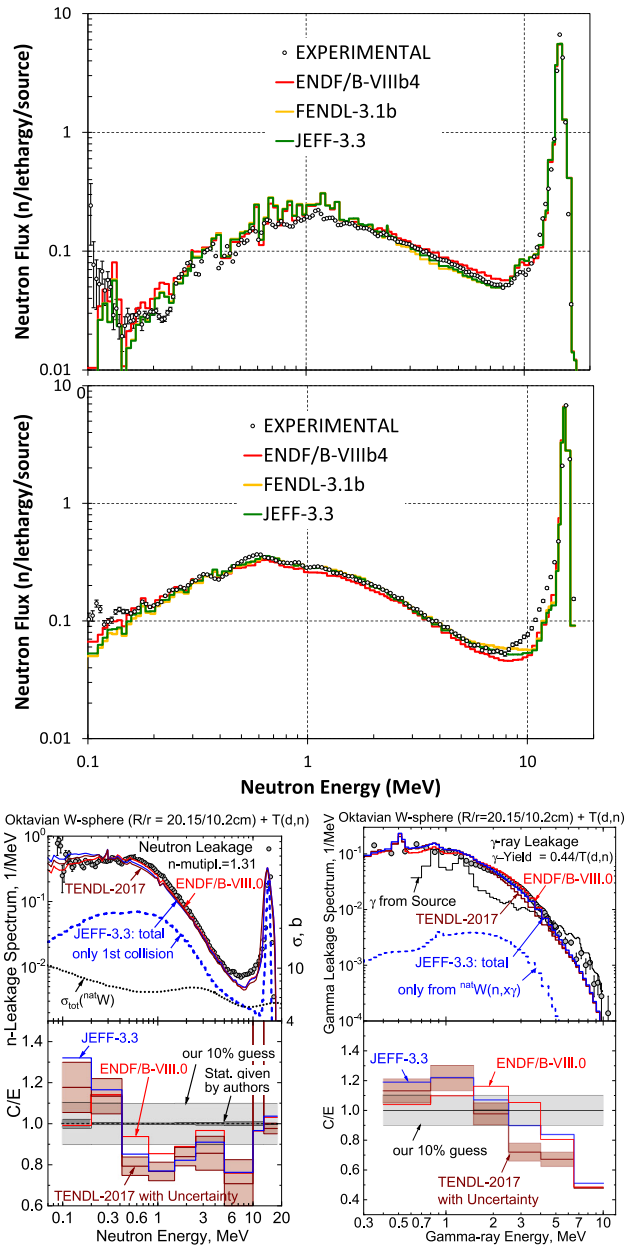

Fig. 70 Comparison of leakage spectra in OKTAVIAN/ToF spheres. Top: neutrons from a 40 cm Cr sphere, middle: neutrons from a 61 cm Mo sphere, bottom: leakage spectra from a 40 cm tungsten sphere; bottom left: neutrons, bottom right: gammas [367]

For W neutron and gamma leakage spectra are shown for the thickest sphere (40 cm diameter) along with C/E ratios (Fig. 70). The total leakage and partial contributions from the first neutron collisions or γ-rays created by the dT source assembly are shown. The uncertainties given by the authors of the experiments include only statistics, so we have added an additional 10% as a rough approximation to the total uncertainty. The uncertainties of the calculated neutron and gamma leakage spectra were propagated by Monte Carlo sampling using TENDL-2015 random files. The resulting uncertainties are between 5 and 10%. Strong energy-energy correlations below 1 MeV follow from this approach. Considering both the experimental and nuclear data uncertainties, JEFF-3.3 performance is similar to ENDF/B-VIII.0 and TENDL-2017. For all three libraries leakage spectra are overestimated up to 30% and underestimated up to 50%. The overestimation tends to occur at low energy and the overestimation at high neutron energy (but below 14 MeV) or gamma energy. This implies that the impact on reaction rates will strongly vary with reaction threshold and more generally the reaction excitation function.

As an example for FNS, Fig. 71 shows calculations compared with data for leakage neutron spectra from Be and Pb at an angle of 0° with the deuteron beam. Table 43 summarises C/E for the energy-averaged angular flux for a cylindrical slab of diameter 31.4 cm with a thickness of 5, 20 and 40 cm of iron, 5.06, 20.24 and 40.48 cm of graphite and 5.06 and 15.24 cm of beryllium. Two different angles are reported 24.90° and 66.80°.

For the MCNP-6 shielding suite, three experiments were considered for iron and SS-304. These consisted of cylindrical slabs (configurations 1, 3 and 7). The MCNP-6 suite also includes a set of eleven LLNL pulsed sphere benchmarks for different target materials: Be, C, concrete, Fe, Pb, Li, N_2, ^{239}Pu, ^{235}U, ^{238}U and water. Results for the LLNL pulsed sphere experiments for ^{235}U and ^{238}U can be seen in Fig. 72.

As mentioned above the comparison of the experimental data for leakage neutron spectra measured by the time-of-flight technique for dT neutrons has shown a good performance for JEFF-3.3. In some cases, slightly better than the other libraries. The main conclusions of this comparison can be summarized as follows:

- **Be**: JEFF-3.3 showed much better agreement than ENDF/B-VIII.0 and FENDL-3.1b for the LLNL pulsed sphere included in the MCNP-6 suite. However, FNS-TOF shows angle-dependent underestimation from 1 to 10 MeV.
- **C**: For FNS, there are large differences between FENDL-3.1b and JEFF-3.3 at large angles for 50 mm and 200 mm thick C shells below 1 MeV in FNS. In general, FENDL-3.1b showed better agreement. This is also true for the slabs in the above Table 43 except for the higher energies at 66.8°.
- **Pb, Li_2O, N_2 and O_2**: The JEFF-3.3 library shows good agreement for FNS.
- ^{238}**U**: For the LLNL pulsed sphere, JEFF-3.3 shows overestimation from 18 to 26 ns (so, high neutron energy, see Fig. 72).
- **Fe**: JEFF-3.3 shows a good agreement for FNS, as do ENDF/B-VIII.0 and FENDL-3.1b (see Table 43) and the LLNL pulsed sphere.

Table 42 Results of OKTAVIAN experiments with spherical vessels. Values of C/E averaged leakage neutron spectra. The libraries are ENDF/B-VIII.0 (E), FENDL-3.1b (F) and JEFF-3.3 (J). The energy groups (E_n) are given in MeV

E_n (MeV)	Al (40 cm)			As (40 cm)			Co (40 cm)		
	E	F	J	E	F	J	E	F	J
10–16	1.01	1.01	1.01	0.82	–	0.83	0.81	0.83	0.83
5–10	0.91	0.90	0.90	0.88	–	0.92	0.89	0.55	0.55
1–5	0.91	0.91	0.91	1.22	–	1.14	0.69	0.64	0.64
0.5–0.1	0.93	0.93	0.94	1.12	–	1.08	0.58	0.61	0.62
0.1–0.5	1.41	1.38	1.41	1.23	–	1.27	0.64	0.77	0.78
E_n (MeV)	Cr (40 cm)			Cu (61 cm)			LiF (61 cm)		
	E	F	J	E	F	J	E	F	J
10–16	0.92	0.93	0.93	0.91	1.02	1.15	1.05	1.05	1.05
5–10	1.18	1.06	1.07	1.58	1.31	1.28	0.87	0.88	0.87
1–5	1.17	1.12	1.14	1.01	1.12	1.07	0.88	0.88	0.88
0.5–0.1	1.15	1.25	1.23	0.99	1.01	0.93	0.67	0.65	0.67
0.1–0.5	1.16	1.07	1.05	1.15	1.11	1.16	0.85	0.82	0.85
E_n (MeV)	Mn (61 cm)			Mo (61 cm)			Nb (61 cm)		
	E	F	J	E	F	J	E	F	J
10–16	0.98	0.98	0.92	0.85	0.83	0.83	0.85	0.83	0.83
5–10	1.02	1.02	1.00	0.86	1.04	0.97	0.86	1.04	0.97
1–5	0.95	0.96	1.13	0.96	1.05	1.04	0.96	1.05	1.04
0.5–0.1	0.87	0.87	1.00	0.84	0.90	0.90	0.84	0.90	0.90
0.1–0.5	1.25	1.24	1.16	0.98	0.92	0.95	0.98	0.92	0.95
E_n (MeV)	Se (40 cm)			Si (60 cm)			Teflon (40 cm)		
	E	F	J	E	F	J	E	F	J
10–16	0.97	–	0.94	0.87	0.87	0.9	0.66	0.65	0.66
5–10	0.74	–	1.28	1.03	1.03	0.96	0.66	0.64	0.66
1–5	1.25	–	1.21	1.05	1.06	0.99	0.61	0.63	0.61
0.5–0.1	1.21	–	1.12	1.18	1.18	1.13	0.61	0.58	0.61
0.1–0.5	1.5	–	1.54	1.26	1.24	1.18	0.79	0.68	0.80
E_n (MeV)	Ti (40 cm)			W (40 cm)			Zr (40 cm)		
	E	F	J	E	F	J	E	F	J
10–16	0.93	0.93	0.93	0.87	0.87	0.88	0.97	0.94	0.94
5–10	1.26	1.25	1.18	0.81	0.81	0.8	0.96	1.03	1.05
1–5	1.28	1.28	1.26	0.94	0.94	0.87	1.19	1.09	1.10
0.5–0.1	1.24	1.25	1.22	0.81	0.81	0.74	1.07	1.06	1.03
0.1–0.5	1.69	1.67	1.68	1.07	1.06	1.13	1.23	1.44	1.38

- In OKTAVIAN, JEFF-3.3 shows good results for Cu, Mn, Nb, Mo and As, overestimation for Al (in the range 0.1–0.5 MeV), Ti, Cr, Se and Zr and underestimation for Co and W as well as LiF and teflon.

3.3.2 SINBAD for Pb, Bi, Fe and O

Several shielding benchmarks from the SINBAD databases were used for the validation of lead, bismuth, iron and oxygen cross sections.

The following was observed:

- For **lead**, good agreement for the Grenoble lead slowing down experiment was observed [261] for both JEFF-3.2 and JEFF-3.3. Differences between the libraries are, however, substantial and given the importance of lead for lead-cooled fast reactors or accelerator driven systems they should be validated further.
- For **bismuth**, good agreement with the IPPE shielding benchmark was observed.
- For **iron**:

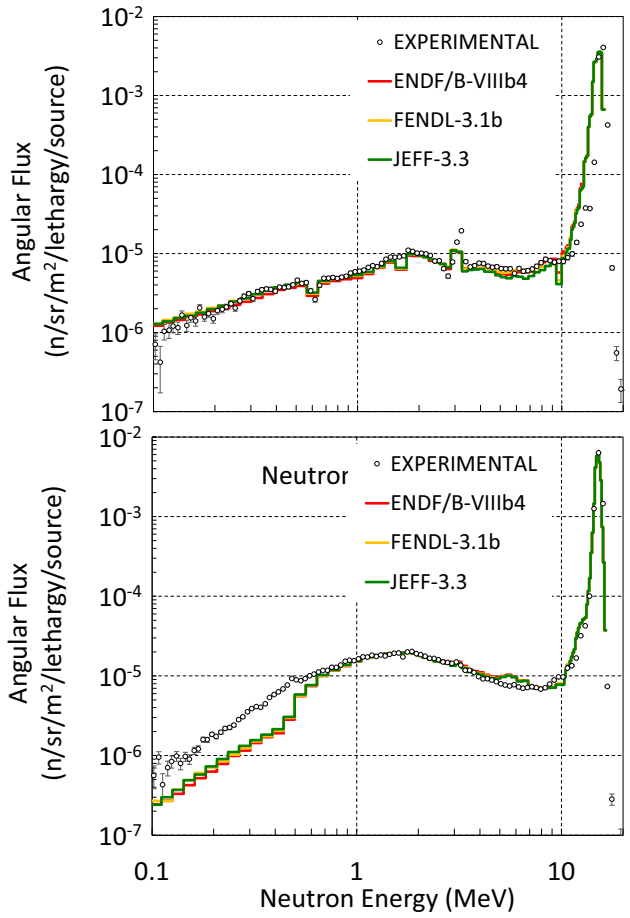

Fig. 71 Comparison of leakage neutron spectra in FNS/ToF cylinder. Top: 31.4 cm ∅ × 5.08 cm Be cylinder and fixed cone bias detector at 0 deg, Bottom: 31.4 cm ∅ × 5.06 cm Pb cylinder and fixed cone bias detector at 0 deg

  - **ASPIS-IRON88**: The ^{115}In(n,n') data are reproduced well suggesting that the lower part of the fast neutron spectrum is well described with the JEFF-3.3 iron data (Fig. 73). Significant discrepancies and differing trends were found for JEFF-3.3 and ENDF/B-VIII for ^{32}S(n,p) reaction rates sensitive to neutrons above 2 MeV. These differed up to a factor of 2 ([393], Fig. 73). However, using the covariance data from JEFF-3.3 the calculated reaction rates agree with experiment within one standard deviation. This indicates that JEFF-3.3 (and also ENDF/B-VII.1 and JENDL-4.0u) covariance matrices are reasonably realistic, with no clear trends of over or under estimation.
  - **TIARA** indicates good agreement up to 40 cm thick iron and overestimation for the thicker spheres by as much as a factor 2 near 10 MeV for the 1 m thick iron sphere using JEFF-3.3 (Fig. 74).

- For **oxygen**: For the FNS Liquid Oxygen experiment, relatively good agreement is observed between the measured and calculated spectra using JEFF-3.3 with no significant trends with increasing angle (Fig. 74). However, measurements cover only the energy range above 0.1 MeV, and the experiment may not be representative for all applications.

3.3.3 The FNG experiment for Cu

Besides occasional use in critical fissioning systems for which JEFF-3.2 and predecessors performed poorly, copper is widely used in fusion tokamaks. Examples are components of the heat sink, in particular the divertor and first wall, magnets, diagnostics, mirrors, waveguides, etc. Remarkably, the cross sections at the neutron energies relevant to fusion are not well assessed.

A benchmark experiment on a 60 × 60 × 70 cm^3 block of pure copper was performed at the 14 MeV Frascati neutron generator (FNG) in Italy. At 8 positions between 4 and 57 cm on the central axis of the block activation foils were irradiated to study the neutron flux and its energy distribution from thermal energies up to 14 MeV. The reactions used were ^{197}Au(n, γ)^{198}Au, ^{186}W(n, γ)^{187}W, ^{55}Mn(n, γ)^{56}Mn, ^{58}Ni(n, p)^{58}Co, ^{115}In(n, n')^{115m}In, ^{27}Al(n, α)^{24}Na, ^{93}Nb(n, 2n)^{92}Nb, and ^{197}Au(n, 2n)^{196}Au.

The experiment was simulated using MCNP-6. A detailed geometrical model of the whole experimental set-up was prepared. The neutron emission from the FNG target was accurately simulated by an ad hoc routine developed by ENEA and JSI [394]. Reaction rates and C/E values of irradiated activation foils at different penetration depths, and neutron and gamma-ray spectra, were determined. Figure 75 shows results for four threshold dosimetry reactions ^{115}In(n, n')^{115m}In, ^{27}Al(n, α)^{24}Na, ^{197}Au(n, 2n)^{196}Au and ^{93}Nb(n, 2n)^{92m}Nb with increasing thresholds (0.34, 3.25, 8.11 and 8.93 MeV). The experimental data are compared with estimates using the JEFF-3.2 and 3.3, as well as the TENDL-2015 nuclear data libraries. The reaction rates highlight an important feature shared with all shielding benchmarks: the strong attenuation of the flux and therefore the reaction rates with penetration depth over 4 to 5 orders of magnitude. The overall trend and magnitude of this attenuation with penetration depth is well reproduced by the calculations. On the other hand the C/E values show that the deviations may amount to 50% for the higher penetration depths. The main conclusions are

- JEFF-3.3 and TENDL-2015 agree best with the indium inelastic scattering dosimetry reaction showing a nearly constant under estimation of about 20% of the experiment. JEFF-3.2 (and JEFF-3.1.1) is nearly equal to JEFF-3.3 at 4 cm penetration depth but decreases to underestimate by about 50% and 30% at 57 cm.

Table 43 FNS slabs measured in time-of-flight. Energy-averaged and angle-dependent leakage-neutron C/E values for slab thicknesses of 5, 20 and 40 cm. The energy group in column E_n is given in MeV. The libraries are ENDF/B-VIII.0 (E), FENDL-3.1b (F) and JEFF-3.3 (J)

	Iron slabs of 31.4 cm ∅						Graphite slabs of 31.4 cm ∅						Beryllium slabs of 31.4 cm ∅					
	5.0 cm						5.06 cm						5.06 cm					
	Angle = 24.90°			Angle = 66.80°			Angle = 24.90°			Angle = 66.80°			Angle = 24.90°			Angle = 66.80°		
E_n	E	F	J	E	F	J	E	F	J	E	F	J	E	F	J	E	F	J
10–16	1.20	1.26	1.27	0.62	0.59	0.58	1.30	1.18	1.30	1.05	0.94	1.05	0.96	0.95	0.95	0.65	0.61	0.62
5–10	0.95	0.98	1.00	0.74	0.74	0.75	1.16	1.11	1.16	1.08	1.01	1.08	1.02	0.97	0.81	1.00	0.90	0.85
1–5	0.92	0.95	0.95	0.87	0.90	0.89	0.82	1.13	0.82	0.83	1.13	0.83	0.92	0.96	0.93	0.90	0.88	0.84
0.5–1	1.03	0.99	1.00	0.95	0.91	0.91	0.95	1.12	0.95	0.86	0.99	0.86	0.85	0.92	0.95	0.79	0.84	0.88
0.1–0.5	1.23	1.09	1.12	1.00	0.90	0.91	–	–	–	–	–	–	0.95	1.04	1.04	0.89	0.95	0.98
	20.0 cm						20.24 cm						15.24 cm					
	Angle = 24.90°			Angle = 66.80°			Angle = 24.90°			Angle = 66.80°			Angle = 24.90°			Angle = 66.80°		
E_n	E	F	J	E	F	J	E	F	J	E	F	J	E	F	J	E	F	J
10–16	0.99	1.04	1.04	0.82	0.77	0.76	1.11	0.98	1.11	1.00	0.85	1.00	0.96	0.95	0.95	0.71	0.67	0.67
5–10	0.81	0.91	0.92	0.81	0.89	0.89	1.06	0.96	1.06	1.05	0.92	1.05	1.07	1.00	0.86	0.98	0.90	0.83
1–5	0.88	0.98	0.97	0.85	0.96	0.94	0.88	1.04	0.88	0.88	1.01	0.88	0.97	0.95	0.90	0.94	0.89	0.84
0.5–1	0.99	1.01	0.99	0.96	0.98	0.96	0.84	1.07	0.84	0.80	1.03	0.80	0.89	0.90	0.90	0.85	0.86	0.86
0.1–0.5	1.08	1.00	1.04	1.02	0.95	0.97	–	–	–	–	–	–	1.02	1.02	1.03	0.97	0.96	0.97

	40.0 cm						40.48 cm					
	Angle = 24.90°			Angle = 66.80°			Angle = 24.90°			Angle = 66.80°		
E_n	E	F	J	E	F	J	E	F	J	E	F	J
10–16	0.93	0.92	0.95	0.67	0.63	0.63	0.89	0.75	0.89	0.79	0.64	0.79
5–10	0.80	0.97	0.94	–	–	–	1.01	0.86	1.01	1.05	0.85	1.05
1–5	0.95	1.15	1.11	0.74	0.94	0.88	0.83	0.85	0.83	0.86	0.84	0.86
0.5–1	0.98	1.07	1.01	0.87	0.97	0.92	0.82	0.94	0.82	0.89	1.03	0.89
0.1–0.5	0.97	0.96	0.96	0.84	0.82	0.85	–	–	–	–	–	–

- JEFF-3.3 (JEFF-3.1.2) and TENDL-2015 show overall good agreement with the ^{27}Al(n, α) data, with best agreement for JEFF-3.3 as it stays within 20% of the data, throughout and is well within 10% up to 30 cm penetration depth.
- For the ^{93}Nb(n,2n) and ^{197}Au(n,2n) dosimetry reactions JEFF-3.3 is clearly best staying within 10% of the data in both cases. The other libraries underestimate the rates remaining within 25% of the data.
- Non-threshold reactions (not shown here) show even larger underestimation (up to 60% for ^{186}W(n,γ)^{187}W), than indium inelastic scattering with the C/E decreasing as a function of the penetration depth. All libraries considered give similar results.

Clearly the new JEFF-3.3 evaluation for copper improves agreement with the FNG benchmark compared with (JEFF-3.1.2) JEFF-3.2 answering at least in part to the suggestions in Refs. [395,396]. Even if covariance data could be further improved it was concluded earlier that the uncertainties calculated using the available nuclear data were realistic ([397], Sect. 4.2.2). In combination with the results from criticality benchmarking we may conclude that JEFF-3.3 contains a substantially improved set of copper files compared with earlier versions of the library.

3.3.4 IPPE Shielding experiments for Fe and U

Neutron leakage spectra from natural iron spheres of various diameters with a ^{252}Cf source in the center were measured at IPPE [23,398]. The results of the comparison between measurement and a Monte-Carlo simulations using JEFF-3.2, JEFF-3.3 and ENDF/B-VIII.0 for the largest sphere with diameter 70 cm are shown in Fig. 76. As the Fe files are the same there is no difference between JEFF-3.2 and JEFF-3.3 and both libraries agree with the measurement within 1–2 times the experimental uncertainties (except at 0.3 MeV). Above 0.7 MeV ENDF/B-VIII.0 significantly underestimates the data by as much as 35%. For JEFF-3.3 this was the main reason to leave the existing JEFF-3.2 evaluation unchanged and not adopt the outcome of the CIELO project.

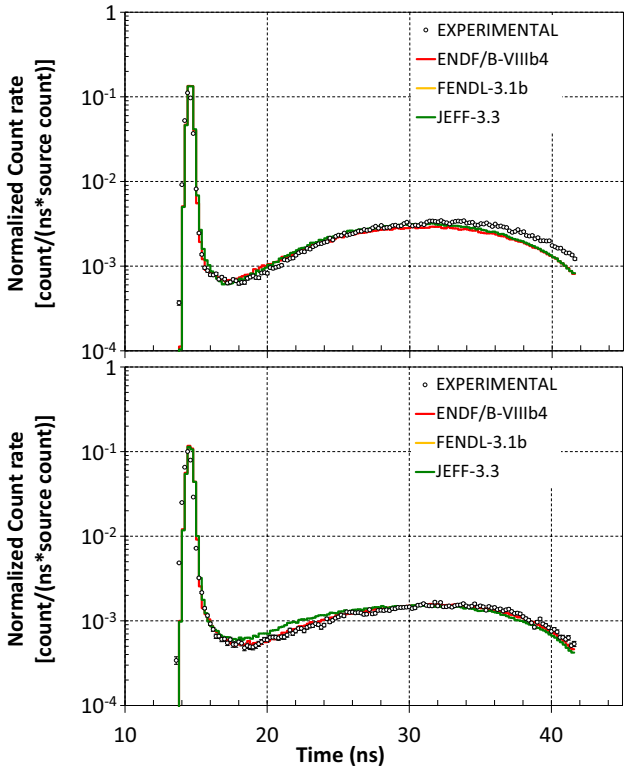

Fig. 72 Comparison of leakage neutron spectra of the LLNL time-of-flight pulsed spheres. Top: U-235, 0.7 mean free path (mfp), NE213-A detector at 30°, Bottom: U-238, 0.8 mean free path, Pilot-B detector at 30°

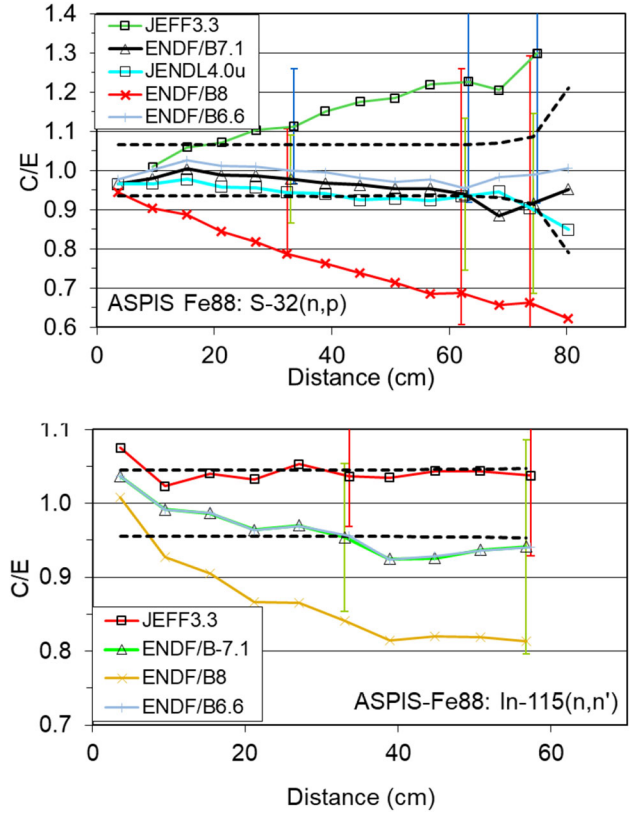

Fig. 73 Comparison of the C/E ratios calculated with MCNP for JEFF-3.3, ENDF/B-VI.6, -VII.1 and -VIII.0 for the ^{32}S(n,p) (top) and ^{115}In(n,n') (bottom) reaction rates measured in the ASPIS-IRON88 experiment. The error bars represent nuclear data uncertainties calculated from JEFF-3.3 and ENDF/B-VII.1 covariance matrices (Sect. 4.2.2)

Neutron leakage spectra from a depleted uranium sphere of 24 cm diameter with a ^{252}Cf source measured at IPPE [399] are compared with the same libraries. As seen in Fig. 76, the calculated spectra with JEFF-3.2 and JEFF-3.3 reproduce the experiment practically within the uncertainties and ENDF/B-VIII.0 agrees similarly. These experimental data confirm that above 100 keV the JEFF-3.3 and ENDF/B-VIII.0 U-238 evaluations show similar good performance for shielding.

3.3.5 The Řež shielding experiments for Fe

Neutron shielding experiments were made at the Řež Research Institute for iron shells of 20, 30, 50 and 100 cm diameter using a ^{252}Cf neutron source placed in the center (Fig. 77).

The detectors are based on detection of the hydrogen recoil following np scattering in either a spherical proportional counter or in a stilbene scintillator. The proportional counter is used at three different pressures (100, 400, 1000 kPa) to cover the neutron energy range from 0.01 to 1.3 MeV. The derivative method is used for spectrum unfolding. The measured data are corrected for proton escape from the detector. The center of the sphere and the detector are placed 2 m above the floor in a room without nearby objects that are not needed as support. The ambient background and the background due to room return neutrons is measured with a shielding cone between the sphere and the detector (Fig. 77). The proportional counter has a low sensitivity to gamma-rays. Electron-escape from the detector sensitive volume leads to a so-called physical threshold for gamma-rays. For a detector of 400 kPa hydrogen in a 4 cm diameter volume this threshold is 120 keV. By accepting only pulses with a pulse height above this threshold only recoil protons (neutrons) are detected. Pulse-shape discrimination is used with the stilbene detector to remove the gamma-ray contribution.

The data for the stilbene detector is in fact an average spectrum from 4 measurements made by different lead scientists: L.A. Trykov (Obninsk, 1–17 MeV, Řež experiment), F. Cvachovec, (Brno, 0.8–10 MeV, Řež experiment), M. Kostal, (Řež, 1–10 MeV, Řež experiment), A.M. Adams, (NIST, 0.57–4.5 MeV, NIST experiments with a large ROSPEC proportional counter). The NIST experiment used a sphere of 50.7 cm diameter. The NIST spectra were rescaled to represent a sphere of 50 cm by using the ratio of two simulations, one for a sphere of 50.7 cm and the other with 50 cm. The correction factor varied from 0.99 at 0.1 MeV to 1.02 at 1 MeV

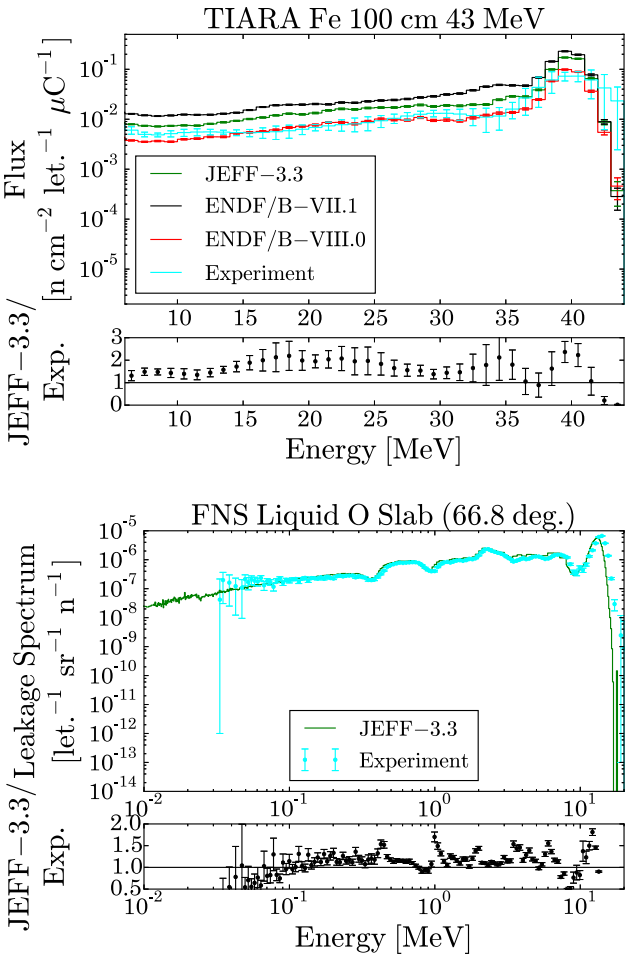

Fig. 74 Comparison of measured and calculated neutron spectra for 5 different iron shield thicknesses of the TIARA benchmark (top). The 10 cm results are multiplied by 10 for clarity. Comparison of measured and calculated neutron spectra for the FNS-O benchmark at an angle of 66° (bottom). The JEFF-3.3 evaluation was used for the calculations. Here, let. means lethargy or, equivalently, ln(E) ($d\Phi/d(\ln(E)) = E\, d\Phi/dE$, where Φ is flux)

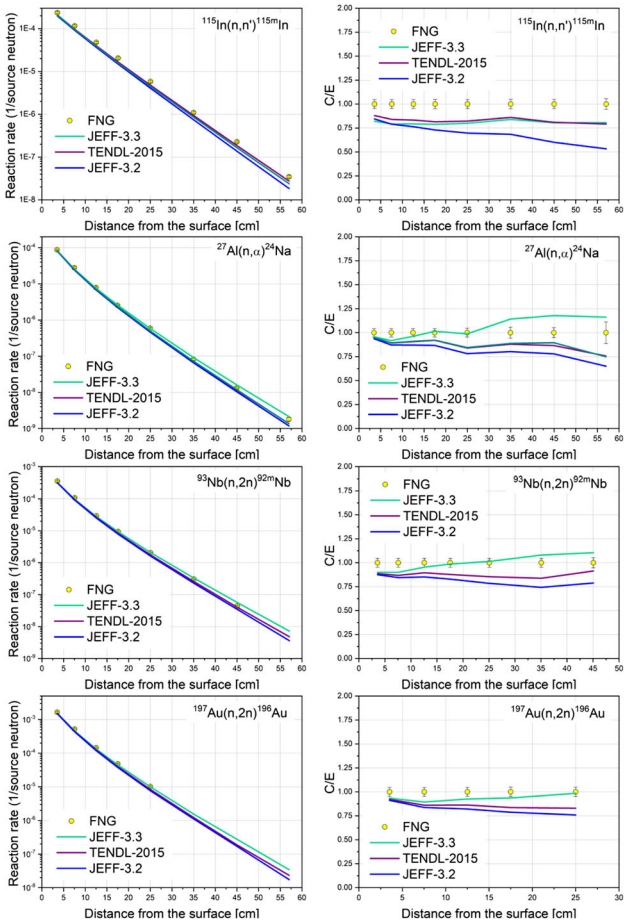

Fig. 75 Comparison of measured and calculated reaction rates for the FNG copper shielding experiment. From top to bottom reaction rates (C/E) are shown on left (right) for the ^{115}In(n,n'), ^{27}Al(n, α), ^{93}Nb(n,2n)^{92m}Nb and ^{197}Au(n,2n) reactions, respectively

and 1.06 at 4 MeV. The data were averaged after representing them on a group structure with 100 keV bins.

Results for the two detectors using different spheres and distances are given in Fig. 78. For both detectors $4\pi R^2\phi(E)/Q$ is shown (in units of 1/MeV) where R is the distance between the center of the sphere and the center of the detector, E is the energy of the detected neutron, ϕ is neutron flux per unit energy of the detected neutron and Q is the number of neutrons emitted by the source per second. The calculated results are obtained using the neutron source spectrum from the standards [40] and an MCNP simulation. The calculated results are broadened but still have a higher resolution than the data leading to obvious differences. For the stilbene detector $4\pi R^2\phi(E)/Q$ is shown in units of 1/MeV. The differences seem less significant but are masked by the many decades on the vertical axis.

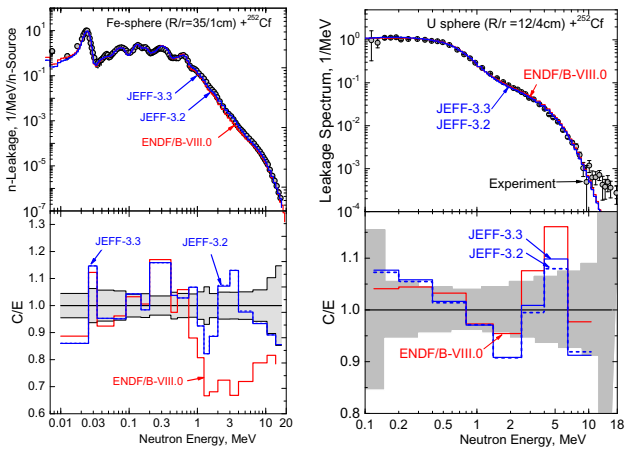

Fig. 76 Neutron leakage spectra (top) from spheres with a ^{252}Cf neutron source and C/E ratios (bottom). Left: a 70 cm ∅ Fe sphere; circles: experiment of L. Trykov [23,398], curves: calculations with JEFF-3.3 (blue curves), JEFF-3.2 (dashed blue) and ENDF/B-VIII.0 (red). Right: a 24 cm ∅^{dep}U sphere; circles experiment of S. Simakov [399], curves calculations with JEFF-3.3 (blue curve), JEFF-3.2, (dashed blue) and ENDF/B-VIII.0 (red)

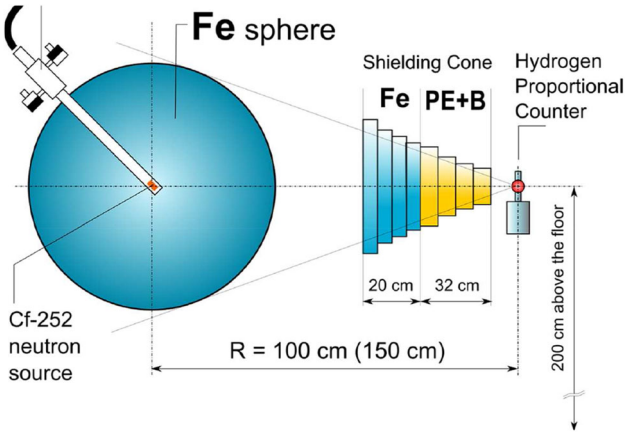

Fig. 77 Řež shielding experiments with iron spheres of varying diameter, a ^{252}Cf neutron source and proton-recoil based detectors. The shielding cone consisting of iron and borated polyethylene is placed between the sphere and the detector to determine the background

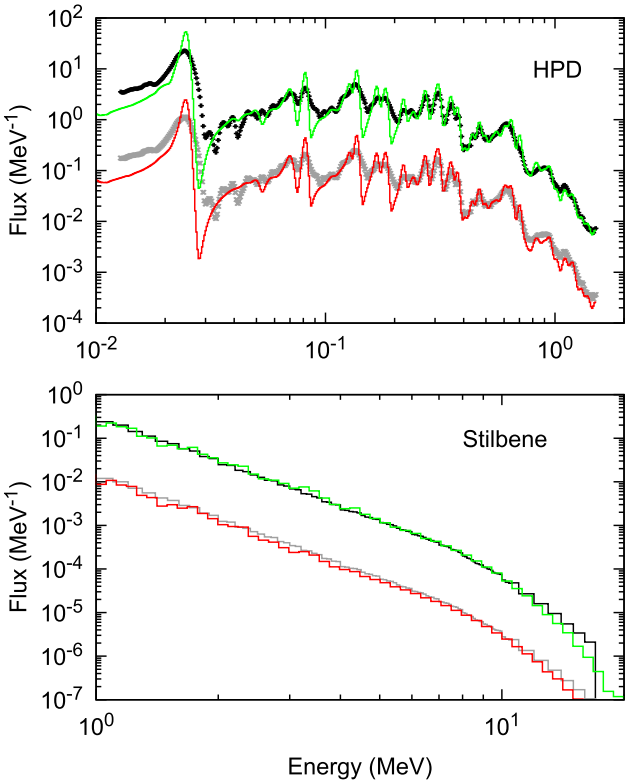

Fig. 78 Fe shielding experiment with ^{252}Cf at Řež. Data (black) versus JEFF-3.3 (green) and data (grey, divided by 20) versus ENDF/B-VIII.0 (red, divided by 20). The top figure shows the data for the energy range 0.01–1.3 MeV obtained with proportional counters. The iron sphere has a diameter of 100 cm and the center of the detector is at 3 cm from the surface of the sphere. The bottom figure (0.9–10 MeV) shows the data obtained with the stilbene scintillator. The sphere has a diameter of 50 cm and the center of the detector is at 100 cm from the center of the sphere

Tables 44 and 45 show C/E on a coarse group structure to highlight the energy averaged difference in the leakage spectra. Calculated results are shown for JEFF-3.3, -3.2 and -3.1.1 and ENDF/B-VIII.0. Differences for the JEFF libraries cannot be due to changes in the file for n+Fe since there weren't any.

Table 44 Coarse energy group C/E values for the Řež 100 cm diameter iron sphere measured with proportional counters at 3 cm from the surface

En.range[MeV]		C/E			
From	To	ENDF/BVIII.0	JEFF-3.1	JEFF-3.2	JEFF-3.3
0.013	1.290	1.045	1.054	1.066	1.052
0.013	0.033	0.9138	0.9822	0.9867	0.9948
0.033	0.060	0.9005	1.015	0.9757	1.020
0.060	0.090	0.9702	0.9779	0.9781	0.9885
0.090	0.150	0.9934	1.003	1.008	1.006
0.150	0.200	1.037	1.018	1.021	1.008
0.200	0.250	1.028	1.021	1.022	1.013
0.250	0.289	1.036	1.017	1.023	1.005
0.289	0.333	1.333	1.245	1.276	1.230
0.333	0.367	1.305	1.269	1.303	1.268
0.367	0.410	1.191	1.183	1.216	1.170
0.410	0.520	1.033	1.089	1.115	1.079
0.520	0.780	1.089	1.07	1.102	1.062
0.780	1.060	0.7834	1.053	1.076	1.048
1.060	1.290	0.7584	0.8655	0.8912	0.8646

C/E<0.90
0.90<C/E<0.95
0.95<C/E<1.05
1.05<C/E<1.10
C/E>1.10

Table 45 Coarse energy group C/E values for the Řež 50 cm diameter iron sphere measured with stilbene scintillator at 100 cm. Coloring as in Table 44

En.range[MeV]		C/E			
From	To	ENDF/BVIII.0	JEFF-3.1	JEFF-3.2	JEFF-3.3
1.0	10.0	0.8442	0.9746	0.9744	0.9756
1.0	1.2	0.8396	0.8963	0.8964	0.8748
1.2	1.4	0.8781	0.9853	0.9850	0.9905
1.4	1.6	0.7347	0.8640	0.8622	0.8800
1.6	1.8	0.9308	1.0690	1.0690	1.0970
1.8	2.0	0.8911	1.0690	1.0710	1.0950
2.0	3.0	0.8390	1.1020	1.1020	1.1150
3.0	4.0	0.8102	1.1850	1.1870	1.1910
4.0	5.0	0.8416	1.1250	1.1170	1.1130
5.0	6.0	0.8557	1.0060	1.0070	1.0030
6.0	7.0	0.8708	1.0270	1.0280	1.0300
7.0	8.0	0.8755	1.0350	1.0370	1.0500
8.0	9.0	0.9337	1.1030	1.1020	1.1140
9.0	10.0	0.8906	1.0280	1.0430	1.0580
10.0	12.0	0.8707	0.9366	0.9324	0.9408
12.0	14.0	0.7554	0.7897	0.7423	0.7728
14.0	16.0	0.6235	0.5624	0.5850	0.5581

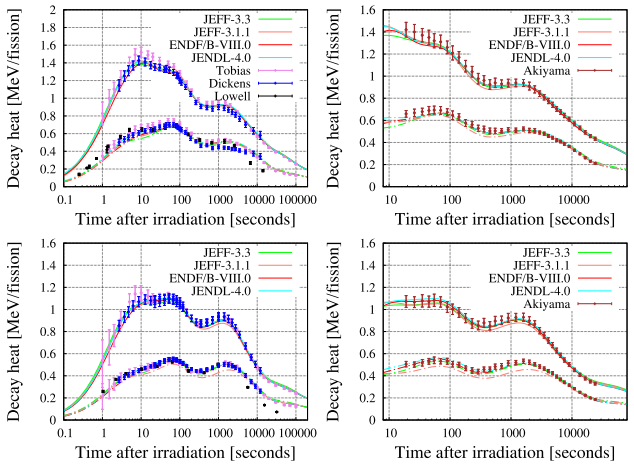

Fig. 79 Total and gamma decay heat for fission pulses of ^{235}U (top) and ^{239}Pu (bottom) induced by thermal (left) or fast (right) neutrons

The JEFF libraries are within 5% of the data up to 0.29 MeV. All four libraries overpredict the data from 0.29 to 0.4 MeV by 20–30%. From 0.4 to 1.3 MeV this overprediction gradually changes to an underprediction by more than 10%. The change is more pronounced for ENDF/B-VIII.0. Above 1.2 MeV ENDF/B-VIII.0 remains below the data by more than 10% (C/E-1 from −7 to −38%). The JEFF files stay closer to the data varying in C/E-1 between −23 and 19%, except for the final group of 14–16 MeV where the deviation is −44%.

As the results were deemed to agree better with the JEFF libraries than the iron evaluations developed by the CIELO collaboration and adopted in ENDF/B-VIII.0, the decision was taken to leave the JEFF evaluation for ^{56}Fe untouched. However, clear data deficiencies remain near 300 keV and between 3 to 5 MeV as shown in Tables 44 and 45.

3.4 Fission and fusion decay heat

At the UK Atomic Energy Authority the FISPACT-II inventory code [401] was used to simulate a suite of fission-pulse decay heat measurements [402] and for a benchmark against fusion decay heat measurements [403] obtained at the JAEA Fusion Neutron Source (FNS) [404,405].

Figure 79 shows the decay heat following a pulse of fission of ^{235}U and ^{239}Pu induced by thermal and fast neutrons. The evaluated experimental data are from Tobias [406,407], Dickens [408,409], the University of Massachusetts at Lowell [410–412] and Akiyama and An [413]. The more recent libraries benefited from a re-evaluation of the decay data correcting the partitioning of the decay energy between gamma and beta radiation. This effect is commonly known as the pandemonium effect [322].

For thermal fission of ^{235}U the estimated total decay heat agrees well with the data. From 10 to 100 s all evaluations favor the Dickens data over the higher data by Tobias. The gamma decay heat from 5 to 30 s reduces compared with JEFF-3.1.1 on account of new decay data. From 500 to 5000 s the evaluations follow the Tobias gamma heat data instead of the lower data by Dickens and the different trend of the Lowell data.

For thermal fission of ^{239}Pu there is again good agreement for the total heat but there is a slight underestimation of the data (one standard deviation) for the total decay heat between 400 and 2000 s. Here JEFF-3.1.1 is clearly low by about 5% indicating an effective improvement of fission yields and/or decay data in JEFF-3.3. For the gamma heat component JEFF-3.1.1 is clearly low by 5–10% between 8 and 4000 s, while JEFF-3.3, ENDF/B-VIII.0 and JENDL-4.0 as modified in 2015 show excellent agreement with the data. The pandemonium effect is therefore remedied for this system.

For fast fission of ^{235}U there is overall good agreement with a tendency for underestimation of the data below 100 s for both the total and the gamma decay heat. There is a clear improvement in both total and gamma heat between 100 and 3000 s. Also for ^{239}Pu agreement is excellent with the gamma decay heat being somewhat low (1–2 standard deviations) between 300 and 2000 s indicating that a further repartitioning of beta and gamma decay heat will be beneficial. The improvement in gamma decay heat over JEFF-3.1.1 is excellent from 20 to 8000 s and noticeable from 400 to 3000 s for the total decay heat.

Fusion decay heat measurements were made at FNS with a dT neutron source. Here results are shown for Cr, Fe, Ni, Cu, W and Pb (Fig. 80) during 1-h of cooling after a 5 min irradiation and for between 50 and 450 days of cooling following 7 h irradiations (Fig. 81) [400,403]. These elements were chosen as examples here, as they are important constituents of steel (Cr, Fe, Ni), of a fusion device's divertor and inner wall (W), and of the electric and power, and cooling infrastructure (Cu) of fusion reactors. Lead features as the neutron moderator in several of the tritium-breeding blanket concepts in fusion power plant designs [414].

In the simulations of the 5-min irradiations, there is an important difference for nickel where all libraries underestimate decay heat significantly, except JEFF-3.3 and FENDL/A-3.0, which are within one standard uncertainty from the data. These two libraries correctly predict the production of two metastable cobalt nuclides, which the others all miss [403]. For tungsten, JEFF-3.3 and JEFF-3.2 improve agreement compared with JEFF-3.1.2 but both underestimate decay heat significantly for the first 15 min and overestimate it by about a factor 2 after 20 min. The latter feature is shared with all other libraries except JEFF-3.1.2, but ENDF/B-VIII.0 and FENDL/A-3.0 are much closer to the data during the first 15 min due to the correct prediction of production of the ^{185m}W metastable radionuclide via

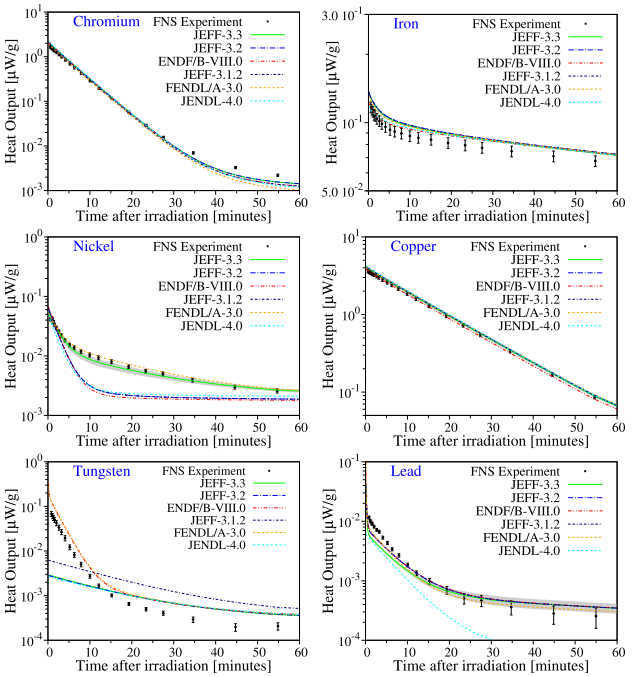

Fig. 80 Decay heat simulations and measurements from the JAEA fusion neutron source, considering chromium, iron, nickel, copper, tungsten and lead following irradiation for 5 min and 1 h cooling time. JEFF-3.3 is compared with JEFF-3.2, JEFF-3.1.2, ENDF/B-VIII.0, FENDL/A-3.0, JENDL-4.0 and the experimental data

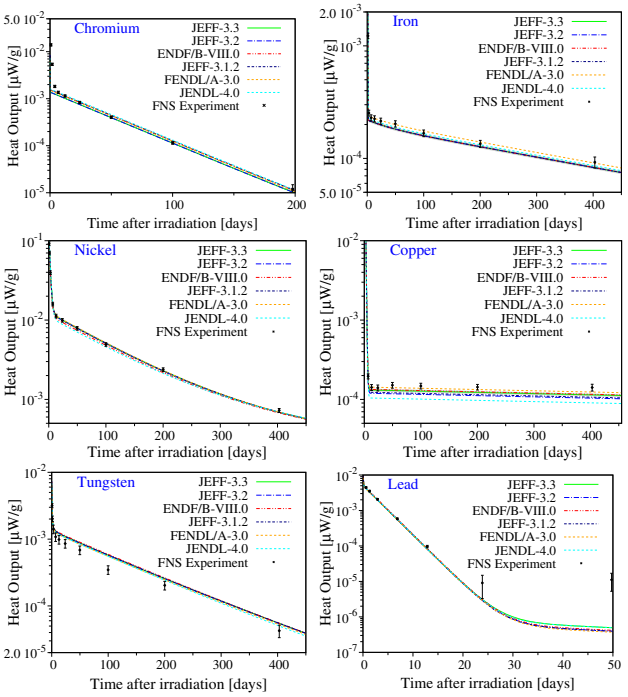

Fig. 81 Decay heat simulations and measurements from the JAEA Fusion Neutron Source, considering chromium, iron, nickel, copper, tungsten and lead following irradiation for 7 h and cooling of 50 (lead), 200 (chromium) and 450 (iron, nickel, copper, tungsten) days. JEFF-3.3 is compared with JEFF-3.2, JEFF-3.1.2, ENDF/B-VIII.0, FENDL/A-3.0, JENDL-4.0 and the experimental data

(n,2n) reactions on ^{186}W. For lead, JENDL-4 differs significantly from the data while the other libraries are a good match except during the first 10 min of cooling (controlled by ^{208}Pb(n,p)^{208}Tl). Agreement between the simulations and the experiments for iron and chromium is less good due to experimental uncertainties, particularly beyond 40' min of cooling in Cr, where sample impurities (of aluminium and iron) are thought to play a role [400,404]. For copper the agreement with all libraries is excellent.

In the simulations of the 7-h experiments, all libraries are in good agreement with each other, reflecting the fact that important long-lived radionuclides dominate and have been well characterised for many years. However, there are significant differences between the simulations and experiment during the first week of cooling in the chromium experiment due to the same aluminium and iron impurities that caused the disagreement in the 5-min experiments above. For iron, copper and nickel there is excellent agreement between the library predictions with FISPACT-II and the experimental measurements, although for iron FENDL/A-3.0 is a slightly better match than the rest. In tungsten, the simulations overestimate the decay heat during 400 days of cooling. As noted in [400], this overestimate could be caused by incorrect (n,2n) cross sections on W isotopes. In lead, there is excellent agreement between simulation and experiment during the first 20 days of cooling where ^{204}Pb(n,2n)^{203}Pb dominates, but significant underestimation with all libraries at experimental cooling times of 24 and 50 days [403]. This latter result could point to an need to improve the (n,α) cross section on ^{206}Pb, which leads to ^{203}Hg ($T_{1/2}$ = 46.6 days).

The JEFF-3.3 library adopted several additional activation channels not present in earlier versions from the TENDL project. The overall picture from the decay-heat benchmark is that the inclusion of several activation channels, particularly isomeric production, gives JEFF-3.3 an advantage over other libraries, such as ENDF/B-VIII.0 and JENDL-4.0u. In many cases, these are taken from TENDL evaluations, which explains the agreement with the JEFF-3.3/A activation files, which are special-purpose formatted TENDL.

Figure 82 highlights the recent improvements in JEFF-3.3/A in comparison to earlier JEFF versions. Decay heat calculations divided by experimental measurements (C/E) values are shown as a function of mass number of the daughter nucleus producing the decay heat. Integral values of decay heat are taken from the experiments where there is one dominating activation product produced by a single dominant reaction during some of the cooling period in a particular experiment (in practice this means that each FNS experiment may contribute multiple values to Fig. 82). The C/E value shown corresponds to the time at which the reaction first becomes dominant (see [403] for more details). If there

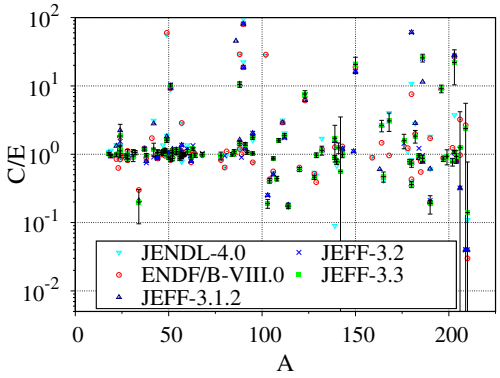

Fig. 82 Comparison between calculated and experimental cross sections for three versions of the JEFF library as well as JENDL-4.0 and ENDF/B-VIII.0, taken from the FNS integral decay-heat benchmark [400]. Calculation/experiment (C/E) ratios for reactions are plotted against the baryon number of the daughter nuclide. C/E values were taken from the simulation versus experiment comparison at the cooling time where the reaction first becomes dominant (according to the simulations). Error bars shown (for the JEFF-3.3 data points only) correspond to the experimental uncertainty

are multiple contributing activation products or competing pathways to the same product during a particular cooling phase of an experiment, then it is not possible to attribute C/E values to a single reaction. Improvements due to new input parameter evaluations and elimination of erroneous database entries has resulted in improved C/E values for several reactions with JEFF-3.3/A compared to earlier versions, although there are a few cases where ENDF/B-VIII.0 and more rarely JENDL-4.0 are still outperforming JEFF, particularly at high mass number.

3.5 Maxwellian-averaged cross-sections

Maxwellian-averaged cross sections (MACS) in the 10 s of keV energy range have a particular interest for astrophysics and in particular for nucleosynthesis by the s-process. In view of this interest a considerable amount of work was directed at establishing a reliable database of cross sections, reaction rates and so-called s-factors [415]. Recommendations for these cross sections based on the combined use of experiment and modeling were compiled by Bao et al. [416] and, more recently, the online KADoNiS database [417].[8] A large subset of the KaDoNis database is based on experimental data obtained with the activation technique or the neutron time-of-flight technique and many of the measurements provide at least the 30 keV MACS [415]. The results for 30 keV are then extended to cover the range of temperatures of interest in nucleosynthesis either directly from the data or by modeling.

[8] We have used the KaDoNiS-1.0 database as much as possible (exp-astro.de/kadonis1.0).

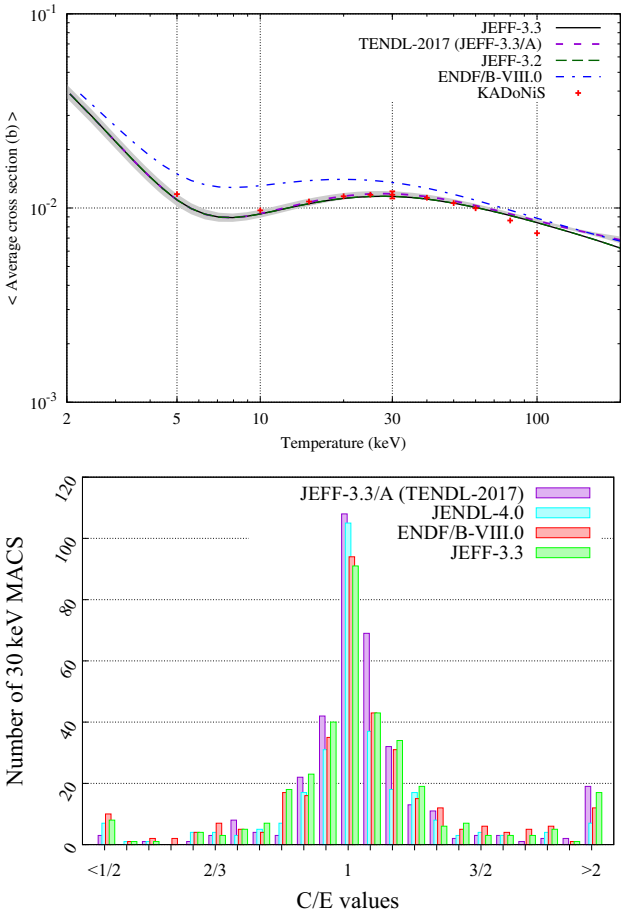

Fig. 83 Top: temperature dependent MACS for ^{56}Fe. The uncertainty band is from TENDL-2017 (JEFF-3.3/A). Bottom: histogram of C/E values for the 30 keV MACS. Absent cross sections are omitted in the comparison

Taking advantage of this work by the astrophysics community the KaDoNiS database was used as a comprehensive test [273]. Figure 83 shows an example of the temperature dependence of the MACS for ^{56}Fe. Covariances from TENDL-2017 are used to calculate the one-group cross section uncertainties. We recall that the JEFF-3.3 transport file and the JEFF-3.3 activation file differ. JEFF-3.3/A is a file produced from TENDL-2017 by processing the latter into an activation file. This implies that (1) cross sections are not the same between JEFF-3.3 and JEFF-3.3/A and (2) the processing eliminates data from the TENDL-2017 file such as resonance parameters and covariances. Despite these differences the figure shows no impact on the energy dependence and magnitude of the MACS for ^{56}Fe and excellent agreement with KaDoNiS except at 90 keV and higher. In contrast there is an important difference with ENDF/B-VIII.0, which does not agree with KaDoNiS.

The overall agreement between KaDoNiS and several evaluations is shown in Fig. 83 for the 30 keV MACS by a C/E

histogram comparing KaDoNiS with JEFF-3.3, JEFF-3.3/A, ENDF/B-VIII.0 and JENDL-4.0. Note that several reaction channels are missing in the non-JEFF evaluations, with only the activation file containing all cross sections and JEFF-3.3 missing only 11 cases of 357. The overall distributions are very similar with TENDL peaking higher than the others indicating a somewhat smaller distribution. It appears that most values lie within a factor 2 from those in KaDoNiS with some notable exceptions that should be inspected more closely.

3.6 Data processing

As any nuclear data file JEFF-3.3 is stored in the ENDF format that requires 'processing' in order to prepare the data in a format used by transport or other application codes. An example is the ACE format used by the MCNP Monte Carlo transport and criticality code. Besides allowing for the testing described in the previous and next section, processing codes verify completeness, correctness and fit-for-purpose of the components of the evaluated nuclear data file or perform transformations such as pointswise cross section reconstruction and Doppler broadening. To guarantee proper functioning of the evaluated data file and avoid misuse processing must be standardized for reliability of use of the library. In the framework of verification and validation of the JEFF-3.3 library, the evaluated files were processed using the following codes:

NJOY: a LANL comprehensive computer package for the processing of nuclear data evaluations,
PREPRO: a modular set of computer codes [300] owned and maintained by the IAEA,
ENDF-6 Checking & Utility Codes: a suite of computer codes to evaluate the consistency of the evaluated files with the underlying nuclear physics and with the ENDF-6 format.

To allow broad application of the JEFF-3.3 libraries, the evaluated files were processed into several application formats, including ACE, G4NDL [418] and WIMSD, which can be used in several application codes. Some details are given below.

3.6.1 Processing neutron-induced data

Codes used for neutron transport or criticality estimation require either pointwise linear continuous energy data or energy group data for which the effect of the temperature of the material is accounted for – the data are Doppler broadened. This implies that processing needs to decide on an energy grid for piecewise linear interpolation or an energy group structure, reconstruct the cross sections on that grid or group structure from the (resonance) parameters provided by the evaluation. For group cross sections and or in the unresolved energy range resonance self-shielding must be accounted for. Important response functions are provided, for instance for heating and damage estimates. Finally a file structure must be delivered that is read by the application code. Testing that the existing processing codes are capable of processing a submitted evaluated file, in particular correctly treating the resolved and unresolved resonance region, is a fundamental task in the sequence of nuclear data verification and validation.

This highlights the potential need for corrections to the evaluations and that reference input parameters for standard processing codes should be provided alongside the evaluated files.

Many Monte Carlo transport and reactor physics codes use nuclear data files in 'A Compact ENDF' (ACE) format, a derived format that contains most of the information available in ENDF-6 files. These are mostly prepared by the NJOY code, although recently there are other options. NJOY consists of a set of codes that read and write ENDF files in sequence producing the required ACE file at the end.

As an outcome of the dedicated JEFF group for processing and verification [368], the following standard sequence of NJOY modules was set up and optimal input parameters were identified to process the JEFF-3.3 incident-neutron data into ACE format:

RECONR: the ENDF-6 file is converted into pointwise-ENDF (PENDF) format, where sufficient energy grid points are introduced to ensure that linear-linear interpolation reproduces the original evaluations within an accuracy of 0.1%. When resolved resonance parameters are provided, RECONR evaluates the corresponding cross sections on the energy-grid.
BROADR: cross sections are Doppler-broadened at 293.6 K[9] up to the end of the resolved resonance region maintaining the accuracy requirement of 0.1%.
THERMR: the thermal scattering law accounting for atomic motion is applied below 10 eV on a scattering grid of 20 equi-probable angles. The free-gas model is used unless a material relevant thermal scattering law is available such as for H in liquid light water or O in liquid heavy water.
UNRESR: effective self-shielded cross sections in the unresolved resonance region are calculated using the Bondarenko method and six levels of background cross sections: infinite, 10^4 b, 10^3 b, 10^2 b, 10 b and 1 b.
PURR: probability tables are generated using 20 probability bins and 64 resonance ladders.

[9] This is the standard temperature for testing. ACE files at other temperatures are provided for reactor applications.

Table 46 Number of covariance files present in JEFF-3.3, JEFF-3.2 and ENDF/B-VIII.0

Covariance type	JEFF-3.3	JEFF-3.2	ENDF/B-VIII.0
MF31 – fission multiplicities	50	17	73
MF32 – resonance parameters	352	181	118
MF33 – cross sections	442	218	220
MF34 – angular distributions	359	158	108
MF35 – energy distributions	36	3	65
MF40 – activation cross sections	286	137	32

HEATR: partial kerma and damage energy production cross sections are calculated. Redundant cross sections for gas production are calculated.
ACER: the ACE file is created.

3.6.2 Processing covariance data

One of the remarkable efforts made by JEFF for its new release was to enlarge the number of files that contained covariance sections. Several new evaluations were made and covariances were extensively imported from the TENDL library. Table 46 shows the progress in covariance evaluation during the development of JEFF-3.3.

The covariances were converted with NJOY into the BOXER format, a format recognised by the well-known NEA visualization tool JANIS and by sensitivity codes such as NDaST [419].

4 Impact studies

Here we report on the impact of JEFF-3.3 on criticality and uncertainty estimation for a number of applications and we show how the new evaluations with their covariance information can be used for adjustment of the library to critical experiments.

4.1 Criticality

4.1.1 Spent fuel cask

A reactivity benchmark (BUC/Phase-VII) for computational transport packages was organized by the OECD NEA Expert Group on Burn-up Credit Criticality Safety. Figure 84 shows the k_{eff} values calculated with several codes and nuclear data libraries considering fresh fuel and room temperature (20 °C). JEFF-3.3 and ENDF/B-VIII values are compared with those in Ref. [420]. JEFF-3.3 is in excellent agreement with the mean-value in Ref. [420] from the 13 participating codes and libraries showing a small negative bias that is perhaps 10% of the 260 pcm standard deviation.

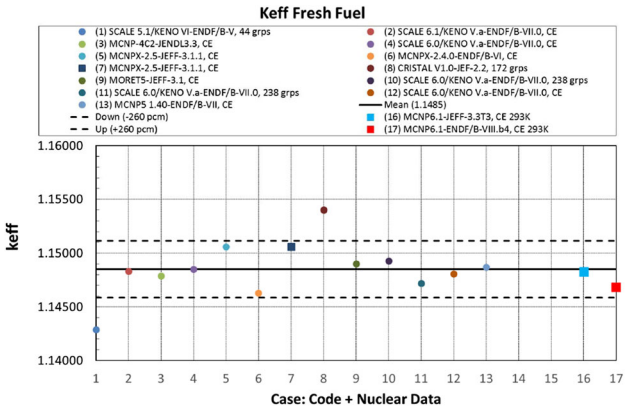

Fig. 84 Comparison of k_{eff} results for fresh fuel for the 13 organizations participating in the benchmark Phase VII exercise with the criticality codes and nuclear data used. JEFF-3.3T3 and ENDF/B-VIII are shown. The mean value of the participants' k_{eff} results for the representative fuel cask is 1.1485. Lower and upper bands represent the standard deviation values (±260 pcm) of the participants' k_{eff} results

4.1.2 Gen-IV reactor concepts

The impact of JEFF-3.3 on new GEN IV reactor concepts with large development programmes was investigated for

ASTRID: the Advanced Sodium Technological Reactor for Industrial Demonstration [421];
MYRRHA: the Multi-purpose hYbrid Research Reactor for High-tech Applications [422];
ALFRED: the Advanced Lead Fast Reactor European Demonstrator [423].

Since these MOX-fuelled reactors are cooled with different materials (i.e. lead, bismuth, sodium) a larger range of evaluations impacts k_{eff} estimates of the designs.

From a sensitivity analysis, the following nuclear data evaluations were identified as of major importance for these reactor concepts:

- plutonium, ^{239}Np and ^{23}Na for ASTRID;
- plutonium, lead and bismuth for MYRRHA;
- plutonium and lead for ALFRED.

Table 47 k_{eff} of GEN IV concepts with different versions of the JEFF library. The Monte Carlo statistical uncertainty is 1 pcm

	JEFF-3.2	JEFF-3.3	Difference (pcm)
MYRRHA	1.00475	1.00722	247
ASTRID	0.99838	1.00252	414
ALFRED	0.9922	0.99937	717

Table 48 Differences in fission rates, capture rates and fission neutron multiplicities calculated with MCNP6.1.1b for ASTRID, MYRRHA and ALFRED using JEFF-3.3 and JEFF-3.2

	ASTRID	MYRRHA (%)	ALFRED (%)
Δ fission rate	1.1	1.0	1.5
Δ capture rate	−0.6	−0.5	−0.4
$\Delta\,\overline{\nu}$	−0.7	−0.8	−0.8

The impact of the new JEFF-3.3 evaluations on k_{eff} was assessed using MCNP6.1.1b [390]. Table 47 shows that JEFF-3.3 produces an increase in k_{eff} for the three models when compared to JEFF-3.2. The increase is least for MYRRHA (about 250 pcm) and most for ALFRED (about 700 pcm). Given that these are design estimates with only limited validation of some of the important data, in particular lead for MYRRHA and ALFRED, the changes are what may be expected from the nuclear data uncertainties (see below). For the system for which the data should be best established (ASTRID) the estimates of both JEFF-3.2 and JEFF-3.3 are within 300 pcm of 1. The same is true for ALFRED and JEFF-3.3, but the result is not consistent with that for MYRRHA. The deviation of the JEFF-3.3 calculation from the VENUS-F experimental result seems consistent with the estimate for MYRRHA.

For the same systems, Table 48 reports the variations of fission rate, capture rate and fission neutron muliplicities calculated using JEFF-3.2 and JEFF-3.3. For ASTRID, JEFF-3.3 produced an increase in fission rate together with a decrease of the capture rate and fission neutron multiplicity of the system. The difference in the total fission rate mainly comes from the ^{239}Pu, with a 2.4% fission rate increase calculated with the JEFF-3.3 the library, which is only partially compensated by 2.7% and 0.6% fission rate reductions for ^{238}U and ^{241}Pu. The differences in the capture rate come from ^{238}U (decrease of 1.2%), which is partially compensated by other isotopes. The three systems behave rather similarly. No significant differences were generated by the different evaluations for sodium, lead and bismuth. The table clearly shows that an uncertainty smaller than 0.5% is only achievable through a careful balancing of effects of very similar magnitude. Designs will have to allow for the inherent uncertainty of modeling also with the new library.

4.2 Uncertainty estimation

This section describes testing and verification of JEFF-3.3 covariance data. We have propagated the nuclear data uncertainties and their correlations for some of the calculations discussed above in the benchmarking and testing section. The comparison of benchmark/experimental uncertainties and uncertainties inferred from propagating the nuclear data covariances allows an assessment of the reliability of uncertainty estimates based on the JEFF-3.3 library and it allows an assessment which benchmarks may be used. Here we must pay attention to the role of the discrepancies between, for instance, calculated and benchmark k_{eff} values as already summarized above.

4.2.1 Criticality

Here we consider the propagation of uncertainties and covariance data to estimates of k_{eff} for benchmarks given in the ICSBEP Handbook [23]. A small study is presented for which a complete propagation was carried out and two large studies are presented that use the NDaST tool [424] developed at OECD-NEA which propagates uncertainties based on precompiled sensitivity profiles available in DICE [425].

Full covariance propagation The uncertainty of k_{eff} ($u_{k_{\text{eff}}}$) due to nuclear data uncertainties was evaluated at NRG for seven benchmarks taken from the NEA extended Mosteller suite (Sect. 3.1.1). Uranium and plutonium systems were considered covering the fast, intermediate and thermal energy ranges. Covariance data were considered for ^{235,238}U, ^{239,240,241}Pu and the (n,el), (n,inl), (n,2n), (n,f) and (n,γ) reaction cross sections as well as $\overline{\nu}$. Of the non-actinides ^{1}H, ^{16}O, $^{\text{nat}}$C, ^{27}Al, ^{10}B were considered with the (n,el), (n,inl) and (n,γ) reaction cross sections. JEFF-3.3, ENDF/B-VII.1 and JENDL-4 data covariances were propagated using linear perturbation theory with sensitivity vectors calculated by the Iterated Fission Probability (IFP) method implemented in MCNP6. NJOY was used to produce ACE files and covariance matrices, MCNP6 KSEN provided the sensitivity profiles and SUSD3D was used to combine sensitivity profiles with nuclear data covariances to produce the system uncertainties. It was found that $\overline{\nu}$ uncertainties play an important role, especially in the uranium systems, and are therefore essential for a full description of the uncertainty associated with fissionable nuclides [426].

The results are presented in Table 49 showing the benchmark uncertainty, the absolute deviation between calculated and benchmark k_{eff} and the overall k_{eff} uncertainty $u_{k_{\text{eff}}}$ for JEFF-3.3, ENDF/B-VII.1 and JENDL-4. For most cases, there is good agreement between the uncertainties calculated using JEFF-3.3 and ENDF/B-VII.1. The exception is the intermediate energy range for which there are also larger

Table 49 Uncertainties $u_{k_{eff}}$ for the effective neutron multiplication factor k_{eff} of selected critical benchmarks. Uncertainties represent one standard deviation and are given in pcm (parts per 100,000). Calculated values (C) are for the JEFF-3.3, ENDF/B-VII.1 and JENDL-4.0 libraries. The experimental k_{eff} value is E and its uncertainty u_E. The absolute deviation between experiment and calculations is |C-E|. Calculations have ∼20 pcm statistical uncertainty

		JEFF-3.3		ENDF/B-VII.1		JENDL-4	
Case	u_E	|C-E|	$u_{k_{eff}}$	|C-E|	$u_{k_{eff}}$	|C-E|	$u_{k_{eff}}$
hmf1	100	39	1331	49	1201	249	861
hmi6-1	80	77	1241	483	2123	162	596
hst32-1	260	475	1390	204	1422	272	410
lct8-1	120	212	692	19	748	112	445
pmf1	110	14	501	21	612	185	599
pci1-1	380	168	2112	1119	538	1376	512
pst11-18-6	520	948	945	556	912	448	671

differences in the k_{eff} estimates. JENDL-4 does not have covariance matrices for ^{1}H yielding lower overall uncertainty estimates for thermal systems and this is the main difference with other libraries.

It is found that:

- the experimental uncertainty u_E is between 80 and 520 pcm,
- the calculated k_{eff} uncertainties are between 500 and 2100 pcm for JEFF-3.3 and similar for ENDF/B-VII.1 and 400 and 900 pcm for JENDL-4,
- |C-E| for JEFF-3.3 are less than $2u_E$ reflecting the choices made in the evaluation process to achieve good performance for the extended Mosteller suite (hmf1, hmi6-1, pmf1 and pci1-1 deviate less than u_E),
- all calculated uncertainties for JEFF-3.3 cover the observed deviation between benchmark and calculated k_{eff}, while for ENDF/B-VII.1 and JENDL-4 this is not true for pci1-1,
- Besides the generally lower uncertainty in JENDL-4, there are significant differences in uncertainty between JEFF-3.3 and ENDF/B-VII.1 for hmi6-1 and pci1-1.

The small deviation and rather small uncertainty for pmf1 in the case of JEFF-3.3 is the result of a Bayesian adjustment performed during the evaluation process making use of exactly that benchmark and no others.

Even if the total calculated uncertainty compares well between the different libraries, the constituents contributing to the total uncertainty differ. For example, when comparing the calculated total uncertainty on k_{eff} of the pst11-18-6 benchmark with ^{239}Pu as fissile constituent Table 50 shows the resulting total uncertainty for all three libraries are comparable. Here the total uncertainty contribution of ^{239}Pu was

Table 50 Total uncertainties of k_{eff} in pcm for the pst11-18-6 benchmark as a result of the covariances on nuclear data for ^{239}Pu. The last line shows k_{eff}-1 in pcm with a statistical uncertainty of the simulation of 18 pcm

Isotope	JEFF-3.3	ENDF/B-VII.1	JENDL-4.0
^{239}Pu	512	637	639
^{239}Pu $\bar{\nu}$	473	171	80
Total unc.	697	660	644
$k_{eff} - 1$	− 386	15	− 1

obtained by adding the uncertainties due to $\bar{\nu}$ and the cross sections in quadrature, so assuming no correlations. However, the variance of k_{eff} due to the ^{239}Pu(n,f) and ^{239}Pu(n, γ) reactions (Table 51) shows significant differences between the JEFF-3.3 library and the ENDF/B-VII.1 and JENDL-4.0 libraries: (1) the uncertainty related to the (n, γ) reaction channel of ^{239}Pu in the JEFF-3.3 library is much larger than those of the other two libraries, and (2) the cross-correlation between the (n, f) and (n, γ) reactions differs in both sign and magnitude. These differences ultimately reflect the evaluation method and the associated method for fixing the covariance data for each library. Changes of a similar nature may be expected in the future as each library project continues to develop its own evaluation methods with its associated assessments of uncertainties and their correlations.

Finally, it was found that the group structure of covariance data is also important, as can be seen from the results of the intermediate spectrum benchmarks, where a coarse group structure used to represent the covariance data of ^{239}Pu in the JEFF-3.3 library leads to higher uncertainty estimates.

Uncertainties by precompiled sensitivities

Table 52 gives the average uncertainty contributions in pcm in k_{eff} calculated with the NDaST [419,424] tool for 4519 cases from the ICSBEP Handbook [23] with the precalculated sensitivities available in DICE [425]. Results are averaged by fissile material and spectrum and compared with the average experimental uncertainty. Only the covariances for the four major actinides (^{233,235,238}U and ^{239}Pu) are propagated and the contributions due to cross section σ, mean neutron multiplicity $\bar{\nu}$ and the prompt fission neutron spectrum χ_ν are separated. For the prompt fission neutron spectrum the covariances at 1 MeV incident neutron energy are used. JEFF-3.3 is compared with results from the SCALE-6.2rev8 [427] system. The latter is based on the ENDF/B-VII.1 covariance library and is a well-known reference for the criticality safety community.

It is clear that the JEFF-3.3 uncertainty in $\bar{\nu}$ and therefore its impact on k_{eff} is larger than that for ENDF/B-VII.1 and therefore SCALE. Also the uncertainty for the prompt fission neutron spectrum for plutonium is clearly larger for JEFF-3.3 than for ENDF/B-VII.1, while for ^{235}U it is comparable. Except for a few cases the uncertainty due to the

Table 51 Variance and covariance for k_{eff} of the pst11-18-6 benchmark due to the ^{239}Pu(n,f) and ^{239}Pu(n, γ) reactions

	JEFF-3.3		ENDF-B/VII.1		JENDL-4	
^{239}Pu	(n, f)	(n, γ)	(n, f)	(n, γ)	(n, f)	(n, γ)
(n, f)	2.5E−05	−1.4E−05	2.1E−05	5.7E−06	2.1E−05	5.6E−06
(n,γ)	−1.4E−05	3.0E−05	5.7E−06	8.4E−06	5.6E−06	8.2E−06

Table 52 Uncertainty contributions to k_{eff} due to cross sections σ, mean neutron multiplicity $\overline{\nu}$ and prompt fission neutron spectrum χ_ν from the covariances data for ^{233,235,238}U and ^{239}Pu. JEFF-3.3 is compared with the SCALE-6.2rev8 system. 4519 benchmark cases from ICSBEP are considered and averages per fissile material (mat.) and spectrum (sp.) category are given (notation as in footnote 5; a is all, # is the number of cases). Uncertainties are given in pcm, u_E is the average experimental uncertainty

				SCALE-6.2rev8			JEFF-3.3		
mat.	sp.	#	u_E	σ	$\overline{\nu}$	χ_ν	σ	$\overline{\nu}$	χ_ν
HEU	f	463	227	1157	92	201	1062	515	259
	i	21	310	1534	161	374	1060	543	326
	m	78	416	1046	171	346	674	539	360
	t	807	477	234	366	623	332	560	903
	a	1369	375	602	262	465	619	543	617
IEU	f	57	201	1649	205	512	1369	477	685
	i	8	220	1614	193	324	1287	501	402
	m	8	360	745	244	379	588	533	456
	t	142	512	298	361	773	356	555	945
	a	215	398	722	309	673	717	528	826
LEU	f	1	274	1126	90	216	932	506	323
	m	5	353	878	140	200	751	505	290
	t	1494	255	411	361	265	412	537	328
	a	1500	255	413	360	264	413	537	328
MIX	f	44	305	629	90	155	547	356	254
	i	2	253	635	106	116	815	426	203
	m	1	270	395	151	99	777	404	177
	t	364	462	549	198	229	511	431	514
	a	411	435	558	159	221	519	419	470
PU	f	152	355	305	76	110	259	414	308
	i	4	612	568	85	96	1283	460	238
	m	9	587	357	118	274	741	447	570
	t	607	400	506	176	285	526	463	885
	a	772	395	467	156	250	477	453	735
SPEC	f	6	333	346	22	96	672	388	399
U233	f	8	174	779	216	107	861	217	114
	i	29	670	341	323	981	352	315	997
	m	8	601	283	368	996	287	363	1018
	t	194	600	203	447	842	203	446	866
	a	239	591	242	422	839	260	412	857

cross section is very similar. For ^{233}U there are few differences. The average experimental uncertainty per category is between 200 and 650 pcm and these are clearly exceeded by the uncertainty of JEFF-3.3 (577–1603 pcm, 2-8 × u_E) and that of SCALE (333-1739 pcm, 1-9 × u_E. As is clear from the discussion above SCALE has smaller combined uncertainties for plutonium holding systems than JEFF-3.3 while for uranium systems combined uncertainties are very similar.

Uncertainties for the NRG suite

In the above analysis uncertainties were stated for any case in ICSBEP for which sensitivity profiles are available regardless of whether there was an evaluation of k_{eff} for JEFF-3.3. For the 2172 cases of the NRG suite for which k_{eff} predictions were discussed in Sect. 3.1.2, Table 53 shows an analysis of k_{eff} uncertainties obtained with NDaST using nuclear data covariances for ^{233,235,238}U, ^{239,240,241}Pu, ^{232}Th, ^{237}Np, ^{1,2}H, ^{16}O, Al, Fe, Cu, Zr and W. The average k_{eff} C/E-1 has a bias of 68 pcm so it is very close to 0. By fuel category it varies

Table 53 Deviations and uncertainties for the NRG suite of 2172 cases from ICSBEP (Sect. 3.1.2, [373]): mean relative deviation (col. C/E-1) and its standard spread (col. $s_{C/E}$), average standard benchmark uncertainty u_E, average standard uncertainty due to JEFF-3.3 covariances u_{ND}, number of cases $\#_E$ with C/E-1 within u_E and within u_{ND} ($\#_{ND}$). The comparison is split by fuel category (mat) and the number of cases per category is in column #

mat	#	$\frac{C}{E}$-1	$s_{C/E}$	u_E	u_{ND}	$\#_E$	$\#_{ND}$
HEU	800	104	754	361	1446	35	89
IEU	98	154	412	465	1423	69	100
LEU	497	− 1	513	258	959	53	88
PU	483	223	727	408	1650	57	91
MIX	198	− 240	903	418	913	29	65
U233	96	− 267	1184	583	800	34	51
All	2172	68	744	369	1316	45	87

Table 54 Computed versus experimental uncertainties (u_E) in % for the ASPIS IRON-88 benchmark. The penetration depth is d (in cm)

Reaction	d	Uncertainty			u_E
		JEFF-3.3	ENDF/B-VII.1	JENDL4	
^{32}S(n,p)	26	13	12	17	7
	52	25	21	35	7
	62	29	25	43	9
^{115}In(n,n')	26	7	11	15	5
	46	11	15	18	5
^{103}Rh(n,n')	26	6	8	9	5
	62	12	19	15	5
^{27}Al(n, α)	26	19	32	30	5
^{197}Au(n, γ)	26	5	10	9	4
	46	4	9	9	4
	62	4	8	9	4

between − 267 and + 223 pcm so on average the bias per fuel is within 300 pcm (see Sect. 3.1 for a further discussion). Concerning the distribution 45% of the benchmarks lie within 1 experimental standard deviation, a fact also noted in Sect. 3.1. In contrast nearly 90% of the NRG-suite cases lie within the estimated standard uncertainty using the JEFF-3.3 covariance data. Both these percentages are contrary to expectation in the case of a normal distribution. As mentioned earlier the first percentage highlights the role of outliers/discrepancies, while the second shows that uncertainties for k_{eff} propagated from (JEFF-3.3) nuclear data uncertainties that are primarily based on input from microscopic data alone are very conservative, while nothing was done to account for benchmark discrepancies. The average uncertainty per category due to JEFF-3.3 covariance data is consistent with that found for the full study in Table 52 and the limited study with full covariance propagation (Table 49).

Summary of k_{eff} uncertainty prediction Both the evaluation of covariance matrices for nuclear data from models and microscopic experimental data and the inclusion of integral experiments in evaluations with its implied impact on covariance data, are active fields of research and development. Here, we can only reflect the present state of the art. The estimated uncertainties clearly exceed experimental uncertainties for k_{eff}. It is therefore obvious that an inclusion of benchmark k_{eff} data in the nuclear data and covariance evaluation process will lead to smaller a posteriori uncertainties for an adjusted evaluation. The discussion of outliers and the residuals distribution presented above in the criticality benchmarking of Sect. 3.1 provided clear evidence of a considerable number of discrepancies between benchmark and calculation. It should be quite clear that reduced uncertainties from an adjustment to benchmarks will only lead to reliable a posteriori covariances if these discrepancies are removed by the adjustment process and consistency with the much larger database of microscopic experimental nuclear data is maintained. In cases where such a satisfactory outcome is not achieved dedicated work should address these discrepancies and NDaST is a valuable tool for identifying issues by nuclide or by benchmark [419,424]. The program sketched above is a major challenge for the next generation of nuclear data evaluations.

4.2.2 Shielding

Cross-section sensitivity and uncertainty analyses of several SINBAD [367,393,428] shielding benchmarks, such as the ASPIS-Iron88 and the FNG experiments were performed using the SUSD3D [305] perturbation code, based on the direct and adjoint neutron flux moments calculated by the DORT/TORT code system [429].

The uncertainties for the ASPIS-Iron88 reaction rates due to ^{56}Fe cross sections were assessed for several penetration depths in the experimental block using covariance matrices from JEFF-3.3, ENDF/B-VII.1 and JENDL-4.0u. The largest contributions to the uncertainties are due to the uncertainty in the ^{56}Fe inelastic, elastic and capture cross-sections [428] (Tables 54, 55 and Fig. 73). Reasonable agreement can be observed between different evaluations. The |C/E-1| results are mostly within the 1σ for all evaluations, even for the very discrepant results such as those of ^{32}S(n,p) (Fig. 73). A similar situation, where large C/E discrepancies are within the uncertainties predicted due to the cross section covariances, was observed for the FNG Copper benchmark [393,396] (see Table 56). This suggests that for the above cases the covariance matrices seem to be, on the average, relatively realistic, with no clear trends of over- or under-estimation. This is in contradiction to the observed overestimations of the nuclear data uncertainties when compared to the C/E values of the

Table 55 ^{56}Fe secondary angular distribution uncertainties (SAD; in %) for the ASPIS IRON-88 benchmark. The penetration depth is d (in cm)

Reaction	d	SAD Uncertainty		
		JEFF-3.3	ENDF/B-VII.1	JENDL-4
^{32}S(n,p)	26	1.3	1.3	2.9
	52	2.1	2.1	6.0
	62	2.3	2.3	7.2
^{115}In(n,n')	26	0.6	0.6	2.3
	46	1.0	1.0	3.2
^{103}Rh(n,n')	26	0.3	0.3	1.0
	62	0.3	0.3	1.1
^{27}Al(n,α)	26	3.4	3.4	1.4
^{197}Au(n,γ)	26	0.03	0.1	0.3
	46	0.1	0.1	0.3
	62	0.1	0.1	0.3

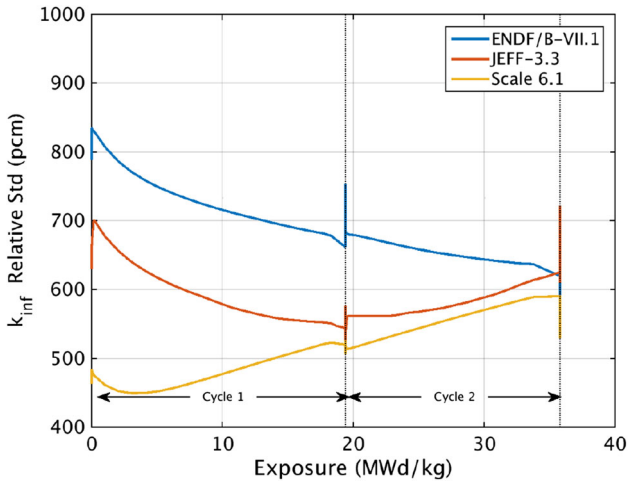

Fig. 85 Evolution of the k_{inf} relative standard deviation of a typical PWR assembly. Various covariance matrices are considered from JEFF-3.3 and other well-known libraries

critical benchmarks. This may therefore be an artefact of the use of certain critical benchmarks both in the nuclear data evaluation process.

The contribution of the uncertainty of the secondary angular distribution (SAD) of elastic scattering was also studied using the MF34 covariance data available in JEFF-3.3 for several isotopes. For ^{56}Fe the JEFF-3.3 ENDF/B-VII.1 and JENDL-4.0u evaluations only have the covariance data for P_1. For the ASPIS-Iron88 benchmark, significant contributions of SAD uncertainties were found for the ^{32}S and ^{27}Al reaction rates. As shown in Table 55 the JEFF-3.3 data predict reasonable uncertainties, consistent with most other evaluations (ENDF/B-VII.1, JENDL-4.0) as well as with the observed C/E ratios (Fig. 73).

The same is not true for some other isotopes such as ^{238}U. As shown in Table 57, MF34 covariances predict an excessively large uncertainty of 1.33% in k_{eff} for the pmf6 (FLATTOP-Pu) benchmark, much larger than JENDL-4.0 nuclear data evaluation, and largely exceeding the uncertainty contributions of all other nuclear data uncertainty terms together.

Table 56 Uncertainty due to transport cross-sections of different origin compared to the C/E values for the FNG-Cu benchmark. The penetration depth is d

Reaction	d	Uncertainty (%)		
	(cm)	JEFF-3.3	ENDF/B-VI.8	TENDL-2013
^{58}Ni(n,p)	35	5	14	23
	57	9	27	42
^{115}In(n,n')	35	8	9	12
	57	13	19	24
^{27}Al(n,α)	57	13	33	52
^{93}Nb(n,2n)	57	13	35	53
^{197}Au(n,γ)	57	15	20	19
^{186}W(n,γ)	57	23	29	27

Table 57 Uncertainty in k_{eff} in pcm for the FLATTOP-Pu (pmf6) and SNEAK-7A critical benchmarks due to secondary angular distribution uncertainties taken from the JEFF-3.3, JENDL-4.0 and ENDF/B-VII.1 libraries

FLATTOP-Pu	JEFF-3.2	JENDL-4.0	ENDF/B-VII.1
MF31–MF33	891	701	548
MF34 (^{238}U P_1)	1340	312	–
SNEAK-7A			
MF31–MF33	766	616	763
MF34 (^{238}U P_1)	590	144	–

4.2.3 Burnup

An example of application for the covariance information in the JEFF-3.3 library is given in Fig. 85: a 4.1% enriched PWR assembly is irradiated during two cycles in a Swiss nuclear power plant. The evolution of its k_{inf} uncertainty due to nuclear data uncertainty is depicted. The uncertainty propagation calculation has been carried out with CASMO-5 [430] and the SHARK-X [431–433] platform. For the sake of comparison, the results of JEFF-3.3 are shown together with other covariance libraries from ENDF/B-VII.1 [121] and Scale-6.1 [427]. All possible nuclide reaction pairs (cross sections, fission spectrum and averaged number of neutron per fission) have been perturbed, i.e.all isotopes available in both covariance libraries and the CASMO-5 library. A 19 energy group representation of the covariance libraries is used to be consistent with the group structure of CASMO-5. The representation was produced with the NJOY code [41]. ^{235}U (MT = 452 – total number of neutrons per fission) uncer-

tainties are not available in the JEFF-3.3 library, only uncertainties for the average number of prompt neutrons produced by fission is provided (MT = 456). Due to limitations in the SHARK-X methodology, such information cannot be handled and as such, MT452 is perturbed using the covariances of MT = 456.

At Beginning of Life (BOL), the major contributors to the uncertainties are the same between the various sources of covariance matrices: average number of neutron produced by fission, fission cross section and spectrum of ^{235}U, capture cross sections of ^{235}U and ^{238}U. Their contribution to the total uncertainty is however different. Both ENDF/B-VII.1 and JEFF-3.3 have ^{235}U as the largest contributor to k_{inf} uncertainty. The consumption of ^{235}U during irradiation explains the global decrease of k_{inf} uncertainty with exposure. The lower k_{inf} uncertainty at BOL in Scale 6.1 is due to the relatively low uncertainty in ^{235}U. Moreover, the increase of the k_{inf} uncertainty with exposure in Scale 6.1 is due to ^{239}Pu whose uncertainty is overestimated. Both input uncertainties have been changed in Scale 6.2 [434]. The evolution of the k_{inf} uncertainties with exposure obtained the JEFF-3.3 covariances appear reasonable. A more in-depth analysis of the JEFF-3.3 covariance matrices will be given elsewhere.

4.2.4 GEN-IV reactor concepts

JEFF-3.3 neutron reaction covariances were used for the uncertainty quantification of the GEN-IV reactor concepts MYRRHA, ALFRED and ASTRID with the SUMMON methodology [435]. These uncertainties were compared against results obtained using the new ENDF/B-VIII.0 nuclear data library covariances [180]. Results for the uncertainty quantification of MYRRHA shows that the total k_{eff} uncertainty is very similar: 814 pcm and 769 pcm for JEFF-3.3 and ENDF/B-VIII.0 respectively, The main contributions to this uncertainty differ a lot which denotes noteworthy differences between covariance evaluations. ^{238}U, ^{239}Pu, ^{240}Pu and ^{241}Pu are the main contributors to the uncertainty using both nuclear data library covariances. ^{238}U inelastic scattering and fission reactions, including its cross-correlations with other reactions are of special importance.

Moreover, ^{209}Bi elastic scattering is one of the main contributors to the uncertainty. The uncertainty analysis for ALFRED shows 905 pcm and 760 pcm for JEFF-3.3 and ENDF/B-VIII.0 respectively. Analogous conclusions to the analysis performed with MYRRHA can be extracted for ALFRED. For ASTRID, the total k_{eff} uncertainty predicted by both covariance evaluations is also very similar: 994 pcm and 832 pcm for JEFF-3.3 and ENDF/B-VIII.0, respectively.

The uncertainties for MYRRHA and ALFRED approximately account for the difference between experimental and predicted k_{eff} values for VENUS-F (Sect. 3.1.7).

4.3 Adjustment to benchmarks

Uncertainties estimated on the basis of evaluations accounting only for microscopic data are substantially larger than those of criticality benchmarks (Sect. 4.2.1). Developing proper methods for adjusting evaluations to benchmarks is an active field of research [436–438] and without presenting final conclusions on what may be achieved, we show here two recent examples based on JEFF-3.3.

The JAEA adjustment In support of the development of advanced fast reactors of Generation-IV type the JAEA adjustment methodology was applied to JEFF-3.3 using the methods, benchmarks and experimental quantities established by recent OECD-NEA WPEC expert groups [436,437, 439–442]. Important aspects of the methods proposed are to maintain agreement with the unadjusted data within one standard deviation (before adjustment) and to avoid adjustment to integral data that are initially more than two benchmark standard uncertainties discrepant. These constraints avoid unphysical modifications of the nuclear data.

The quantities[10] considered are given in Table 58. The reaction rates are taken at the center of the critical assembly.

The cross sections and covariances from JEFF-3.3 that were used are those for neutron-induced reactions on ^{10}B, ^{16}O, ^{23}Na, ^{52}Cr, ^{56}Fe, ^{58}Ni, ^{235,238}U, ^{239,240,241}Pu. Data and covariances for ^{242}Pu were also needed and taken from JENDL-4. These uncertainty data in the fast energy range are based only on microscopic experimental data.

The results before and after the adjustment with the JAEA method are compared with those for JENDL-4 in Fig. 86 which presents the ratio of calculated to experimental data. C/E values for both JEFF-3.3 and JENDL-4 look good in general and with few exceptions are very similar after adjustment regardless of initial differences. For both libraries the k_{eff} estimates which were already quite good improve by the adjustment. This is particularly noteworthy for the initial larger deviations for SNEAK and Proteus and to a lesser extent ZPR6/7-st. These six case were well outside one benchmark standard uncertainty and after adjustment either agree within one standard uncertainty (ZPR6/7-st, ZPR6/7 ^{240}Pu, Proteus core 8) or within 2 standard uncertainties. Jezebel (pmf1) reaction rates are similarly off for JENDL-4 and JEFF-3.3 before the adjustment, but JEFF-3.3 is closer to experiment after the adjustment. In contrast the two SVR values for ZPPR-9, which were more than 10% off before the adjustment in the case of JEFF-3.3, remain between 5 and 7% after

[10] Xnm denotes a reaction rate. X = F for fission and C for capture. The charge number is Z = 90+n. The mass number is A = 230+m. F28 is therefore the rate of the ^{238}U(n,f) reaction, F25 for ^{235}U(n,f), F49 for ^{239}Pu(n,f), F37 for ^{237}Np(n,f), C28 for ^{238}U(n, γ). F28/F25 denotes the reaction rate for ^{238}U(n,f) divided by that of ^{235}U(n,f). Such a ratio is called a spectral index.

Table 58 Integral quantities[10] used in the JAEA adjustment of JEFF-3.3. SVR is the sodium void reactivity swing, CVR the coolant void reactivity swing

Benchmark	Quantities
Jezebel ^{239}Pu, pmf1	k_{eff}, F28/F25, F49/F25, F37/F25
Jezebel ^{240}Pu, pmf2	k_{eff}
Flattop-Pu, pmf6	k_{eff}, F28/F25, F37/F25
ZPR6-7 st, mcf1	k_{eff}, F28/F25, F49/F25, C28/F25
ZPR6-7 ^{240}Pu, mcf2-1	k_{eff}
ZPPR-9	k_{eff}, F28/F25, F49/F25, C28/F25, SVR-central, SVR-leakage dominated
Joyo	k_{eff}
Proteus core-7 (water)	k_{inf}, C28/F49, F28/F49, F25/F49, F41/F49, C42/F49, CVR
Proteus core-8 (unmod)	k_{inf}, C28/F49, F28/F49, F25/F49, F41/F49, C42/F49
SNEAK-7A MOX	k_{eff}
SNEAK-7B MOX,$^{\text{nat}}UO_2$	k_{eff}

the adjustment, while for JENDL-4 they improve to 2–4% overestimation. An adjustment may also worsen agreement with experiment, as is evident for the ratio of the ^{238}U(n,f) to ^{235}U(n,f) reaction rates for ZPR6/7-st. Further analysis of the effect for the SVR of ZPPR-9 suggests a further investigation of ^{239}Pu neutron capture and $\overline{\nu}$, and ^{23}Na elastic scattering are warranted.

The PSI adjustment To complement criticality benchmarking a comparative study between JEFF-3.3 and TENDL-2017 was conducted at Paul Scherrer Institut (PSI) for reaction rates measured for a number of fast critical experiments. Mean values and uncertainties were analysed in a consistent manner. The necessary specifications were taken from the ICSBEP [23] and IRPhE [443] databases.

The TENDL data and covariances were generated on the basis of random files available on the web [189]. For JEFF-3.3 covariances are taken from the evaluation or were delivered in the appropriate formats by the NEA. The latter were produced with NJOY [41] from the ENDF formatted files.

The deterministic code system ERANOS (Edition 2.2-N) [444] was used to compute the integral parameters along with the uncertainties due to nuclear data uncertainties, by using the P_1S_{16} approximation in the required forward and adjoint transport calculations. For both JEFF-3.3 and TENDL only the ten most important nuclides with respect to the chosen benchmarks were used. These nuclides are ^{16}O, ^{23}Na, ^{52}Cr, ^{56}Fe, ^{58}Ni, ^{235}U, ^{238}U, ^{239}Pu, ^{240}Pu and ^{241}Pu. We also note that for these the fission spectra, secondary energy/angular distributions and background cross sections, as well as the data for all other nuclides, are stemming from the original JEFF-3.1 based ERANOS library. The quantities[10] which are considered are similar to that of Table 58 but reaction rates for the Flattop-^{235}U (hmf28) and BigTen experiments (imf7) were included as well. The

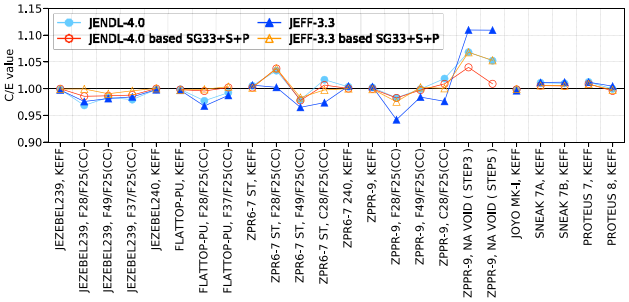

Fig. 86 Calculated over experimental (C/E) values of the quantities given in Table 58 before and after adjustment. JEFF-3.3 and JENDL-4. The label 'based on SG33+S+P' is the adjusted result and refers to the benchmark quantities defined by WPEC Subgroup-33 with the SNEAK and PROTEUS k_{eff} added on recommendation of Subgroup-39 [436,437]

reaction rates were measured in the center of the core relative to the fission of ^{235}U. For the adjustment the so-called APIA method was used – asymptotic Progressing Incremental nuclear data Adjustment – [445,446]. Of the 34 available quantities only 6 were used in the adjustment: The Godiva reaction rate ratios for ^{238}U(n,f), ^{239}Pu(n,f) and ^{238}Np(n,f) relative to ^{235}U(n,f) and the ZPPR-9 reaction rates for ^{238}U(n,f), ^{239}Pu(n,f) and ^{238}U(n, γ) also relative to ^{235}U(n,f). This leaves 28 quantities to compare with that were not included.

Figure 87 shows the absolute residual χ before and after adjustment for the experiments considered. For clarity χ is $\chi = \left|\frac{C-E}{u_{\text{E}}}\right|$, with, as usual, C for the calculated value, E for the experimental one and u_{E} its standard uncertainty.

On average, before and after adjustment JEFF-3.3 agrees better with the benchmark data than TENDL. Exceptions are ^{238}U capture (C28/F25) and k_{eff} for ZPPR-9, ZPR-6/7 and SNEAK 7B for which the prior values are better for TENDL.

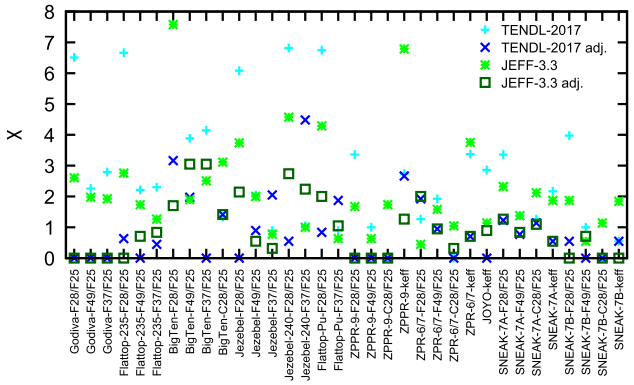

Fig. 87 Results of the PSI adjustment of JEFF-3.3 and TENDL-2017 to Godiva and ZPPR-9 reaction rates using the APIA method [438]

Table 59 Results of the PSI calculations with uncertainties for Big Ten (imf7). JEFF-3.3 is in column JEFF, TENDL-2017 in column TENDL [438]

Quantity		C and u_C			
	E	prior		posterior	
	u_E	JEFF	TENDL	JEFF	TENDL
F28/F25	0.0374	0.0348	0.0334	0.0368	0.0363
	0.0003	0.0017	0.0007	0.0012	0.0006
F49/F25	1.194	1.178	1.161	1.219	1.177
	0.008	0.049	0.022	0.020	0.014
F37/F25	0.322	0.315	0.310	0.331	0.322
	0.003	0.017	0.004	0.011	0.004
C28/F25	0.110	0.101	0.106	0.106	0.106
	0.003	0.005	0.002	0.003	0.001

After adjustment JEFF-3.3 and TENDL both improve significantly and only SNEAK-7B k_{eff} is still better with TENDL. The initial number of deviations greater than 2 standard uncertainties of the experimental data is very large for both libraries. Even if the number of data used for the adjustment is small the overall improvement is very good for both libraries: 4-5 cases remain deviating 2 standard uncertainties or more.

As for the estimated standard uncertainties u_C due to nuclear data uncertainties, clear trends are observed, namely that (1) in most cases the computed prior uncertainties are larger than the benchmark uncertainties i.e.$u_C > u_E$, and (2) the JEFF-3.3 prior uncertainty is even more conservative than TENDL. Table 59 for the BigTen (imf7) benchmark serves as an illustrative example. It further shows that also the posterior uncertainty for JEFF-3.3 is larger than that of TENDL and remains larger than for the benchmark. It may however be noted that the JEFF-3.3 uncertainties are such that the deviations between C and E are within at most $2u_E$ both for the prior and the posterior, giving some credit to the applicability of the larger JEFF-3.3 uncertainties.

5 Conclusions

A comprehensive description of the JEFF-3.3 – joint evaluated nuclear data library for fission and fusion, version 3.3 – was presented with a focus on evaluations for neutron induced reactions. Important differences with earlier releases of the library include

- the new major actinide evaluations,
- a number of new evaluations for structural and shielding materials, coolants and fission products,
- considerable improvements for photon emission,
- a consistent approach for delayed neutrons,
- a new decay data library,
- a new fission yields library and
- new thermal scattering evaluations.

JEFF-3.3 has a much larger set of covariance files associated with the evaluations. Of particular importance are covariances for the major actinides, but also many other new evaluations have covariance data. A considerable number of complete and partial evaluations for neutron-induced reactions were taken from the TENDL library, making the JEFF-3.3 library more complete and consistent and furnishing a considerable number of nuclide evaluations with covariances. JEFF-3.3 adopted the TENDL-2017 libraries for photon, proton, deuteron, triton, helion and alpha induced reactions. These replace the proton library of JEFF-3.1 and previous activation libraries. For light elements a selection of files were taken from ENDF/B-VIII.0.

The present paper summarizes the developments since JEFF-3.1.1, for which the last comprehensive report was made. The paper includes descriptions for (partial) evaluations already in JEFF-3.1.2 or JEFF-3.2 if these were kept for JEFF-3.3. We also clearly indicate the origin of evaluated files in case these were not developed by the JEFF community.

Evaluations Focusing on the neutron transport sublibrary, the foremost changes were the major actinides ^{235}U, ^{238}U and ^{239}Pu. These were re-evaluated in the resonance and in the fast energy range with a close adherence to the cross sections obtained by the neutron standards working group in 2009. For the fast range, the evaluation was performed with the TALYS code. For uranium and plutonium, the fission channel was consistently evaluated using all available data for the respective isotopic chain, substituting only the standard cross sections of ^{235}U and ^{238}U for the model theoretical one. This ensures a consistent physics approach for the remaining reaction channels with the exception of the elastic channel, which accommodates the difference in the fission channel between theory and the standard. The major actinide evaluations include new evaluations of the prompt neutron

multiplicity as a function of energy and of the fission neutron spectrum. The latter is based on a new fit with the Madland and Nix model. A new feature is the inclusion of prompt fission gamma evaluations based on recent experimental data obtained by Oberstedt et al.

For the minor actinides and the actinides of the Th-U fuel-cycle, files were adopted from earlier evaluations. Special mention is made here of ^{241}Am and the curium isotopes (A = 240–250), which were evaluated for JEFF-3.2 and adopted in JEFF-3.3.

For the time dependence of the emission of delayed neutrons, the 8 group structure was adopted as consistently as possible. It was imposed on all evaluations taken from other libraries whenever the relevant recommendation was provided by WPEC Subgroup 6.

Discussions of evaluations for neutron-induced reactions were also presented for deuterium, sodium, aluminum, chromium, iron, nickel, copper, zirconium, cadmium, hafnium, tantalum, tungsten, gold, lead and bismuth. These evaluations were performed for JEFF-3.2 or JEFF-3.3. For aluminum, lead and bismuth, these include only minor modifications. Iron was not changed.

From TENDL-2015, 312 evaluations are adopted in the JEFF-3.3 neutron sublibrary. Of these, 111 are stable nuclides ranging from ^{17,18}O to ^{203,205}Tl. This implies that many of the fission product evaluations that were left untouched since JEFF-3.0 are now from TENDL. The same holds for certain (structural) materials not mentioned above.

Special attention was given to the inclusion of gamma-ray emission data for the neutron sublibrary. For fission products these are based on TALYS calculations. For iron, silver, indium, ^{113}Cd, ^{155,157}Gd and hafnium, these are obtained from a combination of the EGAF database and TALYS calculations. For the actinides, the available prompt fission gamma data were included. For a number of nuclides (in particular fission products), the correlated emissions of gamma-rays from inelastic scattering were included.

The new fission yields library includes 19 neutron induced fission yield files with thermal, fast (E_n = 0.5 MeV) and high-energy (14 MeV) evaluations. Spontaneous fission yields files are given for ^{252}Cf, ^{242}Cm and ^{244}Cm. The choice of evaluations is based on the contribution of these nuclides to the number of fissions in thermal and fast thorium, uranium and MOX-fuelled reactors. The methodology of the evaluation and the new data included in addition to those of the previous evaluation are summarized. Of particular interest for burnup analysis is the cumulative yield of ^{148}Nd.

The new decay data evaluation contains 3852 radionuclides recognizing and incorporating the most rigorous available evaluation for each of these nuclides. The source libraries for the evaluations are NUBASE (2295), ENSDF (849), DDEP (140), UKPADD-6.12 (441), UKHEDD-2.6 (59), IAEA (66) and IRDFF (2). The TAGS data of Greenwood et al. and the TAGS data of the Valencia and Nantes groups obtained at Jyväskylä were included. This leads to an improved partitioning of the total decay energy over the energy carried away by gamma-rays and by beta-rays.

The neutron activation sublibrary is a specially processed version of the TENDL-2017 library which replaces EAF-2010. This accommodates users needing activation data in the well-known EAF-format.

The thermal scattering library was expanded with 9 new evaluations: hydrogen in liquid ortho and para hydrogen, polyethylene, ice, mesytylene, toluene; deuterium in liquid ortho and para deuterium; deuterium and oxygen in heavy water, Al and O in sapphire/alumina, Si in silicon metal. The evaluations are based on scattering data analysed with models developed and adjusted at Bariloche.

Testing As an application library in the field of nuclear energy, JEFF-3.3 was tested and benchmarked for fission and fusion. It was demonstrated to process with common tools such as NJOY and PREPRO and certain dedicated tools of interest to the co-authors. Benchmarking concerned criticality estimation, shielding, delayed neutron yields, decay heat and Maxwellian averaged cross sections. The impact on criticality estimation of the new extended set of covariances was surveyed and highlighted by examples. A first demonstration of using these covariances for data adjustment was presented.

The 123 criticality benchmarking cases of the NEA Mosteller suite were inspected after each of four beta-releases to monitor progress in performance and guide choices of evaluations. For these benchmarks, the library has an excellent Chi-square that is substantially better than that of previous releases. It also compares well with the recently released ENDF/B-VIII.0 library. However, inspection of larger suites (van der Marck; IAEA) with more than 2000 benchmarks from ICSBEP, analysed statistically, shows an important warning. On average, criticality is predicted well but the distributions of deviations between calculation and experiment do not correspond to stated experimental uncertainties. As discussed in the text, this general conclusion is reflected in each of the smaller suites that are analysed, including the NEA Mosteller suite. Significant discrepancies exist that prevent meaningful statistical inference. This is highlighted also by cumulative Chi-square plots showing large steps. For future progress, these discrepancies need to be understood and dealt with.

For criticality safety, IRSN and PSI analysed suites of benchmarks that are used to validate the reliability of their calculational methods. On the whole JEFF-3.3 performs better than earlier releases, but the conclusion is not uniform: benchmarks may be found for which an earlier release performs better. Typically, JEFF-3.3 predicts a somewhat higher criticality, in particular for light-water uranium-oxide-fueled thermal systems. The same conclusion follows from exper-

iments performed at the Cadarache EOLE and MASURCA critical facilities that are representative for pressurized water reactors and sodium-cooled fast reactors.

An analysis of outliers in criticality benchmarking gives a number of materials that warrant attention of nuclear data evaluators: polyethylene, heavy water, beryllium and beryllium-oxide, carbon, fluor, aluminum, concrete, sulphur, steel, copper, erbium, hafnium, tungsten, lead, thorium and neptunium. For heavy water, considerable improvement was achieved with JEFF-3.3 as confirmed also by the FRM-II criticality estimates, however hst20-5 is still discrepant. The recent VENUS-F critical experiments testing lead and bismuth data for the MYRRHA project confirm the interest in improvement of those data by a substantial overprediction of criticality. A considerable number of outliers have no special materials, emphasizing the continued interest in searching for improvements of the major actinides (^{235}U, ^{238}U ^{239}Pu), water, oxygen and iron. Independently and importantly, the validity and specifications of benchmarks should be re-evaluated to ensure their importance for qualification of nuclear data. This concerns in particular the quality and credibility of uncertainty statements.

Uncertainty estimates for k_{eff} with JEFF-3.3 were given for a wide range of benchmarks comparing with other libraries and analyzing the origin by cross section, mean prompt neutron multiplicity and spectrum. Predicted uncertainties for JEFF-3.3 range from 0.5 to 2% depending on the critical benchmark. These uncertainties are typically larger than the differences between calculation and experiment. These small differences are due to choices in the evaluation process that are guided by comparisons with integral data. For the major actinides, evaluations were also affected by explicit fitting of a few integral data. However, no large scale fitting of integral data was performed, so that the potential reduction of the uncertainties that would have resulted is not effected in the present library. A systematic approach for inclusion of integral data was explored but a more complete use of integral data is deferred to JEFF-4 for which it is a major objective.

Concerning delayed neutron yields, JEFF-3.3 performs well for estimates of β_{eff} and Rossi-α for the 31 benchmarks identified by van der Marck and for VENUS-F. The estimates are slightly worse than those using JEFF-3.1.1 but no deviation is greater than 3 standard deviations. An earlier analysis shows that uncertainties of estimates are of the order of 3% for ^{235}U and ^{239}Pu fueled systems and about 7% for ^{233}U.

For shielding, JEFF-3.3 performs better than earlier releases and is competitive with other libraries. The user must however be aware that in deep penetration experiments the neutron flux drops significantly and differences with experimental dosimeter reaction rates of 20–50% may be found especially at the greater penetration depths. This reflects the state of the art. The improved covariance data lead to one standard deviation intervals around the calculated value that overlap the experimental data. A highlight illustrating these general conclusions is the Frascati 14 MeV copper benchmark. The iron file was not changed due to its good performance for leakage spectra, in particular those from the Řež iron spheres with a ^{252}Cf neutron source.

A first assessment of the new fission yields and decay data is given by the fission pulses for thermal and fast fission of ^{235}U and ^{239}Pu. For cooling periods from several hours to 1 day a comparison with the thermal aggregate data of Tobias, Dickens and the University of Massachussets at Lowell and the fast fission data of Akiyama and An shows a clear improvement of the partitioning of the total decay heat over gamma decay heat and beta decay heat. This change is primarily due to the inclusion of total absorption gamma-ray spectrometry data. Changes to the total decay heat reflect the new fission yields and further modifications of the decay data.

Comparisons with the decay heat data obtained at the JAEA 14 MeV Fast Neutron Source also show significant improvements of the new library. Here this is demonstrated for important elements for fusion reactors: chromium, iron, nickel, copper, tungsten and lead. The decay heat is followed for decay times of 1 h after a 5 min irradiation and decay times of about 1 year after a 7 h irradiation. Here, JEFF-3.3 benefits from the added TENDL evaluations providing isomer production cross sections which are crucial for this type of activation data. Although JEFF-3.3. is a rather good evaluation for this type of calculation, not all deficiencies are remedied and a summary is presented of the nuclide cross sections warranting closer scrutiny in future evaluated libraries.

Outlook. The JEFF development community has agreed to a major change in evaluation methodology for JEFF-4, foreseen for release in 2024. This change aims at a general purpose library produced by state-of-the-art methods leading to evaluations that feature best physics, highly performant in applications, well documented and reproducible. A general purpose library must be applicable in many domains such as

- reactor core design for present, next generation and advanced reactors fostering nuclear power as key component of a sustainable energy supply,
- analysis and prediction of parameters determining reactor operation,
- end of cycle and end of fuel life time inventory and response analyses,
- analysis and prediction of inventories and key responses for intermediate storage, reprocessing, transport and final repositories of spent fuel to meet the environmental challenges of nuclear power,
- detection techniques in security and nuclear safeguards,
- accelerator applications such as MYRRHA,
- medical applications, i.e. production of nuclides,

- applications of neutrinos,
- interests in basic science such as stellar nucleosynthesis.

This will require the inclusion of state of the art experimental data from microscopic nuclear physics measurements, such as cross sections, resonance parameters, spectra, decay data, but also from high quality integral experiments allowing meaningful testing and adjustment of the evaluated data files. Best physics requires besides best experimental data also best modeling. So the best possible support from theoretical insights and codes available among the nuclear physics community should be accessible to and used by the evaluation community. These insights will be critical to make progress with the modeling of the fission, capture and inelastic scattering processes for actinides in particular and for the modeling of non-fissile nuclides such as the important structural materials. In view of these challenges the JEFF project is reaching out to scientists and engineers capable and committed to provide best knowledge for key developments of our society. They will find in the present paper not only the merits of the JEFF-3.3 library, but also the challenges that it has left to tackle.

Acknowledgements The authors would like to thank all contributors to the JEFF project that shared their insights and provided their specific input for the present JEFF-3.3 evaluation and its immediate predecessors JEFF-3.2 and JEFF-3.1.2.

Data Availability Statement This manuscript has no associated data or the data will not be deposited. [Authors' comment: The nuclear data in the JEFF-3.3 library described in this paper are freely accessible from http://www.oecd-nea.org/dbdata/jeff/. There also the nuclear data of earlier versions of the library may be found.]

References

1. The JEFF-3.0 Nuclear Data Library: Synopsis of the General Purpose File. JEFF Report 19, ISBN 92-64-01046-7, NEA No. 3711, OECD Nuclear Energy Agency, France (2005)
2. A. Koning, R. Forrest, M. Kellett, R. Mills, H. Henriksson, Y. Rugama (Eds.) The JEFF-3.1 nuclear data library. JEFF Report 21, ISBN 92-64-02314-3, NEA No. 6190, OECD Nuclear Energy Agency, France (2006)
3. A. Santamarina, D. Bernard, P. Blaise, M. Coste, A. Courcelle, T. Huynh, C. Jouanne, P. Leconte, O. Litaize, S. Mengelle, G. Noguère, J. Ruggiéri, O. Sérot, J. Tommasi, C. Vaglio, J. Vidal, The JEFF-3.1.1 nuclear data library. JEFF Report 22, Validation results from JEF-2.2 to JEFF-3.1.1, ISBN 92-64-02314-3, NEA No. 6190, OECD Nuclear Energy Agency, France (2006)
4. M. Kellett, O. Bersillon, R. Mills, The JEFF-3.1/-3.1.1 radioactive decay data and fission yields sub-libraries. JEFF Report 20, NEA No. 6287, ISBN 978-64-99087-6 (2009)
5. A. Koning, D. Rochman, J.-C. Sublet, N. Dzysiuk, M. Fleming, S. van der Marck, TENDL: complete nuclear data library for innovative nuclear science and technology. Nucl. Data Sheets **155**, 1–55 (2019). Special Issue on Nuclear Reaction Data
6. F. Varaine, G. Rodriguez, J. Hamy, S. Kubo, H. Mochida, U. Kukinori, J.-P. Helle, A. Remy, T. Chauveau, J.-L. Mazel, M. Libessart, R.-P. Benard, M. Fukuie, D. Settimo, V. Gautier, Y. Lhor, M. Lefrancois, ASTRID Project, General Overview and Status Progress in *Proceedings of the ICAPP 2018 International Congress on Advances in Nuclear Power Plants, 8–11 April 2018* (Charlotte, 2018)
7. D. De Bruyn, H. Aït Abderrahim, P. Baeten, C. Angulo Pérez, The Belgian MYRRHA ADS Programme. Part 1: The new phased implementation plan, in *Proceedings of the ICAPP 2018 International Congress on Advances in Nuclear Power Plants, 8–11 April 2018*, (Charlotte, 2018)
8. D. De Bruyn, R. Fernandez, P. Baeten, The Belgian MYRRHA ADS Programme. Part 2: recent developments in the reactor primary system, in *Proceedings of the ICAPP 2018 International Congress on Advances in Nuclear Power Plants, 8–11 April 2018*, (Charlotte, 2018)
9. T. Donné, W. Morris (eds.) European Research Roadmap to the Realisation of Fusion Energy. EUROfusion Programme Management Unit, ISBN 978-3-00-061152-0, November 2018. https://www.euro-fusion.org/eurofusion/roadmap/ (2018)
10. G. Federici, C. Bachmann, L. Barucca, W. Biel, L. Boccaccini, R. Brown, C. Bustreo, S. Ciattaglia, F. Cismondi, M. Coleman, V. Corato, C. Day, E. Diegele, U. Fischer, T. Franke, C. Gliss, A. Ibarra, R. Kembleton, A. Loving, F. Maviglia, B. Meszaros, G. Pintsuk, N. Taylor, M. Tran, C. Vorpahl, R. Wenninger, J. You, DEMO design activity in Europe: progress and updates. Fusion Eng. Des. **136**, 729–741 (2018). Special Issue: Proceedings of the 13th International Symposium on Fusion Nuclear Technology (ISFNT-13)
11. D. Bernardi, F. Arbeiter, M. Cappelli, U. Fischer, A. García, R. Heidinger, W. Krolas, F. Martín-Fuertes, G. Miccichè, A. Muñoz, F. Nitti, M. Pérez, T. Pinna, K. Tian, A. Ibarra, Towards the EU fusion-oriented neutron source: the preliminary engineering design of IFMIF-DONES. Fusion Eng. Des. **146**, 261–268 (2019)
12. P. Romojaro, F. Álvarez Velarde, I. Kodeli, A. Stankovskiy, C. Díez, O. Cabellos, N. García-Herranz, J. Heyse, P. Schillebeeckx, P. Schillebeeckx, G. Van den Eynde, G. Žerovnik, Nuclear data sensitivity and uncertainty analysis of effective neutron multiplication factor in various MYRRHA core configurations. Ann. Nucl. Energy **101**, 330 (2017)
13. Co-ordinated Evaluation of Plutonium-239 in the Resonance Region. Working Party on International Evaluation Co-operation, OECD NEA Nuclear Science Committee, Volume 34, NEA/NSC/WPEC/DOC(2014)447 (2014)
14. M. Chadwick, E. Dupont, E. Bauge, A. Blokhin, O. Bouland, D. Brown, R. Capote, A. Carlson, Y. Danon, C. De Saint Jean, M. Dunn, U. Fischer, R. Forrest, S. Frankle, T. Fukahori, Z. Ge, S. Grimes, G. Hale, M. Herman, A. Ignatyuk, M. Ishikawa, N. Iwamoto, O. Iwamoto, M. Jandel, R. Jacqmin, T. Kawano, S. Kunieda, A. Kahler, B. Kiedrowski, I. Kodeli, A. Koning, L. Leal, Y. Lee, J. Lestone, C. Lubitz, M. MacInnes, D. McNabb, R. McKnight, M. Moxon, S. Mughabghab, G. Noguère, G. Palmiotti, A.

Plompen, B. Pritychenko, V. Pronyaev, D. Rochman, P. Romain, D. Roubtsov, P. Schillebeeckx, M. Salvatores, S. Simakov, E. Soukhovitskii, J. Sublet, P. Talou, I. Thompson, A. Trkov, R. Vogt, S. van der Marck, The CIELO collaboration: neutron reactions on ^{1}H, ^{16}O, ^{56}Fe, ^{235,238}U, and ^{239}Pu. Nucl. Data Sheets **118**, 1 (2014)

15. Collaborative International Evaluated Library Organisation Pilot Project. Working Party on International Evaluation Cooperation, OECD NEA Nuclear Science Committee, Volume 40, NEA/NSC/WPEC/DOC(2019)—in print (2019)
16. G. Žerovnik, F. Álvarez-Velarde, O. Cabellos, L. Fiorito, N. García-Herranz, J. Heyse, I. Kodeli, S. Kopecky, B. Kos, P. Romojaro, P. Schillebeeckx, A. Stankovskiy, G.V. den Eynde, Recommendations for MYRRHA relevant cross section data to the JEFF project. JRC Technical Reports, EUR 28957 EN, Geel, Belgium (2017)
17. U. Fischer, M. Angelone, M. Avrigeanu, V. Avrigeanu, C. Bachmann, N. Dzysiuk, M. Fleming, A. Konobeev, I. Kodeli, A. Koning, H. Leeb, D. Leichtle, F. Ogando, P. Pereslavtsev, D. Rochman, P. Sauvan, S. Simakov, The role of nuclear data for fusion nuclear technology. Fusion Eng. Des. **136**, 162–167 (2018). Special Issue: Proceedings of the 13th International Symposium on Fusion Nuclear Technology (ISFNT-13)
18. G. de Saussure, L.C. Leal, R.B. Perez, N.M. Larson, M.S. Moore, A new resonance region evaluation of neutron cross sections for ^{235}U. Nucl. Sci. Eng. **103**, 109–118 (1989)
19. N. Larson, Updated Users' Guide for SAMMY: multilevel R-matrix fits to neutron data using Bayes' Equations, Oak Ridge National Laboratory Technical Report ORNL. ORNL/TM-9179 R, vol. 8 (2008)
20. S. Cathalau, A. Benslimane, A. Maghnouj, P. Fougeras, V. Ukraintsev, Qualification of the JEF2.2 cross sections in the epithermal and thermal energy ranges using a statistical approach. Nucl. Sci. Eng. **121**(2), 326 (1995)
21. L. Leal, H. Derrien, N. Larson, R. Wright, R-Matrix analysis of ^{235}U neutron transmission and cross-section measurements in the 2.25-keV energy range. Nucl. Sci. Eng. **131**, 230 (1999)
22. M. Fukushima, Y. Kitamura, T. Kugo, S. Okajima, Benchmark models for criticalities of FCA-IX assemblies with systematically changed neutron spectra. J. Nucl. Sci. Technol. **53**, 406–424 (2016)
23. J. Briggs (ed.) International Handbook of Evaluated Criticality Safety Benchmark Experiments. Organization for Economic Cooperation and Development—Nuclear Energy Agency (OECD-NEA) (2009)
24. Uranium-235 Capture Cross-section in the keV to MeV Energy Region. Working Party on International Evaluation Cooperation, OECD NEA Nuclear Science Committee, vol. 29, NEA/NSC/WPEC/DOC(2011)433 (2011)
25. Y. Danon, D. Williams, R. Bahran, E. Blain, B. McDermott, D. Barry, G. Leinweber, R. Block, M. Rapp, Simultaneous measurement of ^{235}U fission and capture cross sections from 0.01 eV to 3 keV using a gamma multiplicity detector. Nucl. Sci. Eng. **187**(3), 291–301 (2017)
26. M. Jandel, T.A. Bredeweg, E.M. Bond, M.B. Chadwick, A. Couture, J.M. OĎonnell, M. Fowler, R.C. Haight, T. Kawano, R. Reifarth, R.S. Rundberg, J.L. Ullmann, D.J. Vieira, J.M. Wouters, J.B. Wilhelmy, C.Y. Wu, J.A. Becker, New precision measurements of the $^{235}U(n,\gamma)$ cross section. Phys. Rev. Lett. **109**, 202506 (2012)
27. A.D. Carlson, V.G. Pronyaev, D.L. Smith, N.M. Larson, C. Zhengpeng, G.M. Hale, F.-J. Hambsch, E.V. Gai, S.-Y. Oh, S.A. Badikov, T. Kawano, H.M. Hofmann, H. Vonach, S. Tagesen, International evaluation of neutron cross section standards. Nucl. Data Sheets **110**, 3215 (2009)
28. R. Spencer, J. Harvey, N. Hill, L. Weston, Parameters of the 1.056-eV resonance in ^{240}Pu and the 2200 m/s neutron total cross sections of ^{235}U, ^{239}Pu, and ^{240}Pu. Nucl. Sci. Eng. **96**, 318 (1987)
29. J. Harvey, N. Hill, F. Perey, G. Tweed, L. Leal, High-resolution neutron transmission measurements on ^{235}U, ^{239}Pu and ^{238}U, in *Proceedings of the International Conference Nuclear Data for Science and Technology, May 30–June 3*, (Mito, 1988), p. 115
30. R. Gwin, R. Spencer, R. Ingle, J. Todd, S. Scoles, Measurements of the neutron fission cross sections of ^{235}U (En = 0.01 eV to 30 keV) and ^{239}Pu (En = 0.01 to 60 eV). Nucl. Sci. Eng. **88**, 37 (1984)
31. L.W. Weston, J.H. Todd, High-resolution fission cross-section measurements of ^{235}U and ^{239}Pu. Nucl. Sci. Eng. **111**, 415–421 (1992)
32. L. Weston, J. Todd, Subthreshold fission cross section of ^{240}Pu and the fission cross sections of ^{235}U and ^{239}Pu. Nucl. Sci. Eng. **88**, 567 (1984)
33. C. Paradela, I. Duran, L. Tassan-Got, L. Audouin, B. Berthier, S. Isaev, C. Le Naour, C. Stephan, D. Tarrío, U. Abbondanno, G. Aerts, H. Álvarez-Pol, F. Álvarez-Velarde, S. Andriamonje, J. Andrzejewski, G. Badurek, P. Baumann, F. Becvar, E. Berthoumieux, F. Calviño, M. Calviani, D. Cano-Ott, R. Capote, C. Carrapiço, P. Cennini, V. Chepel, E. Chiaveri, N. Colonna, G. Cortes, A. Couture, J. Cox, M. Dahlfors, S. David, I. Dillmann, C. Domingo-Pardo, W. Dridi, C. Eleftheriadis, M. Embid-Segura, L. Ferrant, A. Ferrari, R. Ferreira-Marques, K. Fujii, W. Furman, I.F. Gonçalves, E. Gonzalez-Romero, A. Goverdovski, F. Gramegna, C. Guerrero, F. Gunsing, R. Haight, M. Heil, M. Igashira, E. Jericha, Y. Kadi, F. Kaeppeler, D. Karadimos, M. Kerveno, V. Ketlerov, P. Koehler, V. Konovalov, M. Krticka, C. Lampoudis, C. Lederer, H. Leeb, A. Lindote, S. Lukic, J. Marganiec, T. Martinez, S. Marrone, C. Massimi, P. Mastinu, A. Mengoni, P.M. Milazzo, C. Moreau, M. Mosconi, S.J. Pancin, A. Pavlik, P. Pavlopoulos, L. Perrot, R. Plag, A. Plompen, A. Plukis, A. Poch, C. Pretel, J. Praena, J. Quesada, T. Rauscher, R. Reifarth, C. Rubbia, G. Rudolf, P. Rullhusen, J. Salgado, C. Santos, L. Sarchiapone, I. Savvidis, G. Tagliente, J.L. Tain, L. Tavora, R. Terlizzi, P. Vaz, A. Ventura, D. Villamarin, M.C. Vincente, V. Vlachoudis, R. Vlastou, F. Voss, S. Walter, C. Weiss, M. Wiesher, K. Wisshak, High accuracy 235U(n, f) data in the resonance energy region. EPJ Web Conf. **111**, 02003 (2016)
34. C. Wagemans, P. Schillebeeckx, A.J. Deruytter, R. Barthelemy, Subthermal fission cross-section measurements for ^{233}U, ^{235}U and ^{239}Pu. in *Proceedings of the International Conference on Nuclear Data for Science and Technology* ed. by S. Igarashi, p. 91 (Mito, Japan, 1988)
35. J. Wartena, H. Weigmann, C. Burkholz, Nuclear data for the calculation of thermal reactor reactivity coefficients, in *Proceedings of an Advisory Group meeting*, (IAEA, Vienna, Tecdoc, 1987), p. 491
36. H. Weigmann, B. Keck, J. Wartena, P. Geltenbort, K. Schreckenbach, Measurements of η of ^{235}U for subthermal neutron energies. The physics of reactors: operation, design and computation. Volume 3, Marseille, France (1990)
37. R.B. Perez, G. Saussure, E.G. Silver, R.W. Ingle, H. Weaver, Simultaneous measurements of the neutron fission and capture cross sections for Uranium-235 for neutron energies from 8 eV to 10 keV. Nucl. Sci. Eng. **52**, 46–72 (1973)
38. G. de Saussure, R. Gwin, L. Weston, R. Ingle, R. Fullwood, R. Hockenbury, Simultaneous measurements of the neutron fission and capture cross sections for ^{235}U for incident neutron energies from 0.4 eV to 3 keV. Tech. Rep. ORNL-TM-1804, Oak Ridge National Lab., Tenn.; Rensselaer Polytechnic Inst., Troy, N. Y. Dept. of Nuclear Engineering and Science (1967)

39. L. Erradi, A. Santamarina, O. Litaize, The reactivity temperature coefficient analysis in light water moderated UO_2 and UO_2-PuO_2 lattices. Nucl. Sci. Eng. **144**, 47–73 (2003)
40. A. Carlson, V. Pronyaev, R. Capote, G. Hale, Z.-P. Chen, I. Duran, F.-J. Hambsch, S. Kunieda, W. Mannhart, B. Marcinkevicius, R. Nelson, D. Neudecker, G. Noguère, M. Paris, S. Simakov, P. Schillebeeckx, D. Smith, X. Tao, A. Trkov, A. Wallner, W. Wang, Evaluation of the neutron data standards. Nucl. Data Sheets **148**, 143 (2018). Special Issue on Nuclear Reaction Data
41. R. MacFarlane, D. Muir, *The NJOY Nuclear Data Processing System, Version 99* (LANL, Los Alamos, 1999)
42. P. Archier, C. De Saint Jean, O. Litaize, G. Noguère, L. Berge, E. Privas, P. Tamagno, CONRAD evaluation code: development status and perspectives. Nucl. Data Sheets **118**, 488–490 (2014)
43. A. Koning, D. Rochman, Modern nuclear data evaluation with the TALYS code system. Nucl. Data Sheets **113**, 2841–2944 (2012)
44. J. Tommasi, G. Noguère, Analysis of the PROFIL and PROFIL-2 sample irradiation experiments in Phénix for JEFF-3.1 nuclear data validation. Nucl. Sci. Eng. **160**(2), 232 (2008)
45. V. Andreev, Measuremnet of ν(eff) and fission + capture for fast neutrons in ^{235}U and ^{239}Pu. Atmos. Energy **4**, 185 (1958)
46. F. Corvi, P. Giacobbe, Capture to fission ratio of^{235}U from the measurement of low energy gamma-rays. in *Conference on nuclear cross sections and technology*, (Washington, 1975)
47. F. Corvi, L. Calabretta, M. Merla, T. van der Veen, M. Moore, Measurement of neutron capture cross section and alpha of ^{235}U from 2 to 85 keV. Argonne National Laboratory Report series No. 83-4, Argonne, USA (1983)
48. J. Hopkins, B. Diven, Neutron capture to fission ratios in ^{233}U, ^{235}U and ^{239}Pu. Nucl. Sci. Eng. **12**, 169 (1962)
49. J. Hopkins, B. Diven, The measurement of alpha, neutron fission and capture cross sections for ^{235}U and ^{239}Pu for neutron energies from 10 to 80 keV. At. Energy **38**, 82 (1975)
50. G. Muradyan, G. Ustroev, Y. Shchepkin, Y. Adamchuk, M. Voskanyan, L. Prokofeva, Measurement of radiative capture and fission cross sections and their ratio alpha for ^{235}U, in *All union conference on neutron physics, Kiev 18-22 April 1977*, (USSR, Kiev, 1977)
51. P. Spivak, B. Erozolimskij, G. Dorofeev, V. Lavernchik, I. Kutikov, J. Dobrynin, Average number of neutrons ν_{eff} emitted by the isotopes ^{233}U, ^{235}U, ^{239}Pu on capture of neutrons with energies from 30 to 900 keV. At. Energy **1**, 21 (1956)
52. E. Fort, J. Doat, A Code to Calculate Average Parameters from Sets of Resolved Resonance Parameters, tech. rep., CEA Cadarache, 1983. NEA Nuclear Data Committee Report NEANDC-161U (1983)
53. J. Both, Y. Lee, A. Mazzolo, Y. Peneliau, O. Petit, B. Roesslinger, M. Soldevila, Tripoli-4, a three-dimensional poly-kinetic particle transport Monte-Carlo code, in *International Conference on Supercomputing in Nuclear Applications SNA2003* (2003)
54. H. Kim, C. Paradela, I. Sirakov, B. Becker, R. Capote, F. Gunsing, G. Kim, S. Kopecky, C. Lampoudis, Y.-O. Lee, R. Massarczyk, A. Moens, M. Moxon, V. Pronyaev, P. Schillebeeckx, R. Wynants, Neutron catpure cross section measurements for ^{238}U in the resonance region at GELINA. Eur. Phys. J. A **52**, 170 (2016)
55. H. Derrien, L. Leal, N. Larson, A. Courcelle, Neutron resonance parameters and calculated cross sections from Reich–Moore analysis of experimental data in the neutron energy range from 0 to 20 keV. ORNL/TM-2005/241, Oak Ridge National Laboratory (2005)
56. D. Olsen, G. de Saussure, R. Perez, E. Silver, F. Difilippo, R. Ingle, H. Weaver, Precise measurement and analysis of neutron transmission through uranium-238. Nucl. Sci. Eng. **62**, 479–501 (1977)
57. D. Olsen, G. de Saussure, R. Perez, F. Difilippo, R. Ingle, Note on ^{238}U+n resolved resonance energies. Nucl. Sci. Eng. **66**, 141–144 (1978)
58. F. Difilippo, R. Perez, G. de Saussure, D. Olsen, R. Ingle, ^{238}U neutron-induced fission cross section for incident neutron energies between 5 eV and 3.5 MeV. PRC **21**, 1400–1410 (1980)
59. M.C. Moxon, J.B. Brisland, GEEL REFIT, A least squares fitting program for resonance analysis of neutron transmission and capture data computer code. AEA-InTec-0630, AEA Technology, Harwell, UK (1991)
60. C.W. Reich, M.S. Moore, Multilevel formula for the fission process. Phys. Rev. **111**, 929–933 (1958)
61. A. Lane, R. Thomas, R-matrix theory of nuclear reactions. Rev. Mod. Phys. **30**, 257 (1958)
62. P. Schillebeeckx, B. Becker, Y. Danon, K. Guber, H. Harada, J. Heyse, A.R. Junghans, S. Kopecky, C. Massimi, M. Moxon, N. Otuka, I. Sirakov, K. Volev, Determination of resonance parameters and their covariances from neutron induced reaction cross section data. Nucl. Data Sheets **113**, 3054–3100 (2012)
63. W. Mondelaers, P. Schillebeeckx, GELINA, a neutron time-of-flight facility for high-resolution neutron data measurements. Notizario Neutroni e Luce di Sincrotrone **11**, 19–25 (2006)
64. A. Trkov, G. Molnár, Z. Révay, S. Mughabghab, R. Firestone, V. Pronyaev, M.M.A.L. Nichols, Revisiting the ^{238}U thermal capture cross section and Gamma-emission probabilities from Gamma-ray emission probabilities from ^{239}Np decay. Nucl. Sci. Eng. **150**, 336–348 (2005)
65. L. Koester, H. Rauch, E. Seymann, Neutron scattering lengths: a survey of experimental data and methods. At. Data Nucl. Data Tables **49**, 65 (1991)
66. H. Derrien, L. Leal, N. Larson, Neutron Resonance Parameters and Covariance Matrix of ^{239}Pu. ORNL/TM-2008/123, Oak Ridge National Laboratory, Oak Ridge, Tenn (2008)
67. S.F. Mughabghab, *Atlas of Neutron Resonances: Resonance Parameters and Thermal Cross Sections. Z = 1-100* (Elsevier Science, New York, 2006)
68. P. Romain, B. Morillon, H. Duarte, Bruyères-le-Châtel neutron evaluations of actinides with the TALYS code: the fission channel. Nucl. Data Sheets **131**, 222–258 (2016). Special Issue on Nuclear Reaction Data
69. E. Bauge, G. Bélier, J. Cartier, A. Chatillon, J.M. Daugas, J.P. Delaroche, P. Dossantos-Uzarralde, H. Duarte, N. Dubray, M. Ducauze-Philippe, L. Gaudefroy, G. Gosselin, T. Granier, S. Hilaire, H.-T.P. Chau, J.M. Laborie, B. Laurent, X. Ledoux, C. Le Luel, V. Méot, P. Morel, B. Morillon, O. Roig, P. Romain, J. Taieb, C. Varignon, N. Authier, P. Casoli, B. Richard, Coherent investigation of nuclear data at CEA DAM: theoretical models, experiments and evaluated data. Eur. Phys. J. A **48**, 113 (2012)
70. R. Capote, M. Herman, P. Obložinský, P.Y.S. Goriely, T. Belgya, A. Ignatyuk, A. Koning, S. Hilaire, V. Plujko, M. Avrigeanu, O. Bersillon, M. Chadwick, T. Fukahori, Z. Ge, Y. Han, S. Kailas, J. Kopecky, V. Maslov, G. Reffo, M. Sin, E. Soukhovitskii, P. Talou, RIPL—reference input parameter library for calculation of nuclear reactions and nuclear data evaluations. Nucl. Data Sheets **110**(12), 3107 (2009). Special Issue on Nuclear Reaction Data
71. D.G. Madland, J.R. Nix, New calculation of prompt fission neutron spectra and average prompt neutron multiplicities. Nucl. Sci. Eng. **81**(2), 213–271 (1982)
72. X-5 Monte Carlo Team, MCNP—A general Monte Carlo N-particle transport code, version 5. Report LA-UR-03-1987, Los Alamos National Laboratory, USA, rev.10/3/05 (2005)
73. T. Kawano, R. Capote, S. Hilaire, P.C. Huu-Tai, Statistical Hauser–Feshbach theory with width-fluctuation correction including direct reaction channels for neutron-induced reactions at low energies. Phys. Rev. C **94**, 014612 (2016)

74. D. Rochman, E. Bauge, A. Vasiliev, H. Ferroukhi, Correlation in the fast neutron range via integral information. EPJ Nucl. Sci. Technol. **3**, 14 (2017)
75. N.V. Kornilov, F.J. Hambsch, I. Fabry, S. Oberstedt, T. Belgya, Z. Kis, L. Szentmiklosi, S. Simakov, The ^{235}U(n, f) prompt fission neutron spectrum at 100 K input neutron energy. Nucl. Sci. Eng. **165**, 117 (2010)
76. P. Johansson, B. Holmqvist, T. Wiedling, An experimental study of the prompt fission neutron spectrum induced by 0.5-MeV neutrons incident on uranium-235. Nucl. Sci. Eng. **62**, 695 (1977)
77. G.S. Boikov, V.D. Dmitriev, G.A. Kudyaev, Y.B. Ostapenko, M.I. Svirin, G.N. Smirenkin, Neutron spectrum in the fission of Th-232, U-235 and U-238 by neutron with energies 2.9 and 14.7 MeV. Yad. Fyz. **53**, 628 (1991)
78. R. Capote, Y.-J. Chen, F.-J. Hambsch, N.V. Kornilov, J.P. Lestone, O. Litaize, B. Morillon, D. Neudecker, S. Oberstedt, T. Ohsawa, N. Otuka, V.G. Pronyaev, A. Saxena, O. Serot, O. Shcherbakov, N.-C. Shu, D.L. Smith, P. Talou, A. Trkov, A.C. Tudora, R. Vogt, A.S. Vorbyev, Prompt fission neutron spectra of actinides. Nucl. Data Sheets **131**, 1 (2016)
79. A. Tudora, Systematic behavior of the average parameters required for the Los Alamos model of prompt neutron emission. Ann. Nucl. Energy **36**, 72 (2009)
80. V. Maslov, Y. Porodzinskij, M. Baba, A. Hasegawa, N. Kornilov, A. Kagalenko, N. Tetereva, Prompt fission neutron spectra of ^{238}u and ^{232}th above emissive fission threshold. Phys. Rev. C **69**, 034607 (2004)
81. C. Sage, V. Semkova, O. Bouland, P. Dessagne, A. Fernandez, F. Gunsing, C. Nästren, G. Noguère, H. Ottmar, A.J.M. Plompen, P. Romain, G. Rudolf, J. Somers, F. Wastin, High resolution measurements of the ^{241}Am(n,2n) reaction cross section. Phys. Rev. C **81**, 064604 (2010)
82. S. Richard, Z. Igor, C.-D. Mireille, M. Emiliano, S. Simone, M. Emanuele, V. Laurence, S. Nadine, G. Nathalie, APOLLO2 Year 2010. Nucl. Eng. Technol. **5**, 474–499 (2010)
83. G. Noguère, O. Bouland, S. Kopecky, C. Lampoudis, P. Schillebeeckx, A. Plompen, F.G.C. Sage, I. Sirakov, Partial-wave analysis of n + ^{241}Am reaction cross sections in the resonance region. Phys. Rev. C **92**, 014607 (2015)
84. G. Noguère, D. Bernard, P. Blaise, O. Bouland, L. Leal, P. Leconte, O. Litaize, Y. Peneliau, B. Roque, A. Santamarina, J.-F. Vidal, Improved mixed oxide fuel calculations with the evaluated nuclear data library JEFF-3.2. Nucl. Sci. Eng. **182**(2), 135 (2016)
85. C. Lampoudis, S. Kopecky, O. Bouland, F. Gunsing, G. Noguère, A.J.M. Plompen, C. Sage, P. Schillebeeckx, R. Wynants, Neutron transmission and capture cross section measurements for ^{241}Am at the GELINA facility. Eur. Phys. J. Plus **128**, 86 (2013)
86. M. Jandel, T. Bredeweg, E. Bond, M. Chadwick, R. Clement, A. Couture, J. O'Donnell, R. Haight, T. Kawano, R. Reifarth, R. Rundberg, J. Ullmann, D. Vieira, J. Wilhelmy, J. Wouters, U. Agvaanluvsan, W. Parker, C. Wu, J. Becker, Neutron capture cross section of ^{241}Am. Phys. Rev. C **78**, 034609 (2008)
87. G. Vanpraet, E. Cornelis, S. Raman, G. Rohr, Neutron capture measurements on 241Am. Radiat. Eff. **93**(1–4), 157–161 (1986)
88. H. Derrien, B. Lucas, The total cross section and the fission cross section of ^{241}Am in the resonance region Resonance parameters, tech. rep., CEA, Cadarache, France. CEA-CONF–3057 (1975)
89. J.W.T. Dabbs, C.H. Johnson, C.E. Bemis Jr., Measurement of the ^{241}Am neutron fission cross section. Nucl. Sci. Eng. **83**(1), 22–36 (1983)
90. B. Becker, K. Kauwenberghs, S. Kopecky, H. Harada, M. Moxon, P. Schillebeeckx, Implementation of an analytical model accounting for sample inhomogeneities in REFIT, Tech. Rep. JRC 86936, ISBN-79-35095-5, JRC Geel, 01 (2013)
91. B. Becker, S. Kopecky, H. Harada, P. Schillebeeckx, Measurement of the direct particle transport through stochastic media using neutron resonance transmission analysis. Eur. Phys. J. Plus **129**, 58 (2014)
92. C. Porter, R. Thomas, Fluctuations of nuclear reaction widths. Phys. Rev. **104**, 483–491 (1956)
93. T.W. Phillips, R.E. Howe, Total neutron cross section for Americium-241. Nucl. Sci. Eng. **69**(3), 375–377 (1979)
94. D.B. Gayther, B.W. Thomas, in *Proceedings of the IV National Soviets Conference on Neutron Physics, III, 3*, (Kiev, 1977)
95. E.S. Soukhovitskii, R. Capote, J.M. Quesada, S. Chiba, Dispersive coupled-channel analysis of nucleon scattering from ^{232}Th up to 200 MeV. Phys. Rev. C **72**, 024604 (2005)
96. P. Talou, T. Kawano, P.G. Young, M.B. Chadwick, R.E. MacFarlane, Improved evaluations of neutron-induced reactions on Americium isotopes. Nucl. Sci. Eng. **155**(1), 84–95 (2007)
97. C. De Saint Jean, G. Noguère, B. Habert, B. Iooss, A Monte Carlo approach to nuclear model parameter uncertainties propagation. Nucl. Sci. Eng. **161**, 363 (2009)
98. G. Noguère, J.-C. Sublet, A nuclear data oriented interface code for processing applications. Ann. Nucl. Energy **35**(12), 2259–2269 (2008)
99. H. Kim, C. Gil, Y. Lee, Simultaneous evaluation of fission cross sections for Cm isotopes. Eur. Phys. J. Web Conf. **2**, 14004 (2010)
100. H. Kim, C. Gil, Y. Lee, Evaluation of neutron cross section with uncertainties for complete Cm isotopic family. J. Korean Phys. Soc. **59**, 839 (2011)
101. K. Shibata, O. Iwamoto, T. Nakagawa, N. Iwamoto, A. Ichihara, S. Kunieda, S. Chiba, K. Furutaka, N. Otuka, T. Ohsawa, T. Murata, H. Matsunobu, A. Zukeran, S. Kamada, J. Katakura, JENDL-4.0: a new library for nuclear science and engineering. J. Nucl. Sci. Technol. **48**, 1 (2011)
102. M. Herman, R. Capote, B. Carlson, P. Obložinský, M. Sin, A. Trkov, H. Wienke, V. Zerkin, Empire: nuclear reaction model code system for data evaluation. Nucl. Data Sheets **108**, 2655 (2007)
103. H. Kim, M. Herman, S. Mughabghab, P. Oblozinsky, D. Rochman, Y. Lee, Evaluation of Neutron Cross Sections for a Complete Set of Nd Isotopes. Report BNL-77775-2007-IR Brookhaven National Laboratory, NY, USA, KAERI/TR-3354-2007, KAERI, Korea (2007)
104. R. Capote, S. Chiba, E. Soukhovitskii, J. Quesada, E. Bauge, A global dispersive coupled-channel optical model potential for actinides. J. Nucl. Sci. Technol. **45**, 333 (2008)
105. V. Plujko, S. Ezhov, M. Kavatsyuk, A. Grebenyuk, R. Yermolenko, Testing and improvements of Gamma-ray strength functions for nuclear model calculations. J. Nucl. Sci. Technol. **39**, 811 (2002)
106. H. Fernández Gianotti, Fast-neutron cross sections for curium-244. Nucl. Sci. Eng. **65**, 164 (1978)
107. B. Fursov et al., Fast neutron induced fission cross sections of some minor actinides. in *Proceedings of the International Conference on Nuclear Data for Science and Technology* vol. 1, ed. by G. Reffo, A. Ventura, C. Grandi, (Trieste, Italy), p. 488, Editrice Compositori, 40128 Bologna, Italy, May 19–24 (1997)
108. E. Fomushkin, G. Novoselov, V. Gavrilov, Y. Vinogradov, Measurements of highly active isotope fission cross-sections with nuclear explosion neutrons, in *Proceedings of International Conference for Nuclear Data for Science and Technology*, (Juelich, Germany, 1991), p. 439
109. E. Fomushkin, G. Novoselov, Y. Vinogradov, V. Vyachin, V. Gavrilov, V. Zherebcon, A. Koshelev, V. Polynov, V. Surin, A. Shvetsov, Fission cross-section of ^{243}Cm and ^{247}Cm by fast neutrons. At. Energy **62**, 278 (1987)
110. E. Fomushkin, G. Novoselov, Y. Vinogradov, V. Gavrilov, B. Maslennikov, Y. Odintsov, Measurements of the energy dependence fo the cross sections of ^{245}Cm fission by fast neutrons. At. Energy **63**, 242 (1987)
111. M. Moore, G. Keyworth, Analysis of the fission and capture cross sections of the Curium isotopes. Phys. Rev. C **3**, 1656 (1971)

112. H. Maguire Jr., C. Stopa, R. Block, D. Harris, R. Slovacek, J. Dabbs, R. Dougan, R. Hoff, R. Lougheed, Neutron-induced fission cross-section measurements of ^{244}Cm, ^{246}Cm, and ^{248}Cm. Nucl. Sci. Eng. **89**, 293 (1985)
113. I. Ivanin, Y. Khoklov, V. Inkov, Y. Vinogradov, E. Fomushin, L. Danli, V. Polynov, Measurements of fission cross sections for curium isotopes, in *Proceedings of the International Conference on Nuclear Data for Science and Technology*, vol. 1 ed. by G. Reffo, A. Ventura, C. Grandi (Trieste, Italy), p. 488, Editrice Compositori, 40128 Bologna, Italy, May 19–24 (1997)
114. P. Vorotnikov, S. Dmitriev, Y. Molchanov, G. Otroshchenko, V. Pchelin, L. Chistyakov, A.N. Smirnov, Cross section measurements for fission of ^{242}Cm induced by neutrons with energies of 0.1-1.4 MeV performed with nanogram amounts of substance. Yad. Fyz. **40**, 1141 (1984)
115. B. Alam, R. Block, R. Slovacek, R. Hoff, Measurement of the neutron-induced fission cross sections of ^{242}Cm and ^{238}Pu. Nucl. Sci. Eng. **99**, 267 (1988)
116. M. Silbert, Fission cross section of ^{243}Cm. Report LA-6239-MS, Los Alamos Scientific Laboratory, NM, USA (1976)
117. R. Fullwood, D. Dixon, R. Lougheed, Fission cross sections from Pommard. Report LA-4420, Los Alamos Scientific Laboratory, NM, USA (1970)
118. Y. Danon, R. Slovacek, R. Block, R. Lougheed, R. Hoff, M. Moore, Fission cross-section measurements of ^{247}Cm, ^{254}Es, and ^{250}Cf from 0.1 eV to 80 keV. Nucl. Sci. Eng. **109**, 341 (1991)
119. R. White, J. Browne, Neutron induced fission cross section measurements and calculations of selected transplutonic isotopes. in *Proceedings of the International Conference on Nuclear Data for Science and Technology* ed. by K. Böckhoff (Antwerp, Belgium, 1982), p. 218
120. R. Capote, L. Leal, P. Liu, T. Liu, P. Schillebeeckx, M. Sin, I. Sirakov, A. Trkov, Evaluated nuclear data for nuclides within the thorium–uranium fuel cycle. Vienna, International Atomic Energy Agency, Report STC/PUB/1435, www.iaea.org/books (2010)
121. M.B. Chadwick, M. Herman, P. Obložinský, M.E. Dunn, Y. Danon, A.C. Kahler, D.L. Smith, B. Pritychenko, G. Arbanas, R. Arcilla, R. Brewer, D.A. Brown, R. Capote, A.D. Carlson, Y.S. Cho, H. Derrien, K. Guber, G.M. Hale, S. Hoblit, S. Holloway, T.D. Johnson, T. Kawano, B.C. Kiedrowski, H. Kim, S. Kunieda, N.M. Larson, L. Leal, J.P. Lestone, R.C. Little, E.A. McCutchan, R.E. MacFarlane, M. MacInnes, C.M. Mattoon, R.D. McKnight, S.F. Mughabghab, G.P.A. Nobre, G. Palmiotti, A. Palumbo, M.T. Pigni, V.G. Pronyaev, R.O. Sayer, A.A. Sonzogni, N.C. Summers, P. Talou, I.J. Thompson, A. Trkov, R.L. Vogt, S.C. van der Marck, A. Wallner, M.C. White, D. Wiarda, P.G. Young, ENDF/B-VII.1 nuclear data for science and technology: cross sections, covariances, fission product yields and decay data. Nucl. Data Sheets **112**, 2887 (2011)
122. K. Shibata, T. Kawano, T. Nakagawa, O. Iwamoto, J. Katakura, T. Fukahori, S. Chiba, A. Hasegawa, T. Murata, H. Matsunobu, T. Ohsawa, Y. Nakajima, T. Yoshida, A. Zukeran, M. Kawai, M. Baba, M. Ishikawa, T. Asami, T. Watanabe, Y. Watanabe, M. Igashira, N. Yamamuro, H. Kitazawa, N. Yamano, H. Takano, Japanese evaluated nuclear data library version 3 revision-3: JENDL-3.3. J. Nucl. Sci. Technol. **39**, 1125 (2002)
123. G. Rudstam, P. Finck, A. Filip, A. D'Angelo et al., Delayed Neutron Data for the Major Actinides. A report by the Working Party on International Evaluation Co-operation of the OECD NEA Nuclear Science Committee, vol. 6 (2002)
124. V. Piksaikin et al., Energy dependence of relative abundances and periods of delayed neutrons from neutron-induced fission of ^{235}U, ^{238}U and ^{239}Pu in 6- and 8-group model representation. Progr. Nucl. Energy **41**(1–4), 203–222 (2002)
125. D. Foligno, P. Leconte, Uncertainty and covariances of the newly derived 8-groups delayed-neutrons abundances set. EPJ Nucl. Sci. Technol. **4**, 31 (2018)
126. G. R. Keepin, T. F. Wimett, R. K. Zeigler, Delayed neutros from fissionable isotopes of uranium, plutonium, and thorium. Phys. Rev. **107**, 1044 (1957)
127. A. Zoia, C. Jouanne, P. Siréta, P. Leconte, G. Braoudakis, L. Wong, Analysis of dynamic reactivity by Monte Carlo methods: the impact of nuclear data. Ann. Nucl. Energy **110**, 11–24 (2017)
128. M. Brady, T. England, Delayed neutron data and group parameters for 43 fissioning systems. Nucl. Sci. Eng. **103**, 129–149 (1989)
129. M.B. Chadwick, P. Obložinský, M. Herman, N.M. Greene, R.D. McKnight, D.L. Smith, P.G. Young, R.E. MacFarlane, G.M. Hale, S.C. Frankle, A.C. Kahler, T. Kawano, R.C. Little, D.G. Madland, P. Moller, R.D. Mosteller, P.R. Page, P. Talou, H. Trellue, M.C. White, W.B. Wilson, R. Arcilla, C.L. Dunford, S.F. Mughabghab, B. Pritychenko, D. Rochman, A.A. Sonzogni, C.R. Lubitz, T.H. Trumbull, J.P. Weinman, D.A. Br, D.E. Cullen, D.P. Heinrichs, D.P. McNabb, H. Derrien, M.E. Dunn, N.M. Larson, L.C. Leal, A.D. Carlson, R.C. Block, J.B. Briggs, E.T. Cheng, H.C. Huria, M.L. Zerkle, K.S. Kozier, A. Courcelle, V. Pronyaev, S.C. van der Marck, ENDF/B-VII.0: next generation evaluated nuclear data library for nuclear science and technology. Nucl. Data Sheets **107**, 2931 (2006)
130. A. Trkov, R. Capote, E. Soukhovitskii, L. Leal, M. Sin, I. Kodeli, D. Muir, Covariances of evaluated nuclear cross section data for 232Th, 180,182,183,184,186W and 55Mn. Nucl. Data Sheets **112**, 3098 (2011)
131. V. McLane, ENDF-201, ENDF/B-VI summary documentation supplement I, ENDF/HE-VI Summary documentation. BNL-NCS-17541, [ENDF-201], 4th edn., [ENDF/B-VI Supplement, National Nuclear Data Center, Brookhaven National Laboratory, Upton, New York 11973-5000 (1996)
132. B. Morillon, R. Lazauskas, J. Carbonell, Influence of the ab initio n-d cross sections in the critical heavy-water benchmarks. Ann. Nucl. Energy **54**, 167 (2013)
133. R. Malfliet, J. Tjon, Three nucleon calculations with local tensor forces. Phys. Lett. B **30**, 293 (1969)
134. P. Doleschall, I. Borbély, Z. Papp, W. Plessas, Nonlocality in the nucleon–nucleon interaction and three-nucleon bound states. Phys. Rev. C **67**, 064005 (2003)
135. R. Lazauskas, J. Carbonell, Three-neutron resonance trajectories for realistic interaction models. Phys. Rev. C **71**, 044004 (2005)
136. W. Dilg, L. Koester, W. Nistler, The neutron–deuteron scattering lenghts. Phys. Lett. B **36**, 208 (1971)
137. L.A. Rayburn, E.O. Wollan, Total neutron cross sections at 1.44 eV. Nucl. Phys. **61**, 381 (1965)
138. E. Fermi, L. Marshall, Spin dependence of slow neutron scattering by deuterons. Phys. Rev. **75**, 578 (1949)
139. L.J. Rainwater, W.W. Havens Jr., J.R. Dunning, C.S. Wu, Slow neutron velocity spectrometer studies of H, D, F, Mg, S, Si, and quartz. Phys. Rev. **73**, 733 (1948)
140. H.B. Hanstein, Interaction experiments with resonance neutrons. Phys. Rev. **59**, 489 (1941)
141. P. Stoler, N.N. Kaushal, F. Green, E. Harms, L. Laroze, Total neutron cross section of deuterium below 1000 keV. Phys. Rev. Lett. **29**, 1745 (1972)
142. P. Stoler, N.N. Kaushal, F. Green, Total cross section of neutrons on deuterium in the keV region. Phys. Rev. C **8**, 1539 (1973)
143. T. Phillips, B. Berman, J. Seagrave, Total neutron cross section for tritium. Phys. Rev. C **22**, 384 (1980)
144. J.M. Clement, P. Stoler, C.A. Goulding, R.W. Fairchild, Hydrogen and deuterium total neutron cross sections in the MeV region. Nucl. Phys. A **183**, 51 (1972)
145. J. Davis, H. Barschall, Fast neutron total cross section of deuterium. Phys. Rev. C **3**, 1798 (1971)

146. H.B. Willard, J.K. Bair, C.M. Jones, n-d scattering: a search for effects due to the dineutron. Phys. Lett. **9**, 339 (1964)
147. A. Bratenahl, J. Peterson, J. Stoering, Neutron total cross sections in the 7 to 14-MeV region. Phys. Rev. **110**, 927 (1958)
148. J.M. Peterson, A. Bratenahl, J.P. Stoering, Neutron total cross sections in the 17- to 29-mev region. Phys. Rev. **120**, 521 (1960)
149. W.P. Abfalterer, F.B. Bateman, F.S. Dietrich, R.W. Finlay, R.C. Haight, G.L. Morgan, Measurement of neutron total cross sections up to 560 MeV. Phys. Rev. C **63**, 044608 (2001)
150. R. Riddle, A. Langsford, P. Bowen, G. Cox, The neutron–neutron and neutron–deuterium total cross section in the energy range 15–120 MeV. Nucl. Phys. **61**, 457 (1965)
151. P. Schwarz, H.O. Klages, P. Doll, B. Haesner, J. Wilczynski, B. Zeitnitz, Elastic neutron–deuteron scattering in the energy range from 2.5 mev to 30 mev. Nucl. Phys. A **398**, 1 (1983)
152. E. Pirovano, R. Beyer, A.R. Junghans, N. Nankov, R. Nolte, M. Nyman, A. Plompen, Backward–forward reaction asymmetry of neutron elastic scattering on deuterium. Phys. Rev. C **95**, 024601 (2017)
153. P. Archier, G. Noguère, C. De Saint Jean, A. Plompen, C. Rouki, New JEFF-3.2 sodium neutron induced cross-sections evaluation for neutron fast reactors applications: from 0 to 20 MeV. Nucl. Data Sheets **118**, 140 (2014)
154. C. De Saint Jean, B. Habert, O. Litaize, G. Noguère, C. Suteau, Status of CONRAD, a nuclear reaction analysis tool. EDP Sci. **1**, 251–254 (2008)
155. J. Raynal, Notes on ECIS94, Tech. Rep. CEA-N-2772, Commissariat à l'Énergie Atomique, Saclay, France (1994)
156. F. Rahn, H.S. Camarda, G. Hacken, W.W. Havens, H.I. Liou, J. Rainwater, U.N. Singh, M. Slagowitz, S. Wynchank, Neutron resonance spectroscopy. XIII. Na to 320 keV. Phys. Rev. C **8**, 1827–1832 (1973)
157. D. Larson, J. Harvey, N. Hill, Measurement of the Neutron Total Cross Section of Sodium from 32 keV to 37 MeV. Tech. Rep. ORNL-TM-5614, Oak Ridge National Laboratory (1976)
158. C. Rouki, P. Archier, C. Borcea, C. De Saint Jean, J. Drohé, S. Kopecky, A. Moens, N. Nankov, A. Negret, G. Noguére, A. Plompen, M. Stanoiu, High resolution measurement of neutron inelastic scattering cross-sections for ^{23}Na. Nucl. Instrum. Methods Phys. Res. A **672**, 82 (2012)
159. B. Morillon, P. Romain, Bound single-particle states and scattering of nucleons on spherical nuclei with a global optical model. Phys. Rev. C **76**, 044601 (2007)
160. P. Pereslavtsev, A. Konobeyev, L. Leal, U. Fischer, Evaluation of ^{50}Cr, ^{52}Cr, ^{53}Cr, ^{54}Cr neutron cross section data for energies up to 200 MeV. J. Korean Phys. Soc. **59**, 931 (2011)
161. L. Leal, H. Derrien, K. Guber, G. Arbanas, D. Wiarda, Evaluation of the chromium resonance parameters including resonance parameter covariance. J. Korean Phys. Soc. **59**, 1644 (2011)
162. A.Y. Konobeyev, U. Fischer, A.J. Koning, P.E. Pereslavtsev, M. Blann, Implementation of the geometry dependent hybrid model in TALYS. J. Korean Phys. Soc. **59**, 935 (2011)
163. M. Bormann, A. Behrend, I. Riehle, O. Vogel, Measurement of (n,2n) excitation functions. Nucl. Phys. A **115**, 309 (1968)
164. Y. Ikeda, C. Konno, K. Oishi, T. Nakamura, H. Miyade, K. Kawade, H. Yamamoto, T. Katoh, Activation cross section measurements for fusion reactor structural materials at energies from 13.3 to 15.0 MeV using FNS facility. JAERI report 1312, Tokai-mura, Japan (1988)
165. H. Liskien, M. Uhl, M. Wagner, G. Winkler, The excitation function for the reaction ^{52}Cr(n,2n)^{51}Cr. Private communication, EXFOR nr. 22124 [179] (1989)
166. M. Wagner, G. Winkler, H. Vonach, C. Buczko, J. Csikai, Measurement of the cross sections for the reactions ^{52}Cr(n,2n)^{51}Cr, ^{66}Zn(n,2n)Zn^{65}, ^{89}Y(n,2n)^{88}Y and ^{96}Zr(n,2n)^{95}Zr from 13.5 to 14.8 MeV. Ann. Nucl. Energy **16**, 623 (1989)
167. S. Iwasaki, T. Win, S. Matsuyama, N. Odano, Measurement of (n,2n) cross-sections for Sc, Mn,Cr and In between 12 and 19 MeV with activation technique. Proceedings of the 1996 Symposium on Nuclear Data, Nov. 21–22, JAERI, Tokai (1996)
168. Y. Uno, Y. Uwamino, T. Soewarsono, T. Nakamura, Measurement of neutron activation cross sections of ^{12}C, ^{30}Si, ^{47}Ti, ^{48}Ti, ^{52}Cr, ^{59}Co and ^{58}Ni between 15 and 40 MeV. Nucl. Sci. Eng. **122**, 247 (1996)
169. N.I. Molla, R.U. Miah, S. Basunia, S.M. Hossain, M. Rahman, Excitation Functions of (n,p), (n,α) and (n,2n) processes on some Isotopes of Cl, Cr, Ge, Mo, and Ce in the energy range 13.57 MeV – 14.71 MeV, May 19–24 (1997)
170. A. Fessler, E. Wattecamps, D.L. Smith, S.M. Qaim, Excitation functions of $(n, 2n)$, (n, p), $(n, np+pn+d)$, and (n, α) reactions on isotopes of chromium. Phys. Rev. C **58**(2), 996 (1998)
171. F.-Q. Zhou, Y.-L. Yi, F. Tuo, X.-X. Cao, X.-Z. Kong, Measurement of cross sections for ^{50}Cr(n,2n)^{49}Cr and ^{52}Cr(n,2n)^{51}Cr reactions induced by 13.5-14.6 MeV neutrons. Phys. Energy Fort. Nucl. **29**, 644 (2005)
172. W. Mannhart, D. Schmidt, Measurement of neutron activation cross sections in the energy range from 8 MeV to 15 MeV. Report PTB-N-53 of the Physikalisch-Technischen Bundesanstalt, Braunschweig, Germany (2007)
173. D. Smith, J. Meadows, Cross section measurement for the ^{52}Cr(n, p)^{52}V reaction near threshold. Nucl. Sci. Eng. **76**, 43 (1980)
174. S. Ghorai, J. Williams, W. Alford, The (n,2n) excitation function for ^{50}Cr and the (n,2n) and (n, p) excitation functions for ^{52}Cr. J. Phys. G **13**, 405 (1987)
175. M. Viennot, M. Berrada, G. Paic, S. Joly, Cross section measurements of (n, p) and (n, np+pn+d) reactions for some titanium, chromium, iron, cobalt, nickel and zinc isotopes around 14 MeV. Nucl. Sci. Eng. **108**, 289 (1991)
176. Y. Kasugai, H. Yamamoto, K. Kawade, T. Iida, Measurement of (n, p) cross sections for shortlived products by 13.4-14.9 MeV neutrons. Ann. Nucl. Energy **25**, 23–45 (1998)
177. L. Mihailescu, C. Borcea, A. Koning, A. Plompen, High resolution measurement of neutron inelastic scattering and (n,2n) cross-sections for ^{52}Cr. Nucl. Phys. A **786**, 1 (2007)
178. A. Negret, L.C. Mihailescu, C. Borcea, P. Dessagne, K.H. Guber, M. Kerveno, A.J. Koning, A. Olacel, A.J.M. Plompen, C. Rouki, G. Rudolf, Cross section measurements for neutron inelastic scattering and the (n, 2nγ) reaction on ^{206}Pb. Phys. Rev. C **91**, 064618 (2015)
179. N. Otuka, R. Capote, V. Semkova, T. Kawai, G. Noguère, Experiments in the EXFOR library for evaluation of thermal neutron constants. EPJ Web Conf. **146**, 07005 (2017)
180. D. Brown, M. Chadwick, R. Capote, A. Kahler et al., ENDF/B-VIII.0: the 8th major release of the nuclear reaction data library with CIELO-project cross sections, new standards and thermal scattering data. Nucl. Data Sheets **148**, 1 (2018)
181. C. Vaglio-Gaudard, A. Santamarina, D. Bernard, G. Nogueère, J. Ruggieri, J. Vidal, A. Lyoussi, New ^{56}Fe covariances for the JEFF3 file from the feedback of integral benchmark analysis. Nucl. Sci. Eng. **166**, 267 (2010)
182. R. Beyer, R. Schwengner, R. Hannaske, A. Junghans, R. Massarczyk, M. Anders, D. Bemmerer, A. Ferrari, A. Hartmann, T. Kögler, M. Röder, K. Schmidt, A. Wagner, Inelastic scattering of fast neutrons from excited states in ^{56}Fe. Nucl. Phys. A **927**, 41 (2012)
183. A. Negret, C. Borcea, P. Dessagne, M. Kerveno, A. Olacel, A. Plompen, M. Stanoiu, Cross-section measurements for the ^{56}Fe(n, xnγ) reactions. Phys. Rev. C **90**, 034602 (2014)
184. A. Negret, M. Sin, C. Borcea, R. Capote, P. Dessagne, M. Kerveno, N. Nankov, A. Olacel, A. Plompen, C. Rouki, Cross-section

measurements for the ^{57}Fe(n, nγ)^{57}Fe and ^{57}Fe(n,2nγ)^{56}Fe reactions. Phys. Rev. C **96**, 024620 (2017)
185. A. Olacel, C. Borcea, M. Boromiza, P. Dessagne, G. Henning, M. Kerveno, L. Leal, A. Negret, M. Nyman, A. Plompen, Neutron inelastic scattering on ^{54}Fe. Eur. Phys. J. A **54**, 183 (2018)
186. E. Pirovano, R. Beyer, M. Dietz, A. Junghans, S. Müller, R. Nolte, M. Nyman, A. Plompen, M. Röder, T. Szücs, M. Takacs, Cross section and neutron angular distribution measurements of neutron scattering on natural iron. Phys. Rev. C **99**, 024601 (2019)
187. F. Garner, Radiation damage in austenitic steels. Compr. Nucl. Mater. **4**, 33–95 (2012)
188. H. Gruppelaar et al., Evaluation of neutron cross sections and photon-production data for Ni-isotopes in the energy range 0–20 MeV, tech. rep., ECN (1990)
189. A. Koning, D. Rochman, Towards sustainable nuclear energy: putting nuclear physics to work. Ann. Nucl. Energy **35**(11), 2024–2030 (2008)
190. P. Helgesson, H. Sjöstrand, D. Rochman, Uncertainty-driven nuclear data evaluation including thermal (n,α) applied to ^{59}Ni. Nucl. Data Sheets **145**, 1–24 (2017)
191. P. Helgesson, D. Rochman, H. Sjöstrand, E. Alhassan, A. Koning, UO_2 vs MOX: propagated nuclear data uncertainty for k_{eff}, with burnup. Nucl. Sci. Eng. **177**, 321–336 (2014)
192. J. Harvey, J. Halperin, N. Hill, S. Raman, R. Macklin, (n, alpha),(n, p),(n, gamma), and total neutron-cross- section measurements on ^{59}Ni. Bull. Am. Phys. Soc. **21**, 536 (1976)
193. J. Harvey, J. Halperin, N. Hill, S. Raman, R. Macklin, (n, alpha),(n, p),(n, gamma), and total neutron-cross- section measurements on ^{59}Ni. Bull. Am. Phys. Soc. **20**, 1195 (1975)
194. J. Harvey, J. Halperin, N. Hill, S. Raman, R. Macklin, in *Proceedings of International Conference Interactions of Neutrons with Nuclei, 6–9 July 1976*, EXFOR entry 10680 [179] ed. by E. Sheldon (Lowell, Massachussets, 1976), p. 143
195. H. Tsuchiya, H. Harada, M. Koizumi, F. Kitatani, J. Takamine, M. Kureta, H. Iimura, A. Kimura, B. Becker, S. Kopecky, K. Kauwenberghs, W. Mondelaers, P. Schillebeeckx, Impact of systematic effects on results of neutron resonance transmission analysis. Nucl. Instrum. Methods Phys. Res. Sect. A Accel. Spectrom. Detect. Assoc. Equip. **767**, 364–371 (2014)
196. H. Weigmann, J. Winter, Neutron radiative capture in Cu. Zeitschrift für Physik A Hadrons and nuclei **213**, 411–419 (1968)
197. F. Ma, C. Paradela, G. Alaerts, H. Harada, J. Heyse, F. Kitatani, S. Kopecky, P. Schillebeeckx, H. Tsuchiya, R. Wynants, Experimental verification of an analytical transmission expression for homogeneous samples not fulfilling good transmission geometry conditions (2019) (**to be published**)
198. V. Sobes, L. Leal, K. Guber, B. Forget, S. Kopecky, P. Schillebeeckx, P. Siegler, New resolved resonance region evaluation for ^{63,65}Cu for nuclear criticality safety program. Nucl. Data Sheets **118**, 155 (2014)
199. P. Pereslavtsev, L. Leal, A. Konobeyev, U. Fischer, New evaluations of n + Cu and n + Zr cross-section data for neutron energies up to 200 MeV. Eur. Phys. J. Web Conf. **146**, 02039 (2017)
200. W. Dilg, W. Schantl, H. Vonach, M. Uhl, Level density parameters for the back-shifted Fermi gas model in the mass range 40<A<250. Nucl. Phys. A **217**, 269 (1973)
201. H. An, C. Cai, Global deuteron optical model potential for the energy range up to 183 MeV. Phys. Rev. C **73**, 054605 (2006)
202. V. Avrigeanu, P.E. Hodgson, M. Avrigeanu, Global optical potentials for emitted alpha particles. Phys. Rev. C **49**, 2136 (1994)
203. P. Pereslavtsev, U. Fischer, A.Y. Konobeyev, L. Leal, V. Soves, New evaluation of n+Cu-63,65 nuclear cross section data up to 200 MeV neutron energy. Nucl. Data Sheets **118**, 158 (2014)
204. K. Takamiya, Y. Ota, M. Akamine, S. Shibata, T. Shibata, Y. Ito, M. Imamura, Y. Uwamino, N. Nogawa, M. Baba, S. Iwasaki, S. Matsuyama, Excitation function for ^{63}Cu(n,p)^{63}Ni reaction in neutron energy range up to 15 MeV. Appl. Radiat. Isot. **66**(10), 1321–1324 (2008)
205. A. Trkov, P. Griffin, S. Simakov, L. Greenwood, K. Zolotarev, R. Capote, D. Aldama, V. Chechev, C. Destouches, A. Kahler, C. Konno, M. Kostal, M. Majerle, E. Malambu, M. Ohta, V. Pronyaev, V. Radulovic, S. Sato, M. Schulc, E. Simeckova, I. Vavtar, J. Wagemans, M. White, H. Yashima, IRDFF-II: a new neutron metrology library. Nucl. Data Sheets **163**, 1 (2020)
206. K. Volev, A. Borella, S. Kopecky, C. Lampoudis, C. Massimi, A. Moens, M. Moxon, P. Schillebeeckx, P. Siegler, I. Sirakov, A. Trkov, R. Wynants, Evaluation of resonance parameters for neutron induced reactions in cadmium. Nucl. Instrum. Methods Phys. Res. Sect. B Beam Interact. Mater. Atoms **300**, 11–29 (2013)
207. I. Sirakov, S. Kopecky, C. Massimi, M. Moxon, V. Pronyaev, P. Schillebeeckx, A. Trkov, K. Volev, R. Wynants, ENDF-6 compatible evaluation of neutron induced reaction cross sections for ^{106,108,110,111,112,113,114,116}Cd. JRC Scientific and Policy Reports, Report EUR 25800 EN (2013)
208. C. Dean, T. Ware, D. Weaver, M. Moxon, R. Hiles, P. Schillebeeckx, S. Kopecky, Evaluation of neutron cross sections for hafnium in the resolved resonance range. J. Korean Phys. Soc. **59**, 1884 (2011)
209. G. Noguère, E. Rich, C. De Saint Jean, O. Litaize, P. Siegler, V. Avrigeanu, Average neutron parameters for hafnium. Nucl. Phys. A **831**(1), 106–136 (2009)
210. G. Noguère, P. Blaise, O. Litaize, D. Bernard, J.-M. Ruggieri, Group-average covariance matrices for the hafnium isotopes of interest for light water reactor applications. Ann. Nucl. Energy **36**(8), 1059–1069 (2009)
211. M.J. Trbovich, D.P. Barry, R.E. Slovacek, Y. Danon, R.C. Block, N.C. Francis, M. Lubert, J.A. Burke, N.J. Drindak, G. Leinweber, R. Ballad, Hafnium resonance parameter analysis using neutron capture and transmission experiments. Nucl. Sci. Eng. **161**(3), 303–320 (2009)
212. T. Ware, *Measurement and analysis of the resolved resonance cross sections of the natural hafnium isotopes*. Ph.D. thesis, University of Birmingham (2010). http://etheses.bham.ac.uk/807/
213. P. Siegler, K. Dietze, P. Ribon, Testing of neutron data by comparison of measured and calculated average transmissions. J. Nucl. Sci. Technol. **39**(sup2), 936–939 (2002)
214. M. Moxon, D. Endacott, T. Haste, J. Jolly, J. Lynn, M. Sowerby, Differential neutron cross-sections of natural hafnium and its isotopes for neutron energies up to 30 keV, Tech. Rep. Harwell Report AERE-R 7864, UKAEA, Harwell, UK (1974)
215. B. Habert, C. De Saint Jean, G. Noguère, L. Leal, Y. Rugama, Retroactive generation of covariance matrix of nuclear model parameters using marginalization techniques. Nucl. Sci. Eng. **166**(3), 276–287 (2010)
216. B. Morillon, P. Romain, Dispersive and global spherical optical model with a local energy approximation for the scattering of neutrons by nuclei from 1 keV to 200 MeV. Phys. Rev. C **70**, 014601 (2004)
217. B. Morillon, P. Romain, Bound single-particle states for neutrons from a global spherical optical model. Phys. Rev. C **74**, 014601 (2006)
218. V. Avrigeanu, S. Chuvaev, R. Eichin, A. Filatenkov, R. Forrest, H. Freiesleben, M. Herman, A. Koning, K. Seidel, Pre-equilibrium reactions on the stable tungsten isotopes at low energy. Nucl. Phys. A **765**, 1 (2006)
219. E. Rich, A. Tudora, G. Noguère, J. Tommasi, J.-F. Lebrat, Modeling of the n + ^{242}Pu reactions for fast reactor applications. Nucl. Sci. Eng. **162**(2), 178–191 (2009)
220. J. Palau, Correlations entre donnees nucleaires et experiences integrales a plaques: le cas du Hafnium, Tech. Rep. Report CEA-R-5843, CEA-DEN Cadarache (1999)

221. P. Blaise, J.-F. Vidal, A. Santamarina, Validation of the REL2005 code package on Gd-poisoned PWR type assemblies through the CAMELEON experimental program, in *Proceedings of 2009 International Congress on Advances in Nuclear Power Plants*, (Japan, 2009), p. 2572
222. C. Vaglio-Gaudard, O. Leray, M. Lemaire, A. Colombier, J. Hudelot, First feedback with the AMMON integral experiment for the JHR calculations. EPJ Web Conf. **42**, 05001 (2013)
223. S.K. Mukherjee, H. Bakhru, Some (n,alpha) reaction cross-sections and the resulting radio-isotopes. Nucl. Solid State Phys. A Symp, Bombay (1963), p. 244
224. L. Veeser, E. Arthur, P. Young, Cross sections for (n,2n) and (n,3n) reactions above 14 MeV. Phys. Rev. C **16**(5), 1792 (1977)
225. J. Fréhaut, A. Bertin, R. Bois, J. Jary, Status of (n,2n) cross section measurements at Bruyères-le-Châtel, in *Symposium on Neutron Cross Sections from 10-50 MeV, BNL-NNDC, May 12–14*, (Upton, 1980)
226. S. Simakov, G. Lovchikova, O. Salnikov, G. Kotelnikova, A. Trufanov, Elastic and inelastic scattering of the neutrons with the energies from 5 to 8 MeV on bismuth and tantalum. Yad. Konst. **49**, 17 (1982)
227. A. Takahashi, E. Ichimura, Y. Sasaki, H. Sugimoto, Double and single differential neutron emission cross sections at 14.1 mev. vol. 1. Osaka University Report OKTAVIAN A-87-03 (1987)
228. R. Wölfle, A. Mannan, S.M. Qaim, H. Liskien, R. Widera, Excitation Functions of ^{93}Nb(n,2n)^{92m}Nb, ^{93}Nb(n, α)^{90m,g}Y, ^{139}La(n, α)^{136}Cs and ^{181}Ta(n, p)^{181}Hf Reactions in the Energy Range of 12.5-19.6 MeV. Appl. Radiat. Isot. **39**(5), 407–412 (1988)
229. H.-L. Lu, D.-H. Wang, Y.-J. Xiu, Y.-F. Cui, P.-L. Chen, IAEA Report INDC(CPR)-16, Vienna (1989)
230. X. Kong, Y. Wang, J. Yang, J. Yuan, X. Wang, Cross section measurements for ^{98}Mo(n, α)^{95}Zr, ^{95}Mo(n,p)^{95m}Nb, ^{95}Mo(n,p)^{95g}Nb and ^{181}Ta(n,p)^{181}Hf reaction. Chin. J. Nucl. Phys. **14**, 239 (1992)
231. S.P. Simakov, G.N. Lovchikova, V.P. Lunev, V.G. Pronyaev, N.N. Titarenko, A.M. Trufanov, Neutron inelastic scattering at 5–8.5 MeV for ^{59}Co, ^{89}Y, ^{93}Nb, ^{93}Mo, ^{115}In, ^{181}Ta and ^{209}Bi Nuclei. Yad. Konst. **4**, 74 (1992)
232. Y. Kasugai, M. Asai, A. Tanaka, H. Yamamoto, I. Jun, T. Iida, K. Kawade, Measurement of activation cross sections on tantalum and tungsten with 14 MeV neutrons. J. Nucl. Sci. Technol. **31**(12), 1248 (1994)
233. A. Majdeddin, V. Semkova, R. Doczi, C. Buczko, J. Csikai, Investigations on (n,α) cross sections in the 14 MeV region. INDC report INDC(HUN)-031, IAEA, Vienna, Austria (1997)
234. S. Begun, I. Kadenko, V. Maidanyuk, V. Neplyuev, G. Primenko, V. Tarankanov, Determination of the cross section of (n, x) nuclear reactions on Y, La, Ta, Pb and Bi at the energy of neutrons about 14 MeV. J. Nucl. Sci. Technol. **S2**, 425 (2002)
235. A.A. Filatenkov, S.V. Chuvaev, Measurement of a set of badly known neutron induced cross sections. Khlopin Radium Institute Report RI-258, St Petersburg (2001)
236. P. Young, E. Arther, M. Chadwick, Comprehensive nuclear model calculations: introduction to the theory and use of the GNASH code. Report LA-12343-MS, Los Alamos National Laboratory, NM, USA (1992)
237. A.J. Koning, J.P. Delaroche, Local and global nucleon optical models from 1 keV to 200 MeV. Nucl. Phys. A **713**, 231 (2003)
238. J. Bojowald, H. Machner, H. Nann, W. Oelert, M. Rogge, P. Turek, Elastic deuteron scattering and optical model parameters at energies up to 100 MeV. Phys. Rev. C **38**, 1153 (1988)
239. S. Watanabe, High energy scattering of deuterons by complex nuclei. Nucl. Phys. **8**, 484 (1958)
240. F. Becchetti, G. Greenlees, in *Polarization phenomena in Nuclear Reactions* ed. by H.H. Barschall, W. Haeberly (University of Wisconsin Press, 1971)
241. J. Kopecky, M. Uhl, Test of gamma-ray strength functions in nuclear reaction model calculations. Phys. Rev. C **41**, 1941 (1990)
242. G. Gurevich, L.E. Lazareva, V.M. Mazur, S.Y. Merkulov, G.V. Solodukhov, V.A. Tyutin, Total nuclear photoabsorption cross section in the region 150<A<190. Nucl. Phys. A **351**, 257 (1981)
243. C. Kalbach, Surface and collective effects in preequilibrium reactions. Phys. Rev. C **62**, 044608 (2000)
244. A. Konobeyev, Y. Korovin, Calculation of deuteron spectra for nucleon induced reactions on the basis of the hybrid exciton model taking into account direct processes. Kerntechnik **61**, 45 (1996)
245. P. Pereslavtsev, U. Fischer, Evaluation of n + W cross section data up to 150 MeV neutron energy. Proceedings of the International Conference on Nuclear Data for Science and Technology - ND2004, Sep. 26–Oct. 1, 2004, Santa Fe, USA, AIP Conference proceedings 769, Melville, NY (2005)
246. F. Emiliani, K. Guber, S. Kopecky, C. Lampoudis, C. Massimi, P. Schillebeeckx, K. Volev, Evaluation of stable tungsten isotopes in the resolved resonance region. EPJ Web Conf. **42**, 02002 (2013)
247. H.S. Camarda, H.I. Liou, G. Hacken, F. Rahn, W. Makofske, M. Slagowitz, S. Wynchank, J. Rainwater, Neutron resonance spectroscopy. XII. The separated isotopes of W. Phys. Rev. C **8**, 1813 (1973)
248. R.L. Macklin, D.M. Drake, E.D. Arthur, Neutron capture cross sections of ^{182}W, ^{183}W, ^{184}W, and ^{186}W from 2.6 to 2000 keV. Nucl. Sci. Eng. **84**(2), 98 (1983)
249. K. Knopf, W. Waschkowski, Wechselwirkung von neutronen mit wolfram und seinen isotopen. Z. Naturf. A **42**, 909–916 (1987)
250. S.J. Friesenhahn, E. Haddad, F.H. Fröhner, W.M. Lopez, The neutron capture cross section of the tungsten isotopes from 0.01 to 10 electron volts. Nucl. Sci. Eng. **26**(4), 487–499 (1966)
251. C. Massimi, A. Borella, S. Kopecky, C. Lampoudis, P. Schillebeeckx, M. Moxon, G. Vannini, Neutron resonance parameters of ^{197}Au from transmission, capture and self-indication measurements at GELINA. J. Korean Phys. Soc. **59**, 1689–1692 (2012)
252. R. Capote, K.I. Zolotarev, V.G. Pronyaev, A. Trkov, Updating and extending the IRDF-2002 dosimetry library. J. ASTM Int. **9**, 1 (2012)
253. I. Sirakov, B. Becker, R. Capote, S. Kopecky, C. Massimi, V. Pronyaev, P. Schillebeeckx, A. Trkov, G.Žerovnik, Evaluation of neutron induced reaction cross sections on gold. JRC Scientfic and Policy Report, Report EUR 25803 EN (2013)
254. N.E. Holden, K.A. Holden, Re-examination of 2200 m/s cross section experiments for neutron capture and fission standards. Pure Appl. Chem. **61**, 1505–1510 (1989)
255. K. Seth, Neutron total cross sections and intermediate resonances. Phys. Lett. **16**, 306–308 (1965)
256. O. Purtov, L. Litvinskiy, A. Murzin, G. Novoselov, Total neutron cross-sections and average resonance parameters of gold. At. Energy **77**, 536–539 (1994)
257. C. Massimi, B. Becker, E. Dupont, S. Kopecky, C. Lampoudis, R. Massarczyk, M. Moxon, V. Pronyaev, P. Schillebeeckx, I. Sirakov, R. Wynants, Neutron capture cross section measurements for ^{197}Au from 3.5 to 84 keV at GELINA. Eur. Phys. J. A **50**, 124 (2014)
258. I. Sirakov, R. Capote, F. Gunsing, P. Schillebeeckx, A. Trkov, An ENDF-6 compatible evaluation for neutron induced reactions of ^{232}Th in the unresolved resonance region. ANE **35**, 1223–1231 (2008)
259. E. Soukhovitski, S. Chiba, R. Capote, J. Quesada, S. Kunieda, G. Mororovskij, Supplement to OPTMAN Code, Manual Version 10 (2008). JAEA-Data/Code 2008-025, Japan Atomic Energy Agency (2008)

260. S. Badikov, C. Zhenpeng, A. Carlson, G.H.E.V. Gai, F.-J. Hambsch, H. Hofmann, T. Kawano, N. Larson, V. Pronyaev, D.L. Smith, S.-Y. Oh, S. Tagesen, H. Vonach, International evaluation of neutron cross-section standards. IAEA Report, STI/PUB/1291 (2007)
261. L. Perrot, A. Billebaud, R. Brissot, A. Giorni, D. Heuer, J.-M. Loiseaux, O. Méplan, J.-B. Viano, Precise validation of database (n,γ) cross sections using a lead-slowing-down spectrometer and simulation from 0.1 ev to 30 kev: Methodology and data for a few elements. Nucl. Sci. Eng. **144**(2), 142 (2003)
262. L.C. Mihailescu, C. Borcea, P. Baumann, P. Dessagne, E. Jericha, H. Karam, M. Kerveno, A.J. Koning, N. Leveque, A. Pavlik, A.J.M. Plompen, C. Quétel, G. Rudolf, I. Trešl, A measurement of (n, xnγ) cross sections for ^{208}Pb from threshold up to 20 MeV. Nucl. Phys. A **811**, 1–27 (2008)
263. L.C. Mihailescu, Neutron (n,xnγ) cross-section measurements for ^{52}Cr, ^{209}Bi and ^{206,207,208}Pb from threshold up to 20 MeV. Ph.D. thesis, University of Bucharest (2007). EUR 22343 EN—ISBN 92-79-02885-5
264. L.C. Mihailescu, C. Borcea, A. Koning, A. Pavlik, A.J.M. Plompen, High resolution measurement of neutron inelastic scattering and (n,2n) cross-sections for ^{209}Bi. Nucl. Phys. A **799**, 1–29 (2008)
265. K. Saito, M. Igashira, T. Ohsaki, T. Obara, H. Sekimoto, Measurement of cross sections of the 210-Po production reaction by keV-neutron capture of 209-Bi, in *JAERI Conference Proceedings, vol. 6* (2003), p. 133
266. A. Borella, T. Belgya, S. Kopecky, F. Gunsing, M. Moxon, M. Rejmund, P. Schillebeeckx, L. Szentmiklosi, Determination of the ^{209}Bi(n, γ)^{210}Bi and ^{209}Bi(n, γ)^{210m,g}Bi reaction cross sections in a cold neutron beam. Nucl. Phys. A **850**, 1–21 (2011)
267. A. Borella, T. Belgya, E. Berthoumieux, N. Colonna, C. Domingo-Pardo, J. Drohe, F. Gunsing, S. Marrone, T. Martinez, C. Massimi, P. Mastinu, P. Milazzo, P. Schillebeeckx, G. Tagliente, J. Tain, R. Terlizzi, R. Wynants, Measurements of the branching ratio of the ^{209}Bi(n, γ)^{210g}Bi/^{209}Bi(n, γ)^{210m}Bi reactions at GELINA, in *Proceedings of International Conference on Nuclear Data for Science and Technology 2007*, ed. by O. Bersillon, F. Gunsing, E. Bauge, R. Jacqmin, S. Leray (EDP Sciences, 2007), p. 563
268. D. Rochman, A. Koning, How to randomly evaluate nuclear data: a new data adjustment method applied to ^{239}Pu. Nucl. Sci. Eng. **169**, 68 (2011)
269. A.J. Koning, Bayesian Monte Carlo method for nuclear data evaluation. Eur. Phys. J. A **51**, 184 (2015)
270. P. Helgesson, H. Sjostrand, A. Koning, J. Ryden, D. Rochman, E. Alhassan, S. Pomp, Combining total Monte Carlo and Unified Monte Carlo: Bayesian nuclear data uncertainty quantification from auto-generated experimental covariances. Progr. Nucl. Energy **96**, 76 (2017)
271. D. Rochman, O. Leray, A. Vasiliev, H. Ferroukhi, A. Koning, M. Fleming, J. Sublet, A Bayesian Monte Carlo method for fission yield covariance information. Ann. Nucl. Energy **95**, 125–134 (2016)
272. A. Trkov, M. Herman, D. Brown, ENDF-6 Formats Manual, Data Formats and Procedures for the Evaluated Nuclear Data Files ENDF/B-VI, ENDF/B-VII and ENDF/B-VIII. CSEWG Document ENDF-102, Report BNL-203218-2018-INRE, SVN Commit: revision 215 (2012)
273. M. Fleming, J-Ch. Sublet, J. Kopecky, Integro-differential verification and validation, FISPACT-II & TENDL-2017 nuclear data libraries. UK Atomic Energy Authority, report UKAEA-R(18)004 (2018)
274. D. Rochman, A. Koning, J. Kopecky, J.-C. Sublet, P. Ribon, M. Moxon, From average parameters to statistical resolved resonances. Ann. Nucl. Energy **51**, 60 (2013)
275. J. Kopecky, M. Delfini, H.V. der Kamp, D. Nierop, Revisions and extensions of neutron capture cross-sections in the European Activation File EAF-3. Tech. Rep. ECN Petten Report ECN-C-92-051, The Netherlands (1992)
276. IAEA-CRP, Database of Prompt Gamma Rays for slow Neutron Capture for elemental analysis. IAEA Report STI/PUB/1263, consulted June 2019, IAEA, Wagramerstrasse 5, Vienna, Austria (2007). www-nds.iaea.org/pgaa/egaf.html
277. G. Rimpault, A. Courcelle, D. Blanchet, Needs for accurate measurements of spectrum and multiplicity of prompt γ-emitted in fission. Entries 421 and 422 (2006). https://www.oecd-nea.org/science/wpec/hprl/
278. G. Rimpault, D. Bernard, D. Blanchet, C. Vaglio-Gaudard, S. Ravaux, A. Santamarina, Needs of accurate prompt and delayed gamma spectrum and multiplicity for nuclear reactor designs. Phys. Procedia **31**, 3–12 (2012)
279. A. Luthi, R. Chawla, G. Rimpault, Improved gamma-heating calculational methods for fast reactors and their validation for plutonium-burning configurations. Nucl. Sci. Eng. **138**(3), 233 (2001)
280. A. Oberstedt, T. Belgya, R. Billnert, R. Borcea, T. Bryś, W. Geerts, A. Göök, F.-J. Hambsch, Z. Kis, T. Martinez, S. Oberstedt, L. Szentmiklosi, K. Takàcs, M. Vidali, Improved values for the characteristics of prompt-fission γ-ray spectra from the reaction ^{235}U($n_{\rm th}$, f). Phys. Rev. C **87**, 051602 (2013)
281. M. Lebois, J.N. Wilson, P. Halipré, A. Oberstedt, S. Oberstedt, P. Marini, C. Schmitt, S.J. Rose, S. Siem, M. Fallot, A. Porta, A.-A. Zakari, Comparative measurement of prompt fission γ-ray emission from fast-neutron-induced fission of ^{235}U and ^{238}U. Phys. Rev. C **92**, 034618 (2015)
282. J. Wilson, M. Lebois, private communication (2016)
283. A. Gatera, T. Belgya, W. Geerts, A. Göök, F.-J. Hambsch, M. Lebois, B. Maróti, A. Moens, A. Oberstedt, S. Oberstedt, F. Postelt, L. Qi, L. Szentmiklósi, G. Sibbens, D. Vanleeuw, M. Vidali, F. Zeiser, Prompt-fission gamma-ray spectral characteristics from Pu-239(n(th), f). Phys. Rev. C **95**, 064609 (2017)
284. S. Oberstedt, R. Billnert, T. Belgya, T. Bryś, W. Geerts, C. Guerrero, F.-J. Hambsch, Z. Kis, A. Moens, A. Oberstedt, G. Sibbens, L. Szentmiklosi, D. Vanleeuw, M. Vidali, High-precision prompt-γ-ray spectral data from the reaction ^{241}Pu($n_{\rm th}$, f). Phys. Rev. C **90**, 024618 (2014)
285. V. Verbinski, H. Weber, R. Sund, Prompt gamma-rays from U-235(n, f), Pu-239(n, f), and spontaneous fission of Cf-252. Phys. Rev. C **7**, 1173 (1973)
286. R. Peelle, F. Maienschein, Spectrum of photons emitted in coincidence with fission of U-235 by thermal neutrons. Phys. Rev. C **3**, 373 (1971)
287. F. Pleasonton, R. Ferguson, H. Schmitt, Prompt gamma-rays emitted in thermal-neutron-induced fission of U-235. Phys. Rev. C **6**, 1023 (1972)
288. F. Pleasonton, Prompt gamma-rays emitted in thermal-neutron-induced fission of U-233 and Pu-239. Nucl. Phys. A **213**, 413 (1973)
289. S. Oberstedt, R. Borcea, T. Bryś, T. Gamboni, W. Geerts, F.-J. Hambsch, A. Oberstedt, M. Vidali, Artificial diamonds as radiation-hard detectors for ultra-fast fission-fragment timing. Nucl. Instrum. Methods Phys. Res. Sect. A Accel. Spectrom. Detect. Assoc. Equip. **714**, 31–37 (2013)
290. K.-H. Schmidt, B. Jurado, C. Amouroux, C. Schmitt, General description of fission observables: GEF model code. Nucl. Data Sheets **131**, 107 (2016). Special Issue on Nuclear Reaction Data
291. P. Talou, T. Kawano, I. Stetcu, J.P. Lestone, E. McKigney, M.B. Chadwick, Late-time emission of prompt fission γ rays. Phys. Rev. C **94**, 064613 (2016)
292. R. Vogt, J. Randrup, Improved modeling of photon observables with the event-by-event fission model FREYA. Phys. Rev. C **96**, 064620 (2017)

293. O. Litaize, O. Serot, L. Berge, Fission modelling with FIFRELIN. Eur. Phys. J. A **51**, 177 (2015)
294. W. Hauser, H. Feshbach, The inelastic scattering of neutrons. Phys. Rev. **87**, 366–373 (1952)
295. F. Becvar, Simulation of γ cascades in complex nuclei with emphasis on assessment of uncertainties of cascade-related quantities. Nucl. Instrum. Methods Phys. Res. A **417**(2), 434–449 (1998)
296. O. Litaize, O. Serot, Investigation of phenomenological models for the Monte Carlo simulation of the prompt fission neutron and γ emission. Phys. Rev. C **82**, 054616 (2010)
297. D. Regnier, O. Litaize, O. Serot, An improved numerical method to compute neutron/gamma deexcitation cascades starting from a high spin state. Comput. Phys. Commun. **201**, 19–28 (2016)
298. R. Billnert, F.-J. Hambsch, A. Oberstedt, S. Oberstedt, New prompt spectral gamma-ray data from the reaction Cf-252(sf) and its implication on present evaluated nuclear data files. Phys. Rev. C **87**, 024601 (2013)
299. A. Oberstedt, R. Billnert, S. Oberstedt, Predictions of characteristics of prompt-fission γ-ray spectra from the n $+^2$ 38U reaction up to $E_n = 20$MeV. Phys. Rev. C **96**, 034612 (2017)
300. D.E. Cullen, PREPRO 2018: 2018 ENDF/B Pre-processing Codes. Report IAEA-NDS-39 Rev. 18, June 20 (2018)
301. M.R. Bhat, Evaluated nuclear structure data file (ENSDF), in *Proceedings of International Conference on Nuclear Data for Science and Technology*, ed. by S.M. Qaim (Springer, Berlin, 1992), p. 817
302. Investigation of Covariance Data in General Purpose Nuclear Data Libraries. Working Party on International Evaluation Co-operation, OECD NEA Nuclear Science Committee, Volume 44, in print (2019)
303. E. Axton, Evaluation of the thermal constants of ^{233}U, ^{235}U, ^{239}Pu and ^{241}Pu, and the fission neutron yield of ^{252}Cf, Tech. Rep. GE/PH/01/86, JRC-Geel (1986)
304. C. De Saint Jean, E. Privas, P. Archier, G. Noguère, Estimation of nuclear reaction model parameter covariances and the related neutron induced cross sections with physical constraints. Nucl. Data Sheets **118**, 336–340 (2014)
305. I. Kodeli, S. Slavič, SUSD3D Computer Code as Part of the XSUN-2017 Windows Interface Environment for Deterministic Radiation Transport and Cross Section Sensitivity-Uncertainty Analysis, Science and Technology of Nuclear Installations **2017**, ID 1264736 (2017)
306. L. Fiorito, A. Stankovskiy, G.V. den Eynde, C. Diez, O. Cabellos, P. Labeau, Generation of fission yield covariances to correct discrepancies in the nuclear data libraries. Ann. Nucl. Energy **88**, 12–23 (2016)
307. N. Terranova, O. Serot, P. Archier, C. De Saint Jean, M. Sumini, Covariance Matrix Evaluations for Independent Mass Fission Yields. Nuclear Data Sheets **123**, 225–230 (2015). Special Issue on International Workshop on Nuclear Data Covariances April 28–May 1, 2014, Santa Fe, New Mexico, USA http://t2.lanl.gov/cw2014
308. M.J. Norgett, M.T. Robinson, I.M. Torrens, A proposed method of calculating displacement dose rates. Nucl. Eng. Des. **33**, 50 (1975)
309. K. Nordlund, A. Sand, F. Granberg, S. Zinkle, R. Stoller, R. Averback, T. Suzudo, L. Malerba, F. Banhart, W. Weber, F. Willaime, S. Dudarev, D. Simeone, Primary Radiation Damage in Materials. Report NEA/NSC/DOC(2015)9 (2015)
310. K. Nordlund, Primary Radiation Damage Cross Sections. Report INDC(NDS)- 0691, IAEA (2015)
311. P. Jung, *Production of Atomic Defects in Metals. Landolt–Beirnstein, Group III: Crystal and Solid State Physics* (Springer, Berlin, 1991)
312. M.T. Robinson, Basic physics of radiation damage production. J. Nucl. Mater. **216**, 1 (1994)
313. C.H.M. Broeders, A.Y. Konobeyev, Defect production efficiency in metals under neutron irradiation. J. Nucl. Mater. **328**, 197 (2004)
314. K. Nordlund, Private communication (2016)
315. A.Y. Konobeyev, U. Fischer, Y.A. Korovin, S.P. Simakov, Effective threshold displacement energies and other data required for the calculation of advanced atomic displacement cross-sections. NET **3**, 169 (2017)
316. R.W. Mills, A new UK fission yield evaluation UKFY3.7. EPJ Web Conf. **146**, 04008 (2017)
317. R.W. Mills, Fission product yield evaluation. Ph.D. thesis, University of Birmingham (1995). http://etheses.bham.ac.uk/4353/
318. G. Audi, O. Bersillon, J. Blachot, A.H. Wapstra, The nubase evaluation of nuclear and decay properties. Nucl. Phys. A **729**, 3 (2003)
319. R.J. Perry, C.J. Dean, A.L. Nichols, Actinide, activation product and fission product decay data for reactor-based applications. Nucl. Data Sheets **120**, 261 (2014)
320. M.A. Kellett, O. Bersillon, The decay data evaluation project (DDEP) and the JEFF-3.3 radioactive decay data library: combining international collaborative efforts on evaluated decay data. EPJ Web Conf. **146**, 02009 (2017)
321. M.A. Kellett, A.L. Nichols, Library of Recommended Actinide Decay Data, 2011. No. 1618 in IAEA-STI/PUB, International Atomic Energy Agency (2013)
322. J.C. Hardy, L.C. Carraz, B. Jonson, P.G. Hansen, The essential decay of pandemonium: a demonstration of errors in complex beta-decay schemes. Phys. Lett. B **71**(2), 307–310 (1977)
323. Assessment of Fission Product Decay Data for Decay Heat Calculations. A report by the Working Party on International Evaluation Co-operation of the OECD NEA Nuclear Science Committee, vol. 25, ISBN 978-92-64-99034-0, NEA No. 6284 (2007)
324. R.C. Greenwood, R.G. Helmer, M.H. Putnam, K.D. Watts, Measurement of β^--decay intensity distributions of several fission-product isotopes using a total absorption γ-ray spectrometer. Nucl. Instrum. Methods Phys. Res. **A390**, 95 (1997)
325. A. Algora, D. Jordan, J.L. Tain, B. Rubio, J. Agramunt, A.B. Perez-Cerdan, F. Molina, L. Caballero, E. Nacher, A. Krasznahorkay, M.D. Hunyadi, J. Gulyas, A. Vitez, M. Csatlos, L. Csige, J. Aysto, H. Penttila, I.D. Moore, T. Eronen, A. Jokinen, A. Nieminen, J. Hakala, P. Karvonen, A. Kankainen, A. Saastamoinen, J. Rissanen, T. Kessler, C. Weber, J. Ronkainen, S. Rahaman, V. Elomaa, S. Rinta-Antila, U. Hager, T. Sonoda, K. Burkard, W. Huller, L. Batist, W. Gelletly, A.L. Nichols, T. Yoshida, A.A. Sonzogni, K. Perajarvi, Reactor decay heat in ^{239}Pu: solving the γ discrepancy in the 4–3000-s cooling period. Phys. Rev. Lett. **105**, 202501 (2010)
326. E. Valencia, J.L. Tain, A. Algora, J. Agramunt, E. Estévez, M.D. Jordan, B. Rubio, S. Rice, P. Regan, W. Gelletly, Z. Podolyák, M. Bowry, P. Mason, G.F. Farrelly, A.A. Zakari-Issoufou, M. Fallot, A. Porta, V.M. Bui, J. Rissanen, T. Eronen, I. Moore, H. Penttilä, J. Äystö, V.V. Elomaa, J. Hakala, A. Jokinen, V.S. Kolhinen, M. Reponen, V. Sonnenschein, D. Cano-Ott, A.R. Garcia, T. Martínez, E. Mendoza, R. Caballero-Folch, B. Gomez-Hornillos, V. Gorlichev, F.G. Kondev, A.A. Sonzogni, L. Batist, Total absorption gamma-ray spectroscopy of ^{87}Br, ^{88}Br and ^{94}Rb β-delayed neutron emitters. Phys. Rev. C **95**, 024320 (2016)
327. A.A. Zakari-Issoufou, M. Fallot, A. Porta, A. Algora, J.L. Tain, E. Valencia, S. Rice, V.M. Bui, S. Cormon, M. Estienne, J. Agramunt, J. Äystö, M. Bowry, J.A. Briz, R. Caballero-Folch, D. Cano-Ott, A. Cucoanes, V.V. Elomaa, T. Eronen, E. Estévez, G.F. Farrelly, A.R. Garcia, W. Gelletly, M.B. Gomez-Hornillos, V. Gorlychev, J. Hakala, A. Jokinen, M.D. Jordan, A. Kankainen, P. Karvonen, V.S. Kolhinen, F.G. Kondev, T. Martínez, E. Mendoza, F. Molina, I. Moore, A.B. Perez-Cerdán, Z. Podolyák, H. Pentillä, P.H. Regan, M. Reponen, J. Rissanen, B. Rubio, T. Shiba, A.A. Sonzogni, C. Weber, and the IGISOL Collaboration, Total absorp-

tion spectroscopy study of ^{92}rb decay: A major contributor to reactor antineutrino spectrum shape. Phys. Rev. Lett. **115**, 102503 (2015)
328. R.W. Mills, D.J. Mountford, J.P. Coleman, C. Metelko, M. Murdoch, Y.-J. Schnellbach, Modelling of the anti-neutrino production and spectra from a magnox reactor. Eur. Phys. J. Web Conf. **170**, 07008 (2018)
329. M. Estienne, M. Fallot, A. Algora, J. Briz-Monago, V. Bui, S. Cormon, W. Gelletly, L. Giot, V. Guadilla, D. Jordan, L.L. Meur, A. Porta, S. Rice, B. Rubio, J. Taín, E. Valencia, A.-A. Zakari-Issoufou, Updated summation model: an improved agreement with the daya bay antineutrino fluxes. Phys. Rev. Lett. **123**, 022502 (2019)
330. X. Mougeot, Reliability of the usual assumptions in the calculation of β and ν spectra. Phys. Rev. C **92**, 059902 (2015)
331. J. Sublet, L.W. Packer, J. Kopecky, R.A. Forrest, A.J. Koning, D.A. Rochman, The European Activation File: EAF-2010 neutron-induced cross section library. EASY Documentation Series CCFE-R (10) (2010)
332. R.A. Forrest, The European Activation File: EAF-2007 decay data library, Tech. Rep. UKAEA-FUS–537, EURATOM/CCFE (2007)
333. R. Forrest, M. Pillon, J. Kopecky, A. Klix, S.P. Simakov, J.-C. Sublet, P. Bém, M. Honusek, E. Šimecková, Validation of EASY-2007 using integral measurements, Tech. Rep. UKAEA-FUS–547, UKAEA, UK (2008)
334. M. Gilbert, Validation of EAF-style TENDL-2017 neutron cross section library for activation calculations, Tech. Rep. 2M8JK4, EUROfusion (2018)
335. L. Alianelli, M.S. del Rıo, R. Felici, K. Andersen, E. Farhi, A novel Monte Carlo algorithm for simulating crystals with McStas. Phys. B Condens. Matter **350**(1–3), E725–E729 (2004)
336. A.K. Freund, Cross-sections of materials used as neutron monochromators and filters. Nucl. Instrum. Methods Phys. Res. **213**(2–3), 495–501 (1983)
337. F. Sanchez et al., Irradiation facilities performance at RA-10. 16th IGORR (2014)
338. F. Cantargi, J. Granada, R. Mayer, Thermal neutron scattering kernels for sapphire and silicon single crystals. Ann. Nucl. Energy **80**, 43–46 (2015)
339. R. Brugger, R. Fluharty, P. Lisowski, C. Olsen, Neutron total cross section of single crystal silicon at 21 K, tech. rep., Los Alamos Scientific Lab., NM (USA) (1979)
340. J.A. Young, J.U. Koppel, Slow neutron scattering by molecular hydrogen and deuterium. Phys. Rev. **135**(3A), A603 (1964)
341. R. MacFarlane, New thermal neutron scattering files for ENDF/B-VI release 2. Los Alamos National Laboratory Report LA–12639-MS (1994)
342. M. Zoppi, A. Soper, R. Magli, F. Barocchi, U. Bafile, N. Ashcroft, Structure factor of compressed liquid deuterium close to the melting transition. Phys. Rev. E **54**(3), 2773 (1996)
343. J. Granada, V. Gillette, A new thermal neutron scattering kernel for liquid hydrogen. Phys. B Condens. Matter **348**(1–4), 6–14 (2004)
344. M. Celli, N. Rhodes, A. Soper, M. Zoppi, The total neutron cross section of liquid para-hydrogen. J. Phys. Condens. Matter **11**(50), 10229 (1999)
345. K. Grammer, R. Alarcon, L. Barrón-Palos, D. Blyth, J. Bowman, J. Calarco, C. Crawford, K. Craycraft, D. Evans, N. Fomin et al., Measurement of the scattering cross section of slow neutrons on liquid parahydrogen from neutron transmission. Phys. Rev. B **91**(18), 180301 (2015)
346. M. Kasprzak, Ultracold neutron converters, Ph.D. Thesis. University of Vienna (2008)
347. F. Atchison, B. van den Brandt, T. Bryś, M. Daum, P. Fierlinger, P. Hautle, R. Henneck, K. Kirch, J. Kohlbrecher, G. Kühne et al., Measured total cross sections of slow neutrons scattered by gaseous and liquid 2H(2). Phys. Rev. Lett. **94**(21), 212502 (2005)
348. W. Seiffert, Messung der Streuquerschnitte von flüssigem und festem Wasserstoff, Deuterium und Deuteriumhydrid für thermische Neutronen. Ph.D. thesis, Technische Universität München (1970). also published as Euratom report No. EUR 4455d
349. V. Ananiev, A. Belyakov, M. Bulavin, E. Kulagin, S. Kulikov, K. Mukhin, T. Petukhova, A. Sirotin, D. Shabalin, E. Shabalin et al., The world's first pelletized cold neutron moderator at a neutron scattering facility. Nucl. Instrum. Methods Phys. Res. Sect. B Beam Interact. Mater. Atoms **320**, 70–74 (2014)
350. M.H. Parajon, E. Abad, F. Bermejo, A review of the cold neutron moderator materials: neutronic performance and radiation effects. Phys. Procedia **60**, 74–82 (2014)
351. I. Natkaniec, K. Holderna-Natkaniec, J. Kalus, I. Majerz, Vibrational spectra of selected methyl derivatives of benzene and their solutions as potential materials for cold moderators, in *Proceedings of 16th meeting of the international collaboration on advanced neutron sources (ICANS-XVI), Düsseldorf-Neuss, Germany* (2003)
352. F. Cantargi, J. Granada, Thermal neutron cross-section libraries for aromatic hydrocarbons. Nucl. Instrum. Methods Phys. Res. B **268**(16), 2487 (2010)
353. J. Granada, V. Gillette, L. Torres, M. Sbaffoni, F. Cantargi, Preliminary evaluation of the cold neutron cross sections ch4 - hydrate, in *Proceedings of the 6th International Workshop on Advanced Cold Moderators held at Forschungszentrum Julich from 11 to 13 September 2002* (2002)
354. K. Nünighoff, C. Pohl, V. Bollini, A. Bubak, H. Conrad, D. Filges, H. Glückler, F. Goldenbaum, G. Hansen, B. Lensing et al., Ice moderator experiments at very low temperatures. Eur. Phys. J. A Hadron. Nuclei **22**(3), 519–528 (2004)
355. Regulations for the safe transport of radioactive material. IAEA safety standard series, ISSN 1020-525X, ISBN 978-92-0-133310-0, no. SSR-6d (2012)
356. A. Kolesnikov, V. Sinitsyn, E. Ponyatovsky, I. Natkaniec, L. Smirnov, Neutron scattering studies of the vibrational spectrum of high-density amorphous ice in comparison with ice ih and vi. J. Phys. Condens. Matter **6**(2), 375 (1994)
357. L. Torres, J. Granada, J. Blostein, Total cross sections of benzene at 90 K and light water ice at 115 K. Nucl. Instrum. Methods Phys. Res. Sect. B Beam Interact. Mater. Atoms **251**(1), 304–305 (2006)
358. J.I. Marquez Damian, D. Malaspina, J.R. Granada, CAB models for water: a new evaluation of the thermal neutron scattering laws for light and heavy water in ENDF-6 format. Ann. Nucl. Energy **65**, 280 (2014)
359. M. Mattes, J. Keinert, Thermal neutron scattering data for the moderator materials H2O, D2O and ZrHx in ENDF-6 format. INDC (NDS)-0470. IAEA (2005)
360. A. Soper, C. Benmore, Quantum differences between heavy and light water. Phys. Rev. Lett. **101**(6), 065502 (2008)
361. J.I. Marquez Damian, D. Malaspina, J. Granada, Vibrational spectra of light and heavy water with application to neutron cross section calculations. J. Chem. Phys. **139**(2), 024504 (2013)
362. J.I. Marquez Damian et al., Measurement of the total cross section of heavy water in the 0.1 meV-1 eV energy range at 20 and 50 ° C. Nuovo Cimento C **38**, 178 (2016)
363. J.I. Marquez Damian, J. Granada, D. Roubtsov, Improvement on the calculation of D2O moderated critical systems with new thermal neutron scattering libraries. Ann. Nucl. Energy **71**, 206–210 (2014)
364. D. Roubtsov, J. Chow, J.I. Marquez Damian, J. Granada, Application of the CAB evaluation of thermal scattering law for heavy water to ZED-2 critical benchmarks at room temperature. Ann. Nucl. Energy **110**, 958 (2017)

365. L. Maul, J.I.M. Damián, G. Braoudakis, M. Ho, G.H. Yeoh, Perturbation scheme for estimating uncertainties in thermal scattering cross sections of water. Ann. Nucl. Energy **121**, 232–249 (2018)
366. D. Rochman, W. Zwermann, S. Marck, A. Koning, H. Sjöstrand, P. Helgesson, B. Krzykacz-Hausmann, Efficient use of monte carlo: uncertainty propagation. Nucl. Sci. Eng. **177**(3), 337–349 (2014)
367. I. Kodeli, A. Milocco, P. Ortego, E. Sartori, 20 Years of SINBAD (Shielding Integral Benchmark Archive and Database). Progr. Nucl. Sci. Technol. **4**, 308–311 (2014)
368. O. Cabellos, F. Alvarez-Velarde, M. Angelone, C. Diez, J. Dyrda, L. Fiorito, U. Fischer, M. Fleming, W. Haeck, I. Hill, R. Ichou, D. Kim, A. Klix, I. Kodeli, P. Leconte, F. Michel-Sendis, E. Nunnenmann, M. Pecchia, Y. Peneliau, A. Plompen, D. Rochman, P. Romojaro, A. Stankovskiy, J. Sublet, P. Tamagno, S. van der Marck, Benchmarking and validation activities within JEFF project. Eur. Phys. J. Web Conf. **146**, 06004 (2017)
369. B. Cochet, A. Jinaphanh, L. Heulers, O. Jacquet, Capabilities overview of the MORET 5 Monte Carlo code. Ann. Nucl. Energy **82**, 74–84 (2015). Joint International Conference on Supercomputing in Nuclear Applications and Monte Carlo 2013, SNA+ MC 2013. Pluri- and Trans-disciplinarity, Towards New Modeling and Numerical Simulation Paradigms
370. W. Haeck, GAIA User's Manual—Version 1.0.0, Tech. Rep. IRSN Report PSN-EXP/SNC/2015-165, Institut de Radioprotection et de Sûreté Nucléaire (2015)
371. R.D. Mosteller, F.B. Brown, B.C. Kiedrowski, An expanded criticality validation suite for MCNP. Los Alamos National Laboratory LA-UR-11-05076 (2011)
372. R.D. Mosteller, Comparison of results from the MCNP criticality validation suite using ENDF/B-VI and preliminary ENDF/B-VII nuclear data, in *Proceedings of International Conference on Nuclear Data for Science and Technology - ND2004, Sep. 26–Oct. 1, 2004, Santa Fe, USA, AIP Conference proceedings 769*, (Melville, 2005), p. 390–393
373. S.C. van der Marck, Benchmarking ENDF/B-VII.1, JENDL-4.0 and JEFF-3.1.1 with MCNP6. Nucl. Data Sheets **113**(12), 2935–3005 (2012). Special Issue on Nuclear Reaction Data
374. R. Ichou, N. Leclaire, L. Leal, W. Haeck, B. Morillon, P. Romain, H. Helder Duarte, Use of integral experiments for the assessment of a new ^{235}U IRSN-CEA evaluation. EPJ Web Conf. **146**, 02046 (2017)
375. E. Kolbe, A. Vasiliev, H. Ferroukhi, The effect of modern thermal neutron scattering sublibraries on criticality safety evaluations of wet storage pools. Ann. Nucl. Energy **37**, 371 (2010)
376. A. Trkov, On the Benchmarking of New Evaluated Nuclear Data Libraries. INDC(NDS)-0751, IAEA, Vienna, Austria (2018)
377. P.J. Finck, J.C. Cabrillat, M. Martini, R. Soule, G. Rimpault, R. Jacqmin, The CIRANO experimental programme in support of advanced fast reactor physics, in *International Conference on the Physics of Reactors PHYSOR96*, vol 2, (Japan, 1996), p. 673
378. J.F. Vidal, A. Calloo, P. Blaise, *Qualification of Apollo28/jeff-311 Code Package for the Calculations of PWR Plutonium Recycling Using the Epicure Experiments* (American Nuclear Society-ANS, New York, 2010)
379. S. Cathalau, J.C. Cabrillat, J.P. Chauvin, P.J. Finck, P. Fougeras, G. Flamenbaum, H. Matsu-ura, M. Ueji, T. Yamamoto, MISTRAL: an experimental programme in the EOLE facility devoted to 100% MOX core physics, in *International conference on the physics of reactors PHYSOR96*, vol 3 (Japan, 1996), p. 605
380. C. Vaglio-Gaudard, A. Santamarina, P. Blaise, O. Litaize, A. Lyoussi, G. Noguère, J.M. Ruggieri, J.F. Vidal, Interpretation of PERLE Experiment for the Validation of Iron Nuclear Data Using Monte Carlo Calculations. Nuclear Science and Engineering **166**(2), 89–106 (2010)
381. E. Brun, F. Damian, C. Diop, E. Dumonteil, F. Hugot, C. Jouanne, Y. Lee, F. Malvagi, A. Mazzolo, O. Petit, J. Trama, T. Visonneau, A. Zoia, TRIPOLI-4, CEA, EDF and AREVA reference Monte Carlocode. Annals of Nuclear Energy **82**, 151–160 (2015). Joint International Conference on Supercomputing in Nuclear Applications and Monte Carlo 2013, SNA + MC 2013. Pluri- and Trans-disciplinarity, Towards New Modeling and Numerical Simulation Paradigms
382. A. Kochetkov, G. Vittiglio, J. Wagemans, W. Uyttenhove, A. Krása, J. Hernandez, The Lead-Based VENUS-F Facility: Status of the FREYA Project. EPJ Web of Conferences **106**, 06004 (2016)
383. A. Krása, A. Kochetkov, P. Baeten, G. Vittiglio, J. Wagemans, V. Bécares, Comparative study on neutron data in integral experiments of MYRRHA mockup critical cores in the VENUS-F reactor. EPJ Web Conf. **146**, 06019 (2017)
384. A. Röhrmoser, Hafnium data for description of criticality of FRM II reactor with control and safety rods, in *Proceedings of the European Research Reactor conference-RRFM2018, Munich 11–15 March 2018* (2018)
385. O. Cabellos, L. Fiorito, Examples of Monte Carlo Techniques applied for nuclear data uncertainty propagation EPJ Web Conf. **211**, 07008 (2019)
386. S.C. van der Marck, Benchmarking ENDF/B-VII.0. Nucl. Data Sheets **107**(12), 3061–3118 (2006). Evaluated Nuclear Data File ENDF/B-VII.0
387. H. Paxton, Fast critical experiments. Progr. Nucl. Energy **7**, 151 (1981)
388. I.-A. Kodeli, Sensitivity and uncertainty in the effective delayed neutron fraction (β_{eff}). Nucl. Instrum. Methods Phys. Res. Sect. A Accel. Spectrom. Detect. Assoc. Equip. **715**, 70–78 (2013)
389. X. Doligez, A. Billebaud, S. Chabod, T. Chevret, D. Fourmentel, A. Krasa, A. Kochetkov, F.R. Lecolley, J.L. Lecouey, G. Lehaut, N. Marie, F. Mellier, G. Vittiglio, J. Wagemans, Effective delayed neutron fraction measurement in the critical VENUS-F reactor using noise techniques, in *2015 4th International Conference on Advancements in Nuclear Instrumentation Measurement Methods and their Applications (ANIMMA)* (2015), p. 1–6
390. E.D.B. Pelowitz, MCNP6 User's Manual. Version 1.0. Report LA-CP-13-00634, Rev.0, Los Alamos National Laboratory, USA (2013)
391. U. Fischer, K. Kondo, M. Angelone, P. Batistoni, R. Villari, T. Bohm, M. Sawan, B. Walker, C. Konno, Benchmarking of the fendl-3 neutron cross-section data library for fusion applications, Tech. Rep. INDC(NDS)—0631, IAEA, International Atomic Energy Agency (IAEA) (2014)
392. R. Mosteller, Validation Suites for MCNP, Tech. Rep. LA-UR-02-0878, Los Alamos National Laboratory (2002)
393. I. Kodeli, G. Zerovnik, A. Milocco, Examples of use of SINBAD database for nuclear data and code validation. EPJ Web Conf. **153**, 02010 (2017)
394. A. Milocco, M. Pillon, A. Trkov, A Monte Carlo model for low energy D–D neutron generators. Nucl. Instrum. Methods Phys. Res. B **271**, 6 (2012)
395. M. Angelone, D. Flammini, S. Loreti, F. Moro, M. Pillon, R. Villari, A. Klix, U. Fischer, I. Kodeli, R. Perel, W. Pohorecky, Copper benchmark experiment for the testing of JEFF-3.2 nuclear data for fusion applications. EPJ Web Conf. **146**, 09004 (2017)
396. M. Angelone, D. Flammini, S. Loreti, F. Moro, M. Pillon, R. Villari, Copper benchmark experiment at the Frascati neutron generator for nuclear data validation. Fusion Eng. Des. **109–111**, 843–847 (2016). (**Proceedings of the 12th International Symposium on Fusion Nuclear Technology-12 (ISFNT-12)**)
397. I. Kodeli, K. Kondo, R. Perel, U. Fischer, Cross-section sensitivity and uncertainty analysis of the FNG copper benchmark experiment. Fusion Eng. Des. **109–111**, 1222–1226 (2016). (**Proceedings of the 12th International Symposium on Fusion Nuclear Technology-12 (ISFNT-12)**)

398. L. Trykov, J. Kolevatov, A. Nikolaev, I. Buryan, M. Marek, B. Yanskiy, M. Tikhiy, P. Otopal, Experimental Researches of Outow Spectra of Neutron and Gamma Radiations for Spheres from Iron, Tech. Rep. Preprint IPPE-943, IPPE (1979) (**(in Russian); Numerical data and additional references are available in ALARM-CF-FE-SHIELD-001 of ICSBEP)**)
399. S.P. Simakov, M.G. Kobosev, A.A. Lychagin, V.A. Talalaev, D.Y. Chuvilin, V.M. Maslov, Benchmarking of uranium-238 evaluations against spherical transmission and (n, xn)-reaction experimental data. AIP Conf. Proc. **769**(1), 67–70 (2005)
400. M. Gilbert, J.-C. Sublet, Experimental decay-heat simulation-benchmark for 14 MeV neutrons & complex inventory analysis with FISPACT-II. Nucl. Fusion **59**, 086045 (2019)
401. J.-C. Sublet, J. Eastwood, J. Morgan, M. Gilbert, M. Fleming, W. Arter, FISPACT-II: an advanced simulation system for activation, transmutation and material modelling. Nucl. Data Sheets **139**, 77–137 (2017). Special Issue on Nuclear Reaction Data
402. M. Fleming, J-Ch. Sublet, Validation of FISPACT-II decay heat and inventory predictions for fission events, Tech. Rep. UKAEA-R(18)003, UKAEA (2018)
403. M. Gilbert, J-Ch. Sublet, Decay heat validation, FISPACT-II & TENDL-2017, JEFF-3.3, ENDF/B-VIII.0, EAF2010, and IRDFF-1.05 nuclear data libraries, Tech. Rep. UKAEA-CCFE-R(18)002, CCFE (2018)
404. F. Maekawa, Y. Ikeda, Decay heat experiment on thirty-two fusion reactor relevant materials irradiated by 14-MeV neutrons. Fusion Eng. Des. **47**(4), 377–388 (2000)
405. F. Maekawa, K. ichiro Shibata, M. Wada, Y. Ikeda, H. Takeuchi, Comprehensive activation experiment with 14-MeV neutrons covering most of naturally existing elements: 5 min irradiation experiment. J. Nucl. Sci. Technol. **39**(sup2), 990–993 (2002)
406. A. Tobias, Decay heat. Technical Report, Central Electricity Generating Board, Berkeley Nuclear Laboratories, Berkeley, Gloucestershire GL13 9PB, England (1979)
407. A. Tobias, Derivation of decay heat benchmarks for U-235 and Pu-239 by a least squares fit to measured data. Technical Report, Central Electricity Generating Board (1989)
408. J. Dickens, J. Emery, T. Love, J. McConnell, K. Northcutt, R. Peelle, H. Weaver, Fission product energy release for times following thermal-neutron fission of U-235 between 2 and 14,000 s. Technical Report, ORNL/NUREG-14, Oak Ridge National Laboratory (1979)
409. J. Dickens, Current status of decay heat measurements, evaluations and needs. Technical Report ORNL/TM-10094, Oak Ridge National Laboratory (1986)
410. S. Li, Beta Decay Heat Following ^{235}U, ^{238}U and ^{239}Pu Neutron Fission. PhD thesis, University of Massachusetts Lowell, Department of Physics (1997)
411. H.V. Nguyen, Gamma-ray Spectra and Decay Heat Following ^{235}U Thermal Neutron Fission. Ph.D. thesis, University of Massachusetts Lowell, Department of Physics (1997)
412. E. Seabury, Gamma-ray Decay Heat Measurements Following ^{238}U(n,f) and ^{239}Pu(n,f). Ph.D. thesis, University of Massachusetts Lowell, Department of Physics (1997)
413. M. Akiyama, S. An, Measurements of fission product decay heat for fast reactors. Conf. on Nucl. Data for Sci. and Technol., Antwerp 1982 (1983)
414. G. Federici, W. Biel, M.R. Gilbert, R. Kemp, N.P. Taylor, R. Wenninger, European DEMO design strategy and consequences for materials. Nucl. Fusion **57**, 092002 (2017)
415. F. Käppeler, R. Gallino, S. Bisterzo, W. Aoki, The s process: nuclear physics, stellar models and observations. Rev. Mod. Phys. **83**, 157 (2011)
416. Z. Bao, H. Beer, F. Käppeler, F. Voss, K. Wisshak, T. Rauscher, Neutron cross sections for nucleosynthesis studies. At. Data Nucl. Data Tables **76**(1), 70 (2000)
417. I. Dillmann, M. Heil, F. Käppeler, T. Rauscher, KADoNiS v0.3—the third update of the Karlsruhe astrophysical database of nucleosynthesis in stars. Luxembourg, Publications Office of the European Union, JRC 56548, EUR 23883 EN, ISBN 978-92-79-11705-3. https://doi.org/10.2787/23116, Printed in Geel, Belgium (2010)
418. E. Mendoza, D. Cano-Ott, T. Koi, C. Guerrero, New standard evaluated neutron cross section libraries for the GEANT4 code and first verification. IEEE Trans. Nucl. Sci. **61**, 2357–2364 (2014)
419. O. Cabellos, J. Dyrda, N. Soppera, Checking, processing and verification of nuclear data covariances. Eur. Phys. J. Nucl. Sci. Technol. **4**, 39 (2018)
420. G. Radulescu, J. Wagner, Burn-up Credit Criticality safety Benchmark Phase VII—UO_2 fuel: study of spent fuel compositions for long-term disposal, Tech. Rep. OECD/NEA-6998, Working Party on Nuclear Criticality Safety (2012)
421. J. Bess, J.C. Bosq, C. Bouret, C. De Saint Jean, T. Fanning, P. Finck, J.C. Garnier, H. Khalil, R. Lavastre, P. Marsault, G. Palmiotti, P. Salvatores, M. Sciora, T. Sofu, T. Sumner, F. Varaine, A. Zaetta, DOE–CEA benchmark on SFR ASTRID innovative core: neutronic and safety transients simulation. International Atomic Energy Agency (IAEA): IAEA (2015)
422. J. Engelen, H.A. Abderrahim, P. Baeten, D.D. Bruyn, P. Leysen, MYRRHA: preliminary front-end engineering design. Int. J. Hydrogen Energy **40**(44), 15137–15147 (2015). The 4th International Conference on Nuclear and Renewable Energy Resources (NURER2014), 26-29 October 2014, Antalya, Turkey
423. D. De Bruyn, A. Alemberti, L. Mansani, G. Grasso, G. Bandini, C. Artioli, E. Bubelis, G. Mueller, J. Wallenius, A. Orden, S. Michiels, *Main Achievements Of The FP7-LEADER Collaborative Project Of The European Commission Regarding The Design Of A Lead-Cooled Fast Reactor* (Korean Nuclear Society, 4 2013), p. 281
424. J. Dyrda, N. Soppera, I. Hill, M. Bossant, J. Gulliford, New features and improved uncertainty analysis in the NEA nuclear data sensitivity tool (NDaST). EPJ Web Conf. **146**, 06026 (2017)
425. A. Nouri, P. Nagel, J.B. Briggs, T. Ivanova, DICE: database for the international criticality safety benchmark evaluation program handbook. Nucl. Sci. Eng. **145**(1), 11–19 (2003)
426. B. Erasmus, A comparison of JEFF-3.3(T4), ENDF/B-VII.1 and JENDL-4.0u covariance data. JEF/DOC-1888 (2017)
427. B. Rearden, M. Jessee, SCALE Code System, Version 6.2.3, Tech. Rep. ORNL/TM-2005/39, Oak Ridge National Laboratory, Oak Ridge, Tennessee, (2018) (**Available from Radiation Safety Information Computational Center as CCC-834**)
428. I. Kodeli, Transport and S/U analysis of the ASPIS-IRON88 Benchmark using recent and older iron cross-section evaluations, in *Proc. of PHYSOR 2018, Reactor physics paving the way towards more efficient systems, 22–26 April 2018*, (Cancun, Mexico, 2018)
429. W. Rhoades et al., DOORS-3.2, One-, two-, three-dimensional discrete ordinates neutron/photon transport code system. CCC-650, Radiation Safety Information Computational Center, Oak Ridge National Laboratory (1998)
430. J. Rhodes, K. Smith, D. Lee, CASMO-5 development and applications, in *Proceedings of the PHYSOR-2006 conference, ANS Topical Meeting on Reactor Physics (Vancouver, BC, Canada, 2006) B*, vol. 144 (2006)
431. O. Leray, H. Ferroukhi, M. Hursin, A. Vasiliev, D. Rochman, Methodology for core analyses with nuclear data uncertainty quantification and application to Swiss PWR operated cycles. Ann. Nucl. Energy **110**, 547–559 (2017)
432. W. Wieselquist, T. Zhu, A. Vasiliev, H. Ferroukhi, PSI methodologies for nuclear data uncertainty propagation with CASMO-5M and MCNPX: Results for OECD/NEA UAM benchmark phase I. Sci. Technol. Nucl. Install. **2013**, 15 (2013)

433. M. Hursin, M. Scriven, G. Perret, A. Pautz, Uncertainty quantification and representativity analysis of LWR-PROTEUS Phase III experiments using SHARKX. Ann. Nucl. Energy **91**, 48–58 (2016)
434. W.J. Marshall, M.L. Williams, D. Wiarda, B.T. Rearden, M.E. Dunn, D.E. Mueller, J.B. Clarity, development and testing of Neutron cross-section covariance data for SCALE 6.2, in *International Conference on Nuclear Criticality Safety (ICNC 2015) Charlotte, NC, USA, September 13–17, 2015, ISBN: 978-0-89448-723-1*, p. 1213 (2015)
435. P. Romojaro, F. Alvarez-Velarde, N. Herranz, Summon: a sensitivity and uncertainty methodology for monte carlo codes, in *International Conference on Mathematics and Computational Methods Applied to Nuclear Science and Engineering*, (Jeju, Korea, 2017)
436. Methods and Issues for the Combined Use of Integral Experiments and Covariance Data. Working Party on International Evaluation Co-operation, OECD NEA Nuclear Science Committee, Volume 33, NEA/NSC/WPEC/DOC(2013)445 (2012)
437. Methods and approaches to provide feedback from nuclear and covariance data adjustment for improvement of nuclear data files. Working Party on International Evaluation Co-operation, OECD NEA Nuclear Science Committee, Volume 39, in print (2019)
438. S. Pelloni, D. Rochman, Performance assessment of adjusted nuclear data along with their covariances on the basis of fast reactor experiments. Ann. Nucl. Energy **121**, 361 (2018)
439. K. Yokoyama, M. Ishikawa, Use and impact of covariance data in the Japanese latest adjusted library ADJ2010 based on JENDL-4.0. Nucl. Data Sheets **123**, 97 (2015)
440. G. Palmiotti, M. Salvatores, G. Aliberti, A priori and a posteriori covariance data in nuclear cross section adjustment: issues and challenges. Nucl. Data Sheets **123**, 41 (2015)
441. M. Salvatores, G. Palmiotti, G. Aliberti, P. Archier, C. De Saint Jean, E. Dupont, M. Herman, M. Ishikawa, T. Ivanova, E. Ivanov, S.-J. Kim, I. Kodeli, G. Manturov, R. McKnight, S. Pelloni, C. Perfetti, A. Plompen, B. Rearden, D. Rochman, K. Sugino, A. Trkov, W. Wang, H. Wu, W.-S. Yang, Methods and issues for the combined use of integral experiments and covariance data: Results of a nea international collaborative study. Nucl. Data Sheets **118**, 38 (2014)
442. Methods and Approaches to Provide Feedback from Nuclear and Covariance Data Adjustment for Improvement of Nuclear Data Files. OECD Nuclear Energy Agency, Nuclear Science, NEA/NSC/R(2016)6 (2017)
443. International Reactor Physics Experiment Evaluation project, IRPhE Handbook. OECD-NEA. https://www.oecd-nea.org/science/wprs/irphe/handbook.html, Paris (2018)
444. G. Rimpault, D. Plisson, J. Tommasi, R. Jacqmin, J.-M. Rieunier, The ERANOS data and code system for fast reactor neutronic analyses, in *Proceedings of the International Conference on the New Frontier of Nuclear Technology: Reactor Physics, Safety and High-Performance Computing (PHYSOR 2002)* (2002)
445. S. Pelloni, D. Rochman, Cross-section adjustment in the fast energy range on the basis of an asymptotic progressing nuclear data Incremental Adjustment (APIA) methodology. Ann. Nucl. Energy **115**, 323 (2018)
446. S. Pelloni, Comparison of progressive incremental adjustment sequences for cross-section and variance/covariance data adjustment by analyzing fastspectrum systems. Ann. Nucl. Energy **106**, 33 (2017)

A. J. M. Plompen is an experimental nuclear physicist working at the accelerator laboratories of the European Commission, Joint Research Centre in Geel, Belgium. He received his doctorate degree in 1993 from the Vrije Universiteit Amsterdam, The Netherlands. Presently, he chairs the Coordination Group of the Joint Evaluated Fission and Fusion nuclear data library, a collaborative project of the Databank of the Nuclear Energy Agency of the OECD in Paris.